VNIVERSITAT DE VALÈNCIA

Doctorado en Biomedicina y Farmacia

Tesis doctoral

Pharmacometrics model-informed strategies for improving the pharmacokinetic/pharmacodynamic properties and clinical decision-making processes of drugs

Karine E. Rodríguez Fernández

Directores:
Dr. Victor Mangas Sanjuán
Dra. Mónica Climente Martí
Dra. Elena Gras Colomer

Valencia, Febrero 2025

VNIVERSITAT DE VALÈNCIA

Pharmacometrics model-informed strategies for improving the pharmacokinetic/pharmacodynamic properties and clinical decision-making processes of drugs

Tesis doctoral

Doctorado en Biomedicina y Farmacia

Karine E. Rodríguez Fernández

Directores:

Dr. Víctor Mangas Sanjuán
Dra. Mónica Climente Martí
Dra. Elena Gras Colomer

Tutora:

Dra. Matilde Merino Sanjuán

Departamento de Farmacia y Tecnología Farmacéutica y Parasitología

Valencia, Febrero 2025

Cover page designed by Adrián Sanz Berbegal (LLAR digital)

To my family

Dr. Víctor Mangas Sanjuán, Profesor Titular del Departamento de Farmacia y Tecnología Farmacéutica y Parasitología de la Universidad de Valencia, Dra. Mónica Climente Martí, Jefa del Servicio de Farmacia del Hospital Universitario Dr. Peset de Valencia, Doctora en Farmacia y Profesora Asociada del Departamento de Farmacia y Tecnología Farmacéutica y Parasitología de la Universidad de Valencia, Dra. Elena Gras Colomer, Directora General de Farmacia de la Conselleria de Sanidad de la Generalitat Valenciana, Doctora en Farmacia, por igual en condición de directores, y Dra. Matilde Merino Sanjuán, Catedrática del Departamento de Farmacia y Tecnología Farmacéutica y Parasitología de la Universidad de Valencia, en condición de tutora,

CERTIFICAN

Que la Memoria realizada por Dña. Karine Elena Rodríguez Fernández para optar al grado de Doctor titulada:

Pharmacometrics model-informed strategies for improving the pharmacokinetic/pharmacodynamic properties and clinical decision-making processes of drugs

se ha desarrollado bajo su dirección y supervisión, y reúne todos los requisitos necesarios para su juicio y calificación.

El que subscriben en Burjassot a 4 de febrero de 2025.

Fdo. Víctor Mangas Sanjuán

MANGAS SANJUAN VICTOR - 48575410P

Firmado digitalmente por MANGAS SANJUAN VICTOR - 48575410P
Fecha: 2025.02.04 15:41:31 +01'00'

Fdo. Mónica Climente Martí

MONICA| CLIMENTE| MARTI

Firmado digitalmente por MONICA| CLIMENTE|MARTI
Fecha: 2025.02.05 10:29:01 +01'00'

Fdo. Elena Gras Colomer

Firmat per Elena Gras Colomer, el 04/02/2025 11:55:46
Càrrec: Directora General de Farmacia

Fdo. Matilde Merino Sanjuán

MARIA MATILDE| MERINO| SANJUAN

Firmado digitalmente por MARIA MATILDE|MERINO| SANJUAN
Fecha: 2025.02.04 14:10:19 +01'00'

Table of Contents

Acknowledgments

Todo comenzó una calurosa tarde en el Malecón de La Habana acompañados de la brisa marina y de colegas maravillosos. Allí, junto al Dr. Víctor Mangas inicié mi camino hacia el doctorado que después de mucha dedicación, tiempo y esfuerzo acaba con la realización de esta Tesis doctoral. Gracias a la colaboración y apoyo de las personas que se mencionan a continuación ha sido posible transitar este camino.

Quisiera agradecer al Dr. Víctor Mangas por su entrega incondicional en cada proyecto, por confiar en mi cuando ni yo misma lo hacía y por su persistencia infatigable, de la cual espero haberme contagiado un poco. Gracias por mi maestro y a la vez amigo. Todos necesitamos un Víctor en la vida para crear nuestra mejor versión.

A mi tutora Dra. Matilde Merino (Mati), gracias por siempre estar, por acogerme como parte de vuestro equipo, y por compartir tantos conocimientos y experiencias.

A mis directoras de Tesis Dras. Mónica Climente y Elena Gras, y a la Dra. Marina Saez. Gracias por vuestros consejos y guía en el trabajo de día a día. Os admiro muchísimo.

Por la gran disposición y compromiso con el proyecto de psoriasis agradezco a los dermatólogos Dra. Almudena Mateu y Dr. Antonio Martorell. Al personal de los servicios de Farmacia y Dermatología de los hospitales Doctor Peset y de Manises gracias por vuestra ayuda. Gracias de todo corazón al servicio de Dermatología del Peset, por hacerme sentir tan arropada mientras estuve en el hospital.

A los pacientes con psoriasis que aceptaron participar en el estudio, gracias por su disponibilidad y generosidad.

Agradezco enormemente al Dr. Jorge Duconge de la Universidad de Puerto Rico (EE. UU.), por la oportunidad de trabajar con el proyecto de warfarina.

My gratitude to Dr. Jose David Gomez Mantilla and Dr. Sheila Peters for the 180-degree-turn opportunity in my professional career during my internship in BI. Thanks to you and the rest of BI colleagues not only for sharing with me some of your wide-ranging expertise in PBPK modeling but also for making me feel like one more among you.

A mis compañeros de grupo *UVmetriX,* Javi Reig, Javi Zarzoso, Kike, Aymara, Marina y Cristian. Gracias por los momentos compartidos y

por vuestra invaluable contribución en los proyectos de esta Tesis doctoral.

Gracias a mi familia por animarme en todo momento, en especial a mi madre por inculcarme la disciplina y la fuerza de voluntad que me han permitido llegar hasta aquí. A mi hermana por entenderme como nadie y por ser mi soporte incondicional. Gracias a ti y a mi cuñado por estar siempre pendientes. A mis bendiciones por tantas alegrías. Gracias Tati por tu ayuda y afecto desde siempre y durante estos años de doctorado. A David, gracias por estar always and forever y por ayudarme a hacer realidad mis sueños. Mi especial agradecimiento a la familia que con tanto cariño me ha acogido aquí, en especial a Enrique. Gracias por no rendirte nunca, por tu apoyo y por el amor que me has dado estos últimos años, han sido el impulso que necesitaba para acabar mi doctorado.

A mis amigos cuyas historias de lucha y superación al emigrar son un ejemplo para mí. Gracias por las llamadas tan poco frecuentes, pero que nos alimentan el alma.

Quisiera agradecer también a mis profesoras y amigas Dras. Leyanis Rodriguez y Gledys Reynaldo, presentes siempre en cada proyecto de mi vida profesional y personal. Leyi que con su visión de futuro impulsó el desarrollo de la famacometría en Cuba y nos enseñó el camino para llevar nuestras carreras hacia lo más alto. Gledys las palabras que busco no existen, pues mi agradecimiento y sentimientos hacia ti no tienen comparación. Eres uno de esos ángeles que habitan la tierra que el UNIVERSO pone en nuestro camino para cambiarnos la vida. No hay lección que no me hayas dado. Por siempre serás mi "tutora integral".

¡A todos muchas gracias!

List of publications

The following articles provided the fundamentals for the current Thesis:

1. **Pharmacometric characterization of entero-hepatic circulation processes of orally administered formulations of amiodarone under complex binding kinetics**.
   K. Rodríguez-Fernández, E. Gras-Colomer, M. Climente-Martí, V. Mangas-Sanjuán, M. Merino-Sanjuán
   Eur J Pharm Sci. 2022 Jul 1; 174:106198
   Journal statistics: IF 4.3, Q1 (Pharmacology & Pharmacy)
2. **New insights into the role of VKORC1 polymorphisms for optimal warfarin dose selection in Caribbean Hispanic patients through an external validation of a population PK/PD model.**
   K. Rodríguez-Fernández, G. Reynaldo-Fernández, S. Reyes-González, C. de las Barreras, L. Rodríguez-Vera, C. Vlaar, J-C M. Monbaliu, T. Stelzer, J. Duconge, V. Mangas-Sanjuán
   Biomed Pharmacother. 2024 Jan;170:115977
   Journal statistics: IF 6.9, Q1 (Pharmacology & Pharmacy)
3. **Model-Informed Precision Dosing for Personalized Ustekinumab Treatment in Plaque Psoriasis.**
   K. Rodríguez-Fernández, J. Zarzoso-Foj, M. Saez-Bello, A. Mateu-Puchades, A. Martorell-Calatayud, M. Merino-Sanjuán, E. Gras-Colomer, M. Climente-Martí and V. Mangas-Sanjuán
   Pharmaceutics. 2024 Oct 4;16(10):1295
   Journal statistics: IF 4.9, Q1 (Pharmacology & Pharmacy)
4. **Personalized Secukinumab Treatment in Patients with Plaque Psoriasis Using Model-Informed Precision Dosing.**
   K. Rodríguez-Fernández, J. Zarzoso-Foj, M. Saez-Bello, A. Mateu-Puchades, A. Martorell-Calatayud, M. Merino-Sanjuán, E. Gras-Colomer, M. Climente-Martí and V. Mangas-Sanjuán
   Pharmaceutics. 2024 Dec 10;16(12):1576.
   Journal statistics: IF 4.9, Q1 (Pharmacology & Pharmacy)
5. **Evaluation of solubility-limited absorption as a surrogate to predicting positive food effect of BCS II/IV drugs.**
   K. Rodriguez-Fernandez, J-D Gómez-Mantilla, S. Shukla, P. Stopfer, P. Sieger, V. Mangas-Sanjuán and S-A. Peters.
   Clin Pharmacokinet. 2025 Feb 3. Epub ahead of print.
   Journal statistics: IF 4.6, Q1 (Pharmacology & Pharmacy)

List of abbreviations

-2LL:	-2xlog likelihood
AM:	Amiodarone
AUC:	Area under the curve
BCS:	Biopharmaceutical classification system
CI:	Confidence intervals
CL:	Clearance
C_{max}:	Maximum concentration
CYP2C9:	Cytochrome P4502C9 gene
CYP3A:	Cytochrome P450 3A
DV:	Dependent variable
EHR:	Entero-hepatic reabsorption
FaSSIF:	Fasted state simulated intestinal fluid
FaSSIF/D:	Dose-adjusted FaSSIF solubility
FE:	Food effect
GOF:	Goodness of fit
IC_{50}:	Concentration of the drug needed to inhibit 50% of the response
IIV:	Interindividual variability
IL:	Interleukin
I_{max}:	Maximum inhibition drug effect
INR:	International normalized ratio
IV:	Intravenous
IVIV:	*in vitro - in vivo*
k_a:	First-order absorption rate constant
mAb:	Monoclonal antibody
MCMC:	Markov Chain Monte Carlo
MIPD:	Model-informed precision dosing
NLME:	Nonlinear mixed effects
NPDE:	Normalized prediction distribution errors
OFV:	Objective function's minimum value
OR:	Oral
PASI:	Psoriasis Area and Severity Index
PBPK:	Physiologically based pharmacokinetic
pc-VPC:	Prediction-corrected visual predictive check
PD:	Pharmacodynamic

PK:	Pharmacokinetic
PK/PD:	Pharmacokinetic/pharmacodynamic
PMx:	Pharmacometrics
PRED:	Population prediction
RSE:	Relative standard error
RUV:	Residual unexplained variability
SCK:	Secukinumab
SLA:	Solubility-limited absorption
SmPC:	Summary of product characteristics
SR:	Sensitivity range
TDM:	Therapeutic drug monitoring
UTK:	Ustekinumab
V_d:	Central volume of distribution
***VKORC1*:**	Vitamin K epoxide reductase complex subunit 1 gene

Síntesis

Síntesis

Introducción

La disciplina farmacometría representa una convergencia entre múltiples campos desarrollada con la finalidad de estudiar el comportamiento de los fármacos y optimizar los efectos terapéuticos. Se define como "la ciencia de desarrollar y aplicar métodos matemáticos y estadísticos para caracterizar, comprender y predecir el comportamiento farmacocinético, farmacodinámico y resultante de biomarcadores de un fármaco", los cuales permiten estudiar los efectos de los medicamentos y la variabilidad en la exposición y respuesta a los mismos. Tradicionalmente, el desarrollo de fármacos ha sido un proceso de baja precisión y no muy eficiente. Sin embargo, la expansión de la farmacometría a finales del siglo XX y la aparición del paradigma de descubrimiento y desarrollo de fármacos basados en modelos (del inglés *Model-Informed Drug Discovery and Development*), ha permitido la incorporación de metodologías basadas en modelos y simulaciones con el fin de aumentar la eficiencia en el desarrollo de fármacos, al minimizar la necesidad de abordar cada cuestión de forma experimental e iterativa.

En las agencias reguladoras, como la de EE. UU. (*United States Food and Drug Administration*, FDA) y la europea (*European Medicines Agency,* EMA), la farmacometría desempeña un papel primordial al respaldar la toma de decisiones basada en datos durante los procesos de aprobación de medicamentos. Más allá del desarrollo de fármacos, la farmacometría resulta de utilidad también en la práctica clínica. Utilizando técnicas de modelado y simulación los datos de los ensayos clínicos pueden combinarse con los obtenidos en práctica clínica habitual, para analizar el comportamiento del fármaco en estos contextos más amplios y adaptar la farmacoterapia a las necesidades clínicas del paciente en función de factores ambientales, de estilo de vida e internos pertinentes. Con el fin de optimizar e individualizar las posologías de moléculas de síntesis y fármacos biológicos se ha utilizan la monitorización terapéutica de fármacos y, más recientemente, la dosificación de precisión informada por modelos (del inglés *model-informed precision dosing* [MIPD]), ambos procedimientos basados en programas informáticos donde ha sido implementada la predicción bayesiana.

Dentro de la farmacometría se engloban una amplia gama de metodologías que, en orden creciente de complejidad, se conocen como modelos empíricos, semimecanicistas y mecanicistas. Los

modelos empíricos llevan a cabo las correlaciones entre la exposición y el efecto del fármaco sin tener en cuenta los fundamentos mecanicistas causales. Estos modelos se desarrollan utilizando el enfoque "top-down", que se basa en los datos clínicos disponibles. Este tipo de modelos son únicamente predictivos en escenarios que han sido apropiadamente descritos a través de los datos utilizados para generar el modelo. Por lo tanto, su capacidad para extrapolar más allá de estos casos es muy limitada. Los modelos mecanicistas representados por los modelos farmacocinéticos fisiológicos caracterizan detalladamente los procesos fisiológicos de un organismo vivo, y su estructura se corresponden con los tejidos y órganos que lo constituyen, todos ellos conectados por los flujos sanguíneos del sistema cardiovascular. Esta metodología se basa en el enfoque "bottom-up", con multitud de extrapolaciones *in vitro-in vivo*. La principal ventaja de los modelos farmacocinéticos fisiológicos, cuando se comparan con los modelos empíricos, es que ofrecen una gran capacidad para llevar a cabo la extrapolación en situaciones complejas como las interacciones entre fármacos o el deterioro de órganos, así como desde voluntarios adultos sanos hasta poblaciones especiales como niños u obesos. Al integrar los cambios en la fisiología y las propiedades relacionadas con los principios activos, los modelos farmacocinéticos fisiológicos se pueden utilizar para simular la farmacocinética de un compuesto en condiciones de alimentación o ayuno, al tiempo que integran las propiedades del fármaco como la solubilidad o la permeabilidad, entre otras. Como resultado, los modelos farmacocinéticos fisiológicos pueden emplearse para evaluar los efectos de la ingesta de alimentos en la absorción de fármacos, mayormente de clase II y IV según el sistema de clasificación biofarmacéutica. La finalidad de utilizar estos modelos es la de identificar la necesidad y el momento adecuado para llevar a cabo un ensayo clínico pivotal que determine los efectos de los alimentos sobre los fármacos, lo que representa un gran ahorro de tiempo y recursos para la industria farmacéutica. No obstante, cuando el modelo se torna más complejo, tal como sucede en los modelos farmacocinéticos fisiológicos, siempre existen retos en el momento de seleccionar el más adecuado. Por lo tanto, el desarrollo de modelos semimecanicistas, con la aproximación "middle-out", proporciona un balance entre los enfoques empíricos y mecanicistas. Por su menor complejidad, se consiguen tiempos de ejecución de programas informáticos más breves para los modelos semimecanicistas. Estos modelos han demostrado su utilidad en casos de resistencia a los antimicrobianos y en la detección de las características farmacocinéticas y farmacodinámicas de los medicamentos antibacterianos. También

resultan beneficiosos para evaluar efectos adversos en otras áreas terapéuticas como la oncología y la reumatología, siendo capaces de describir la mielosupresión causada por la quimioterapia y la inducción de la cascada hematopoyética.

Los modelos no lineales de efectos mixtos basados en el análisis poblacional, se consideran el estándar de excelencia para la estimación de parámetros farmacocinéticos y farmacodinámicos. El objetivo de los modelos no lineales de efectos mixtos es determinar simultáneamente los efectos fijos, los cuales representan la tendencia típica de la población, y los efectos aleatorios, que incorporan la variabilidad individual asociada a estos parámetros y a las concentraciones experimentales. En el análisis poblacional se pueden estimar parámetros mediante diseños de muestreo intensivos o dispersos, o mediante la fusión de ambos. Otra fortaleza del modelado no lineal de efectos mixtos es que permite cuantificar la incertidumbre asociada tanto a los parámetros farmacocinéticos / farmacodinámicos poblacionales como a los parámetros individuales. La incertidumbre representa el nivel de confianza o precisión relacionado con la estimación de los parámetros. El proceso de seleccionar y evaluar un modelo farmacocinético/farmacodinámico poblacional que logre describir todos los datos, puede ser complejo. El resultado que se espera de un análisis poblacional es establecer el modelo más sencillo (*lex parsimoniae* o principio de parsimonia) que describa de manera aceptable tanto los perfiles individuales del fármaco como la tendencia en la población, y que, además, sea clínicamente verosímil e interpretable. Para refinar los modelos farmacocinéticos / farmacodinámicos poblacionales se emplean diversas estrategias, que abarcan tanto estimaciones numéricas, evaluaciones gráficas y ejercicios de simulación. En ningún caso, una técnica en sí misma es definitiva y, por lo tanto, solo la combinación de los resultados logrados a través del uso de múltiples estrategias ofrece una perspectiva global sobre la fiabilidad del ajustado y, en consecuencia, facilita el proceso de selección y evaluación de modelos. Los métodos diagnósticos más utilizados son la comparación de modelos anidados mediante la prueba de razón logarítmica de verosimilitud, las gráficas de bondad de ajuste y el procedimiento de exploración predictiva visual. Una de las principales características de los modelos no lineales de efectos mixtos es que permiten realizar simulaciones deterministas y / o estocásticas de datos no observados con fines de inferencia. La simulación determinista es un método de simulación que omite el paso de estimación y donde se asigna valor de cero a los efectos aleatorios. Esto

simula el individuo típico de la población. La simulación estocástica, crea datos seleccionando aleatoriamente distribuciones de probabilidad indicativas de los efectos aleatorios.

Los beneficios que ofrece la farmacometría se presentan en todas las etapas del desarrollo de medicamentos, desde los estudios preclínicos hasta la farmacovigilancia después de su comercialización. Tanto la farmacocinética como la farmacodinámica del fármaco, así como los objetivos clínicos y los desafíos a resolver influyen en la selección del enfoque farmacométrico más adecuado para cada análisis. Los modelos PBPK son fundamentales en fases preclínicas, ya que ayudan a determinar dosis y esquemas de administración seguros y efectivos, además de identificar las moléculas más prometedoras. A través de simulaciones, estos modelos facilitan la traducción de datos *in vitro* y de estudios en animales hacia aplicaciones en humanos Durante las siguientes etapas del desarrollo, la farmacometría se utiliza principalmente para desarrollar modelos farmacocinéticos / farmacodinámicos poblacionales y de progresión de enfermedades. Caracterizar la relación entre la exposición al fármaco y la respuesta, tanto beneficiosa (eficacia) como adversa (seguridad) es crucial durante las fases 1 y 2. Asimismo, los estudios en estas etapas buscan identificar y cuantificar la variabilidad individual en la exposición y la respuesta, lo que se logra analizando las covariables que influyen en los parámetros específicos del sistema. En las etapas finales, la farmacometría permite perfeccionar modelos farmacocinéticos y farmacodinámicos para optimizar las dosis, integrando datos escasos provenientes de ensayos clínicos con información recopilada en previas etapas de desarrollo. Además, la determinación de los parámetros individuales puede contribuir a explicar toxicidades o fallos terapéuticos, mejorando así los resultados del tratamiento.

En casos de medicamentos ampliamente utilizados en la práctica clínica y con una larga trayectoria en el mercado, la farmacometría aplicada en los estudios postcomercialización ha demostrado gran utilidad a pesar de que su uso estuviera limitado durante las fases iniciales de desarrollo e investigación. La incorporación de modelos farmacométricos y las posteriores simulaciones en la dosificación de precisión ha consolidado la dosificación de precisión informada por modelos como un paradigma novedoso para respaldar la toma de decisiones clínicas para la individualización de la dosis. La dosificación de precisión informada por modelos combina el uso de varios enfoques de modelado en el contexto concreto del paciente y su enfermedad con el objetivo de orientar la optimización de posologías efectivas, seguras y eficientes. La

dosificación de precisión informada por modelos permite reducir la variabilidad en la respuesta a los medicamentos, tanto en condiciones ideales (ensayos clínicos) como en situaciones de práctica clínica habitual. Este enfoque vincula el conocimiento adquirido durante el desarrollo del medicamento y la optimización de posologías en grupos de poblaciones específicos. Su implementación ha sido especialmente destacada en antibioticoterapia, inmunosupresión y onco-hematología. A pesar de los avances y el gran potencial de la dosificación de precisión informada por modelos, su implementación en la atención sanitaria aún requiere un esfuerzo conjunto entre profesionales sanitarios, académicos, reguladores, pacientes y otros actores relevantes para generar evidencia sólida y promover su integración sistemática en el sistema de salud.

Hipótesis y Objetivos

La utilización de tratamientos personalizados, seguros, efectivos y eficientes para el tratamiento de diferentes patologías representa un desafío considerable, y los métodos tradicionales han demostrado ser insuficientes para abordar esta necesidad. El empleo de la farmacometría representa una solución innovadora, ya que esta disciplina ofrece una herramienta predictiva que ayuda a analizar el comportamiento de los medicamentos en distintas poblaciones y entornos clínicos, promoviendo el desarrollo de ensayos clínicos más efectivos, impulsando la medicina personalizada y asegurando el cumplimiento de los estándares regulatorios. En esencia, la farmacometría influye significativamente en la mejora de las propiedades farmacocinéticas / farmacodinámicas y los procesos de toma de decisiones clínicas de los medicamentos, permitiendo un tratamiento óptimo de los pacientes, logrando los objetivos terapéuticos y obteniendo así mejores resultados en materia de atención sanitaria.

Por todo lo anteriormente expuesto, **objetivo general** de esta Tesis doctoral es:

Desarrollar, validar e implementar estrategias guiadas por farmacometría para optimizar los procesos de investigación, desarrollo y toma de decisiones clínicas de medicamentos.

Los **objetivos específicos** son:

1. Explorar un enfoque novedoso para predecir el efecto de los alimentos positivo en los fármacos de clase II/IV del sistema

de clasificación biofarmacéutica, utilizando un modelo farmacocinético fisiológico simplificado, reconociendo la solubilidad limitada en la absorción como el único impulsor del efecto de los alimentos positivo en los fármacos de clase II/IV.
2. Caracterizar las propiedades de absorción de diferentes formulaciones de amiodarona administradas por vía oral en ratas para optimizar el desarrollo de nuevas formulaciones orales.
3. Evaluar las estrategias óptimas de dosificación de warfarina en pacientes hispanos del Caribe basados en un modelo farmacocinético / farmacodinámico poblacional de warfarina en la práctica clínica.
4. Proponer una estrategia de individualización posológica de ustekinumab y secukinumab en pacientes con psoriasis en placas crónica de moderada a grave a partir de la incertidumbre de los parámetros individuales de un modelo farmacocinético / farmacodinámico poblacional.

Resultados y Discusión

Parte 1: Predicción in silico de los Efectos de los Alimentos

En esta parte se resumen los principales resultados referentes al objetivo específico 1.

Los alimentos pueden alterar significativamente la farmacocinética de los fármacos administrados por vía oral al modificar la velocidad y el grado de absorción del fármaco, lo que repercute tanto en su eficacia terapéutica como en su seguridad. Los modelos farmacocinéticos fisiológicos se utilizan cada vez más para predecir el efecto de los alimentos, pero la parametrización de estos modelos se ve comprometida por las desconexiones *in vitro-in vivo* y / o problemas de identificación de parámetros. Para superar estas dificultades, se ha propuesto un método novedoso capaz de establecer un marco cuantitativo para la predicción temprana del efecto de los alimentos mediante la estimación de un rango de sensibilidad de valores obtenidos a partir de la interacción de la solubilidad del fármaco en un medio biorrelevante de fluido intestinal simulado en estado de ayuno (FaSSIF por sus siglas en inglés) y de la dosis de cada fármaco (FaSSIF/D). La predicción del efecto de los alimentos se realizó de manera conservativa y no conservativa. La predicción conservativa se ejecutó para 26 fármacos a los cuales se les determinó la solubilidad FaSSIF en el laboratorio de la empresa farmacéutica Boehringer

Ingelheim. Como resultado se obtuvieron valores de FaSSIF/D conservativos donde los compuestos con FaSSIF/D inferiores a $3x10^{-5}$ 1/ml, es probable que presenten efecto de los alimentos positivo. Si FaSSIF/D es mayor que $1x10^{-3}$ 1/ml, es probable que no presenten efecto de los alimentos. Si el valor de FaSSIF/D se encuentra entre $3x10^{-5}$ y $1x10^{-3}$ 1/ml, la determinación de la absorción limitada por solubilidad con simulaciones a partir de modelos farmacocinéticos fisiológicos simplificados puede ayudar a predecir si es probable que el fármaco tenga o no efecto de los alimentos, siempre y cuando la tasa de extracción intestinal del fármaco sea baja. La predicción no conservativa se efectuó tras la inclusión de valores de FaSSIF/D de 25 compuestos adicionales con datos de solubilidad FaSSIF reportados en la literatura. Estos valores se derivan de determinaciones en diferentes laboratorios y sus condiciones experimentales son desconocidas, por lo que se considera como una predicción no conservativa. Los límites del rango de sensibilidad no conservativo son comparables a los límites obtenidos utilizando el método conservativo. Con este estudio se demostró que FaSSIF/D puede discriminar entre fármacos con o sin efecto de los alimentos, siempre y cuando los fármacos estén fuera del rango de sensibilidad.

Para la determinación de la absorción limitada por solubilidad, se llevaron a cabo simulaciones con modelos farmacocinéticos fisiológicos utilizando valores de solubilidad máxima, los cuales eran mayores que los valores de solubilidad optimizados (o determinados experimentalmente, según el compuesto). Como para este trabajo se utilizó la plataforma PK-Sim®, de los 20 compuestos dentro del rango de sensibilidad, solo 6 tenían un modelo farmacocinético fisiológico disponible en dicha plataforma. Si el perfil cinético simulado con la solubilidad máxima es distintito al obtenido con la solubilidad optimizada, la solubilidad *in vivo* del fármaco puede ser aumentada por los alimentos a través de su influencia en uno o más factores (pH gástrico, tasa de vaciamiento gástrico, así como concentraciones de fármaco y sales biliares). Este fue el caso de los compuestos carbamazepina y efavirenz. Por el contrario, los fármacos digoxina y acido mefenámico presentaron perfiles cinéticos similares, por lo que su absorción no está limitada por la solubilidad y pueden ser candidatos para no tener efecto de los alimentos.

Este método no es apropiado para compuestos con un metabolismo elevado en el intestino o que son sustratos de transportadores intestinales, como ocurre con felodipino y clopidogrel, que presentan

un elevado aclaramiento y un metabolismo intestinal relevante mediado por la enzima Citocromo P450 3A4. Consecuentemente, la biodisponibilidad de estos fármacos está condicionada por efectos de primer paso más que por su capacidad para solubilizarse. Este fenómeno puede identificarse en modelos farmacocinéticos fisiológicos cuando la concentración máxima simulada supera a la concentración máxima observada, ya que es improbable que la solubilidad en el medio FaSSIF sea mayor que la solubilidad *in vivo*. Sin embargo, las contribuciones individuales de la solubilidad y el metabolismo intestinal a la limitación en la absorción del fármaco no pueden diferenciarse, ya que la optimización de la modelo basada en las concentraciones plasmáticas observadas del fármaco solo puede resolver la incertidumbre en un parámetro a la vez. En el caso de fármacos afectados por metabolismo intestinal, este fenómeno genera un enmascaramiento que lleva a estimaciones conservadoras del impacto de los alimentos, siempre que sea posible aplicar el enfoque propuesto. Sin embargo, lograr una predicción cuantitativa fiable del metabolismo intestinal es todo un desafío, incluso para sustratos de Citocromo P450 3A4. Afortunadamente, la mayoría de los fármacos con alto aclaramiento suelen identificarse durante las etapas iniciales de optimización, y los medicamentos con bajo aclaramiento no suelen verse afectados por el metabolismo intestinal. Por ello, se espera que la proporción de fármacos para los cuales no se puede predecir con precisión el efecto de los alimentos mediante este método sea baja.

La dificultad para verificar los mecanismos subyacentes en la disolución, la precipitación y la solubilización, incluidos en los modelos farmacocinéticos fisiológicos, resulta en un modelo con muchas suposiciones que pueden ajustarse a los datos observados, pero no pueden predecir de manera confiable un escenario no probado (por ejemplo, efecto de los alimentos). Con este estudio se propone un marco básico para evaluar la predicción del efecto de los alimentos basado en un modelo fisiológico simplificado, donde la absorción limitada por solubilidad es el sustituto del efecto de los alimentos. Esto permite que el único parámetro que afecta al efecto de los alimentos (solubilidad) se optimice frente a los datos observados para los fármacos que no se metabolizan ampliamente en el intestino, lo que da lugar a una predicción del efecto de los alimentos más fiable. La ampliación de este trabajo en el futuro para cubrir todos los compuestos dentro del rango de sensibilidad valdrá para aumentar la confianza en el uso de la absorción limitada por solubilidad para

identificar fármacos que probablemente exhiban un efecto de los alimentos positivo.

Parte 2: Caracterización Preclínica de los Procesos Circulatorios Enterohepáticos de la Amiodarona

En este apartado se sintetizan los resultados más relevantes vinculados al objetivo específico 2.

Amiodarona es un fármaco lipofílico utilizado principalmente para tratar arritmias supraventriculares, sin embargo, su empleo presenta ciertas limitaciones. Su estrecho margen terapéutico supone un alto riesgo de toxicidad, especialmente durante la administración crónica. Además, la absorción oral de amiodarona es baja y variable, lo que genera una marcada variabilidad interindividual en los niveles plasmáticos. Otro desafío asociado es que la formulación intravenosa autorizada, debido a su contenido de alcohol bencílico, no se recomienda para neonatos ni para niños menores de tres años. En este contexto, comprender la farmacocinética de amiodarona es crucial para ajustar las dosis de manera efectiva y minimizar la variabilidad en la respuesta. También es necesario desarrollar formulaciones orales que mejoren la biodisponibilidad del medicamento. Dado que amiodarona presenta una farmacocinética compleja, los modelos predictivos pueden no ser precisos si no consideran adecuadamente todos estos procesos.

El estudio incluyó 96 ratas macho de la cepa Wistar, de 20 semanas de edad, con un peso corporal entre 250 y 320 g, de los cuales se registraron 985 observaciones de amiodarona. Se analizaron las vías de administración intravenosa y oral, utilizando dosis que oscilaron entre 10 y 25 mg, en esquemas de dosificación única y múltiple. La formulación intravenosa empleada fue la presentación comercial de clorhidrato de amiodarona (Trangorex®, 50 mg/ml). Para la administración oral, se evaluaron tres formulaciones: la solución inyectable intravenosa (Trangorex®, denominada Solución I, 50 mg/ml), una suspensión preparada a partir de comprimidos de Trangorex® (denominada Tableta, 200 mg) y una solución en Polisorbato 80 al 5% (denominada Solución II, 5 mg/ml).

Un modelo farmacocinético poblacional previamente desarrollado, que consideraba los procesos de distribución lineales y no lineales de amiodarona tras su administración intravenosa, fue ajustado para analizar los datos disponibles. Este modelo permitió caracterizar los procesos de absorción y reabsorción enterohepática asociados a las tres

formulaciones orales. La reabsorción enterohepática refleja el movimiento de amiodarona libre desde el compartimento central hacia la bilis y posteriormente hacia la luz intestinal, según la evidencia recopilada en los grupos experimentales. El modelo farmacocinético poblacional estimó que el 12,3% de amiodarona experimenta reabsorción enterohepática, mientras que otra fracción se metaboliza. Este hallazgo subraya la importancia de la reabsorción enterohepática en la disposición de amiodarona. Se observaron estimaciones de parámetros finales similares entre el modelo farmacocinético de referencia y el modelo desarrollado en esta investigación.

El modelo farmacocinético poblacional final asume diferentes constantes de velocidad de absorción de primer orden para cada formulación (k_{a1} = 1,33 • 10^{-1} h^{-1}, k_{a2} = 8,20 • 10^{-2} h^{-1} y k_{a3} = 2,05 • 10^{-1} h^{-1}), demostrando que la k_a de las Solución II y I aumentaron 2,5 y 1,62 veces respectivamente, en comparación con la formulación Tableta. Además, la biodisponibilidad en Tableta, Solución I y Solución II fue de 37%, 40% y 50%, respectivamente. Los resultados globales demuestran la contribución de las concentraciones supramicelares de surfactante (polisorbato 80) en la mejora de la absorción oral de amiodarona. Los resultados del análisis realizado basado en simulación de fracciones no unidas / unidas de amiodarona, sugiere que es poco probable que las nuevas formulaciones propuestas para mejorar la biodisponibilidad alteren significativamente las fracciones de amiodarona libre en el plasma o el tiempo necesario para lograr el equilibrio entre las fracciones libres y unidas.

Parte 3: Dosificación de Precisión para Seleccionar Pautas Óptimas de Dosificación

A continuación, se responde a los objetivos específicos 3 y 4.

Rango de Dosis de Warfarina en Pacientes Hispanos del Caribe

Warfarina, un anticoagulante oral utilizado durante décadas para prevenir eventos tromboembólicos, plantea varios desafíos en su manejo clínico, entre los que destacan una ventana terapéutica estrecha, un alto riesgo de hemorragia y una marcada variabilidad en la respuesta individual. Se ha estudiado ampliamente el papel de los polimorfismos genéticos en la respuesta a warfarina, con especial atención a los dos genes más relevantes: *CYP2C9* y *VKORC1*. En el caso de la población hispana del Caribe, el tratamiento con warfarina presenta vacíos terapéuticos debido a la ausencia de guías clínicas que consideren el impacto de los diferentes genotipos en el manejo rutinario del índice

internacional normalizado, lo que deriva en respuestas clínicas subóptimas en esta población. Para abordar este contexto, se desarrolló un modelo farmacocinético / farmacodinámico poblacional basado en datos individuales y registros de dosificación recopilados durante 2 años en pacientes hispanos para optimizar en esta población los regímenes de dosificación. El estudio incluyó a 138 pacientes con una edad promedio de 68 años y un peso medio de 83 kg, en quienes se registraron 1033 observaciones del índice internacional normalizado. Las dosis semanales de warfarina oscilaron entre 7 y 82 mg, con intervalos de dosificación de 24 o 48 horas. Se identificaron ocho variantes genéticas de *CYP2C9* (*1/*2, *1/*3, *1/*5, *1/*8, *2/*2, *2/*3, *2/*5) y tres haplotipos *VKORC1* (G/A, G/G, A/A) entre los pacientes incluidos en el estudio.

Las covariables incluidas en el modelo final fueron el peso corporal en el volumen de distribución y *CYP2C9* en el aclaramiento. Además, los polimorfismos de *VKORC1* se incluyen como una covariable estadísticamente significativa en los valores de índice internacional normalizado basales y la concentración que produce el 50 % del efecto máximo para los parámetros farmacodinámicos. Un hallazgo importante del estudio fue que los valores de concentración que produce el 50 % del efecto máximo obtenidos para cada uno de los haplotipos *VKORC1*, fueron superiores a los reportados previamente en otras poblaciones lo que sugiere una mayor resistencia a la warfarina. Esto implica que los pacientes hispanos del Caribe podrían necesitar regímenes de dosificación más intensivos para alcanzar los niveles terapéuticos de índice internacional normalizado deseados. Además, los análisis de los valores basales de índice internacional normalizado en diferentes haplotipos de *VKORC1*, mostraron niveles más elevados en portadores del haplotipo A/A en comparación con los pacientes con haplotipos que contenían el alelo G. Este fenómeno podría explicarse por tiempos de protrombina más largos y niveles más bajos de factores de coagulación funcionales en los portadores del alelo A, debido a una menor expresión de la enzima hepática *VKORC1,* que desempeña un papel fundamental en el ciclo de la vitamina K en el hígado.

Por último, se realizó un análisis de dosificación de precisión informada por modelos para determinar las pautas de dosificación óptimas mediante simulaciones que evaluaron la probabilidad de alcanzar niveles terapéuticos de respuesta subpoblaciones obtenidas por combinaciones de *CYP2C9* y *VKORC1*. Los resultados indicaron que

dosis diarias de warfarina entre 3 y 5 mg serían suficientes para alcanzar niveles terapéuticos en la mayoría de los casos, mientras que el subgrupo de pacientes con *2/* 2-, * 2/* 3- y *2/*5-A/A requieren 1 mg diario de warfarina para lograr la respuesta terapéutica. Con este enfoque se logra reducir el riesgo de eventos adversos asociados a dosificaciones inadecuadas de warfarina y mejorar los resultados terapéuticos.

Tratamiento Individualizado con Ustekinumab y Secukinumab en Pacientes con Psoriasis

La psoriasis es una enfermedad inflamatoria crónica donde se produces lesiones escamosas y engrosadas en la piel. El desarrollo de la enfermedad esta mediado por procesos como la sobreproducción de interleucinas (IL) proinflamatorias como IL-12, IL-23 e IL-17A. Estas pueden ser inhibidas por anticuerpos monoclonales como ustekinumab y secukinumab. La herramienta más ampliamente utilizada para la medida de la severidad de psoriasis y de la efectividad del tratamiento es el índice de la severidad del área de psoriasis (PASI por sus siglas en inglés).

En este proyecto se realizó un estudio de clínico postautorización, prospectivo, multicéntrico y observacional en pacientes con psoriasis en placas moderada a grave, en tratamiento con ustekinumab y secukinumab. Se incluyeron 23 pacientes tratados con ustekinumab (edad media: 62 años, peso medio: 92 kg) y 117 medidas de efectividad del tratamiento (PASI) y 75 muestras de plasma. En cuanto a la investigación de secukinumab se incluyeron un total de 22 pacientes (edad media: 50 años, peso medio: 74,5 kg), con 85 muestras de plasma y 106 medidas de PASI.

Modelos Farmacocinéticos/Farmacodinámicos Poblacionales

La relación entre la concentración de ustekinumab y las observaciones de PASI se describió utilizando la misma estructura del modelo de referencia de respuesta indirecta, donde ustekinumab inhibió la constante de progresión de orden cero de la lesión cutánea psoriásica a través de un modelo de efecto de fármaco de inhibición máxima. Este modelo también fue seleccionado para describir la relación entre la concentración de secukinumab y el PASI. Para explicar el retraso entre la administración de secukinumab y los efectos observables, se añadió una cadena adicional de 4 compartimentos prePASI, donde cada uno representa un paso en la progresión de la enfermedad. Para secukinumab se incorporó también un mecanismo de tolerancia para

explicar el aumento temporal del PASI. En ambos casos se estimó la constante de remisión de primer orden de la lesión cutánea psoriásica y los niveles basales de PASI. Debido a dificultades durante los procesos de minimización y convergencia, las concentraciones de los fármacos necesarios para inhibir el 50% de la respuesta no pudieron ser estimadas, por lo que se fijaron a los valores publicados (0,07 y 9,35 mg/L para ustekinumab y secukinumab, respectivamente).

Régimen de Dosificación Personalizado

Se desarrolló un procedimiento capaz de individualizar las estrategias de dosificación de ustekinumab y secukinumab en la práctica clínica a partir de la incertidumbre de las estimaciones de los parámetros individuales de un modelo farmacocinético / farmacodinámico poblacional. Además, la inclusión de la incertidumbre durante el paso de simulación facilitó la evaluación del grado de certeza en las predicciones informadas por modelos en el entorno clínico, proporcionando un marco probabilístico para la dosificación de precisión informada por modelos.

Según las simulaciones el 35% de los pacientes incluidos en tratamiento con ustekinumab requerirían una optimización de la pauta posológica, de entre los que hasta un 22% se propone sea un régimen de dosificación no descrito en ficha técnica. Entre los pacientes tratados con secukinumab se sugirió un cambio a un régimen optimizado para el 50%, proponiéndose que esta optimización sea a una pauta posológica no indicada en la ficha técnica (91%). Estos resultados representan una disminución en la exposición a ambos fármacos, pero manteniendo la misma efectividad, por tanto, se logra una mayor seguridad y eficiencia del tratamiento. Se propuso una intensificación de la pauta posológica respecto a la recibida en la práctica clínica en el 26% de los pacientes tratados con ustekinumab. Para los pacientes tratados con secukinumab se indicó una intensificación en el 14%.

A través del modelado farmacocinético / farmacodinámico, este estudio ilustra la dosificación de precisión a nivel individual utilizando datos clínicos reales, lo que implica un uso más exhaustivo de las estrategias de dosificación de precisión informada por modelos para fomentar la efectividad, la seguridad y la eficiencia de tratamientos de alto impacto clínico y económico, como es el caso de medicamentos como ustekinumab y secukinumab. Las mejoras en la recopilación y evaluación de datos de pacientes reales pueden ayudar en el descubrimiento de nuevos algoritmos de dosificación de precisión y la

mejora de los actuales, lo que permite la extensión y modificación continuas de los planes posológicos para adaptarse mejor a los requisitos únicos de cada paciente. Es por ello que nuestra estrategia de dosificación de precisión informada por modelos a partir de datos clínicos podría ser el primer intento para conseguir una dosificación individual más precisa en pacientes con psoriasis en placas tratados con ustekinumab y secukinumab.

Conclusiones

1. La selección del rango de sensibilidad de la solubilidad ajustada a la dosis en un medio biorrelevante y la identificación de la absorción limitada por la solubilidad mediante el modelo farmacocinético fisiológico permite una predicción fiable del efecto de los alimentos, facilitando la toma de decisiones sobre la necesidad de realizar estudios piloto y el momento de los estudios fundamentales del efecto en los alimentos.

2. El modelo farmacocinético poblacional de amiodarona demostró la contribución de la circulación enterohepática a la disposición general y la mejora de la absorción cuando amiodarona se formula con formulaciones supramicelares de polisorbato 80 (Solución II) en comparación con la formulación orales disponible comercialmente (Tableta). Esto puede contribuir al desarrollo de formulaciones de soluciones de OR adecuadas y alternativas para pacientes con dificultades para tragar que podrían mejorar el balance beneficio / riesgo de la amiodarona.

3. Se propusieron recomendaciones personalizadas y precisas de dosificación de warfarina de 1 y de 3 a 5 mg para guiar la terapia anticoagulante en individuos hispanos del Caribe basadas en la capacidad predictiva del enfoque de modelado farmacocinético / farmacodinámico poblacional.

4. La metodología propuesta para individualizar las estrategias de dosificación de ustekinumab y secukinumab considerando la incertidumbre de los parámetros individuales dentro de un modelo poblacional permite optimizar la probabilidad de lograr resultados clínicos específicos en pacientes con psoriasis en placas crónica de moderada a severa, y representa un paso inicial y poco explorado hacia la realización de dosificación de precisión informada por modelos para productos biológicos

que actúan sobre las vías de interleucina, para aumentar la efectividad, seguridad y eficiencia del tratamiento.

5. En general, las estrategias basadas en modelos farmacométricos implementadas en esta tesis han demostrado su relevancia para caracterizar en el entorno preclínico y clínico las propiedades farmacocinéticas / farmacodinámicas de moléculas de síntesis y fármacos biológicos, con el objetivo de guiar el tratamiento óptimo individualizado para los pacientes y mejorar los resultados en la atención sanitaria.

Introduction

Introduction

Pharmacometrics: Concept and Evolution

Traditionally, the drug development process followed a very linear and time-consuming empirical approach, where a sequence of distinct phases or events was needed to confirm the safety and efficacy of a drug. This process often involved extensive testing which took very little into account prior information, high costs, and the risk of failure at later stages [1,2]. Pharmacometrics (PMx) has emerged to improve decision-making and increase the efficiency of the drug discovery and development process (Figure 1). According to the definition presented by Williams and Ette, PMx is "the science of developing and applying mathematical and statistical methods to characterize, understand, and predict a drug's pharmacokinetic (PK), pharmacodynamic (PD), and biomarker-outcomes behavior". As a schematic representation of the drug-biological system interaction, these models can study the effects of drugs, variability in drug exposure and response, and disease progression [3].

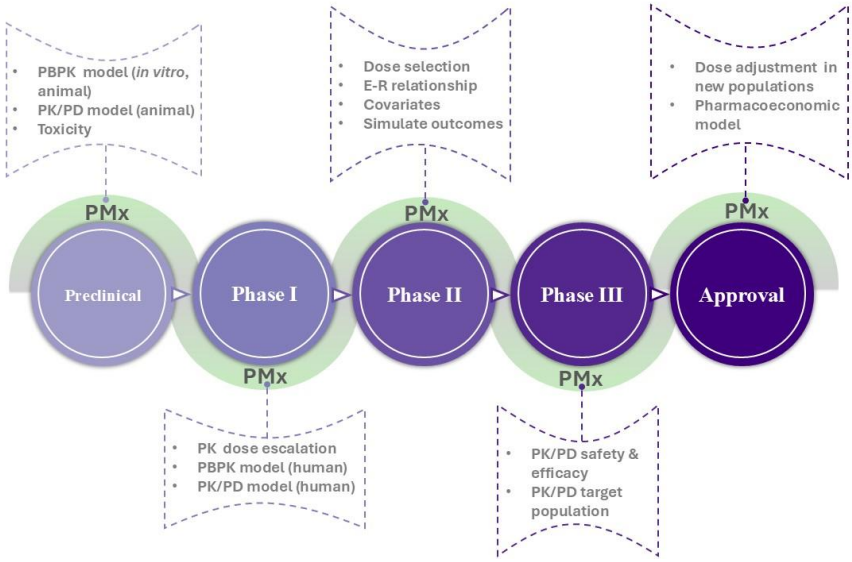

Figure 1. Drug development process guided by PMx. PMx: pharmacometrics; PBPK: physiologically based pharmacokinetic; PK/PD: pharmacokinetic/pharmacodynamic; PK: pharmacokinetic; E-R: exposure-response.

The advent of the Model-Informed Drug Discovery and Development (MID3) paradigm, linked to the learn-confirm technique introduced by

Lewis Sheiner in 1997 Sheiner [4], provided a feasible framework for applying PMx [5]. Thanks to PMx the selected pathway, target, molecule, dose regimen, and patients can be constantly assessed considering the evolving data, which makes possible the integration of the events related to the drug development process. As a result, drug development can lead to faster and less costly procedures as it is conducted utilizing a more rationalizing data-driven decision-making approach that prioritizes comprehension of drug efficacy and safety over efficacy confirmation [1,2,6,7].

Historically, the incorporation of quantitative modeling into regulatory science began to gain traction in the late 20th century as the complexity of drug development increased and the need for more sophisticated analysis methods became apparent [8]. Currently, PMx has become a natural element in most leading regulatory agencies and pharmaceutical companies, allowing agencies to harness quantitative insights for faster, more informed decisions that spotlight patient safety and drug efficacy as much as possible [9,10]. Regulatory agencies, such as the U.S. Food and Drug Administration (FDA) and the European Medicines Agency (EMA), have issued guidances on using PMx to improve general regulatory decision-making, labeling and trial design processes. These guidances give instructions on how to submit physiologically based PK (PBPK) analyses [11,12], population PK analysis results [13,14], and a variety of examples of situations where exposure-response relationships [15] may be useful to give regulatory authorities enough information to evaluate the analysis and conclusions reached.

Following its release onto the market, a drug is administered to a variety of actual patient populations, which frequently diverge greatly from the controlled settings of clinical trials. PMx fills this gap by combining data from clinical trials with real-world evidence and employing modeling and simulation approaches first to examine how the drug behaves in these wider contexts and second for adjusting medication therapy to a patient's needs based on relevant environmental, lifestyle, and inner factors [16]. Traditionally therapeutic drug monitoring (TDM) and more recently model-informed precision dosing (MIPD) are used to support clinical decision-making for dose individualization for small molecules [17] and biologics [18,19]. Individualized dosing through MIPD attempts to modify the dosage schedule by monitoring the drug's concentration in plasma. As a result, the method uses population pharmacokinetic/pharmacodynamic (PK/PD) models generated post-marketing to estimate individual PK/PD parameters as prior knowledge, which is then further refined using a few individual

drug-level measurements [20]. Although the work of Sheiner [21] and Jelliffe [22] first brought in the notion of MIPD in clinical practice more than fifty years ago, the term "MIPD" did not arise until the middle of the 2010s [16]. By including mathematical dosage predictions, considering patient-specific variables (drug measurements, patient characteristics), and contemplating various sources of variability, MIPD goes beyond traditional TDM [20].

Modeling Strategies in Pharmacometrics

PMx encompasses a wide range of sub-areas of quantitative methodologies, as depicted in Figure 2. The quality and extent of accessible data, the stage of drug development, and —above all— the analysis's purpose decide the level of complexity of the model that will be implemented [23].

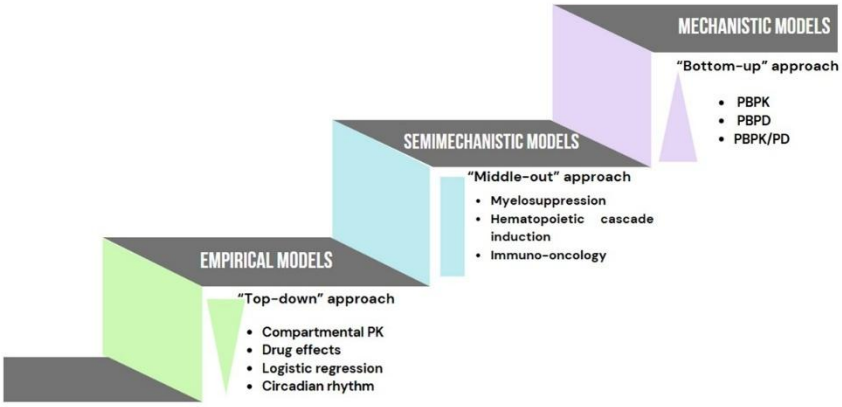

Figure 2. Overview of quantitative methodologies and model examples in PMx. PBPK: physiologically based pharmacokinetic models; PBPD: physiologically based pharmacodynamic models; PBPK/PD: physiologically based pharmacokinetic/pharmacodynamic models.

Empirical Models

Empirical models are non-mechanistic models created using the "top-down" strategy driven by the observed clinical data. Their purpose is to obtain a minimal model for fitting longitudinal data without considering the causal mechanistic bases. By fitting a minimal model, this approach may lack interpretability in terms of molecular and physiological processes. The obtained models may only be predictive

in treatment/disease scenarios that are somehow already covered by the data used to generate the model. Therefore, their ability to extrapolate beyond clinically available data is very limited [24,25]. Empirical models include PK models [26], used for forecasting concentration-time profiles and PK/PD models [27] employed to study over time the exposure-response relationship.

These models aggregate a wide range of different organs and fluids into interconnected hypothetical areas named compartments, assuming that the relative change in drug concentrations over time for these compartments is constant. Differential equations are used to explain mass transfers between compartments [28]. Conventional PK models usually utilize a one-, two- or three-compartment structure to describe drug distribution in the body. They can be used to derive primary PK parameters, such as clearance (CL) [29] and volume of distribution (V_d) [30]. Since the value of V_d is dependent on the concentration measured in a certain bodily space, which is considered to be representative of the concentration in the remainder of the organism, the V_d reflects an apparent volume. Rather than providing information about the process in particular organs or tissues or the rate of distribution, which is typically a determinant of the actual degree of tissue accumulation, V_d relates the amount and concentration of the drug in the system at a given time and gives general information about the degree of distribution in the organism. In addition, PK parameters such as CL and V_d may be distorted by bioavailability. To determine the magnitude of absolute bioavailability, the drug is administered through two different routes: extravascular and intravenous (IV), the latter is used as a reference because it is assumed that 100% of the administered dose enters the systemic circulation unaltered by depositing it directly into the general circulation. When CL and V_d are reported as CL/F and V_d/F respectively, the drug has only been tested in an oral (OR) form. Therefore, with only OR data, the absolute bioavailability of the drug cannot be determined, and the unknown F (bioavailability) factor will be bundled and carried through the calculation of V_d and CL [31,32].

Mechanistic Models

A mechanistic extension of empirical compartmental PK models is the PBPK model. The structure of a PBPK model mimics the physiological and anatomical structures of the organism (the system) under study. This structure is made with a "bottom-up" approach, based on the *in vitro-in vivo* (IVIV) extrapolation process and the data generated from *in*

vitro systems [33,34]. PBPK models incorporate a flow-based type of modeling, together with the implementation of multiple compartments to represent a tissue or an organ of the system. They use the same mathematical framework applied in empirical models (differential equations) [35]. In mechanistic models, it is essential to differentiate between parameters that describe the characteristics of the drug and the biological system. The building blocks of information required for the establishment of PBPK models differentiate in addition to the aforementioned characteristics, the administration protocol and formulation properties [36].

PBPK models are used to estimate the risk for drug-drug interactions [37,38], to predict human PK using *in vitro* and *in silico* data together with preclinical observations during the first-in-human trials [39], to account for pathophysiological changes and to predict the organ impairment in drug exposure [40]. PBPK models also offer an appropriate framework for combining existing information about drugs and systems to forecast system performance in real-world and simulated scenarios, therefore can be applied for instance in regulatory submissions to perform PK predictions in pediatric patients [38,41,42]. One of the examples of major interest in the applications of PBPK models is their use to predict food effects (FE) in biopharmaceutical classification system (BCS) class II and class IV drugs [43-45]. The prediction of FE by the PBPK model has grown as a result of their extension to modeling OR absorption processes and directing formulation development, which allows mechanistically simulating a compound's PK under fed or fasted conditions while integrating changes in physiology and drug properties like solubility and permeability. This leads to a deeper understanding of specific mechanisms influencing the FE and OR drug absorption in general [46]. The purpose of FE prediction is to identify the need and timing of the pivotal FE study [47], saving valuable development time and resources for the pharmaceutical industry. After clinical FE data are available, the model is improved to be applied for providing more mechanistic insights into the observed FE and guide future formulation attempts [48,49].

Semimechanistic Models

For most research-related concerns, empirical models may not be appropriate or useful because, in addition to lacking mechanistic meaning, as the number of parameters in such models is determined

empirically from the available data, differently designed experiments can lead to different models [25]. Along with this, the complex nature of mechanistic models demands more advanced system-related parameters and makes more challenging the model selection and validation processes [34]. Thus, a balance between empirical and mechanistic models is offered by performing semimechanistic models, which maintain a physiological essence only in the fragments of the model relevant to the desired modeling goals [23,25]. The "middle-out" approximation can be applied in developing these models. This approach combines the benefits and strengths of top-down and bottom-up techniques by using clinical data and, at the same time, moving beyond the boundaries of the initial clinical study by using the previous *in vitro* and system information together with the ability to incorporate important aspects of the disease and treatment effects to create the model [34,50,51].

Semimechanistic models make it possible to investigate and validate molecular, genetic, or feedback processes associated with the disease's pathophysiology while producing accurate data that can be replicated or utilized to simulate clinical trials. Compared to full systems biology models, its lower complexity also results in shorter computing running times. In situations of antimicrobial resistance [52] and in identifying the PK and PD properties of antibacterial drugs [53,54], semimechanistic models have demonstrated a significant degree of efficacy. They are also helpful in describing side effects in other disease areas such as thrombocytopenia [55] and rheumatoid arthritis [56], as well as modeling myelosuppression brought on by chemotherapy [57] and hematopoietic cascade induction [58]. These models are also used for bioequivalence studies, where a simulation approach based on a semimechanistic model, which includes systematic and peripheral compartments, lumen, gut, liver, and principal and secondary metabolites compartments, had been applied to the four classes of the BCS to explore in bioequivalence trials scenarios which analyte (parent drug or any of the metabolites) is the most sensitive to changes in drug product performance [59]. In addition, semimechanistic models have been developed to amalgamate both theoretical and evidence-based features of tumor growth and immunological cell-type dynamics [51]. Some examples of these models are the system of three ordinary differential equations built by Kirschner and Panetta [60] for attending to the potential of interleukin (IL)-2 and its effects on tumor relapse and the model developed by Pillis et al. de [61] to justify the need for

taking into consideration multiple cell types (tumor cells, natural killer (NK) cells and CD8 T cells) in the total anti-tumor immune activity.

Theoretical Fundamentals on Pharmacometrics

Nonlinear Mixed Effects Models

The gold standard for PK and PD parameter estimation is the use of nonlinear mixed effects (NLME) models. Before NLME was applied, traditional population analysis techniques like the standard two-stage approach or the naïve pooled data method were used to estimate the parameters PK and PD. The standard two-stage method is based on the individual compartmental analysis of the concentration-time data of each individual included in the study, followed by a statistical analysis of the individual values of the estimated parameters to calculate the mean value and the variances associated with them. In contrast, the naïve pooled data method involves the joint compartmental analysis of all concentration-time data of all individuals included in the study as if they were a single individual. Those approaches need extensive and frequent sampling for each patient and lead to the overestimation of variability and the restricted examination of covariate effects, producing biased estimates of the PK and PD parameters [62].

All individual data is combined and analyzed at the same time in NLME modeling in order to obtain the population parameters, that describe the population's typical tendency, and the individual variability associated with these parameters and with the experimental concentrations. By estimating PK and PD parameters using sample designs that contain either rich or sparse data, or a mix of both, NLME models enable the characterization of kinetic and dynamic behavior in particular populations, including cancer patients, newborns, and the elderly. In comparison to classical analysis, it also enables the simultaneous analysis of heterogeneous data from various sources, improving the ability to detect non-linearities, include extra covariates, or raise the accuracy of PK parameter estimates [63].

The statistical or variance model and the structural model are the two main components of the NLME models (Figure 3). In the first stage, the basic structural model is identified. The structural model is the most accurate explanation for each individual's experimental observations at any given time in the absence of covariates. The PK and PD parameters in this model represent the fixed effects. All research participants share

the fixed effects that characterize the drug's typical behavior in the population under investigation. The worldwide variability in the response obtained in a sample of *n* people is considered by the statistical model.

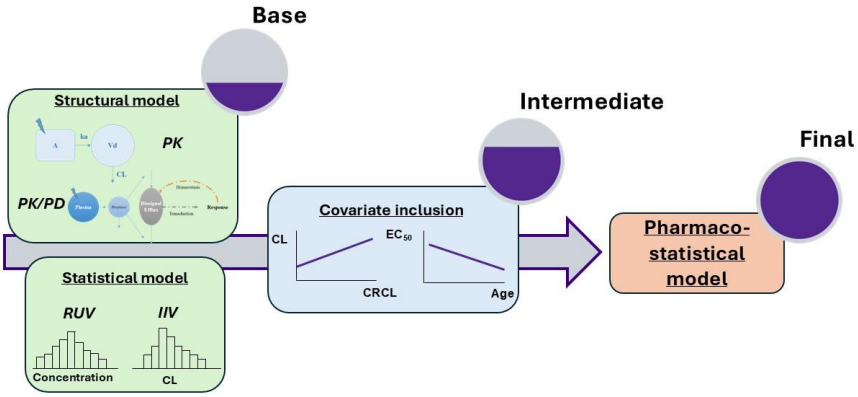

Figure 3. Components of NLME models. PK: pharmacokinetic; PK/PD: pharmacokinetic/pharmacodynamic; RUV: residual unexplained variability; IIV: interindividual variability; CL: clearance; EC_{50}: half maximal effective concentration; CLCR: creatinine clearance.

Both the residual unexplained variability (RUV) and interindividual variability (IIV) are represented by their parameters, which are regarded as random effects. IIV is the differences between the individual and the population PK and PD parameters. RUV quantifies the deviations between the concentrations predicted by the model and the concentrations observed in the individual that cannot be explained by the proposed population model. Following the identification of the base model, the covariate model is eventually developed by incorporating all the prognostic factors (covariables) that could significantly affect any of the base model's PK parameters. In the context of NLME, the regression parameters of the covariables are included as fixed effects in the structural intermediate model. The final pharmaco-statistical model is the one that includes the clinically and statistically relevant covariates [62,63].

Mathematically, NLME models can be represented by the following expression:

$$y_{ij} = f_{ij}(\phi_i, x_{ij}) + \varepsilon_j; i = 1, \dots, N'; j = 1, \dots, n_i$$

where y_{ij} is the jth experimental observation for the ith individual in each of the times x_{ij}, f_{ij} is a non-linear function relating the vector of individual parameters (ϕ_i) and the vector of independent variables (x_{ij}) which represent the structural model, N' is the number of individuals, n_i is the number of observations for the individual ith, and ε_j accounts for the discrepancies between the observations and the model predictions (RUV), which are assumed to be independent random variables following a normal distribution with a mean of zero and a variance of σ^2.

The PK and PD parameters can vary quantitatively from one individual to another, which is represented by the following expression:

$$\phi_i = g\left(z_{ij}, \overline{\theta}\right) + \eta_i$$

where g is a function that describes the expected value of ϕ_i (also referred to as empirical Bayes estimates) which depends on the vector of population parameters or fixed effects ($\overline{\theta}$), and on a set of covariates specific to each individual (z_{ij}), such as weight, age, etc., which may vary over time. The random deviation of ϕ_i is denoted by η_i. It is assumed that their values are independent and describe a symmetric distribution around zero and of variance ω^2, which is indicative of the random IIV linked with $\overline{\theta}$ [62,63]. To explain the variations among studies or research centers, several models incorporate a third degree of variability, such as between-occasion variability (BOV) [64] or inter-study variability (ISV).

Uncertainty Quantification

All models are abstractions and confidence in model predictions depends on the extent of knowledge and data that went into their development. Uncertainty is the degree of accuracy up to which model population (fixed or random effect) or individual parameters can be determined given the available observations, i.e., it represents the level of confidence or precision related to parameter estimation. For the calculation of precision standard error (SE) or confidence intervals (CI) can be used [65].

In terms of population parameter uncertainty, SE values are primarily derived using three methods: (i) the Fisher information matrix (default method implemented in NONMEM software), (ii) log-likelihood

profiling, and (iii) simulation/estimation using bootstrap analysis. Relative standard error (RSE) derived from SE and stated as a percentage, is used to represent the population parameters' uncertainty. While a high RSE number (>50%) is often undesirable and indicates low accuracy in the estimation of the parameter, a small value (<25%) indicates a solid estimation of the parameter [62].

The NONMEM's POSTV matrix provides a straightforward and reliable method for calculating the uncertainty of empirical Bayes estimates. The .phi file from the updated NONMEM 7 version has the POSTV matrix elements as ETC columns. Furthermore, it is possible to compute the estimates of the PK and PD individual parameters as well as the associated uncertainty by determining the individual conditional distributions in Monolix [66]. A Markov Chain Monte Carlo (MCMC) process known as Metropolis-Hastings algorithms is used to determine individual conditional distributions ($p(\psi_i|y_i)$, being ψ_i the individual parameters for individual *i* and y_i represents the data observations for individual *i*. The following expression is used to sample parameter values from these distributions:

$$p(\psi_i|y_i) = \frac{p(y_i|\psi_i) * p(\psi_i)}{p(y_i)}$$

where $p(y_i|\psi_i)$ is the conditional density function of the data when knowing the individual parameter values, $p(\psi_i)$ is the density function for the individual parameters and $p(y_i)$ is constant which represent the likelihood. Reducing uncertainty can be achieved by improving the experiment, expanding the sample size under study, or creating a complementary data [67].

NLME Model Evaluation

Model evaluation enables one to ascertain whether the underlying structural and statistical model assumptions are suitable and to comprehend the model's capacity to sufficiently explain the supplied data. Model assessment is a difficult procedure that involves identifying the model's shortcomings. These methods can be highly helpful during model building as a tool to aid in model differentiation, although they are usually used after the final model has been created. An ideal statistical/graphical tool for choosing and assessing a population PK/PD model does not exist, hence a combination of simulation-

based, graphical, and numerical diagnostics tools should be employed [68,69].

In order to distinguish between two nested models, the numerical methods employ the objective function's minimum value (OFV), which is approximately equal to -2xlog likelihood (-2LL), as a test for statistical significance during model construction. Based on the differences in their OFVs, two nested models may be compared using the log-likelihood ratio test (LRT). When one more parameter is included, a difference in the OFV of 3.84, 6.63, and 10.83 corresponds to the <0.01, <0.05, and <0.001 level of significance, respectively [70]. The Akaike information criterion should be applied in place of the OFV for comparing non-nested models [71].

The most used graphical diagnostics are the goodness-of-fit (GOF) plots, which are based on a collection of graphics that enable evaluating the structural and statistical performance of the model by examining differences between the model's predictions and actual data. To assess the overall performance of the model and the differences explained by IIV, some sample examples of these plots include those that compare the dependent variable (DV) in the actual data to the individual forecasts (IPRED) or population predictions (PRED). If the model is suitable, the points will be evenly distributed around the tendency line and the IPRED will resemble the DV. The PRED is probably going to be comparable to the mean or median of each study's findings. Conditional weighted residuals (CWRESI) vs time or versus PRED are additional instances of GOF plots that are used to examine the structural aspect of the model. These residuals need to be uniformly distributed around the chart axis in this instance, devoid of any discernible tendency. In addition to graphical methods, numerical diagnostics should be used to compare models, give information about the model's robustness, or identify potential over-fits [62,69].

Simulation-based diagnostics are used to create one or more simulated datasets that are then compared to actual data to better understand model attributes and anticipate potential consequences. Prediction discrepancies, posterior predictive checks (PPC), visual predictive checks (VPC), numerical predictive checks (NPC), normalized prediction errors (NPDE), and bootstrap analysis are a few of the options that stand out. VPC is one of the most used tools for assessing model performance, which analyzes the PK/PD model's fixed and random effects components, visually determining whether a model can replicate the observed data's core trend and variability. Due to their

simplicity, visual prediction checks are frequently employed; nevertheless, for them to be informative, the model's and the design's heterogeneity must be minimal. Prediction-corrected VPC (pc-VPC), which normalizes the observed and simulated dependent variable based on the PRED, can be utilized in cases of imbalanced data or discrepancies in the sample time points, dosage regimens, or covariate relationship[72].

Simulation-Based Analysis

An essential part of PMx model assessment and inference is the use of models to simulate data. A simulation is the process of creating data from a model. The model may be used to simulate data that can be directly compared to the index data for assessment purposes. Either a fresh data set (external validation) or a portion of the original database used to derive the model (internal validation) can be utilized to do this. The model is often used to simulate data other than observable data for inference purposes. Simulating non-observed data that falls inside the actual data's limits is known as interpolation. Simulation of non-observed data that fall outside the original data's boundaries is known as extrapolation, which will demand confidence in the assumptions of the primary model [62].

One straightforward method of simulating NLME models is to omit the estimate step and set the residuals $\varepsilon(\sigma^2)$ and the variances of the interindividual random effects $\eta(\omega^2)$ to zero. The predicted concentration values will only be influenced by the doses given, the sampling durations, and the population values of the designated PK and PD parameters (fixed effects). This process, called deterministic simulation, is equivalent to simulating the typical individual of the population. Stochastic simulation, on the other hand, is the most often used method. It creates data by randomly selecting probability distributions that are indicative of the random effects. The fixed effect parameters in the model (θ) and the values of ω^2 and σ^2 must be fixed for this kind of simulation. This makes it possible to gather concentration data and then apply the estimating stage to answer a wide range of queries during the various phases of drug development and clinical usage. To prevent implausible parameter combinations in subjects, it is crucial to understand potential correlations between parameters and consider this element when simulating static models with more than one aleatory effect parameter [73].

Role of Pharmacometrics in Drug Development and Clinical Practice

PMx has emerged as a potent ally in drug research and development by optimizing the information gathered from trials and reducing expenses and time, which are seen as barriers in traditional clinical investigations [6,7,74]. The creation of physiologically based PMx models during preclinical research is crucial during early drug development when the goal is to identify potentially safe and effective dosages and dosing regimens as well as to select promising compounds. Through simulation, these models may improve the extrapolation of *in vitro* and animal data to people by accurately characterizing the PK and PD response to a medicine. Rapid drug candidate screening can be further aided by efficacy and safety models created from preclinical and existing clinical data. PMx mostly contributes to the creation of PK/PD and disease progression models during other phases of drug development [75,76]. Additionally, PMx can be applied during clinical trial simulation models, which are an expert field that creates PK or PD profiles (or both) in virtual participants based on the drug's PK and PD properties, study design and execution, and participant pathophysiologic changes during the trial. Clinical trial simulations may be used to choose between competing study designs by evaluating the power of the various designs for obtaining estimated model parameters with the highest level of precision [77,78].

Throughout phases 1 and 2, PMx is crucial to describe the connection between drug exposure and reaction for both favorable and harmful effects. Also, many studies performed during drug development are aimed at identifying and quantifying the IIV in exposure and response to a drug, which can be explained by determining the covariates and their impact on specific system parameters. During later stages PMx allows the improvement and further development of PK/PD models for dose optimization, using sparse data coupled with previously collected data. Furthermore, estimating individual PK or PD parameters may help explain toxicities or treatment failures [76,79].

The application of PMx is reflected also in post-commercialization stages in drugs that are used in routine clinical practice and that have been on the market for a long time. During their development and research process, PMx has been barely used, hence population-based PK/PD analyses have been established using data developed in animals or from patients in studies carried out time after the drug was available

on the market [80-82]. Moreover, the application of PMx models and simulation in precision dosing has led to MIPD as a novel paradigm to support clinical decision-making for dose individualization [83]. The goal of precision dosing is to prescribe an individualized drug therapy according to patient characteristics that are known to affect drug disposition, and/or response at a given time [84]. This strategy is opposed to the traditionally implemented "one-size-fits-all" approach, where the same dosage regimen is recommended to all patients [85]. The implementation of MIPD offers the potential to overcome the variability in drug response under ideal circumstances (clinical trial conditions) and usual circumstances of healthcare practice [86], leading to improved health outcomes, reduced medication-related harm, and a smaller economic burden [16]. This variability can be observed for example in pharmacological treatments with antibiotics, in oncology, and in immune-mediated diseases, where patients are not equally responsive to beneficial effects, and not equally susceptible to adverse effects [20].

MIPD is an inclusive concept comprehending the use of various mathematical modeling approaches in combination with individually measured patient characteristics and disease characteristics to inform clinical decisions aimed at giving the right drug, in the right dose, to the right patient [20,87,88]. It can be utilized a priori (exclusively relying on patient covariate data) to ascertain the most suitable initial dose, or a posteriori (considering covariate data alongside one or more observed therapeutic drug levels) to produce a Bayesian posterior parameter distribution essential for forecasting the subsequent dose that will achieve optimal drug exposure [89]. In comparison with conventional TDM, in MIPD a sampling scheme is not required because any timed sample can be utilized, allowing interventions at any point, from before the first dose to when a steady state is reached. Also, during TDM a comparison of exposure with a target range is performed, while in MIPD the mode of intervention involves calculating a dose that achieves a predefined PK/PD target [16,20,90]. The application of MIPD has been particularly remarkable for antibiotics considering that one of the largest risks to healthcare is the quick development of antibiotic resistance and the scarcity of new [91] treatments. In addition, MIPD has been often used for antifungals [92], immunosuppressants [93,94] and oncology drugs [95,96]. MIPD may potentially be advantageous in reducing costs without sacrificing efficacy, for instance, in monitoring the concentration of immune checkpoint inhibitors, which may enable dose reductions or longer

treatment intervals [97]. The approach of MIPD has also been applied to PD endpoints, such as the assessment for warfarin of international normalized ratio (INR) [98,99]. Biologic therapies have been a breakthrough for modern-day medicine, delivering targeted therapies that are changing the face of an ever-increasing number of diseases and offer hope for diseases once considered hard to treat even untreatable. While there is most of the available evidence in MIPD studies for anti-TNFs [100,101], there are no prospective studies for anti-interleukins or anti-integrins [87]. Despite the great potential of MIPD, multidisciplinary efforts and cooperation between the medical community, academics, regulators, patients, and other important stakeholders are still necessary for the creation of evidence and the systematic application of MIPD in healthcare [16].

Hypothesis and Objectives

Hypothesis and Objectives

Developing safe, effective, and personalized treatments for medical conditions is one of the greatest challenges in modern-day healthcare. Even with the progress in pharmaceutical science, the traditional methods of drug development and clinical decision-making have proven insufficient in dealing with patient variability, interactions between drugs, and the increasing costs and time limitations for new therapies to enter the market. The variability in drug response, influenced by genetic, physiological, and environmental factors, means that the same drug dosages used to treat a patient can lead to ineffective treatment, threatening certain populations to subtherapeutic treatment or adverse drug events. Given this, there is an urgent need for novel, data-driven approaches to optimize drug development and therapeutic strategies.

With the advent of PMx and the application of mathematical and statistical models to quantify drug behavior, it is possible to offer a transformative solution to these challenges. By integrating PK and PD principles with real-world data, PMx provides a predictive framework capable of quantifying model population (fixed or random effect) or individual parameters and their associated uncertainty for understanding drug behavior across diverse patient populations and scenarios. Its utility covers the whole drug development lifecycle, from preclinical studies to post-market surveillance, facilitating more optimal trial designs, personalized medicine, and compliance with regulatory entities. In essence, the application of PMx significantly enhances the PK/PD properties and clinical decision-making processes of drugs, allowing for more optimal treatment of patients, achieving therapeutic goals and thereby obtaining better healthcare outcomes.

Hence, this Thesis focuses on illustrating the utility of PMx in continuously improving drug development and clinical practice. It also reinforces the need for PMx methods to be integrated into academic research to improve our understanding of how drugs behave and to support the dissemination of data to inform evidence-based decision-making and contribute to the development of precision dosing.

Therefore, the **general objective** of the current Thesis is:

To develop, validate and implement pharmacometrics-guided strategies for optimizing research, development and clinical decision-making processes of drugs

The **specific objectives** to attain the previous aim include:

1. To explore a novel approach to predict the positive food effect of BCS II/IV drugs using a simplified PBPK model, recognizing solubility limited absorption as the sole driver of positive food effect for BCS II/IV drugs.
2. To characterize the absorption properties of different orally administered formulations of amiodarone in rats for optimizing the development of new oral formulations.
3. To evaluate optimal dosing strategies of warfarin in Caribbean Hispanic patients based on a population PK/PD model of warfarin in clinical practice.
4. To propose a methodology capable of individualizing dosing strategies of ustekinumab and secukinumab in patients with moderate to severe chronic plaque psoriasis based on the uncertainty of the individual parameters of a population PK/PD model.

Published or accepted works

Chapter 1: Evaluation of Solubility-Limited Absorption as a Surrogate to Predicting Positive Food Effect of BCS II/IV Drugs

Karine Rodriguez-Fernandez[1,2], José David Gomez-Mantilla[3], Suneet Shukla[3], Peter Stopfer[3], Peter Sieger[4], Victor Mangas-Sanjuan[1,2], Sheila Annie Peters[3]

Authors Affiliation: [1]Department of Pharmacy and Pharmaceutical Technology and Parasitology, University of Valencia, Valencia, Spain; [2]Interuniversity Research Institute for Molecular Recognition and Technological Development, Polytechnic University of Valencia-University of Valencia, Valencia, Spain; [3]Translational Medicine and Clinical Pharmacology, Boehringer Ingelheim Pharma GmbH & Co. KG, Binger Strase 173, 55216 Ingelheim am Rhein, Germany; [4]Drug Discovery Sciences, Boehringer Ingelheim Pharma GmbH & Co. KG, 88397 Biberach a.d. Riss, Germany

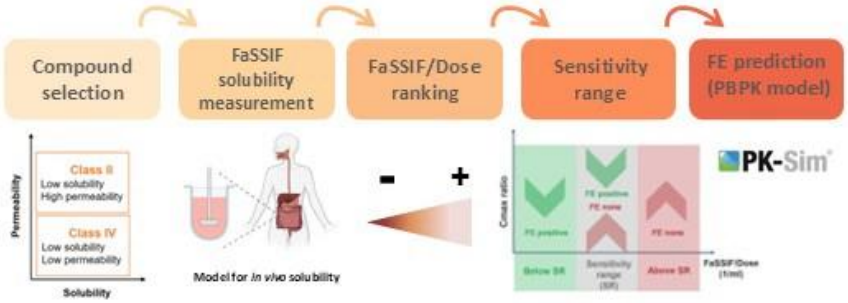

Clin Pharmacokinet. 2025 Feb 3. Epub ahead of print.

1. INTRODUCTION

The effect of food on OR drug absorption is a complex phenomenon that has long captivated the attention of pharmaceutical researchers and clinicians [1]. Food can significantly alter the PK of orally administered drugs by modifying the rate and extent of drug absorption, thereby impacting both their therapeutic efficacy and safety [2]. Food-induced physiological changes affecting absorption include changes in gastric emptying, gastric pH, luminal drug concentrations, bile secretion, and splanchnic blood flow [3]. Understanding the effect of food on the systemic exposure of an orally administered drug is a critical aspect of drug development, regulatory requirements, and clinical practice. During drug development, a pilot FE study is often conducted as part of a phase I clinical trial for drugs that are expected to have low bioavailability to inform dosing with or without food in subsequent trials. Later, a pivotal FE study must be conducted with the final dose and formulation of the drug to inform drug labeling in support of new drug application (NDA) submission [4, 5], unless the investigational drug is a BCS class I drug with an OR bioavailability ≥ 85%. Predictions of FE can significantly streamline drug development by guiding formulation strategies, optimizing clinical trial designs, and informing dosing recommendations. In early clinical development, decisions on the need to conduct a time- and resource-consuming FE study in phase I require a binary (yes/no) prediction with high confidence rather than a quantitative prediction. A reliable, conservative prediction of a lack of FE for the drug of interest can help avert pilot FE studies, as well as delay the pivotal FE study until later in the drug development process when there is more certainty about the drug`s market potential.

Current methods to predict human FE during drug development include *in vitro* and *in silico* tools [6]. *In vitro* methods include simple solubility- and permeability-based models such as BCS classification [7], predictions based on physicochemical properties such as dose number and maximum absorbable dose [8, 9], and compendial dissolution methods using fasted and fed state simulated intestinal fluid (FaSSIF/FeSSIF), as well as complex *in vitro* tools such as TIM and dynamic gastric model (DGM) systems [10]. There is a growing interest in the application of *in silico* PBPK models (e.g., SimCYP, GastroPlus, OSP Suite) that incorporate various factors influencing OR drug absorption for quantitative prediction of FE [11–18]. However, both *in vitro* and *in silico* tools have some limitations in predicting FE on drug

absorption. *In vitro* studies often simplify gastrointestinal environments and operate under static environments leading to IVIV disconnect and resulting in a systematic underprediction of *in vivo* drug absorption. Methods employing dose numbers assume a luminal fluid volume of 250 ml [19], whose relevance *in vivo* is not verifiable. PBPK models describe OR drug absorption with processes such as dissolution, precipitation, solubilization, etc., each with its own set of parameters [20, 21]. The downside of this complexity is that model verification and parameterization are often hindered by the IVIV disconnect and parameter nonidentifiability in "middle-out" approaches-too many parameters with uncertainty and too few observed data (concentration-time data) adversely affecting confidence in model predictions [22-25].

Nonidentifiability issues in a PBPK model may be overcome through model simplification/lumping [26]. In an accompanying article in this issue [22], we proposed a simplified PBPK model in which drug solubility represents all solubility-driven processes (dissolution, precipitation, solubilization, etc.). For a poorly soluble BCS II drug that is not a substrate of cytochrome P450 3A (CYP3A) or intestinal transporters, the *in vitro* solubility employed in the model then becomes the sole parameter associated with uncertainty, which can be readily optimized against observed plasma drug concentrations. The aim of this work is to explore a novel approach to predict positive FE of BCS II/IV drugs using the proposed simplified PBPK model, recognizing solubility limited absorption as the sole driver of positive FE for BCS II/IV drugs. Through a comprehensive analysis, we test the hypothesis that a binary FE prediction using solubility-limited absorption (SLA) identified by a simplified PBPK model in a conservative setting can reliably predict positive FE for BCS II drugs that are not extensively metabolized or effluxed in the gut.

2. MATERIALS AND METHODS

2.1. Compound Selection

A systematic literature search was performed in databases in the field of Health Sciences—Embase, MEDLINE (via PubMed), and Scopus—to find BCS class II and/or IV compounds with a FE clinical study available or at least with information on changes in exposure parameters in the product label after food intake. When more than one clinical FE study was available, the one carried out on healthy individuals with high-fat meals was selected. The categorization of FE type was determined by evaluating the ratio of maximum blood/plasma

concentration (C_{max}) of fed to fasted states using the bioequivalence criteria. If the C_{max} was higher in the fed state compared with the fasted state (ratio > 1.25), it was categorized as a positive FE. Conversely, if C_{max} was greater in the fasted state than in the fed state (ratio < 0.80), it was considered a negative FE. If there was no significant difference in C_{max} when taken with or without food (ratio within 0.8-1.25), it was classified as no FE. The compounds with negative FE were not considered for this investigation. In general, the negative FE observed for a few weak, basic BCS II/IV compounds is attributed to drug precipitation in small intestine due to higher prevailing pH, relative to gastric pH. Although demonstrated *in vitro*, drug precipitation is unlikely under *in vivo* sink conditions. In drugs showing negative FE, the effect sizes are generally small and not linked to safety risks. Therefore, negative FE prediction is generally not considered critical in drug development [22]. In addition to BCS class and FE *in vivo* (positive or none), other information collected from the literature included physical-chemical properties, solubility in FaSSIF, and dose of the drug product.

2.2. FaSSIF Solubility Measurement

The solubility in the FaSSIF medium for a subset of drugs was experimentally measured. The FaSSIF medium was the commercially available product from Biorelevant (www.biorelevant.com). The drug subset was selected based on the availability of the raw materials from Boehringer Ingelheim Pharma: nintedanib, mefenamic acid, phenytoin, ibrutinib, dabigatran etexilate, flibanserin, spironolactone, clopidogrel, progesterone, telmisartan, nefazodone HCl, nevirapine, carbamazepine, amiodarone HCl, digoxin, ibuprofen, meloxicam, and repaglinide were available. Albendazole, crizotinib, efavirenz, felodipine, gefitinib, nelfinavir mesylate, telaprevir, and tizanidine were purchased from Sigma-Aldrich Chemie GmbH. Purity for all drug substance batches was at least 98% or greater and was tested by high performance liquid chromatography (HPLC) before usage. The determination of the equilibrium solubility in FaSSIF medium was performed at 37±1°C by using an in-house built robotic system. Saturated solutions were prepared in well plates by adding an appropriate volume of FaSSIF medium (typically in the range of 0.5-1.0 ml) into each well that contains a known quantity of solid drug substance (typically in the range of 1-2 mg). The well plates were shaken for 24 h and then filtered using PTFE filters with 0.45 μm pore size. Filter absorption was avoided by discarding the first few

drops of filtrate. The amount of dissolved drug substance was determined by UV spectroscopy against a reference solution. In addition, the pH of the aqueous saturated solution was measured using a glass-electrode pH meter. The pH in the final medium was close to 6.5.

2.3. Dose-Adjusted FaSSIF Solubility Estimation

The dose-adjusted FaSSIF solubility (FaSSIF/D) was calculated as the ratio between the solubility in FaSSIF conditions gathered from literature data or measured experimentally and the dose from the *in vivo* FE study for each compound. The compounds were then ranked from the lowest to the highest FaSSIF/D values.

2.4. Sensitivity Range Determination

On the basis of the FaSSIF/D ranking, compounds were subdivided into three categories: (i) drugs with no FE, (ii) drugs with positive FE, and (iii) drugs with positive FE/no FE. The lower and upper limits of the sensitivity range (SR), which included drugs with positive FE/no FE, were established based on the FaSSIF/D values from the upper limit of the drugs with positive FE (below the SR) and the lower limit of the drugs with no FE (above the SR) (Figure 1). The SR was established via two sets of FaSSIF data. The first was the conservative SR determined only for compounds with FaSSIF solubility measured experimentally in this study under the same conditions. The second SR was defined also with the compounds of the conservative SR, as well as using other compounds with literature-reported FaSSIF solubility values assessed under unknown and uncontrolled conditions.

2.5. FE Prediction Through SLA Absorption with PBPK Modeling

The *in vivo* SLA was explored as a surrogate for FE prediction for drugs within the SR for which PBPK models were already available in PK-Sim (Open Systems Pharmacology Suite 11.2, www. open-systems-pharmacology.org, 2023). In these models, the model parameters related to systemic disposition (CL and V_d) were already optimized against observed clinical PK data. The steps for determining SLA are shown in Figure 2. The model-simulated OR PK profile considering the measured FaSSIF solubility was compared with the OR PK profile observed in fasted state. If no relevant differences between the simulated and observed C_{max} were seen, the experimental FaSSIF solubility was considered adequate to describe drug absorption.

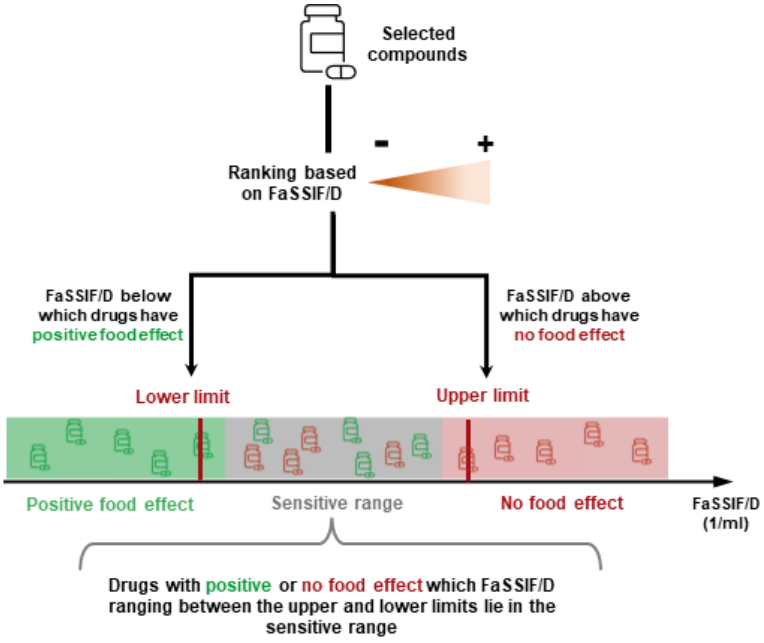

Figure 1. Workflow for SR determination for BCS class II and IV compounds. *D* dose, *FaSSIF* fasted state simulated intestinal fluid, *FaSSIF/D* dose-adjusted FaSSIF solubility, *SR* sensitivity range.

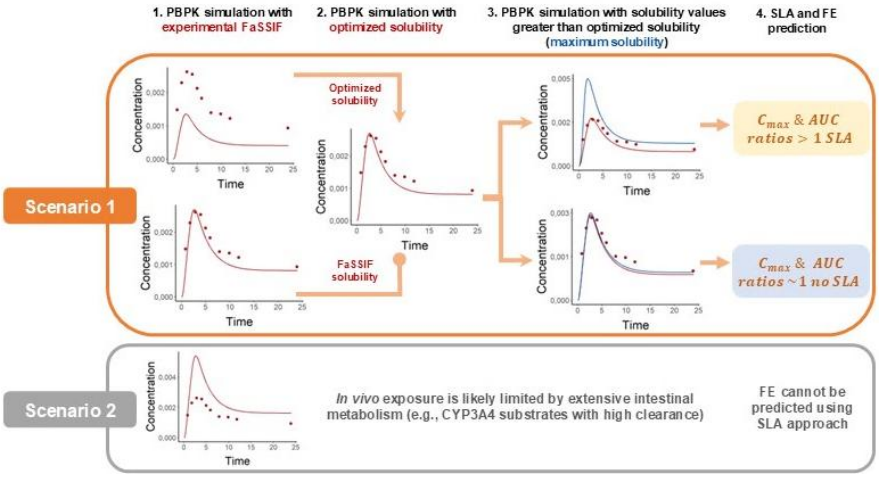

Figure 2. Schematic diagram of the PBPK modeling approach to identify SLA and FE for a drug within the SR. C_{max} maximum blood/ plasma concentration, *FaSSIF* fasted state simulated intestinal fluid

solubility, *FE* food effect, *PBPK* physiologically based pharmacokinetic model, *SLA* solubility-limited absorption, *SR* sensitivity range.

When simulated area under the curve (AUC) and C_{max} were less than the observed parameter values, the measured FaSSIF solubility is said to underpredict *in vivo* drug absorption due to IVIV disconnect. In this case (Figure 2, Scenario 1), the solubility value in the model was increased (optimized solubility) until the simulated AUC and C_{max} matched the observed data. This optimized solubility is referred to as the "at least" *in vivo* solubility [21] since the actual *in vivo* solubility could be even higher than the optimized value if the drug absorption *in vivo* is not limited by solubility. To confirm that absorption of the drug is not limited by solubility *in vivo*, the model solubility value was hypothetically increased beyond the best-fit solubility. Depending on the cases described above, the best-fit solubility could be the measured FaSSIF solubility itself or the optimized solubility. A lack of C_{max} and AUC sensitivity to increases beyond best-fit solubility confirms that *in vivo* drug absorption is not limited by solubility. If a stepwise increase in model value of solubility leads to increases in simulated C_{max} and AUC, the *in vivo* drug absorption is said to be limited by solubility. The value of hypothetically high solubility beyond which there are no changes to simulated AUC and C_{max} is referred to as maximum solubility. If AUC and C_{max} ratios resulting from simulated exposure with maximum solubility and optimized or FaSSIF solubility was > 1, *in vivo* OR drug absorption is solubility limited and suggests a high probability of positive FE. If the ratios are close to 1, then the *in vivo* drug absorption is not limited by solubility [21]. When model-simulated C_{max} was greater than the observed C_{max} gut metabolism- or efflux-limited absorption are assumed to be the driving factors (Figure 2, Scenario 2). This conclusion is justified since the models are already optimized for systemic drug disposition due to CL and V_d using IV PK data. For drugs for which the simulated C_{max} was greater than the observed, it is not possible to apply the proposed method for positive FE prediction. Graphical and numerical analyses were performed using R programming language version 4.3.1 (The R Foundation for Statistical Computing, Vienna, Austria, 2023) and R studio.

3. RESULTS

3.1. Compound Selection

A clinical *in vivo* FE study was reported for 51 compounds showing positive (61%) or no FE (39%), of which 65%, 8%, and 27% were BCS

class II, II/IV, and IV drugs, respectively. Literature-reported solubility in FaSSIF medium was available for 25 compounds, showing positive (76%) or no FE (24%), for which 44%, 8%, and 48% were BCS class II, II/ IV, and IV drugs, respectively (Supplementary Table S1).

3.2. FaSSIF Solubility Measurement

FaSSIF solubility was measured for 26 compounds with positive FE (46%) and no FE (54%) (Table 1), of which 22 belonged to BCS class II. It is noteworthy that 55% of the BCS class II drugs showed no FE *in vivo*. A comparison between experimentally determined FaSSIF values and those from the literature is shown in Figure 3. To quantify the bias in the measurement of FaSSIF, we calculated the average-fold error, which resulted in 0.14, therefore we can affirm that the FaSSIF solubility measured in our laboratory was generally lower compared with literature FaSSIF data.

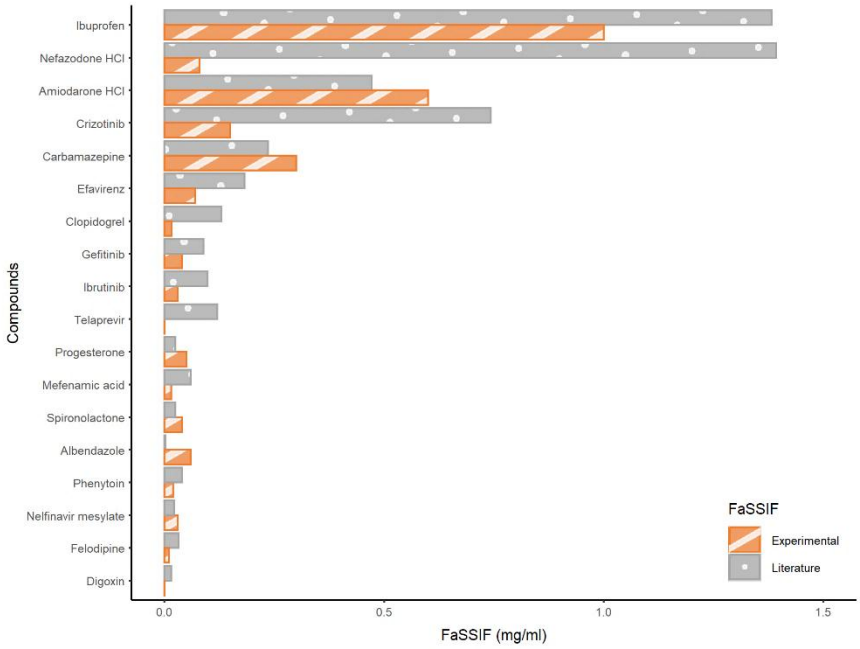

Figure 3. Comparison of experimentally determined and literature-reported FaSSIF values. *FaSSIF* fasted state simulated intestinal fluid solubility.

3.3. Sensitivity Range

First, a conservative SR was assessed using the FaSSIF/D values (Table 1) from the 26 compounds with experimental FaSSIF solubility measured. A total of 20 compounds lay within the conservative SR area (Figure 4). All compounds with FaSSIF/D values less than 3×10^{-5} 1/ml showed only a positive FE while all compounds with FaSSIF/D greater than 1×10^{-3} 1/ml demonstrated no associated FE.

Table 1. Selected compounds for determination of FaSSIF solubility and the conservative SR

Compound	BCS	C_{max} ratio *in vivo*	FE *in vivo*	Dose (mg)	Measured FaSSIF (mg/ml)	FaSSIF/D (1/ml)
Telaprevir	II	5.96	positive[16]	750	0.001	1.33x10^{-06}
Nelfinavir mesylate	II/IV	4.37	positive[16]	1250	0.03	**2.40x10^{-05}**
Nintedanib	II	1.18	none[a]	100	0.003	3.00x10^{-05}
Mefenamic acid	II	1.05	none[33]	250	0.015	6.60x10^{-05}
Phenytoin	II	1.41	positive[34]	300	0.02	6.67x10^{-05}
Ibrutinib	II	2.83	positive[35]	420	0.03	7.14x10^{-05}
Dabigatran etexilate	II	0.96	none[a]	110	0.008	7.27x10^{-05}
Flibanserin	II	1	none[a]	100	0.008	8.00x10^{-05}
Efavirenz	II	1.79	positive[36]	600	0.07	1.17x10^{-04}
Albendazole	II/IV	5.93	positive[37]	400	0.06	1.50x10^{-04}
Gefitinib	II	1.32	positive[38]	250	0.04	1.60x10^{-04}
Spironolactone	II	2.1	positive[39]	200	0.04	2.00x10^{-04}
Clopidogrel	II	6.5	positive[40]	75	0.017	2.27x10^{-04}
Progesterone	II	5.19	positive[41]	200	0.05	2.50x10^{-04}
Telmisartan	II	0.8	none[a]	160	0.05	3.13x10^{-04}
Nefazodone HCl	II	0.93	none[42]	200	0.08	4.00x10^{-04}
Nevirapine	II	1	none[a]	200	0.08	4.00x10^{-04}
Crizotinib	IV	0.86	none[43]	250	0.15	6.00x10^{-04}
Carbamazepine	II	1.35	positive[44]	400	0.3	7.50x10^{-04}
Amiodarone HCl	II	3.68	positive[45]	600	0.6	1.00x10^{-03}
Digoxin	IV	0.8	none[46]	1	0.001	1.00x10^{-03}
Felodipine	II	1.04	none[47]	10	0.01	1.00x10^{-03}
Ibuprofen	II	1.1	none[48]	800	1	**1.25x10^{-03}**
Meloxicam	II	0.8	none[a]	15	0.09	6.00x10^{-03}
Repaglinide	II	0.8	none[a]	2	0.05	2.50x10^{-02}
Tizanidine	II	1.24	none[49]	8	1	1.25x10^{-01}

[a] Food effect information was provided by Boehringer Ingelheim Pharma. The shadow FaSSIF/D area represents the conservative SR, and the red FaSSIF/D values represent the upper and lower limits of the conservative SR.

Since the FaSSIF solubility measured in our laboratory was generally lower compared with literature FaSSIF data (Figure 3), a second SR

was also developed including 25 compounds with FaSSIF solubility from the literature (Supplementary Table S1). The SR with a total dataset of 51 compounds included 10 compounds (all positive FE) with FaSSIF/D lower than the lower limit of the SR, 37 compounds (21 with positive FE and 16 with no FE) within the SR, and 4 compounds (all no FE) with FaSSIF/D values higher than the upper limit of the SR. Overall, the SR showed good agreement with the previous conservative SR, since an equal lower limit was achieved and a slightly higher upper limit of the conservative SR was established (Figure 4).

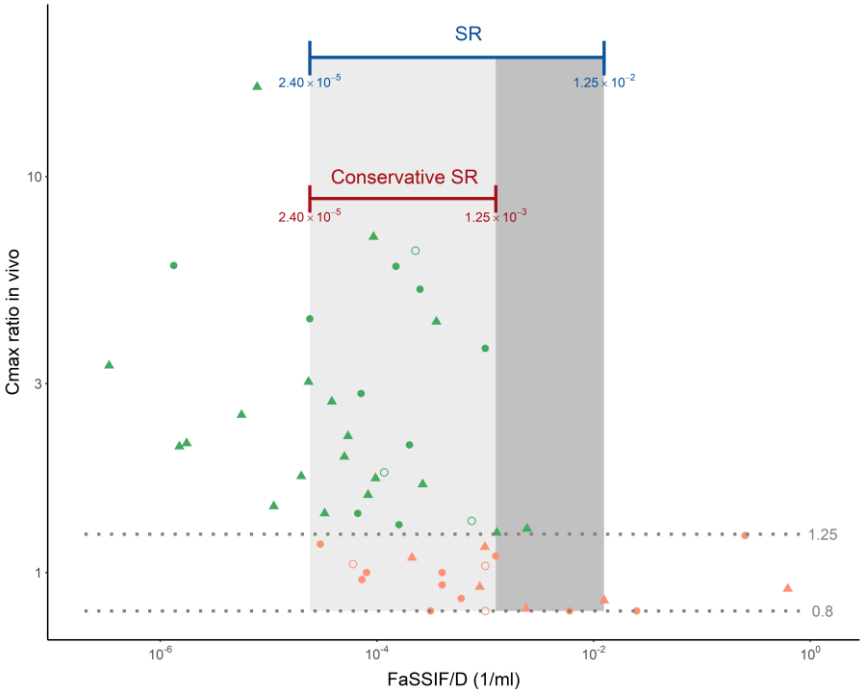

Figure 4. Conservative SR with experimental FaSSIF data and SR with experimental FaSSIF data plus literature FaSSIF data. The shadow grey area represents the SR. Grey dotted lines represent the limits for FE categorization, green filled circles represent the compounds with FE positive and FaSSIF measured experimentally, green filled triangles represent the compounds with FE positive and FaSSIF from literature, orange filled circles represent the compounds with no FE and FaSSIF measured experimentally, orange filled triangles represent the compounds with no FE and FaSSIF from literature, non-filled circles present the compounds with FE positive (green) and no FE (orange) within conservative SR and SR with FaSSIF measured experimentally and selected for PBPK simulations of SLA. *D* dose, *FaSSIF* fasted state

simulated intestinal fluid, *FaSSIF/D* dose-adjusted FaSSIF solubility, *SR* sensitivity range.

3.4. PBPK Simulations for SLA Prediction for Drugs within Conservative SR

PBPK models were available in PK-Sim for 6 out of 20 drugs with a FaSSIF/D ratio within conservative SR. The model parameters impacting absorption, metabolism, distribution, and elimination for these six drugs are presented in Supplementary Table S2. The PBPK simulations of PK profiles of a representative drug with SLA (efavirenz) and another representative drug without SLA (digoxin) are shown in Figure 5. The PBPK simulations of PK profiles of the rest of the compounds are shown in Supplementary Figs. S1 and S2. The values of optimized and maximum solubility for the predicted and observed exposure ratios and *in vivo* and predicted FE from PBPK simulations of all six drugs are presented in Table 2.

For carbamazepine, the first compound in scenario 1 (Supplementary Figure S1), the solubility was optimized to a value almost three times higher than that obtained experimentally and the maximum solubility in this case was greater than the optimized one. Efavirenz is the second case of scenario 1 (Figure 5) where the FaSSIF solubility is very similar to the optimized one, consequently, the experimental FaSSIF solubility was predictive of the observed. Furthermore, we were able to modify up to a maximum solubility greater than the optimized one, which is why efavirenz is a compound sensitive to increasing solubility. Both efavirenz and carbamazepine had C_{max} ratios significantly greater than 1, which represent SLA and support the positive FE observed *in vivo*. The following cases correspond to digoxin and mefenamic where the FaSSIF solubility did not describe the observed behavior. Therefore, the FaSSIF solubility was optimized for these compounds. For both compounds, the OR exposure was not sensitive to an increase in the input solubility beyond the best-fit solubility. Hence, the predicted C_{max} ratios were 1, representing a non-SLA and also predicted no FE *in silico*, which was in agreement with the observed behavior *in vivo*. The *silico/in vivo* ratios of the FE were very close to 1 in all the previous cases.

Table 1. SLA for the prediction of FE using the PBPK modeling approach

Compound		Clopidogrel	Felodipine	Mefenamic acid	Digoxin	Efavirenz	Carbamazepine
Solubility	**FaSSIF**	0.017	0.01	0.015	0.001	0.07	0.3
	Optimized	0.06	0.012	0.5	0.055	0.068	0.85
	Maximum	*	*	0.5	0.055	0.22	1.8
AUC ratio	**Observed**	9.2	1.53	0.97	0.98	1.28	1.12
	Predicted	*	*	1	1	1.44	1.08
C_{max} ratio	**Observed**	6.5	1.04	1.05	0.8	1.79	1.35
	Predicted	*	*	1	1	1.87	1.21
Positive FE *in vivo*		yes	no	no	no	yes	yes
Positive FE predicted by CYP3A4 or UGT substrate?		* CYP3A4	* CYP3A4	no no	no no	yes CYP3A4	yes CYP3A4, UGT
CL (L/h)		84[52]	90[47]	21.23(po)[51]	5.28[51]	9.4 (po)[51]	2.7[50]

* The value could not be determined.

AUC area under the curve, C_{max} maximum blood/plasma concentration, *CL* total body clearance value, *CYP3A4* Cytochrome P450 3A4, *FaSSIF* fasted state simulated intestinal fluid solubility, *Maximum solubility* PBPK model hypothetical solubility that exceeds the optimized solubility that helps to identify SLA, *Optimized solubility* PBPK model hypothetical solubility beyond which there were no further changes between predicted and observed profile, *PBPK* physiologically based pharmacokinetic model, *SLA* solubility-limited absorption, *UGT* uridine diphosphate glucuronosyltransferase

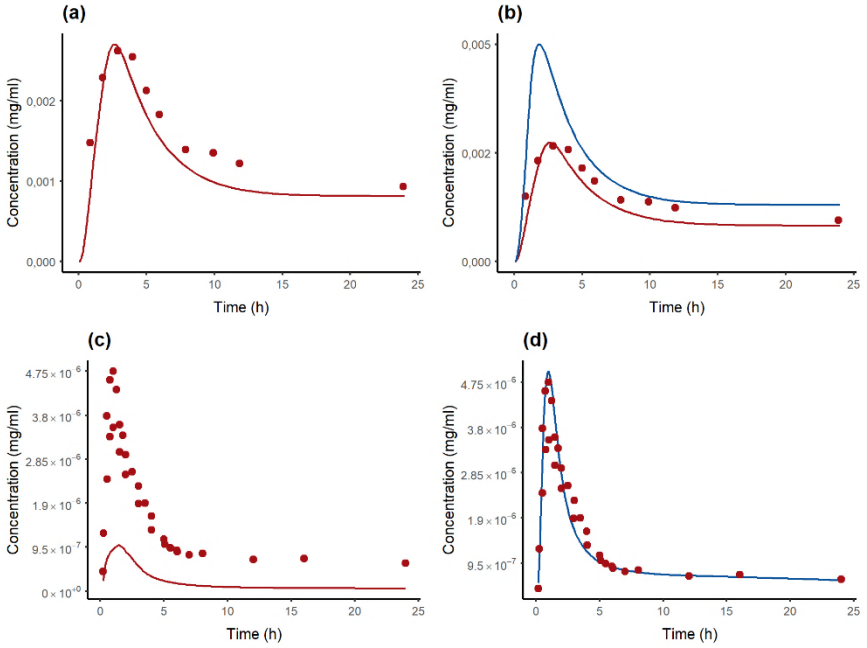

Figure 5. PBPK simulations of fasted PK profiles of efavirenz (a, b) and digoxin (c, d). (a) Efavirenz 600 mg OR administration simulated with measured FaSSIF solubility. (b) Efavirenz 600 mg OR administration simulated with optimized (red line) and maximum solubility (blue line). (c) Digoxin 1 mg OR administration simulated with measured FaSSIF solubility. (d) Digoxin 1 mg OR administration simulated with optimized (red line) and maximum solubility (blue line), in this case, overlapped. *FaSSIF* fasted state simulated intestinal fluid.

The compounds in the second scenario, clopidogrel, and felodipine (Supplementary Figure S2) did show *in vivo* positive FE or no FE, respectively, but it was not possible to describe the change in the observed C_{max} either with the experimental FaSSIF solubility or with a hypothetical increase in solubility, indicating that the exposure of these

drugs is limited by gut metabolism/efflux. Therefore, it was not possible to identify SLA.

4. DISCUSSION

A novel method has been proposed capable of establishing a quantitative framework for the early prediction of FE by estimating a SR range from the interplay of solubility of the drug in biorelevant medium and the dose. This method aims to establish a conservative prediction, with zero uncertainty for both positive FE and non-FE conditions, which enables confident and timely decisions during drug development. Furthermore, it precisely establishes the scope of uncertainty about the impact of food on drug exposure (SR), allowing for simple but informative risk assessment. Although FE impacts the time to reach the maximum blood/plasma concentration (T_{max}), C_{max}, and AUC, compound selection was based on the C_{max} ratio. This is because, C_{max} is likely to be more sensitive to food-induced changes in exposure compared to AUC, while FE changes in T_{max} are likely to be confounded by gastric emptying. The characterization of *in vitro* solubility in physiological pH or FaSSIF and FeSSIF medium are often considered to adequately mimic *in vivo* conditions of orally administered drugs.

However, these measured solubilities may still be conservative as *in vitro* settings may not adequately capture the *in vivo* sink conditions and transit kinetics [10]. Thus, not all BCS II/IV drugs classified based on measured solubility exhibit positive FE. According to a recent publication [18], only 36% of the 111 BCS II/IV approved drugs (25/68 BCS II, 6/25 BCS IV, 9/18 BCS II/IV) exhibit a positive FE, while 60% had no FE and 6% had negative FE. Out of the BCS II drugs exhibiting positive FE, only 15 had FE with significantly increased exposure (AUC ratio ≥ 2.0) [27]. All 15 were drugs with logP > 3 for which enhanced bile solubilization can play an important role in increasing *in vivo* solubility and therefore absorption, supporting that poor solubility is a plausible predictor of positive FE for BCS II drugs. The lack of FE for 60% of BCS II drugs can be explained by a possible misclassification of BCS I drugs as BCS II, based on conservative *in vitro* measures of solubility disconnected from the real *in vivo* solubility. In the previous research article by Owens et al. [27], the authors also showed that negative FEs are mostly seen in BCS III drugs (28% of the 28 drugs) and only 3 of these showed an AUC ratio of < 2.0-fold. Given the weak correlation of FE with BCS classes, the authors concluded that multiple physiological mechanisms impact FE [27].

However, since none of the 25 BCS I drugs in their study showed a positive FE (as expected from this class), it follows that high absorption resulting from high solubility and permeability does guarantee a lack of FE. This implies that mechanisms of FE not mediated by solubility and permeability (food‐drug complexation, lower luminal drug concentration in fed state leading to increased susceptibility of substrates to intestinal efflux and inhibition of CYP3A and/or efflux transporters in gastrointestinal tract) are rare, even if theoretically possible. The absence of positive FE for BCS I drugs also suggests that it is very unlikely for measured solubility to over-predict *in vivo* solubility and misclassify a BCS II as BCS I.

Dose-adjusted solubility provides a drug-independent determinant of OR drug absorption *in vivo*. As adjusted solubility is decreased from a hypothetically high value, the corresponding simulated OR drug absorption is constant at 100% and high, until a critical threshold, below which OR drug absorption starts to decrease. A drug with a dose-adjusted solubility below this critical threshold is said to have SLA (Supplementary Figure S3). The *in vivo* solubility of such a drug may be enhanced by food via its influence on one or more factors (gastric pH and gastric emptying rate, as well as drug and bile salt concentrations). The information provided in Table 1 can aid in early clinical development, if the compound FaSSIF/D values are less than 3×10^{-5} 1/ml (below SR), it is likely to present FE. If FaSSIF/D is greater than 1×10^{-3} 1/ml (above SR), it is likely to exhibit no FE. If the FaSSIF/D value is within the SR area, then SLA determination with PBPK simulations can help to predict if the drug is likely to have FE or not, if the drug is not extensively metabolized in the gut. As can be appreciated, FaSSIF/D can indeed discriminate between drugs with or without FE, under the term that drugs are outside the SR area (Figure 4). A conservative setting for FE prediction was ensured by choosing an upper and lower limit of conservative SR based on a determination of FaSSIF in our laboratory for 26 compounds. The FaSSIF values found in the literature are derived from different laboratories and unreported conditions of measurements. However, despite with literature-reported FaSSIF data provided comparable SR limits to those derived from in-house data (Figure 4).

As previously mentioned, this approach is not valid for compounds with high intestinal metabolism nor substrates of intestinal transporters; both felodipine and clopidogrel are high CL drugs (see Table 2) with extensive Cytochrome P450 3A (CYP3A) 4- mediated

intestinal metabolism. Consequently, the bioavailability of these drugs is limited by metabolism to a much larger extent than limited by solubility. Extensive gut metabolism is likely for very high CL CYP3A4 or uridine diphosphate glucuronosyltransferase (UGT) substrates and can be identified in the PBPK model when the simulated C_{max} with FaSSIF solubility is greater than the observed C_{max} (since it is unlikely that FaSSIF solubility is greater than *in vivo* solubility). However, even when the C_{max} with FaSSIF solubility is lesser than the observed C_{max}, gut metabolism cannot be excluded for CYP3A4 and UGT substrates. The individual contributions of solubility and gut metabolism in limiting drug absorption are nonidentifiable since model optimization against observed plasma drug concentrations can resolve uncertainty only in one parameter. Thus, for drugs with gut metabolism, the resulting masking will provide conservative estimates of FE prediction, if it is possible to apply the proposed approach (C_{max} simulated with FaSSIF < C_{max} observed). Unfortunately, a reliable quantitative prediction of gut metabolism is not easy even for CYP3A substrates [28-30]. However, since most high CL drugs are screened out during lead optimization, and low CL drugs are not likely to be impacted by gut metabolism, the proportion of drugs for which FE cannot be reliably predicted by the method proposed by our work is expected to be low. It is noteworthy that felodipine has no FE despite extensive metabolism by CYP3A4 in the gut, which seems to suggest that the standard high-fat food recommended for FE studies does not impact CYP3A4-driven gut metabolism. This is also consistent with the absence of FE for BCS I drugs [27], many of which are CYP3A4 substrates. However, certain other foods such as grapefruit juice have been shown to selectively inhibit intestinal metabolism [31].

Conventional PBPK models [13, 15-17] that are used for FE predictions include multiple unverifiable processes such as dissolution, precipitation, and solubilization, thus introducing a large array of parameters in the models. Difficulty in verifying underlying mechanisms leads to a model with many assumptions that may fit the observed data but cannot reliably predict an untested scenario (e.g., FE). The parameterization of these models relies on *in vitro* data that are generally under-predictive and cannot be optimized against observed concentration-time profile due to nonidentifiability. Therefore, FE predictions with PBPK models in the traditional setting tend to be conservative and uncertain resulting in unnecessary clinical FE studies [32]. This implies that pilot FE studies would be conducted even for drugs that may not have SLA or FE *in vivo* (e.g., a drug such

as mefenamic acid). We propose here a basic framework to assess FE prediction based on a simplified model, where SLA is the surrogate for FE. This allows the only parameter that impacts FE (solubility) to be optimized against observed data for drugs that are not extensively metabolized/effluxed in the gut, thereby resulting in a more reliable binary FE prediction. However, this is only a retrospective study. In the future, this approach can be applied for prospective predictions. A reliable binary prediction of FE (yes/no) in a conservative setting (no false negatives) using the method proposed in this work is more valuable for making timely decisions on the need for a pilot FE study and timing of a pivotal FE study compared with quantitative prediction by a PBPK in the traditional setting based on several assumptions and uncertain parameters.

5. CONCLUSIONS

The results from this work have demonstrated that dose adjusted FaSSIF solubility can be used to discriminate drugs with positive FE from those with no FE outside SR. Within SR, drugs with SLA identified by PBPK are likely to have FE. Comparable SR limits, with or without the addition of drugs with literature-reported FaSSIF data to drugs with FaSSIF solubility measured in-house, despite interlaboratory differences in the FaSSIF values, show that the SR limits are not too sensitive to these differences and that the SR limits established in this work can be applied to drugs with FaSSIF solubility measured elsewhere. The selection of SR based on conservative, in-house FaSSIF measurements on 26 drugs, and identification of SLA by PBPK allows for reliable prediction of FE to enable decisions on the need for pilot FE study and timing of pivotal FE study. It is important to note that this approach cannot be applied to drugs with extensive gut metabolism or transporter-mediated elimination. The reliability of positive FE prediction using SLA was tested with six compounds within SR, for which PK-Sim models were available. The simplified PBPK model proposed here combines all nonidentifiable parameters into a single identifiable parameter for the purpose of FE prediction, although this may compromise quantitative prediction accuracy. Our work shows that the binary prediction accuracy, which is critical for decision-making in clinical development, is not compromised. Extension of this work in the future to cover all compounds within SR will serve to further enhance confidence in the use of SLA to identify drugs that are likely to exhibit positive FE.

6. SUPPLEMENTARY INFORMATION

The online version contains supplementary material available at **Supplementary file1 (DOCX 192 KB)**

7. ACKNOWLEDGMENTS

The authors acknowledge the leaderships of the Boehringer Ingelheim Pharma departments, especially Translational Medicine & Clinical Pharmacology (TMCP) and Biopharmaceutical Working Group for providing the framework and funding for this research. The authors also thank Ghazal Montaseri from the TMCP Data Science department and Jelisaveta Ignjatović from the Drug Metabolism and Pharmacokinetics DMPK department for all the support to make possible this study.

8. DECLARATIONS

Funding This study was funded by Boehringer Ingelheim Pharma GmbH & Co.

9.CONFLICTS OF INTEREST

José David Gómez-Mantilla, Suneet Shukla, Peter Stopfer, Peter Sieger, and Sheila Annie Peters, are paid employees of Boehringer Ingelheim Pharma GmbH & Co. The authors declare that they do not possess any identifiable financial interests or personal associations that might have appeared to exert an influence on the research presented in this paper.

10. AVAILABILITY OF DATA AND MATERIAL

Data will be made available on request.

11. AUTHOR CONTRIBUTIONS

Investigation, data curation, formal analysis, methodology, visualization, writing-original draft, writing-review and editing: Karine Rodriguez-Fernandez. Investigation, formal analysis, methodology, project administration, supervision, visualization, writing-review and editing: Jose David Gomez-Mantilla. Investigation, methodology, supervision, visualization, writing-review and editing: Shukla Suneet. Conceptualization, funding acquisition, resources, writing-review and editing: Peter Stopfer. Investigation, formal analysis, writing-review and editing: Peter Sieger. Formal analysis, supervision, visualization, writing-original draft, writing-review and editing: Victor Mangas-

Sanjuan. Investigation, conceptualization, formal analysis, methodology, project administration, supervision, visualization, writing-original draft, writing-review and editing: Sheila Annie Peters.

12. REFERENCES

1. Welling PG. Influence of food and diet on gastrointestinal drug absorption: a review. J Pharmacokinet Biopharm. 1977. https:// doi. org/ 10. 1007/ bf010 61694.
2. O'Shea JP, Holm R, O'Driscoll CM, et al. Food for thought: formulating away the food effect—a PEARRL review. J Pharm Pharmacol. 2019. https:// doi. org/ 10. 1111/ jphp. 12957.
3. Deng J, Zhu X, Chen Z, et al. A review of food-drug interactions on oral drug absorption. Drugs. 2017. https:// doi. org/ 10. 1007/ s40265- 017- 0832-z.
4. Eur. European Medicines Agency (EMA) 21 June 2012 CPMP/EWP/560/95/Rev. 1 Corr. 2**, Committee for Human Medicinal Products(CHMP). Guideline on the investigation of drug interactions. https:// www. ema. europa. eu/ en/ docum ents/ scientific- guideline/ guideline- inves tigat ion- drug- inter actio ns- revision-1_ en. pdf. Accessed 11 Arp 2024.
5. US. Food and Drug Administration. Assessing the Effects of Food on Drugs in INDs and NDAs - Clinical Pharmacology Considerations Guidance for Industry, June 2022. https://www.fda. gov/ media/ 121313/ downl oad. Accessed 11 Apr 2024.
6. Lentz KA. Current methods for predicting human food effect. AAPS J. 2008. https:// doi. org/ 10. 1208/ s12248- 008- 9025-8.
7. Amidon GL, Lennernas H, Shah VP, et al. A theoretical basis for a biopharmaceutic drug classification: the correlation of *in vitro* drug product dissolution and *in vivo* bioavailability. Pharm Res. 1995. https:// doi. org/ 10. 1023/a: 10162 12804 288.
8. Gu CH, Li H, Levons J, et al. Predicting effect of food on extent of drug absorption based on physicochemical properties. Pharm Res. 2007. https:// doi. org/ 10. 1007/ s11095- 007- 9236-1.
9. Sugano K, Okazaki A, Sugimoto S, et al. Solubility and dissolution profile assessment in drug discovery. Drug Metab Pharmacokinet. 2007. https:// doi. org/ 10. 2133/ dmpk. 22. 225.

10. Vinarov Z, Butler J, Kesisoglou F, et al. Assessment of food effects during clinical development. Int J Pharm. 2023. https:// doi. org/ 10. 1016/j. ijpha rm. 2023. 122758.
11. Willmann S, Lippert J, Sevestre M, et al. PK-SimR: a physiologically based pharmacokinetic "whole-body" model. Biosilico. 2003. https:// doi. org/ 10. 1016/ S1478-5382(03) 02342-4.
12. Jones HM, Parrott N, Ohlenbusch G, et al. mcPredicting pharmacokinetic food effects using biorelevant solubility media and physiologically based modelling. Clin Pharmacokinet. 2006. https:// doi. org/ 10. 2165/ 00003 088- 20064 5120-00006.
13. Jones HM, Chen Y, Gibson C, et al. Physiologically based pharmacokinetic modeling in drug discovery and development: a pharmaceutical industry perspective. Clin Pharmacol Ther. 2015;97(3):247‐62.
14. GP. Simulations Plus, Manual GastroPlus™, California, EUA; 2010.
15. Tistaert C, Heimbach T, Xia B, et al. Food effect projections via physiologically based pharmacokinetic modeling: predictive case studies. J Pharm Sci. 2019. https:// doi. org/ 10. 1016/j. xphs. 2018. 05. 024.
16. Riedmaier AE, DeMent K, Huckle J, et al. Use of physiologically based pharmacokinetic (PBPK) modeling for predicting drug-food interactions: an industry perspective. AAPS J. 2020. https:// doi. org/ 10. 1208/ s12248- 020-00508-2.
17. Cheng L, Wong H. Food effects on oral drug absorption: application of physiologically-based pharmacokinetic modeling as a predictive tool. Pharmaceutics. 2020. https:// doi. org/ 10. 3390/ pharm aceut ics12 070672.
18. Ezuruike U, Zhang M, Pansari A, et al. Guide to development of compound files for PBPK modeling in the Simcyp populationbased simulator. CPT Pharmacometrics Syst Pharmacol. 2022. https:// doi. org/ 10. 1002/ psp4. 12791.
19. Wuelfing WP, El Marrouni A, Lipert MP, et al. Dose number as a tool to guide lead optimization for orally bioavailable compounds in drug discovery. J Med Chem. 2022. https:// doi. org/ 10. 1021/ acs. jmedc hem. 1c016 87.
20. Shono Y, Jantratid E, Dressman JB. Precipitation in the small intestine may play a more important role in the *in vivo*

performance of poorly soluble weak bases in the fasted state: case example nelfinavir. Eur J Pharm Biopharm. 2011. https:// doi. org/ 10. 1016/j. ejpb. 2011. 04. 005.
21. Fink C, Sun D, Wagner K, et al. Evaluating the role of solubility in oral absorption of poorly water-soluble drugs using physiologically-based pharmacokinetic modeling. Clin Pharmacol Ther. 2019. https:// doi. org/ 10. 1002/ cpt. 1672.
22. Rodriguez-Fernandez K, Gomez-Mantilla J, Shukla S, et al. Solubility-limited absorption identified by a simplified PBPK model for the prediction of positive food effect of BCS II/IV drugs. Clin Pharmacokinet 2024. https:// doi. org/ 10.1007/s40262-025-01472-w.
23. Li M, Zhao P, Pan Y, et al. Predictive performance of physiologically based pharmacokinetic models for the effect of food on oral drug absorption: current status. CPT Pharmacometrics Syst Pharmacol. 2018. https:// doi. org/ 10. 1002/ psp4. 12260.
24. Peters SA, Dolgos H. Requirements to establishing confidence in physiologically based pharmacokinetic (PBPK) models and overcoming some of the challenges to meeting them. Clin Pharmacokinet. 2019. https:// doi. org/ 10. 1007/ s40262- 019- 00790-0.
25. Kesisoglou F. Can PBPK modeling streamline food effect assessments? J Clin Pharmacol. 2020. https:// doi. org/ 10. 1002/ jcph. 1678.
26. Okino MS, Mavrovouniotis ML. Simplification of mathematical models of chemical reaction systems. Chem Rev. 1998. https://doi. org/ 10. 1021/ cr950 223l.
27. Owens K, Argon S, Yu J, et al. Exploring the relationship of drug BCS classification, food effect, and gastric pH-Dependent Drug Interactions. AAPS J. 2021. https:// doi. org/ 10. 1208/s12248- 021- 00667-w.
28. Peters SA, Jones CR, Ungell AL, et al. Predicting drug extraction in the human gut wall: assessing contributions from drug metabolizing enzymes and transporter proteins using preclinical models. Clin Pharmacokinet. 2016. https:// doi. org/ 10. 1007/s40262- 015- 0351-6.
29. Fagerholm U. Prediction of human pharmacokinetics‐gut-wall metabolism. J Pharm Pharmacol. 2007. https:// doi. org/ 10. 1211/jpp. 59. 10. 0002.
30. Davies M, Peramuhendige P, King L, et al. Evaluation of *in vitro* models for assessment of human intestinal metabolism in drug

discovery. Drug Metab Dispos. 2020. https:// doi. org/ 10. 1124/dmd. 120. 000111.
31. Bailey DG, Malcolm J, Arnold O, et al. Grapefruit juice-drug interactions. Br J Clin Pharmacol. 1998. https:// doi. org/ 10. 1046/j. 1365- 2125. 1998. 00764.x.
32. Kesisoglou F, Basu S, Belubbi T, et al. Streamlining food effect assessment - are repeated food effect studies needed? An IQ analysis. AAPS J. 2023. https:// doi. org/ 10. 1208/ s12248- 023- 00822-5.
33. Hamaguchi T, Shinkuma D, Yamanaka Y, et al. Bioavailability of mefenamic acid: influence of food and water intake. J Pharm Sci. 1986. https:// doi. org/ 10. 1002/ jps. 26007 50914.
34. Melander A, Brante G, Johansson O, et al. Influence of food on the absorption of phenytoin in man. Eur J Clin Pharmacol. 1979. https:// doi. org/ 10. 1007/ bf006 18516.
35. de Jong J, Sukbuntherng J, Skee D, et al. The effect of food on the pharmacokinetics of oral ibrutinib in healthy participants and patients with chronic lymphocytic leukemia. Cancer Chemother Pharmacol. 2015. https:// doi. org/ 10. 1007/ s00280- 015- 2708-9.
36. Kaul S, Ji P, Lu M, et al. Bioavailability in healthy adults of efavirenz capsule contents mixed with a small amount of food. Am J Health Syst Pharm. 2010. https:// doi. org/ 10. 2146/ ajhp0 90327.
37. Lange H, Eggers R, Bircher J. Increased systemic availability of albendazole when taken with a fatty meal. Eur J Clin Pharmacol. 1988. https:// doi. org/ 10. 1007/ bf005 40964.
38. Swaisland HC, Smith RP, Laight A, et al. Single-dose clinical pharmacokinetic studies of gefitinib. Clin Pharmacokinet. 2005. https:// doi. org/ 10. 2165/ 00003 088- 20054 4110- 00004.
39. Overdiek HWPM, Merkus FWHM. Influence of food on the bioavailability of spironolactone. Clin Pharmacol Ther. 1986. https:// doi. org/ 10. 1038/ clpt. 1986. 219.
40. Nirogi RV, Kandikere VN, Mudigonda K. Effect of food on bioavailability of a single oral dose of clopidogrel in healthy male subjects. Arzneimittelforschung. 2006. https:// doi. org/ 10. 1055/s-0031- 12967 83.
41. Rangaraj N, Sampathi S, Junnuthula V, et al. Fast-fed variability: insights into drug delivery, molecular manifestations, and regulatory aspects. Pharmaceutics. 2022. https:// doi. org/ 10. 3390/ pharm aceut ics14 091807.

42. Dockens RC, Greene DS, Barbhaiya RH. The lack effect of food on the bioavailability of nefazodone tablets. Biopharm Drug Dispos. 1996. https:// doi. org/ 10. 1002/ (sici) 1099-081x(199603) 17:2%3c135:: aid- bdd947% 3e3.0. co;2-k.
43. Xu H, O'Gorman M, Boutros T, et al. Evaluation of crizotinib absolute bioavailability, the bioequivalence of three oral formulations, and the effect of food on crizotinib pharmacokinetics in healthy subjects. J Clin Pharmacol. 2015. https:// doi. org/ 10. 1002/ jcph. 356.
44. McLean A, Browne S, Zhang Y, et al. The influence of food on the bioavailability of a twice-daily controlled release carbamazepine formulation. J Clin Pharmacol. 2001. https:// doi. org/ 10. 1177/ 00912 70012 20100 05.
45. Meng X, Mojaverian P, Doedee M, et al. Bioavailability of amiodarone tablets administered with and without food in healthy subjects. Am J Cardiol. 2001. https:// doi. org/ 10. 1016/ s0002- 9149(00) 01396-5.
46. Johnson BF, O'Grady J, Sabey GA, et al. Effect of a standard breakfast on digoxin absorption in normal subjects. Clin Pharmacol Ther. 1978. https:// doi. org/ 10. 1002/ cpt19 78233 315.
47. Edgar B, Lundborg P, Regardh CG. Clinical pharmacokinetics of felodipine. A summary. Drugs. 1987. https:// doi. org/ 10. 2165/ 00003 495- 19870 0343- 00005.
48. Pargal A, Kelkar MG, Nayak PJ. The effect of food on the bioavailability of ibuprofen and flurbiprofen from sustained release formulations. Biopharm Drug Dispos. 1996. https:// doi. org/ 10.1002/ (sici) 1099- 081x(199608) 17:6% 3c511:: aid- bdd969% 3e3.0. co;2-y.
49. Shah J, Wesnes KA, Kovelesky RA, et al. Effects of food on the single-dose pharmacokinetics/pharmacodynamics of tizanidine capsules and tablets in healthy volunteers. Clin Ther. 2006. https://doi. org/ 10. 1016/j. clint hera. 2006. 09. 014.
50. Marino SE, Birnbaum AK, Leppik IE, et al. Steady-state carbamazepine pharmacokinetics following oral and stable-labeled intravenous administration in epilepsy patients: effects of race and sex. Clin Pharmacol Ther. 2012. https:// doi. org/ 10. 1038/ clpt. 2011.251.
51. Knox C, Wilson M, Klinger CM, et al. DrugBank 6.0: the drug bank knowledge base for 2024. Nucleic Acids Res. 2024. https://doi. org/ 10. 1093/ nar/ gkad9 76.

52. Duong JK, Nand RA, Patel A, et al. A physiologically based pharmacokinetic model of clopidogrel in populations of European and Japanese ancestry: an evaluation of CYP2C19 activity. Pharmacol Res Perspect. 2022. https:// doi. org/ 10. 1002/ prp2. 946.

Chapter 2: Pharmacometric characterization of entero-hepatic circulation processes of orally administered formulations of amiodarone under complex binding kinetics

Karine Rodríguez-Fernández[1], Elena Gras-Colomer[2], Mónica Climente-Martí[1,3,4], Victor Mangas-Sanjuán[1,5], Matilde Merino-Sanjuán[1]

Authors Affiliation: [1]Department of Pharmacy and Pharmaceutical Technology and Parasitology, University of Valencia, Av Vicent András Estellés, s/n. 46100, Valencia, Burjassot, Valencia, Spain; [2]Department of Pharmacy, Hospital Manises of Valencia, Spain; [3]Department of Pharmacy, University Hospital Doctor Peset of Valencia, Spain; [4]Foundation for the Promotion of Healthcare and Biomedical Research in the Valencian Community (FISABIO), Valencia, Spain; [5]Interuniversity Research Institute for Molecular Recognition and Technological Development, Polytechnic University of Valencia-University of Valencia, Valencia, Spain.

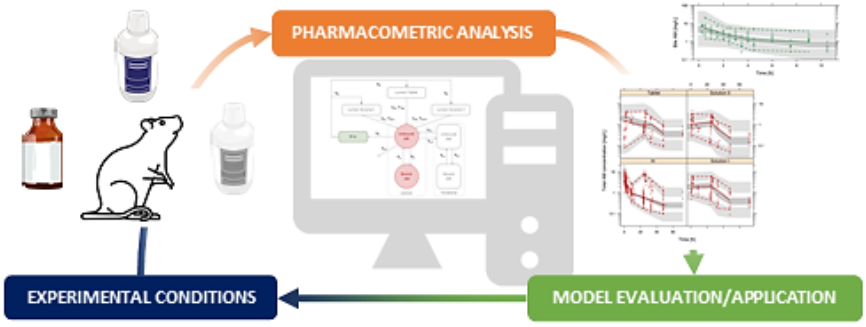

Eur J Pharm Sci. 2022 Jul 1; 174:106198

1. INTRODUCTION

Amiodarone (AM), an iodine-rich benzofuran derivative, is class III antiarrhythmic medication, which is indicated for the treatment of life-threatening ventricular arrhythmia, supraventricular arrhythmia and atrial fibrillation. Despite having demonstrated a high effectiveness as antiarrhythmic medication in clinical practice, long-term therapy can result in a wide variety of side effects affecting several organ systems, some of which can be life threatening (Cahoon et al., 2007; Mujovic et al., 2020). Commercially available AM presentations include IV and OR formulations, the latter indicated in patients with mild and moderate heart disease, whereas IV route of administration is preferred in hemodynamically destabilizing ventricular tachycardia or ventricular fibrillation or when patients are unable to take OR medications (Mujovic et al., 2020). AM is given as a monotherapy or in combination with other drugs (e.g. β-adrenergic antagonists, calcium channel blocking agents or digoxin), showing its effectiveness in several clinical trials (Andrade et al., 2010; Cappelletto et al., 2021; Hamer et al., 1989; Kim et al., 2014; Lupercio et al., 2018; Mitchell et al., 2005; Mooss et al., 1990; Somberg and Molnar, 2016; Somberg et al., 2004). In addition, AM is one of the most effective pharmacological agents with extensive off-label use for the treatment of supraventricular arrhythmia in children (Etheridge et al., 2001; Moak, 2000; Saul et al., 2005). Despite its outstanding pharmacological properties, the slow onset of its antiarrhythmic action, the presence of multiple drug-drug interactions and several safety concerns, including ophthalmological, pulmonary, and neurological toxicity after its chronic administration has limited its use in clinical practice (Mujovic et al., 2020).

AM according to the Biopharmaceutics Classification System (Amidon et al., 1995) is a class III drug, with low solubility (0.35 mg/mL) (Wang et al., 2017) and high permeability drug due to its high lipophilicity, which explains its large distribution into highly perfused and lipophilic tissues. Approved dosing schedules for maintenance regimens ranged from 200 to 400 mg/day (Siddoway, 2003). Slow and variable AM absorption has been reported, reaching a maximal plasma concentration between 3 and 7 h after OR administration and a moderate bioavailability (35–65%). High protein binding (>96%) has been reported (Lalloz et al., 1984; Veronese et al., 1988) predominately to albumin, but also to β-lipoprotein, and large accumulation of AM in liver, lung, adipose tissue, skeletal muscles and skin has been reported (Kodama et al., 1997; Plomp et al., 1987; Singh, 2006; Zimetbaum, 2012). Recently Hashimoto et al. (2021) found serum AM

concentrations increased in patients with hypertriglyceridemia state since as the concentration of LDL/VLDL increases, the fraction of drug bound increases restricting its distribution to other organs/tissues and its hepatic metabolism. AM is metabolized primarily to desethylamiodarone through the cytochrome P450 enzyme CYP3A4, and by CYP2C8. The major route of elimination is hepatic excretion into bile with some degree of hepatic recirculation and the renal excretion for AM is negligible in humans (Haffajee, 1987; Pollak et al., 2000; Somani, 1989). A therapeutic range of AM from 1.0 to 2.5 mg/L has been suggested (Haffajee et al., 1983; Rotmensch et al., 1984), and adverse reactions have been reported at AM concentrations above 2.6 mg/L (Falik et al., 1987; Greenberg et al., 1987; Rotmensch et al., 1984). Complexity in AM pharmacokinetics properties, including the reduced and variable OR absorption, associated with the high IIV in plasma levels, and its narrow therapeutic index due to the high risk of drug toxicity has limited the therapeutic usefulness of AM for its chronic administration. New OR formulations have been developed recently to improve the clinical use of AM focusing on the improvement of its water-solubility and bioavailability, demonstrating the need to improve the technological properties of OR formulations of AM for an optimal therapeutic use (Beig et al., 2015; Creteanu et al., 2015; Elgart et al., 2013; Patel et al., 2015a; Wang et al., 2017).

Preclinical characterization of complex PK properties through model-informed approaches has been widely considered during the drug development process and has demonstrated its utility for an optimal selection of dosing regimens in first-time-in-humans studies (Biliouris et al., 2018; Choi et al., 2019; Dong et al., 2011; Kang et al., 2021; Kwak et al., 2021; Li et al., 2019; Luu et al., 2012; Nirogi et al., 2020; Song et al., 2020; Zou et al., 2012). The advantage of this strategy becomes even more evident when non-linear kinetic processes come into play, since the classical approaches for data analysis are unable to accurately determine the magnitude of the effects together. In this regard, non-linear mixed effects modeling allows to quantitatively characterize the central tendency of the experimental data and the different sources of variability in order to accurately describe the observed behavior (Bonate, 1999). Therefore, the aims of this pre-clinical study are (i) to characterize the absorption properties of different orally administered formulations and at different dose levels, and (ii) to evaluate the impact of entero-hepatic circulation on the time-course of AM in rats in order to optimize the development of new OR formulations of AM.

2. MATERIALS AND METHODS

2.1. Study Design

All PK studies reported here adhere to the Principles of Laboratory Animal Care and were approved by the Research Committee of Animal Use from the Faculty of Pharmacy from University of Valencia (Spain). Data were obtained from the doctoral theses presented by Pascual-Costa (1994) and Chicano-Pia (1998). The experimental dataset consisted of 96 male Wistar rats of 20-weeks, 250-320 g body weight, including 985 AM observations in plasma (n = 901) and bile (n = 84). Wistar rats were housed under pathogen-free conditions, on a 12 h light/dark cycle, with controlled temperature (22-24 ◦C) and humidity (25%). Food and water were given ad libitum. IV and OR routes of administration of AM at different dose levels were evaluated, including single and multiple dosing regimens. Different sampling strategies were considered based on the route of administration and schedule, but all samples were collected to ensure the characterization of the PK profile of each animal. Table 1 summarizes the characteristics of the study, including, dose of AM administered for each administration route and number of animals enrolled and samples available in each group.

IV formulation was the commercial injectable of AM chlorhydrate (Trangorex®, 50 mg/ml). Three OR formulations of AM were evaluated, including the IV injectable (Trangorex®, Solution I, 50 mg/ml), a suspension from Trangorex® tablets (Tablet, 200 mg) and a solution with 5% Polysorbate 80 (Solution II, 5 mg/ml). The composition of the formulations is detailed in Table 2.

Table 1. Summary of study design characteristics

Route of administration	Schedule	Dose (mg)	Formulation	Sample	Nº Animals	Nº Observations
IV	SD	12.5	Solution I	Blood	16	231
			Solution I	Blood, Bile^{NC}	6	84
			Solution I	Blood, Bile^{CC}	6	82
OR	SD	10	Solution II	Blood	8	63
OR	SD	25	Tablet	Blood	8	68
OR	SD	25	Solution I	Blood	8	59
IV+IV	MD	12.5 + 12.5 (t=24h)	Solution I+ Solution I	Blood	8	93
IV+OR	MD	12.5 + 25 (t=24h)	Solution I +Tablet	Blood	8	102
IV+OR	MD	12.5 + 25 (t=24h)	Solution I +Solution I	Blood	8	103
IV+OR	MD	12.5 + 10 (t=24h)	Solution I +Solution II	Blood	8	100

IV: intravenous; OR: oral; SD: single dose; MD: multiple doses, n: number

Table 2. Composition of OR formulations of amiodarone administered

Formulations	Composition	
Solution I	Amiodarone chlorhydrate	0.150 g
	Polysorbate 80	0.300 g
	Benzyl alcohol	0.060 g
	Bidistilled water q.s.	3 mL
Tablet	Amiodarone chlorhydrate	0.200 g
	Lactose	0.071 g
	Cornstarch	0.066 g
	Polividone	0.006 g
	Colloidal silica	0.0024 g
	Magnesium stearate	0.0046 g
Solution II	Amiodarone chlorhydrate	5mg/mL
	Polysorbate 80	5%

2.2. Blood Sampling and Analytical Methods

Twenty-four hours before the administration of AM, the jugular vein, and portions of the bile duct and the small intestine were channeled in the different groups of rats. Prior to the surgical intervention, a dose of 2.7 ml/kg of anesthesia solution was administered by an intraperitoneal injection. The anesthesia was prepared by mixing solutions of 5 mg/ml diazepam, 50 mg/ml ketamine and 1 mg/ml atropine. After surgery and until drug administration, animals were kept fasted overnight with water freely available.

Drug administration of the three OR formulations was performed through a gastric tube. Blood samples (0.5 ml) were withdrawn into heparinized syringes from the jugular vein cannula, then centrifuged at 3000 r.p.m. for 5 min and stored at -20 ◦C. Bile samples were collected from two groups of rats with continuous enterohepatic cycle (CC group) and non-continuous enterohepatic cycle (NC group). In the CC group, the enterohepatic cycle was maintained, and the flowing bile was collected for 5 min before and 5 min after the administration of AM, disconnecting the bridging tubes of the bile duct and small intestine. In the NC group, the enterohepatic cycle was interrupted as soon as AM was administered, disconnecting the bridging tube from the bile duct catheter. Bile samples were stored at 4-8 ◦C (Chicano-Pia, 1998; Pascual-Costa, 1994).

The quantification of AM in plasma and bile samples was performed through high-performance liquid chromatography (HPLC) with spectrophotometric detection under ultraviolet light at a wavelength of 242 nm. The chromatographic method was validated following the recommendations of the International Conference on Harmonization (ICH, 1995) in terms of linearity, precision (intra- and interday), accuracy, limit of detection and quantification, specificity, interval and robustness. The limit of quantification was 0.1 μg/ml.

2.3. Pharmacokinetic Model

The modeling strategy used a previously developed population PK model (Campos Moreno et al., 2007) in rats after IV administration, which contained a two-compartment model with saturable dynamic plasma protein and linear tissular depot binding in the peripheral compartment. Equal PK parametrization of the disposition of AM was assumed as described by Campos Moreno et al. (2007). Then, the model (Figure 1) was adapted to describe the absorption kinetics of AM from the three OR formulations administered to the rats by

assuming linear absorption kinetics. Non-linear absorption kinetics, absorption latency and complex absorption processes (parallel absorption, precipitation, transit compartments, etc.) were also evaluated. Entero-hepatic reabsorption (EHR) of AM was modeled through linear kinetic processes of AM transition into and out of the bile compartment.

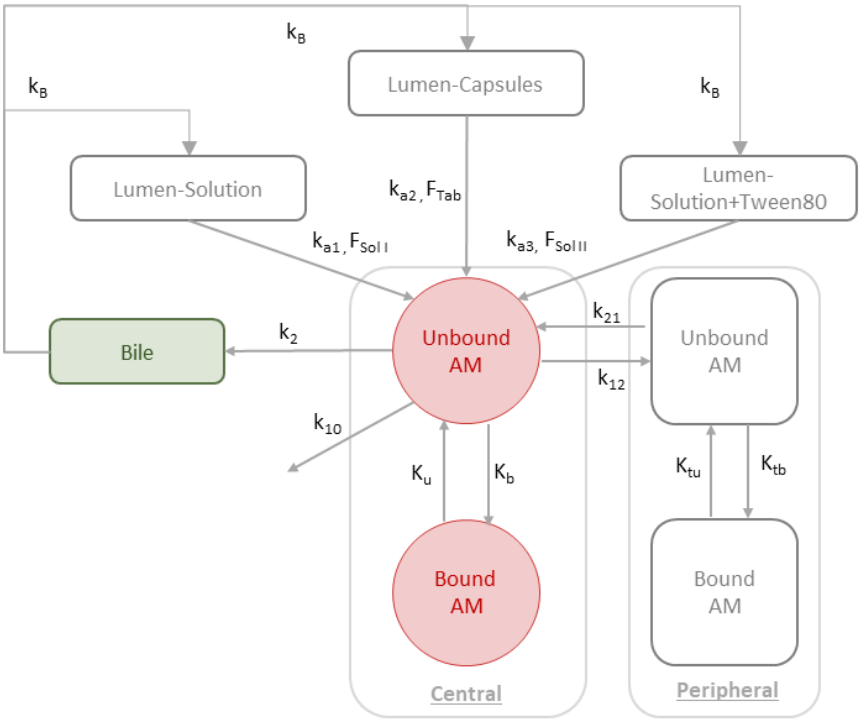

Figure 1. Schematic representation of the final PK model developed. k_B: first-order rate constant from bile, k_{a1}: first-order absorption rate constant of Solution I formulation, $F_{Sol\,I}$: OR bioavailability of Solution I formulation, k_{a2}: first-order absorption rate constant of Tablet formulation, F_{Tab}: OR bioavailability of Tablet formulation, k_{a3}: first-order absorption rate constant of Solution II formulation, $F_{Sol\,II}$: OR bioavailability of Solution II formulation, k_{10}: first-order elimination rate constant, k_2: first-order distribution constant, K_u: rate constant of unbinding in central compartment, K_b: rate constant of binding in central compartment, K_{tu}: rate constant of unbinding in peripheral compartment, K_{tb}: rate constant of binding in peripheral compartment, k_{21}: first-order distribution constant from central to peripheral compartment, k_{12}: first-order rate constant from peripheral to central compartment.

2.4. Data Analysis

Plasma observations were logarithmically transformed. All data analyses were performed based on the population approach with the software NONMEM® (v7.4, ICON plc Development Solutions, Hanover, MD, USA). The population PK parameters were estimated using the Stochastic Approximation of the Expectation Maximization and the Importance Sampling Estimation method.

IIV associated with the PK model parameters was modeled exponentially preventing negative values for the individual estimates, and RUV was described with an additive model on the logarithmic scale. The significance of the non-diagonal elements of the Ω variance-covariance matrix and subject specific RUV were also evaluated.

2.4.1. Model Selection

Model selection was based on physiological and pharmacological rationale with the principle of parsimony (Wade et al., 1994). The minimum value of the OFV provided by NONMEM® and approximately equal to -2LL was used together with the visual inspection of the GOF plots to perform model selection. A decrease in 6.63 points in -2LL value between two nested models differing in one parameter was considered significant at the 1% level.

2.4.2. Model Evaluation

Model evaluation of the selected models was performed through pc-VPC. Briefly, one thousand simulated datasets were simulated; the 2.5th, 50th, and 97.5th percentiles for every simulated study and sampling time-period were calculated. Then, the 95% prediction intervals of the percentiles were calculated and displayed graphically together with corresponding percentiles computed from raw data. In addition, the condition number, computed as the ratio of the largest eigenvalue to the smallest eigenvalue of the variance-covariance matrix, was calculated. A condition number less than 400 was targeted as it indicates good stability in the parameter estimates (Bonate, 1999). Precision of model parameter estimates, defined as the RSE, were calculated from the variance-covariance matrix (when possible) and from the analysis of one thousand simulated bootstrap datasets.

For graphical and statistical analysis, the R software (http://cran.r-project.org, version 4.0.3) was used. Pc-VPC and bootstrap analysis were performed using PsN.

3. RESULTS

3.1. Pharmacokinetic Model

The absorption process after the OR administration of three formulations of AM (Solution I, Tablet and Solution II) were described through a linear process using different first order absorption rate constants for each formulation (k_{a1-3}). The results suggest a major improvement in k_a when AM was administered as solution in the presence of 5% of Polysorbate 80 (Solution II: 250% increase) and 10% of Polysorbate 80 (Solution I: 62% increase) compared to Tablet formulation. Alternative mechanisms were also evaluated (i.e. zero-order absorption, non-linear kinetics, sequential/parallel first-and zero-order processes, transit compartment) but resulted in worse model performance ($p > 0.01$). AM showed a moderate OR bioavailability, which was parametrized independently for each formulation. Tablet showed less OR bioavailability (37%), compared to Solution I (40%) and Solution II (50%). These results reinforce the idea that OR bioavailability of AM could be enhanced by the presence of supramicellar concentration of surfactants that help to increase the AM solubility and dissolution process in the intestinal lumen (Elgart et al., 2013; Wang et al., 2017).

The structural model of AM disposition was adapted from a previous publication (Campos Moreno et al., 2007) in order to characterize PK longitudinal data of AM after IV and OR administration for new dose levels and dosing regimens (Table 1), which included a saturable and non-instantaneous plasma protein binding of AM (B_{max}, C_{50} and K_u) and linear tissue binding in the peripheral compartment (K_{tb} and K_{tu}). The first order binding rate constant (K_b) was derived as K_u/C_{50} and the binding saturation in plasma was modeled considering the available binding capacity. Peripheral distribution of AM occurred only between free fractions of the central and peripheral compartment through linear kinetics (k_{12}, k_{21}), suggesting a large distribution of AM into the peripheral compartment due to its high lipophilicity. The total protein binding in plasma was characterized through the B_{max} parameter, which was assumed as 5.05 mg based on the previous population PK model developed with IV data (Campos Moreno et al., 2007). A more detailed description of the equations governing the PK of AM has been previously published (Campos Moreno et al., 2007). The PK disposition model of AM was expanded by incorporating an EHR process of AM, which assumed a linear distribution process of AM from the unbound central compartment into the bile compartment and

its transit into the lumen through a first-order rate constant (k_B=12.9 h^{-1}). The absence of a gallbladder in rats leads to a constant distribution of the bile content into the lumen, preventing the implementation of more complex EHR models (Ibarra et al., 2021; Jain et al., 2011; Lehr et al., 2009; Okour et al., 2018). An alternative parametrization was evaluated, which included a k_B and a first-order constant into the lumen (k_7) but did not statistically improve the overall fit. The re-absorption of the intestinal process, once the AM returns into the lumen due to the EHR, was assumed to be equal to the initial intestinal absorption after oral AM administration (k_{a1}, k_{a2} and k_{a3}). A reduced fraction of the drug was distributed into the bile (F_{bile}=12.3%), which was calculated as follows (Lehr et al., 2009):

$$F_{bile} = \frac{k_B}{(k_B + k_{10} + k_{12} + K_b)}$$

Where k_B is 1.29x10^1 h^{-1}, k_{10} is 2.98x10^1 h^{-1}, k_{12} is 7.17 x10^1 h^{-1} and K_b is 3.6x10^{-1} $Lh^{-1}mg^{-1}$.

Interindividual random effects were associated to V_2 (46%), k_{12} (24%), K_u (13%), k_{a1} (39%), and k_{a2-3} (34%), showing a moderate-to-high IIV of PK parameters. Non-diagonal elements were explored but did not statistically improve the model performance. The RUV was 46% using an additive error model for log-transformed observations.

1.2. Pharmacokinetic Model Evaluation

Table 3 lists the estimates of the PK model parameters together with their corresponding precision according to the PK model developed (Figure 1). All PK parameters were statistically significant as the 95% confidence intervals (95% CI) did not include the null value. The results from the model evaluation exercise indicate that the model was capable of capturing the longitudinal profiles of the median and the dispersion of the data based on the pc-VPC (Figure 2) and the standard GOF plots (Figure 3).

Table 3. Final population PK parameters after subcutaneous administration of amiodarone in rats

	Population PK model estimates		Bootstrap results	
Fixed-effect	**Value**	**Shrinkage (%)**	**Median**	**95%CI**
k_{a1} (h^{-1})	1.33 x10^{-1}		1.34 x10^{-1}	[1.16-1.49] x10^{-1}
k_{a2} (h^{-1})	8.20 x10^{-2}		8.24 x10^{-2}	[7.69-8.87] x10^{-2}
k_{a3} (h^{-1})	2.05 x10^{-1}		2.02 x10^{-1}	[1.67-2.51] x10^{-1}
$F_{Sol\ I}$ (%)	4.02 x10^{1}		4.03 x10^{1}	[3.71-4.26] x10^{1}
F_{Tab} (%)	3.71 x10^{1}		3.75 x10^{1}	[2.79-4.12] x10^{1}
$F_{Sol\ II}$ (%)	5.05 x10^{1}		5.02 x10^{1}	[4.21-6.19] x10^{1}
k_{12} (h^{-1})	7.17 x10^{1} FIX		7.17 x10^{1} FIX	
k_{21} (h^{-1})	4.64 x10^{-1} FIX		4.64 x10^{-1} FIX	
V_2 (L)	1.44 x10^{-2} FIX		1.44 x10^{-2} FIX	
B_{max} (mg)	5.05 x10^{0} FIX		5.05 x10^{0} FIX	
C_{50} (mg/L)	1.49 x10^{1} FIX		1.49 x10^{1} FIX	
K_u (h^{-1})	5.42 x10^{0} FIX		5.42 x10^{0} FIX	
K_{tb} (h^{-1})	1.63 x10^{-1} FIX		1.63 x10^{-1} FIX	
K_{tu} (h^{-1})	9.87 x10^{-2} FIX		9.87 x10^{-2} FIX	
k_B (h^{-1})	1.29 x10^{1}		1.28 x10^{1}	[1.07-1.42] x10^{1}
k_{10} (h^{-1})	2.98 x10^{1} FIX		2.98 x10^{1} FIX	
Interindividual variability				
k_{a1} (%)	39	16	41	[31-56]
k_{a2-3} (%)	34	21	35	[27-41]
k_{12} (%)	24	32	27	[19-33]
V_2 (%)	46	26	42	[31-58]
K_u (%)	13	38	12	[9-15]
Residual unexplained variability				
Plasma (%)	46	7	45	[42-49]

3.3. Simulation-Based Analysis of Unbound/Bound Fractions of AM

The typical longitudinal ratios between the unbound and bound fractions of AM in the central and peripheral compartments of each OR formulation is depicted in Figure 4, including dose levels evaluated in the current population PK analysis (12.5 and 25 mg) and extrapolated dose levels (50 and 100 mg) of AM. A rapid decrease in the unbound/bound ratio at both compartments is explained by the binding process of AM, achieving steady-state conditions around 24 h, showing the slow binding process of AM. These results show a slight increase in the unbound fraction with the dose level in the central

compartment and irrespective of the OR formulation considered, as expected due to the non-linear binding kinetics of the population PK model. Due to the linear kinetic binding in the peripheral compartment, no differences were observed between the dose levels considered.

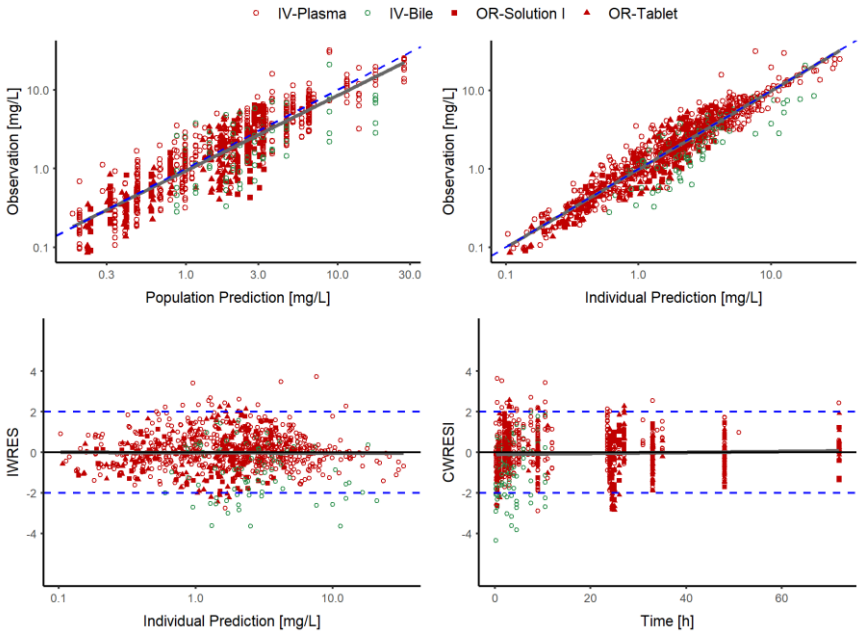

Figure 2. GOF plots of the final population PK model of amiodarone in rats for each OR formulation. The grey solid line represents the non-linear regression, and the blue dotted line represents the line of identity. IWRES: individual weighted residuals, CWRESI: conditional weighted residuals.

4. DISCUSSION

AM is a highly lipophilic drug, showing a unique PK profile. There is a good correlation between plasma concentration of AM and its OR maintenance dose and higher plasma concentration of the drug provides a more effective arrhythmia suppression, but it is associated with a higher risk of drug toxicity. Therefore, in routine clinical practice, the monitoring of total cumulative dose may be more useful than monitoring the plasma AM levels. Hence, a better knowledge of the PK of AM, both in absorption and elimination, will reduce variability and improve dosage adjustment in patients.

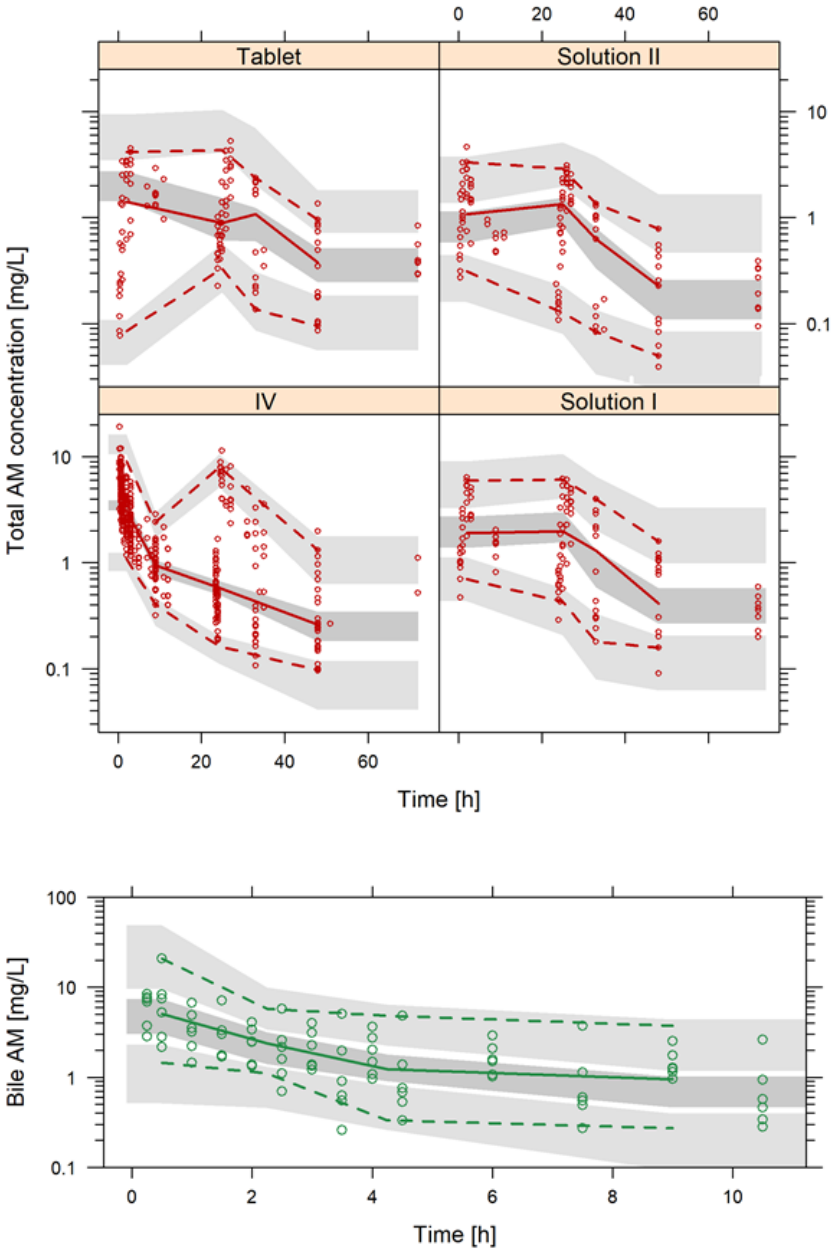

Figure 3. Prediction-corrected visual predictive check of the final population PK model. Shaded areas represent the 95% prediction intervals of the 2.5th, 50th and 97.5th percentiles of the simulated data. Circles represent AM observations and lines represent the 2.5th, 50th and 97.5th percentiles of the raw data.

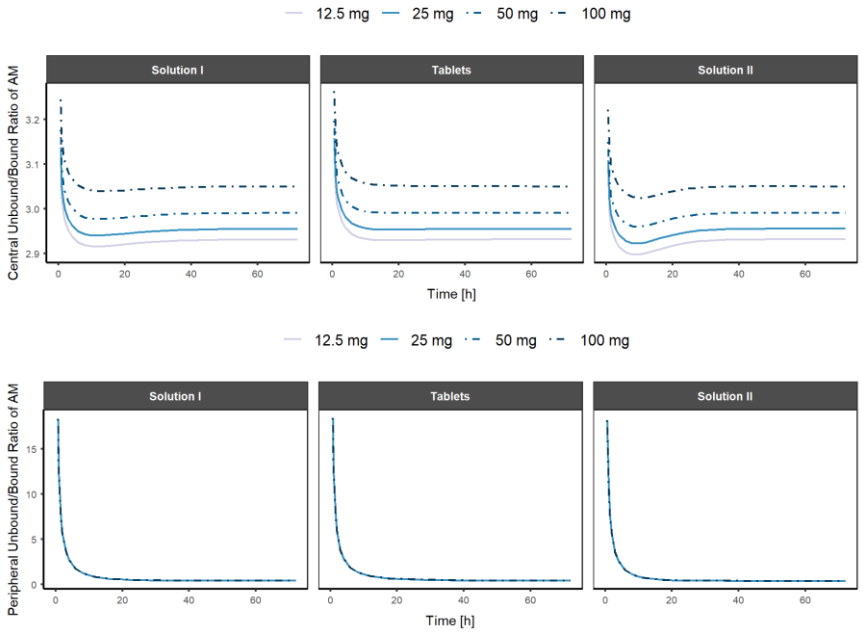

Figure 4. Model predicted unbound/bound ratio of amiodarone in the central (upper) and peripheral (bottom) compartments for each OR formulation after single-dose administration of four dose levels.

In addition, the approved IV formulation of AM contains benzyl alcohol, which is contraindicated in neonates and should be used with caution in infants and children up to 3 years old (Electronic Medicines Compendium, 2022). Therefore, the development of OR formulations able to increase the OR bioavailability of AM are highly needed.

Complex PK processes of drugs, which have not been properly characterized, may increase the IIV of PK parameters and generate unprecise model-predictions. In this sense, the quantitative modeling framework should encompass the biological complexity observed in experimental data in order to serve as a valid tool in the decision-making process of drug development. A population PK model has been successfully applied to characterize the absorption and EHR processes of different OR formulations of AM in rats by adapting a previous population PK model that accounted for the non-linear and linear distribution processes of AM after IV administration. The population PK model assumes different first-order absorption rates constant for each absorption (k_{a3}= $2.05 \cdot 10^{-1}$ h^{-1}). Similar results were obtained for other lipophilic active principles when co-formulated with surfactants (Alqahtani et al., 2013; Chen et al., 2018; Patel et al., 2015b;

Rahman et al., 2016). The current EHR represents the distribution of free AM from the central compartment into the bile and then, into the lumen based on the evidence collected in CC and NC groups. The lack of gallbladder in rats allows assume the continuous emptying of AM into the lumen, which limited the implementation of complex EHR models when the gallbladder exists (Ide et al., 2009; Lehr et al., 2009; Okour et al., 2018; Papathanasiou et al., 2016). The current population PK model quantifies the fraction (12.3%) of AM that suffers EHR and the respective fraction of AM that is metabolized. This result confirms the significant contribution of EHR in the disposition of AM, although due to the absence of experimental observations in the lumen, the fraction excreted via feces could not be estimated.

The development of OR formulations able to increase AM solubility and, ultimately, its absorption rate has been part of research activity recently (Creteanu et al., 2015; Elgart et al., 2013; Wang et al., 2017). In this sense, an increase of absorption rate of drugs in OR formulation with Polysorbate 80 has been hypothesized to be related to the alteration of the intestinal mucus barrier and mucosal barrier, but these results require further clarification (Martin-Algarra et al., 1995; Zhu et al., 2021). On the other hand, the addition of 5% of Polysorbate 80 resulted in a 2.50-fold increase on k_a and 35% increase in its bioavailability compared to Tablet formulation. However, higher concentrations (10%) of Polysorbate 80 in Solution I compared to Tablet formulation only improved by a 1.62-fold the k_a (and 8% its bioavailability), suggesting that increased concentrations of Polysorbate 80 in AM formulations may compromised the absorption process. This phenomenon may be explained by the lipophilic properties of AM and the intramicellar solubilization. Based on this study, 5% concentrations of Polysorbate improve the solubilization of AM in lumen. Higher concentrations of Polysorbate 80 (10%) lead to higher formation of micelles, affecting the release of AM out of the micelles, becoming the PK rate-limiting process (Martin-Algarra et al., 1995).

Model-based approaches currently represent one of the most demanding and increasing areas in the drug discovery and development process. The ability to determine from a very simplistic perspective to a more detailed and complex manner the mechanisms involved in the time-course of a drug clearly contribute to a more efficient and rationale decision-making process. Thus, the re-use of PK models and its integration into new experimental evidence enhances the potential impact and recognition from adjoining areas. The population PK

model externally validates the disposition PK model previously proposed for AM in rats (Campos Moreno et al., 2007) to quantify the contribution of OR formulations and EHR of AM. Similar final parameter estimates were observed between both approaches, demonstrating the adequacy of the population PK model of AM in rats.

Despite the study design characteristics, the reduced number of treatment groups evaluated the PK properties of AM after multiple dose regimens, which might be of relevance in order to better understand how the binding kinetics might be affected when complex and multiple dose levels are administered. Although all formulations contained a polysorbate 80 concentration higher than the CMC, the impact of polysorbate 80 on the AM metabolism could not be assessed due to the lack of hepatic microsomes measurements after its OR and IV administration and the absence of a formulation without polysorbate 80. The complexity of the surgical intervention to collect bile samples resulted in a limited number of observations helping to characterize the EHR process of AM. An 8-fold dose increase (from 12.5 to 100 mg) implies that the unbound/bound ratio of AM only changes by 3% (Figure 4), indicating that at the usual doses the protein plasma binding is not likely to be saturated. In this sense, probably, new formulations that increase the bioavailability of AM do not significantly modify the fractions of free AM in plasma nor the time in which the equilibrium between the free and bound fraction is reached. Alternative preclinical models are encouraged in order to characterize the allometric relationship and the impact of gallbladder emptying that would help to establish accurate and reliable predictions in humans.

5. CONCLUSIONS

In conclusion, the current population PK model of AM demonstrated the absorption enhancement when AM is formulated with supramicellar concentrations of Polysorbate 80 (Solution II) compared to commercially available OR formulation (Tablet). The study design allowed to characterize the EHR of AM and its contribution in the overall AM disposition. The mathematical framework developed based on preclinical evidence on AM could help to optimize the development of new OR formulations able to increase the OR bioavailability of AM at the preclinical and clinical level and assess whether the impact of EHR processes is similar across different species. Furthermore, this study may contribute to the development of OR solution formulations of AM that could improve the benefit/risk balance of AM and its adherence in pediatric patients.

6. CREDIT AUTHORSHIP CONTRIBUTION STATEMENT

Karine Rodríguez-Fernández: Methodology, Software, Formal analysis, Investigation, Writing – original draft, Writing – review & editing. Elena Gras-Colomer: Writing – original draft, Writing – review & editing. Mónica Climente-Martí: Supervision, Writing – original draft, Writing – review & editing. Victor Mangas-Sanjuán: Methodology, Software, Formal analysis, Writing – original draft, Writing – review & editing. Matilde Merino-Sanjuán: Conceptualization, Methodology, Writing – original draft, Writing – review & editing.

7. DECLARATION OF COMPETING INTEREST

Authors declare no conflict of interest.

8. REFERENCES

Alqahtani, S., Alayoubi, A., Nazzal, S., Sylvester, P.W., Kaddoumi, A., 2013. Nonlinear absorption kinetics of self-emulsifying drug delivery systems (SEDDS) containing tocotrienols as lipophilic molecules: *in vivo* and *in vitro* studies. AAPS J. 15, 684–695.

Amidon, G.L., Lennernas, H., Shah, V.P., Crison, J.R., 1995. A theoretical basis for a biopharmaceutic drug classification: the correlation of *in vitro* drug product dissolution and *in vivo* bioavailability. Pharm. Res. 12, 413–420.

Andrade, J.G., Connolly, S.J., Dorian, P., Green, M., Humphries, K.H., Klein, G.J., Sheldon, R., Talajic, M., Kerr, C.R., 2010. Antiarrhythmic use from 1991 to 2007: insights from the Canadian registry of atrial fibrillation (CARAF I and II). Heart Rhythm. 7, 1171–1177.

Beig, A., Agbaria, R., Dahan, A., 2015. The use of captisol (SBE7-β-CD) in oral solubility-enabling formulations: comparison to HPβCD and the solubility-permeability interplay. Eur. J. Pharm. Sci. 77, 73–78.

Biliouris, K., Nestorov, I., Naik, H., Dai, D., Xiao, G., Wang, Q., Pellerin, A., Rabah, D., Lesko, L.J., Trame, M.N., 2018. A pre-clinical quantitative model predicts the pharmacokinetics/pharmacodynamics of an anti-BDCA2 monoclonal antibody in humans. J. Pharmacokinet. Pharmacodyn. 45, 817–827.

Bonate, P.L., 1999. The effect of collinearity on parameter estimates in nonlinear mixed effect models. Pharm. Res. 16, 709–717.

Cahoon, W., Flattery, M.P., Hess, M.L., 2007. Amiodarone: development, clinical indications, and safety. Prog. Cardiovasc. Nurs. 22, 173–176.

Campos Moreno, E., Merino Sanjuan, M., Merino, V., Nacher, A., Martín Algarra, R.V., Casabó, V.G., 2007. Population modelling to describe pharmacokinetics of amiodarone in rats: relevance of plasma protein and tissue depot binding. Eur. J. Pharm. Sci. 30, 190–197.

Cappelletto, C., Gregorio, C., Barbati, G., Romani, S., De Luca, A., Merlo, M., Mestroni, L., Stolfo, D., Sinagra, G., 2021. Antiarrhythmic therapy and risk of cumulative ventricular arrhythmias in arrhythmogenic right ventricle cardiomyopathy. Int. J. Cardiol. Creteanu, A., T`antaru, G., Vieriu, M., Panainte, A.D., Ochiuz, L., 2015. Optimization of the preparation of kollidon SR-based amiodarone hydrochloride tablets with sustained release. Rev. Med. Chir. Soc. Med. Nat. Iasi 119, 1161–1165.

Chen, X.Q., Ziemba, T., Huang, C., Chang, M., Xu, C., Qiao, J.X., Wang, T.C., Finlay, H.J., Salvati, M.E., Adam, L.P., Gudmundsson, O., Hageman, M.J., 2018. Oral delivery of highly lipophilic, poorly water-soluble drugs: self-emulsifying drug delivery systems to improve oral absorption and enable high-dose toxicology studies of a cholesteryl ester transfer protein inhibitor in preclinical species. J. Pharm. Sci. 107, 1352–1360.

Chicano-Piá, P.V., 1998. Study of the first pass effect and the enterohepatic cycle of amiodarone in the rat. (Doctoral Thesis). University of Valencia, Valencia, Spain, p. 180.

Choi, S., Han, S., Jeon, S., Yim, D.S., 2019. Quantitative prediction of human pharmacokinetics and pharmacodynamics of CKD519, a potent inhibitor of cholesteryl ester transfer protein (CETP). Pharmaceutics 11.

Dong, J.Q., Salinger, D.H., Endres, C.J., Gibbs, J.P., Hsu, C.P., Stouch, B.J., Hurh, E., Gibbs, M.A., 2011. Quantitative prediction of human pharmacokinetics for monoclonal antibodies: retrospective analysis of monkey as a single species for first-in-human prediction. Clin. Pharmacokinet. 50, 131–142.

Electronic Medicines Compendium, 2022. Amiodarone hydrochloride 50mg/ml concentrate for solution for injection/infusion. SmPC. Available online: https://www.medicines.org.uk/emc/product/3940/smpc#gref (accessed 2022 March 13).

Elgart, A., Cherniakov, I., Aldouby, Y.,Domb, A.J., Hoffman, A., 2013. Improved oral bioavailability of BCS class 2 compounds by self nano-emulsifying drug delivery systems (SNEDDS): the underlying mechanisms for amiodarone and talinolol. Pharm. Res. 30, 3029–3044.

Etheridge, S.P., Craig, J.E., Compton, S.J., 2001. Amiodarone is safe and highly effective therapy for supraventricular tachycardia in infants. Am. Heart J. 141, 105–110.

Falik, R., Flores, B.T., Shaw, L., Gibson, G.A., Josephson, M.E., Marchlinski, F.E., 1987. Relationship of steady-state serum concentrations of amiodarone and desethylamiodarone to therapeutic efficacy and adverse effects. Am. J. Med. 82, 1102–1108.

Greenberg, M.L., Lerman, B.B., Shipe, J.R., Kaiser, D.L., DiMarco, J.P., 1987. Relation between amiodarone and desethylamiodarone plasma concentrations and electrophysiologic effects, efficacy and toxicity. J. Am. Coll. Cardiol. 9, 1148–1155.

Haffajee, C.I., 1987. Clinical pharmacokinetics of amiodarone. Clin. Cardiol. 10, 16–19.

Haffajee, C.I., Love, J.C., Canada, A.T., Lesko, L.J., Asdourian, G., Alpert, J.S., 1983. Clinical pharmacokinetics and efficacy of amiodarone for refractory tachyarrhythmias. Circulation 67, 1347–1355.

Hamer, A.W., Arkles, L.B., Johns, J.A., 1989. Beneficial effects of low dose amiodarone in patients with congestive cardiac failure: a placebo-controlled trial. J. Am. Coll. Cardiol. 14, 1768–1774.

Hashimoto, N., Doki, K., Kawano, S., Aonuma, K., Ieda, M., Homma, M., 2021. Increased serum amiodarone concentration in hypertriglyceridemic patients: effects of drug distribution to serum lipoproteins. Clin. Transl. Sci.

Ibarra, M., Troconiz, I.F., Fagiolino, P., 2021. Enteric reabsorption processes and their impact on drug pharmacokinetics. Sci. Rep. 11, 5794.

ICH, E.M.A., 1995. CPMP/ICH/381/95- ICH Topic Q2 (R1) validation of analytical procedures: text and methodology. Available online: https://www.ema.europa.eu /en/documents/scientific-guideline/ich-q-2-r1-validation-analytical-procedures-text -methodology-step-5_en.pdf (accessed 2022 March 10).

Ide, T., Sasaki, T., Maeda, K., Higuchi, S., Sugiyama, Y., Ieiri, I., 2009. Quantitative population pharmacokinetic analysis of pravastatin using an enterohepatic circulation model combined with pharmacogenomic Information on SLCO1B1 and ABCC2 polymorphisms. J. Clin. Pharmacol. 49, 1309–1317.

Jain, L., Woo, S., Gardner, E.R., Dahut, W.L., Kohn, E.C., Kummar, S., Mould, D.R., Giaccone, G., Yarchoan, R., Venitz, J., Figg, W.D., 2011. Population pharmacokinetic analysis of sorafenib in patients with solid tumours. Br. J. Clin. Pharmacol. 72, 294–305.

Kang, D.W., Ryu, C.H., Kim, J.H., Choi, G.W., Kim, S., Chon, C.H., Kim, J.H., Cho, H.Y., 2021. Pharmacokinetic-pharmacodynamic modeling approach for dose prediction of the optimal long-acting injectable formulation of finasteride. Int. J. Pharm. 601, 120527.

Kim, H.L., Seo, J.B., Chung, W.Y., Kim, S.H., Kim, M.A., Zo, J.H., 2014. The incidence and predictors of overall adverse effects caused by low dose amiodarone in real-world clinical practice. Korean J. Intern. Med. 29, 588–596.

Kodama, I., Kamiya, K., Toyama, J., 1997. Cellular electropharmacology of amiodarone. Cardiovasc. Res. 35, 13–29.

Kwak, E.Y., Kim, M.J., Park, J.H., Jung, H.W., Jung, M.E., 2021. Target-mediated drug disposition (TMDD) modeling of an anti-TFPI antibody (MG1113) in cynomolgus monkeys to predict human pharmacokinetics and pharmacodynamics. J. Thromb. Haemost. JTH.

Lalloz, M.R., Byfield, P.G., Greenwood, R.M., Himsworth, R.L., 1984. Binding of amiodarone by serum proteins and the effects of drugs, hormones and other interacting ligands. J. Pharm. Pharmacol. 36, 366–372.

Lehr, T., Staab, A., Tillmann, C., Trommeshauser, D., Schaefer, H.G., Kloft, C., 2009. A quantitative enterohepatic circulation model: development and evaluation with tesofensine and meloxicam. Clin. Pharmacokinet. 48, 529–542.

Li, C., Zhang, C., Deng, R., Leipold, D., Li, D., Latifi, B., Gao, Y., Zhang, C., Li, Z., Miles, D., Chen, S.C., Samineni, D., Wang, B., Agarwal, P., Lu, D., Prabhu, S., Girish, S., Kamath, A.V., 2019. Prediction of human pharmacokinetics of antibody-drug conjugates from nonclinical data. Clin. Transl. Sci. 12, 534–544.

Lupercio, F., Romero, J., Peltzer, B., Maraboto, C., Briceno, D., Villablanca, P., Ferrick, K., Gross, J.N., Kim, S., Fisher, J., Di Biase,

L., Krumerman, A., 2018. Efficacy and safety outcomes of direct oral anticoagulants and amiodarone in patients with atrial fibrillation. Am. J. Med. 131, 573 e571-573.e578.

Luu, K.T., Bergqvist, S., Chen, E., Hu-Lowe, D., Kraynov, E., 2012. A model-based approach to predicting the human pharmacokinetics of a monoclonal antibody exhibiting target-mediated drug disposition. J. Pharmacol. Exp. Ther. 341, 702–708.

Martin-Algarra, R.V., Pascual-Costa, R.M., Merino, M., Casabó, V.G., 1995. Effects of polysorbate 80 on amiodarone intestinal absorption in the rat. Int. J. Pharm. 122, 1–8.

Mitchell, L.B., Exner, D.V., Wyse, D.G., Connolly, C.J., Prystai, G.D., Bayes, A.J., Kidd, W. T., Kieser, T., Burgess, J.J., Ferland, A., MacAdams, C.L., Maitland, A., 2005. Prophylactic oral amiodarone for the prevention of arrhythmias that begin early after revascularization, valve replacement, or repair: PAPABEAR: a randomized controlled trial. JAMA 294, 3093–3100.

Moak, J.P., 2000. Supraventricular tachycardia in the neonate and infant. Prog. Pediatr. Cardiol. 11, 25–38. Mooss, A.N., Mohiuddin, S.M., Hee, T.T., Esterbrooks, D.J., Hilleman, D.E., Rovang, K.S., Sketch, M.H., 1990. Efficacy and tolerance of high-dose intravenous amiodarone for recurrent, refractory ventricular tachycardia. Am. J. Cardiol. 65, 609–614.

Mujovic, N., Dobrev, D., Marinkovic, M., Russo, V., Potpara, T.S., 2020. The role of amiodarone in contemporary management of complex cardiac arrhythmias. Pharmacol. Res. 151, 104521.

Nirogi, R., Bhyrapuneni, G., Muddana, N.R., Manoharan, A., Shinde, A.K., Mohammed, A.R., Padala, N.P., Ajjala, D.R., Subramanian, R., Palacharla, V.R.C., 2020. Absorption, distribution, metabolism, excretion (ADME), drug-drug interaction potential and prediction of human pharmacokinetics of SUVN-G3031, a novel histamine 3 receptor (H(3)R) inverse agonist in clinical development for the treatment of narcolepsy. Eur. J. Pharm. Sci. 152, 105425.

Okour, M., Jacobson, P.A., Ahmed, M.A., Israni, A.K., Brundage, R.C., 2018. Mycophenolic acid and its metabolites in kidney transplant recipients: a semimechanistic enterohepatic circulation model to improve estimating exposure. J. Clin. Pharmacol. 58, 628–639.

Papathanasiou, T., Juul, R.V., Gabel-Jensen, C., Kreilgaard, M., Lund, T.M., 2016. Population pharmacokinetic modelling of

morphine, gabapentin and their combination in the rat. Pharm. Res. 33, 2630–2643.

Pascual-Costa, R.M., 1994. Oral bioavailability of amiodarone in the rat. (Doctoral Thesis). University of Valencia, Valencia, Spain, p. 323.

Patel, A., Shelat, P., Lalwani, A., 2015a. Development and optimization of solid self nanoemulsifying drug delivery (S-SNEDDS) using d-optimal design for improvement of oral bioavailability of amiodarone hydrochloride. Curr. Drug Deliv. 12, 745–760.

Patel, A.R., Doddapaneni, R., Andey, T., Wilson, H., Safe, S., Singh, M., 2015b. Evaluation of self-emulsified DIM-14 in dogs for oral bioavailability and in Nu/nu mice bearing stem cell lung tumor models for anticancer activity. J. Controll. Release 213, 18–26 official journal of the Controlled Release Society.

Plomp, T.A., Wiersinga, W.M., Van Rossum, J.M., Maes, R.A., 1987. Pharmacokinetics and body distribution of amiodarone and desethylamiodarone in rats after oral administration. In Vivo 1, 265–279 (Brooklyn).

Pollak, P.T., Bouillon, T., Shafer, S.L., 2000. Population pharmacokinetics of long-term oral amiodarone therapy. Clin. Pharmacol. Ther. 67, 642–652.

Rahman, M.A., Mujahid, M., Hussain, A., 2016. Self-emulsifying pellets prepared by extrusion/spheronization: *in vitro/in vivo* evaluation. Recent Pat. Drug Deliv. Formul. 10, 245–252.

Rotmensch, H.H., Belhassen, B., Swanson, B.N., Shoshani, D., Spielman, S.R., Greenspon, A.J., Greenspan, A.M., Vlasses, P.H., Horowitz, L.N., 1984. Steady-state serum amiodarone concentrations: relationships with antiarrhythmic efficacy and toxicity. Ann. Intern. Med. 101, 462–469.

Saul, J.P., Scott, W.A., Brown, S., Marantz, P., Acevedo, V., Etheridge, S.P., Perry, J.C., Triedman, J.K., Burriss, S.W., Cargo, P., Graepel, J., Koskelo, E.K., Wang, R., 2005. Intravenous amiodarone for incessant tachyarrhythmias in children: a randomized, double-blind, antiarrhythmic drug trial. Circulation 112, 3470–3477.

Siddoway, L.A., 2003. Amiodarone: guidelines for use and monitoring. Am. Fam. Physician 68, 2189–2196.

Singh, B.N., 2006. Amiodarone: a multifaceted antiarrhythmic drug. Curr. Cardiol. Rep. 8, 349–355.

Somani, P., 1989. Basic and clinical pharmacology of amiodarone: relationship of antiarrhythmic effects, dose and drug concentrations to intracellular inclusion bodies. J. Clin. Pharmacol. 29, 405–412. Somberg, J., Molnar, J., 2016. Sotalol versus amiodarone in treatment of atrial fibrillation. J. Atr. Fibrillation 8, 1359.

Somberg, J.C., Timar, S., Bailin, S.J., Lakatos, F., Haffajee, C.I., Tarjan, J., Paladino, W.P., Sarosi, I., Kerin, N.Z., Borbola, J., Bridges, D.E., Molnar, J., 2004. Lack of a hypotensive effect with rapid administration of a new aqueous formulation of intravenous amiodarone. Am. J. Cardiol. 93, 576–581.

Song, L., Yao, X., Liu, Y., Zhong, W., Jiang, J., Liu, H., Zhou, H., Shi, C., Zong, K., Wang, C., Ma, C., Liu, D., Hu, P., 2020. Translational prediction of first-in-human pharmacokinetics and pharmacodynamics of janagliflozin, a selective SGLT2 inhibitor, using allometric scaling, dedrick and PK/PD modeling methods. Eur. J. Pharm. Sci. 147, 105281.

Veronese, M.E., McLean, S., Hendriks, R., 1988. Plasma protein binding of amiodarone in a patient population: measurement by erythrocyte partitioning and a novel glass-binding method. Br. J. Clin. Pharmacol. 26, 721–731.

Wade, J.R., Beal, S.L., Sambol, N.C., 1994. Interaction between structural, statistical, and covariate models in population pharmacokinetic analysis. J. Pharmacokinet. Biopharm. 22, 165–177.

Wang, D., Chen, G., Ren, L., 2017. Preparation and characterization of the sulfobutylether-β-cyclodextrin inclusion complex of amiodarone hydrochloride with enhanced oral bioavailability in fasted state. AAPS PharmSciTech. 18, 1526–1535.

Zhu, Y.T., Yuan, Y.Z., Feng, Q.P., Hu, M.Y., Li, W.J., Wu, X., Xiang, S.Y., Yu, S.Q., 2021. Food emulsifier polysorbate 80 promotes the intestinal absorption of mono-2- ethylhexyl phthalate by disturbing intestinal barrier. Toxicol. Appl. Pharmacol. 414, 115411.

Zimetbaum, P., 2012. Antiarrhythmic drug therapy for atrial fibrillation. Circulation 125, 381–389.

Zou, P., Zheng, N., Yu, Y., Yu, S., Sun, W., McEachem, D., Yang, Y., Yu, L.X., Wang, S., Sun, D., 2012. Preclinical pharmacokinetics of MI-219, a novel human double minute 2 (HDM2) inhibitor and prediction of human pharmacokinetics. J. Pharm. Pharm. Sci. 15,

265–280 a publication of the Canadian Society for Pharmaceutical Sciences, Societe canadienne des sciences pharmaceutiques.

Chapter 3: New insights into the role of VKORC1 polymorphisms for optimal warfarin dose selection in Caribbean Hispanic patients through an external validation of a population PK/PD model

Karine Rodríguez-Fernández[1], Gledys Reynaldo-Fernández[2], Stephanie Reyes-González[3], Camila de las Barreras[2], Leyanis Rodríguez-Vera[4], Cornelis Vlaar[3], Jean-Christophe M. Monbaliu[5], Torsten Stelzer[3,6], Jorge Duconge[3], Victor Mangas-Sanjuan[1,7]

Authors Affiliation: [1]Department of Pharmacy and Pharmaceutical Technology and Parasitology, University of Valencia, Valencia, Spain; [2]Institute of Pharmacy and Foods, University of Havana, Havana 11300, Cuba; [3]Department of Pharmaceutical Sciences, School of Pharmacy, University of Puerto Rico - Medical Sciences Campus, San Juan 00936, PR, USA; [4]Center for Pharmacometrics and System Pharmacology at Lake Nona (Orlando), Department of Pharmaceutics, College of Pharmacy, University of Florida, Orlando, FL 32827, USA; [5]Center for Integrated Technology and Organic Synthesis, MolSys Research Unit, University of Liêge, B-4000 Liêge (Sart Tilman), Liêge, Belgium; [6]Crystallization Design Institute, Molecular Sciences Research Center, University of Puerto Rico, San Juan 00926, PR, USA; [7]Interuniversity Research Institute for Molecular Recognition and Technological Development, Polytechnic University of Valencia-University of Valencia, Valencia, Spain.

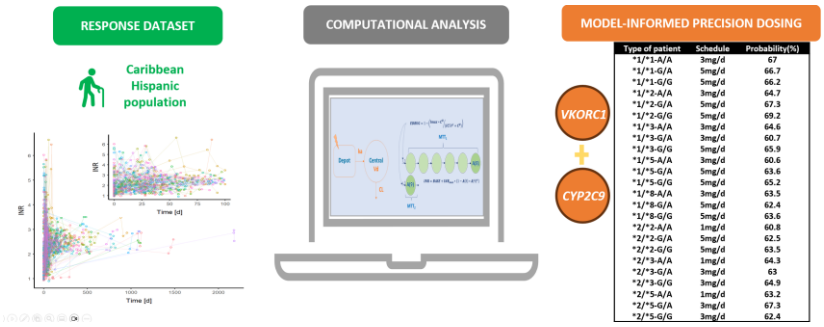

Type of patient	Schedule	Probability(%)
*1/*1-A/A	3mg/d	67
*1/*1-G/A	5mg/d	66.7
*1/*1-G/G	5mg/d	66.2
*1/*2-A/A	3mg/d	64.7
*1/*2-G/A	5mg/d	67.3
*1/*2-G/G	5mg/d	69.2
*1/*3-A/A	3mg/d	64.6
*1/*3-G/A	3mg/d	60.7
*1/*3-G/G	5mg/d	65.9
*1/*5-A/A	3mg/d	60.6
*1/*5-G/A	5mg/d	63.6
*1/*5-G/G	5mg/d	65.2
*1/*6-A/A	3mg/d	63.5
*1/*6-G/A	5mg/d	62.4
*1/*6-G/G	5mg/d	63.6
*2/*2-A/A	1mg/d	60.8
*2/*2-G/A	5mg/d	62.5
*2/*2-G/G	5mg/d	63.5
*2/*3-A/A	1mg/d	64.3
*2/*3-G/A	3mg/d	63
*2/*3-G/G	3mg/d	64.9
*2/*5-A/A	1mg/d	63.2
*2/*5-G/A	3mg/d	67.3
*2/*5-G/G	3mg/d	62.4

Biomed Pharmacother. 2024 Jan;170:115977

1. INTRODUCTION

Warfarin is an OR anticoagulant that has been used for over six decades to prevent thromboembolic events, such as stroke and deep vein thrombosis [1]. It works by inhibiting the synthesis of vitamin K-dependent clotting factors in the liver, thus reducing the production of blood clots [2]. Despite its widespread use, warfarin therapy is associated with several challenges, including a narrow therapeutic window, a high risk of bleeding, and significant interpatient variability in response [3,4]. The management of warfarin therapy involves maintaining a stable therapeutic INR range, which is typically between 2.0 and 3.0 for most indications [5]. However, achieving and maintaining this target range can be challenging due to the wide interpatient variability in warfarin exposure and response. This variability can be attributed to various factors, including age, sex, body weight, diet, comorbidities, and concomitant medications, as well as genetic variations [4].

The impact of genetic polymorphisms on warfarin response has been extensively studied, particularly for two relevant pharmacogenes: the *CYP2C9* gene encodes the cytochrome P450 isoform 2C9, a member of the cytochrome P450 superfamily of enzymes, and the *VKORC1* gene encodes the catalytic subunit 1 of the vitamin K epoxide reductase complex enzyme [3,4]. CYP2C9 is responsible for the metabolism of S-warfarin, the more active enantiomer of warfarin, and genetic polymorphisms in this gene have been associated with altered warfarin CL and higher INR values [4,6,7]. VKORC1 is responsible for the reduction of inactive vitamin K 2,3-epoxide to active vitamin K in the endoplasmic reticulum membrane and, therefore, is involved in the synthesis of vitamin K-dependent clotting factors [6]. Genetic polymorphisms affecting this gene have been associated with reduced sensitivity to warfarin [8,9]. Given the impact of genetic polymorphisms on warfarin response, the use of a pharmacogenetic-driven algorithm has been recommended to guide warfarin dosing in clinical settings, particularly in patients starting warfarin therapy [6,10–12]. The results of genetic testing for *CYP2C9* and *VKORC1* polymorphisms can be used to inform initial warfarin dosing and subsequent dose adjustments, leading to more effective and personalized therapy [6,11–14].

In recent years, population PK and PK/PD models that incorporate genetic information have been developed to predict optimal warfarin doses for individual patients, improving therapeutic efficacy and

reducing the risk of adverse events and thromboembolic events [7,15–19]. The models use a two-step approach: first, a suitable starting dose is estimated based on patient factors that have been previously identified as predictors for dose individualization, which is referred to as a priori individualization. Second, once the treatment has started, the dosing can be further personalized based on feedback observations from the patient, which is referred to as a posteriori individualization [7,15,20].

However, the development of a reliable and accurate PK/PD model that incorporates genetic information can be challenging due to the complex interplay between genetic and non-genetic factors affecting warfarin dosing. Furthermore, the predictive performance and comparability of different PK/PD models that incorporate genetic information have not been extensively evaluated. External validation studies are necessary to assess the accuracy and reliability of these models in different populations, allowing for more personalized and effective warfarin dosing. While PK/PD modeling has shown promise in predicting the optimal warfarin dose for individual patients, most of the studies have been conducted in Caucasian populations, with few studies focusing on non-Caucasian populations. Furthermore, there is limited data on the application of PK/PD models incorporating *CYP2C9* and *VKORC1* genotypes information in Caribbean Hispanic patients.

In this study, we aimed to (i) externally validate a population PK/PD model of INR after concomitant administration of warfarin in clinical practice, and (ii) evaluate optimal dosing strategies of warfarin in Caribbean Hispanic patients based on the selected covariates.

2. MATERIALS AND METHODS

2.1. Ethics Approval

This is a secondary analysis of a previous pharmacogenetic study of warfarin in Puerto Rican patients (IRB approval #A4070109). Proper safeguards against any potential violation of privacy and/or breach of confidentiality will be ensured. Authorization to use the data for the purpose stated in this project was previously obtained from individual patients by an informed consent process. Accordingly, the study was conducted following Helsinki's declaration for human subject protection in clinical surveys.

2.2. Study Design

Data for analyses were available from elderly patients, mostly males, followed upon at the anticoagulation clinic in the Veteran Affairs Caribbean Healthcare System (VACHS) at San Juan, PR. The patients received long-term warfarin anticoagulant therapy for different thromboembolic disorders in total weekly doses ranged from 7 to 82 mg, depending on the 24- or 48-hour dosing interval. Also, they carried eight different *CYP2C9* alleles (*1/*2, *1/*3, *1/*5, *1/*8, *2/*2, *2/*3, *2/ *5) and three *VKORC1* genotypes (G/A, G/G, A/A). Detailed information was recorded, including demographics and clinical response, evaluated longitudinally using the assessment tool INR.

2.3. Base Population PK/PD Model

Due to the absence of longitudinal PK information of warfarin in the current study, a previously published population PK model was implemented to retrieve the structural PK parameter estimates for each sub-group of *CYP2C9* genotype [20]. Given the absence of experimental PK values in the recruited patients, IIV was not associated with the PK parameters.

The structural definition of a previously published PD model for INR was implemented, which relies on an indirect response model coupled to a series of transit compartments to account for the delay between warfarin exposure and INR levels [7,17]. The effect of warfarin concentration was incorporated using a sigmoid response function based on the typical longitudinal PK levels for each *CYP2C9* genotype. IIV associated with the PK/PD model parameters was modeled exponentially preventing negative values for the individual estimates, and RUV was described with a proportional model. The population PD parameters were re-estimated as part of the development of the base PD model from the experimental information (INR) available in the recruited patients. The significance of the non-diagonal elements of the Ω variance-covariance matrix and subject specific RUV were also evaluated.

2.4. Final Population PK/PD Model

A numerical evaluation of the parameter-covariate relationship was performed manually in a univariate testing. A decrease in 6.63 units (p value <0.01) of OFV provided by NONMEM®. Covariates evaluated included: body weight, age, *CPY2C9* and *VKORC1* genotypes, race,

diabetes mellitus and smoking status. For categorical covariates the relative size of the different categories had to be larger than 5% to be considered for covariate testing. Covariates were also investigated for co-linearity. If two covariates had a correlation coefficient > |0.6| then one of the two covariates was excluded from testing.

The assessment of model adequacy was influenced by convergence stability, biological plausibility, and parsimony. An additional evaluation of standard GOF plots together with the NPDE plots was conducted [21].

Model evaluation of the selected models was performed through pc-VPC [22] with 1000 datasets obtained by Monte Carlo simulation using the final parameter estimates for both fixed and random effects. Each simulated dataset has the study design features (covariates, dosing times, PK sampling times) identical to those in the analysis dataset. For each simulated dataset, the 2.5th, 50th, and 97.5th percentiles of the simulated concentrations in each bin were calculated. Then, the 95% prediction intervals of the above-described percentiles were calculated and displayed graphically together with corresponding percentiles computed from raw data.

2.5. Optimal Dosing Regimen Evaluation

A simulation-based analysis using a Monte Carlo approach (n = 10,000) was conducted, assuming log-normal distribution of PD parameters and different combinations of statistically significant covariates. A multiple dose regimen of daily OR administration of 1, 3, 5, 7, and 10 mg of warfarin to achieve steady-state concentrations was assumed. Individual INR levels were computed at 23 h post-dose of the 10th administration cycle (PK steady-state conditions) of warfarin. Dosing regimen selection was established with the goal of achieving the highest probability of INR levels within the therapeutic range (2.0-3.0).

2.6. Data Analysis

All data analyses were performed based on the population approach with the software NONMEM® (v7.5, Icon Development Solutions, Ellicott City, MD). The population parameters were estimated using the Stochastic Approximation of the Expectation Maximization and the Importance Sampling Estimation (SAEM) and the Importance Sampling Estimation (IMP) method.

For graphical and statistical analysis, the R® software v4.2.1 was used (R Foundation for Statistical Computing, Vienna, Austria). The pc-VPC were performed using PsN version 5.0.0 [23].

3. RESULTS

The modelling dataset consisted of 1033 INR observations from 138 patients with Table 1 presenting subject demographics. Figure 1 shows the individual INR (PD) profiles available. Distributions of continuous covariates at baseline are displayed in Supplementary Figure S1.

Table 1. Summary of patients' characteristics

Demographics	Value
N	138
Median age, years (range)	68 (31-90)
Median body weight, kg (range)	83 (51-159)
Race, n (%), self-reported	
White Hispanics	33 (24)
Black Hispanics	26 (19)
Admixed	37 (27)
Others or not reported	42 (30)
Smoking status, n (%)	
Yes	59 (43)
No	79 (57)
type 2 DM status, n (%)	
Yes	39 (28)
No	72 (57)
CYP2C9 genotypes, n (%)	
**1/*1* (wild type)	98 (71)
**1/*2*	21 (15)
**1/*3*	7 (5.1)
**1/*5*	1 (0.72)
**1/*8*	2 (1.44)
**2/*2*	2 (1.44)
**2/*3*	6 (4.34)
**2/*5*	1 (0.72)
VKORC1 haplotypes, n (%)	
G/A	62 (45)
G/G	57 (41.3)
A/A	19 (13.7)

INR, international normalized ratio; DM, diabetes mellitus.

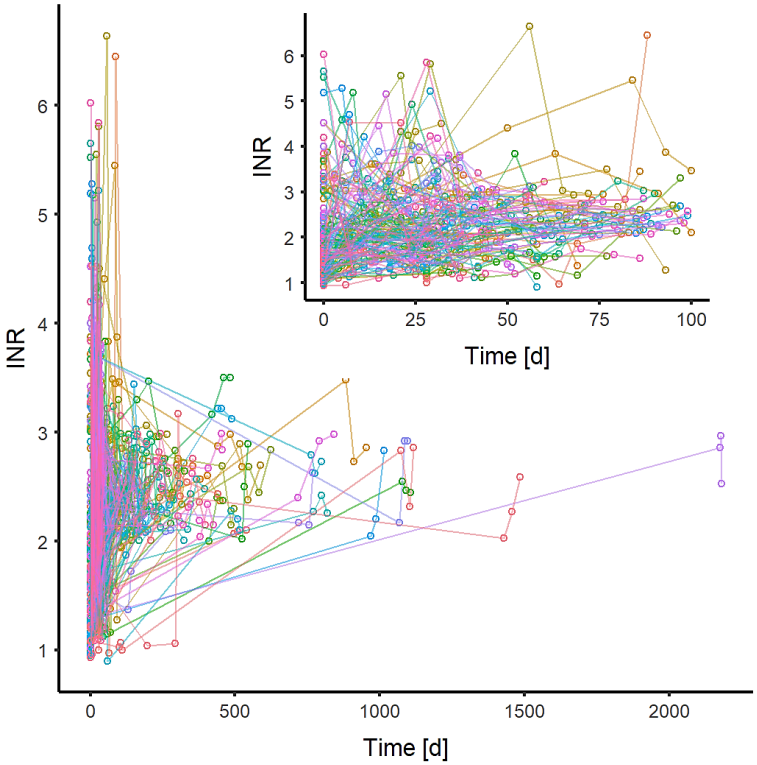

Figure 1. Experimental raw data of INR observations vs time for all subjects included in the study (N = 138). The open circles represent the measured INRs in each patient and each color line represents an individual time profile of INR variations. INR: international normalized ratio.

3.1. Base Population PK/PD Model

A previously developed one-compartment model with first-order OR absorption and *CYP2C9* genotype effect on CL was considered for generating longitudinal PK profiles across different *CYP2C9* genotypes [20]. Since the population PK models were developed from OR administration of warfarin, the bioavailability fraction (F) is unknown, and the estimates of CL and V represent the apparent estimates.

Parameter estimates of the base population PK/PD model are summarized in Supplementary Table S1 and the corresponding GOF, NPDE and VPC are shown in Supplementary Figure S2. The structural definition of the base PK/PD, which incorporates two transit compartment chains with three compartments each to account for the delay between exposure and INR response, can satisfy the overall INR

trend with no appreciable systematic bias that suggests model inadequacies. System-related PD parameters (MTT_1, and MTT_2) were fixed to the values reported by Hamberg et al., 2010 (MTT_1: 27.2 h or 1.13 d, and MTT_2: 110.9 h or 4.62 d). A typical INR at baseline (INR_{base} =1.86) was estimated and the maximum INR was set to 20 as previously reported [7, 17]. An inhibitory sigmoid Emax model of warfarin on the zero-order synthesis rate constants for each chain was assumed. The model assumes a complete (100%) inhibition of warfarin to the vitamin K epoxide reductase, as previously reported [7,17,24], and the Concentration of the drug needed to inhibit 50% of the response (IC_{50}) was estimated (15.4 mg/L). This parametrization helps to enhance model stability. Due to the lack of intensive PD sampling, IIV was only incorporated on INR_{base} (25%) and IC_{50} (35%) parameters.

3.2. Final Population PK/PD Model

The final population PK/PD model incorporates *CYP2C9* on CL and body weight on V_d, as previously reported [20] and for the pharmacodynamic parameters, *VKORC1* polymorphisms as statistically significant covariate on INR_{base} and IC_{50} ($p < 0.01$, ΔOFV=-11.8), respectively (Table 2).

Table 2. Final parameter estimates of the final population PK/PD model of warfarin in Caribbean Hispanic patients

		Population PK Model Estimates		Bootstrap Results	
Fixed-Effect		**Value**	**Shrinkage (%)**	**Median**	**95%CI**
MTT_1 (d)		1.13 FIX		1.13 FIX	
MTT_2 (d)		4.62 FIX		4.62 FIX	
Baseline					
	G/A	1.78		1.76	1.48-1.91
	G/G	1.84		1.85	1.53-2.05
	A/A	2.18		2.14	1.97-2.23
IC_{50}					
	G	5.88		5.91	5.61-6.37
	A	4.61		4.63	4.41-4.98
γ		1.47		1.48	1.27-1.61
Interindividual variability					
Baseline (%)		23	13	24	19-30
IC_{50} (%)		34	44	34	28-39
Residual unexplained variability					
Proportional (%)		27	6	26	22-31

MTT: mean transit time; IC_{50}: concentration resulting in 50% of I_{max}.

Other covariates, binary or (normalized) continuous variables, were investigated during the modeling process, but no statistical improvement ($p < 0.01$) after their inclusion was observed.

Supplementary Figure S3 depicts the eta-distribution values of INR_{base} (ETA1) and IC_{50} (ETA2) across the different covariates available from the base population PK/PD model. Based on the GOF and NPDE plots (Figure S4A), no systematic bias was observed and a slight improvement in the DV vs PRED plot was detected after the inclusion of the covariate effects. Individual observed vs predicted longitudinal INR profiles are shown in Supplementary Figure S4B. The examination of the pc-VPC (Figure 2) suggests a reasonable agreement between the observed data and model predictions for the median (50th percentile) and the variability (2.5th and 97.5th percentiles). The impact of *VKORC1* haplotypes on IC_{50} was modeled by accounting for the effects of individual alleles (G and A), which provides a more robust estimation in uncommon genotypes. The gamma parameter (1.47) of the sigmoid-E_{max} function was estimated, which is in accordance with other published values [7, 15]. Warfarin IC_{50} for G/G, G/A, and A/A were 11.76, 10.49, and 9.22 mg/L, respectively, which are higher than the reported ranges [7, 15,17,25]. The INR_{base} for the G/A, G/G, and A/A *VKORC1* haplotypes were 1.78, 1.84, and 2.18, respectively. After the covariate analysis, the IIV on INR_{base} and IC_{50} were reduced to 23% and 34%, respectively. Supplementary Figure S5 depicts the eta-distribution values of INR_{base} (ETA1) and IC_{50} (ETA2) across the different covariates available from the final population PK/PD model.

3.3. Optimal Dosing Regimen Evaluation

Based on the PD model developed, including the significant covariates on PK (*CYP2C9* genotypes on CL) and PD (*VKORC1* haplotypes on baseline and IC50), we aimed to optimize the oral dosing strategy of warfarin in Caribbean Hispanic patients to achieve the optimal benefit/ risk ratio. Figure 3 represents the simulated INR levels across the dosing regimens tested. Table 3 summarizes the optimal dosing regimen selected for each combination of *CYP2C9* genotypes and *VKORC1* haplotypes.

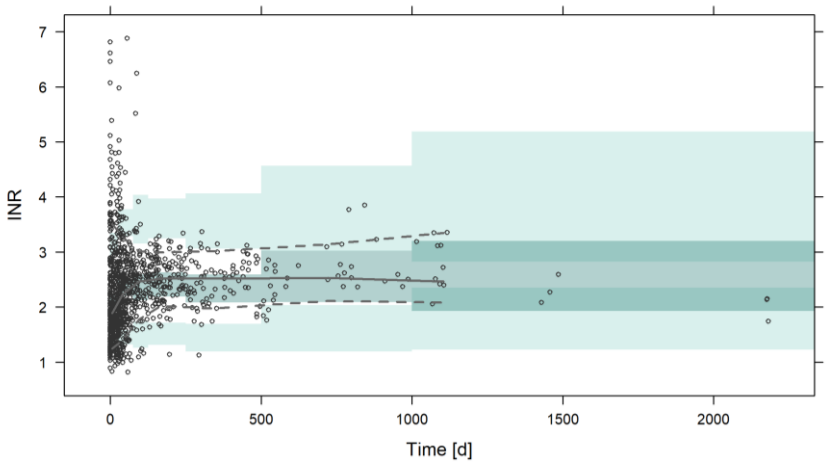

Figure 2. Pc-VPC of the final population PD model of INR after warfarin administration. Grey lines represent the median of 2.5th, 50th and 97.5th percentiles of the experimental INR observations. Green shaded areas encompass the 95% CI of prediction interval at 2.5th, 50th and 97.5th percentiles for the simulated INR data (n = 1000). Empty grey dots represent experimental INR observations. INR: international normalized ratio.

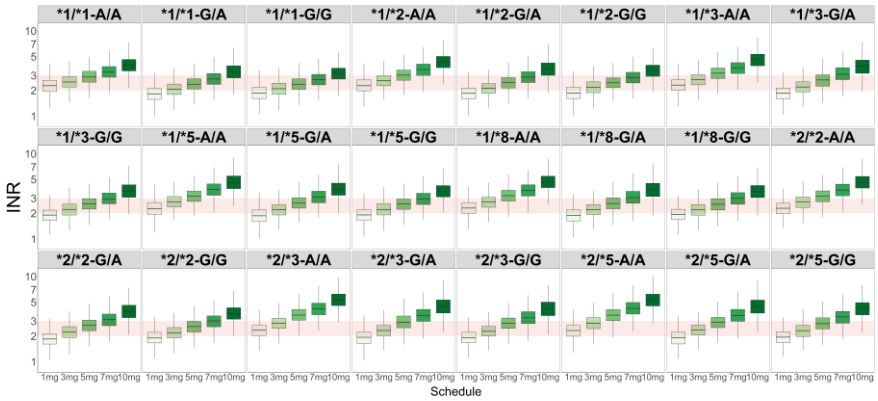

Figure 3. Stochastic simulations (n = 10,000) of INR levels using the final population PK/PD model assuming different daily dosing regimens for each sub-population of *CYP2C9* and *VKORC1* polymorphisms. The red band represents the therapeutic INR interval (2-3). INR: international normalized ratio.

Table 3. Model-informed dosing regimen selection of daily warfarin in patients with combinatorial *CYP2C9* and *VKORC1* polymorphisms

Type of patient	Schedule	Probability
*1/*1-A/A	3mg/d	67
*1/*1-G/A	5mg/d	66.7
*1/*1-G/G	5mg/d	66.2
*1/*2-A/A	3mg/d	64.7
*1/*2-G/A	5mg/d	67.3
*1/*2-G/G	5mg/d	69.2
*1/*3-A/A	3mg/d	64.6
*1/*3-G/A	3mg/d	60.7
*1/*3-G/G	5mg/d	65.9
*1/*5-A/A	3mg/d	60.6
*1/*5-G/A	5mg/d	63.6
*1/*5-G/G	5mg/d	65.2
*1/*8-A/A	3mg/d	63.5
*1/*8-G/A	5mg/d	62.4
*1/*8-G/G	5mg/d	63.6
*2/*2-A/A	1mg/d	60.8
*2/*2-G/A	5mg/d	62.5
*2/*2-G/G	5mg/d	63.5
*2/*3-A/A	1mg/d	64.3
*2/*3-G/A	3mg/d	63
*2/*3-G/G	3mg/d	64.9
*2/*5-A/A	1mg/d	63.2
*2/*5-G/A	3mg/d	67.3
*2/*5-G/G	3mg/d	62.4

4. DISCUSSION

Currently, treatment with warfarin in the Caribbean Hispanic population generates certain therapeutic gaps since there are no clinical guidelines that evaluate the impact of different *CYP2C9* and *VKORC1* genotypes on routine INR measures (efficacy surrogate endpoint) in this population. Consequently, patients show sub-optimal clinical response rates, according to individual INR values. To address this, we have adapted a population PK/PD model of warfarin from individual

data and dose records over 2 years in Caribbean Hispanic patients from a local anticoagulation clinic to optimize the dosing regimens in this population. In this paper, a simulation-based analysis to calculate the probability of guaranteeing therapeutic INR levels (2-3) for different daily regimens of warfarin was performed. The simulations accommodated different patient's genotypes resulting from combinatorial *CYP2C9* and *VKORC1* polymorphisms.

A relevant aspect of this work is that it provides external validation of previously published PK and PD models. The combination of both has made it possible to establish a PK/PD model capable of collecting behavior in the Hispanic Caribbean population, which is different from that used in previous studies. Longitudinal PK model predictions between the structural PK definition of Hamberg *et al.* [7,17] and Reyes-González *et al.* [20] can be found in Figure 4, where no relevant differences were observed across both PK model structures. This highlights the importance of adapting published structural models to predict the behavior of anticoagulant therapy and corroborates their predictive capacity at the structural level.

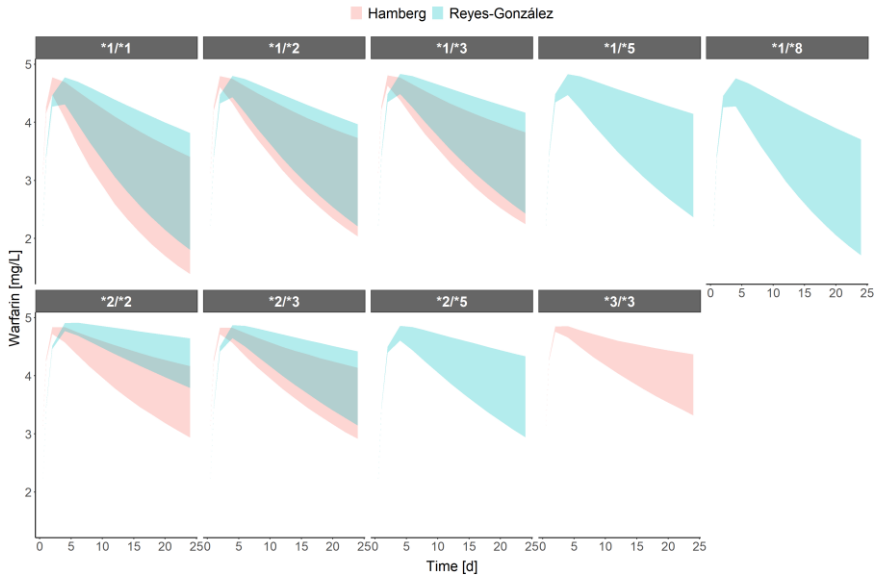

Figure 4. Comparison of the longitudinal PK model predictions between the structural PK definition of Hamberg et al. (2007, 2010) and Reyes-González et al. (2020).

Due to the paucity of longitudinal profiles with a high number of INR samples, the maturation times (MTT_1 and MTT_2) of each of the transit-

compartment chains were fixed to published values. Although some authors propose a kinetic-pharmacodynamic model (K-PD) structure [7], whereby the INR response is not governed by warfarin concentrations, in this article we have generated the PK profiles from the pharmacogenetic information available in each patient to predict the change in response over time as a consequence of warfarin concentrations. Despite the limitation of not having observed concentrations of warfarin and the fact that all patients with the same genetic profile present the same longitudinal profile of warfarin, we believe that this strategy makes it possible to partly mitigate the excessive IIV of warfarin observed in clinical practice.

One of the most surprising results of this study is the IC_{50} values obtained for each of the *VKORC1* haplotypes studied in the Caribbean Hispanic population, which were clearly higher (9.22–11.76 mg/L) than those earlier reported in other populations (1.56–3.11 mg/L) [7,17]. This is consistent with the therapeutic gaps observed in this underrepresented population and suggests increased resistance of Caribbean Hispanic patients to warfarin, who may require more intensive dosing regimens to achieve similar target INR responses. This phenomenon may be the consequence of a longer longitudinal evaluation than in previous studies (>2000 d), as well as a slightly higher distribution of G/G and G/A polymorphisms that may be partially affecting the point estimate. The underlying cause for these increased IC_{50} values remains unclear. However, we also speculate it might in part be linked to the presence of the *NQO1** 2 allele (g .559 C>T, p. P187S) that has been previously associated with warfarin resistance in Hispanics [26,27]. The *NQO1* gene encodes a NAP(H)-dependent quinone oxide reductase enzyme, responsible for catalyzing the reduction of quinones, including vitamin K, into hydroquinone. This mechanism could potentially serve as an alternate vitamin K recycling pathway to VKORC1 in carriers of the haplotype A, who show a lower *VKORC1* gene expression. Nevertheless, this hypothesis needs further validation.

On the other hand, when taking into account the INR_{base} values across different *VKORC1* haplotypes, we observed higher measures in A/A carriers (2.18) compared to those in patients with haplotypes containing the G allele (1.78 and 1.84, respectively). This could be explained by a more prolonged prothrombin time and lower levels of functional (active) prothrombin-dependent coagulation factors in carriers of the *VKORC1*-A allele due to their reduced expression of the

hepatic VKORC1 enzyme, which plays a pivotal role in the vitamin K cycle in the liver [28]. Vitamin K dihydroquinone is oxidized to vitamin K epoxide during this process and γ-glutamyl carboxylase (GGCX) carboxylates the various hypofunctional coagulation factors involved in the clotting cascade including prothrombin (FII). VKORC1 is responsible for the reduction of vitamin K epoxide back to vitamin K1 and vitamin K dihydroquinone, which is the rate-limiting step in vitamin K recycling. Therefore, even in the absence of any competitive inhibition by warfarin (baseline), reduced VKORC1 levels in carriers of the group A haplotype will deplete the formation of vitamin K1 dihydroquinone. Since vitamin K1 dihydroquinone is the essential cofactor to GGCX, further post-translational activation of hypofunctional coagulation factors is critically compromised in this situation. As a result, the prothrombin time will be prolonged, and the INR level will rise accordingly. This would open the door to hypothesize that *VKORC1* polymorphisms not only affect the potency of warfarin but also influence basal INR levels, partially explaining the excessive IIV in INR_{base}.

A model-informed optimal dosing regimen selection has been conducted based on the probability of achieving therapeutic INR levels in a virtual population using the fixed and random parameters from the final population PK/PD model. The different sub-populations considered are the result of the combination of *CYP2C9* and *VKORC1* polymorphisms. Overall, the predicted probability in all scenarios reaches therapeutic INR levels in at least 60% of the patients. Previous authors stated that due to the moderate IIV and residual error and independently of the structural definition of the PK/PD model, probabilities less than 70% are not expected for warfarin dose selection [7, 29]. In this regard, 3–5 mg of daily warfarin would achieve therapeutic INR levels in most of the scenarios considered. The sub-group of patients with * 2/* 2-, * 2/* 3- and * 2/* 5-A/A would require only 1 mg daily of warfarin to achieve therapeutic INR levels at steady state conditions.

The absence of tailored clinical guidelines considering the impact of distinct *CYP2C9* and *VKORC1* genotypes on routine INR measures in Caribbean Hispanics has led to therapeutic gaps, contributing to suboptimal clinical response rates within this population. Through simulation-based analyses encompassing various patient genotypes resulting from *CYP2C9* and *VKORC1* polymorphisms, this study delved into optimizing dosing regimens to ensure therapeutic INR levels. Our findings support the significance and clinical relevance of

using a population PK/PD approach in elucidating the role of genetic polymorphisms (e.g., *CYP2C9* and *VKORC1* haplotypes) for the optimal design of warfarin dosing schemes in Caribbean Hispanic patients. The simulations provided a comprehensive understanding of how a broader range of *CYP2C9* variants and, specifically, the *VKORC1*-1636 A allele influence the PK and PD of warfarin, as well as baseline INR measures, within this diverse population and shed light on potential underlying mechanisms linked to increased IC_{50} values.

The participants in our study are mainly elderly men, which is a limitation of the study as sex differences in warfarin PK have been suggested in previous studies [30,31]. However, the genotypes included as covariates in the PK/PD analyses were based on the *CPY2C9* and *VKORC1* polymorphisms, which are not sex-linked variants and are therefore unlikely to represent significant sex bias.

5. CONCLUSIONS

By performing an external validation of the PK/PD model, we can confidently extrapolate findings from the model to real-world patient scenarios, enabling tailored and precise warfarin dosing recommendations for Caribbean Hispanic individuals. Therefore, this MIPD approach is expected to minimize the risk of adverse events linked to inaccurate warfarin dosing due to genetic differences at individual level and enhance therapeutic outcomes. This strategy will ultimately foster safer and more effective clinical management of personalized anticoagulation therapy in this specific patient subgroup, which is often underrepresented in clinical studies. In conclusion, by adapting this MIPD strategy to the Caribbean Hispanic population's unique characteristics, this research underscores the predictive capacity of the PK/PD modeling approach in guiding anticoagulant therapy.

6. FUNDING

This research was financially sponsored in part by NASA grant # 80 NSSC19M0148 from the EPSCoR program, and by grant # 1R16 GM149372 from the National Institute of General Medical Sciences (NIGMS) of the National Institutes of Health (NIH). The content of this manuscript does not represent the views of the National Institutes of Health, NASA or the United States Government. No funded writing assistance was utilized in the production of this manuscript.

7. CREDIT AUTHORSHIP CONTRIBUTION STATEMENT

Rodríguez-Fernández Karine: Formal analysis, Methodology, Visualization, Writing – original draft, Writing – review & editing. Reynaldo-Fernández Gledys: Data curation, Formal analysis, Methodology, Visualization, Writing – original draft, Writing – review & editing. Reyes-González Stephanie: Data curation, Investigation. de las Barreras Alonso Camila de las Mercedes: Data curation, Formal analysis, Investigation. Rodríguez-Vera Leyanis: Data curation, Methodology. Vlaar Cornelis: Conceptualization, Funding acquisition, Resources. Monbaliu Jean-Christophe M.: Conceptualization, Funding acquisition, Resources. Stelzer Torsten: Conceptualization, Funding acquisition, Resources. Duconge Jorge: Conceptualization, Project administration, Resources, Supervision, Validation, Writing – review & editing. Mangas-Sanjuan Victor: Formal analysis, Supervision, Validation, Visualization, Writing – original draft, Writing – review & editing.

8. DECLARATION OF COMPETING INTEREST

The authors declare that they have no known competing financial interests or personal relationships that could have appeared to influence the work reported in this paper.

9. ACKNOWLEDGEMENTS

We want to thank the patients for voluntarily participating in the original study where data used in this analysis were gathered. A special acknowledgement to the personnel at the Veteran Affairs Caribbean Healthcare System (VACHS) at San Juan, PR for their support.

10. APPENDIX A. SUPPORTING INFORMATION

Supplementary data associated with this article can be found in the online version at doi:10.1016/j.biopha.2023.115977.

11. REFERENCES

[1] J. Ansell, J. Hirsh, E. Hylek, A. Jacobson, M. Crowther, G. Palareti, Pharmacology and management of the vitamin K antagonists: American College of Chest Physicians Evidence-Based Clinical Practice Guidelines (8th Edition), Chest 133 (6 Suppl) (2008) 160s–198s, https://doi.org/10.1378/chest.08-0670.

[2] R. Wallin, S.M. Hutson, Warfarin and the vitamin K-dependent gamma-carboxylation system, Trends Mol. Med. 10 (7) (2004) 299–302, https://doi.org/ 10.1016/j.molmed.2004.05.003.

[3] R. Liu, X. Li, W. Zhang, H.H. Zhou, Comparison of nine statistical model based warfarin pharmacogenetic dosing algorithms using the racially diverse international warfarin pharmacogenetic consortium cohort database, PloS One 10 (8) (2015), e0135784, https://doi.org/10.1371/journal.pone.0135784.

[4] I.G. Asiimwe, M. Pirmohamed, Ethnic diversity and warfarin pharmacogenomics, Front. Pharmacol. 13 (2022), 866058, https://doi.org/10.3389/ fphar.2022.866058.

[5] K. Huynh, Milestone 6: Birth of the INR, Nat. Rev. Cardiol. (2017), https://doi.org/ 10.1038/nrcardio.2017.176.

[6] J.A. Johnson, K.E. Caudle, L. Gong, M. Whirl-Carrillo, C.M. Stein, S.A. Scott, M. T. Lee, B.F. Gage, S.E. Kimmel, M.A. Perera, J.L. Anderson, M. Pirmohamed, T. E. Klein, N.A. Limdi, L.H. Cavallari, M. Wadelius, Clinical Pharmacogenetics Implementation Consortium (CPIC) Guideline for Pharmacogenetics-Guided Warfarin Dosing: 2017 Update, Clin. Pharmacol. Ther. 102 (3) (2017) 397–404, https://doi.org/10.1002/cpt.668.

[7] A.K. Hamberg, M. Wadelius, J.D. Lindh, M.L. Dahl, R. Padrini, P. Deloukas, A. Rane, E.N. Jonsson, A pharmacometric model describing the relationship between warfarin dose and INR response with respect to variations in CYP2C9, VKORC1, and age, Clin. Pharmacol. Ther. 87 (6) (2010) 727–734, https://doi.org/ 10.1038/clpt.2010.37.

[8] International Warfarin Pharmacogenetics Consortium, N.A. Limdi, M. Wadelius, L. Cavallari, N. Eriksson, D.C. Crawford, M.-T.M. Lee, C.-H. Chen, A. Motsinger- Reif, H. Sagreiya, N. Liu, A.H.B. Wu, B.F. Gage, A. Jorgensen, M. Pirmohamed, J.-G. Shin, G. Suarez-Kurtz, S.E. Kimmel, J.A. Johnson, T.E. Klein, M.J. Wagner, Warfarin pharmacogenetics: a single VKORC1 polymorphism is predictive of dose across 3 racial groups, Blood 115 (18) (2010) 3827–3834, https://doi.org/ 10.1182/blood-2009-12-255992.

[9] H.Y. Yuan, J.J. Chen, M.T. Lee, J.C. Wung, Y.F. Chen, M.J. Charng, M.J. Lu, C. R. Hung, C.Y. Wei, C.H. Chen, J.Y. Wu, Y.T. Chen, A novel functional VKORC1 promoter polymorphism is associated with inter-individual and inter-

ethnic differences in warfarin sensitivity, Hum. Mol. Genet. 14 (13) (2005) 1745–1751, https://doi.org/10.1093/hmg/ddi180.

[10] International Warfarin Pharmacogenetics Consortium, T.E. Klein, R.B. Altman, N. Eriksson, B.F. Gage, S.E. Kimmel, M.T. Lee, N.A. Limdi, D. Page, D.M. Roden, M. J. Wagner, M.D. Caldwell, J.A. Johnson, Estimation of the warfarin dose with clinical and pharmacogenetic data, N. Engl. J. Med. 360 (8) (2009) 753–764, https://doi.org/10.1056/NEJMoa0809329.

[11] M. Pirmohamed, G. Burnside, N. Eriksson, A.L. Jorgensen, C.H. Toh, T. Nicholson, P. Kesteven, C. Christersson, B. Wahlstr¨om, C. Stafberg, J.E. Zhang, J.B. Leathart, H. Kohnke, A.H. Maitland-van der Zee, P.R. Williamson, A.K. Daly, P. Avery, F. Kamali, M. Wadelius, A Randomized Trial of Genotype-Guided Dosing of Warfarin, N. Engl. J. Med. 369 (24) (2013) 2294–2303, https://doi.org/10.1056/ NEJMoa1311386.

[12] P.J. Avery, A. Jorgensen, A.K. Hamberg, M. Wadelius, M. Pirmohamed, F. Kamali, A proposal for an individualized pharmacogenetics-based warfarin initiation dose regimen for patients commencing anticoagulation therapy, Clin. Pharmacol. Ther. 90 (5) (2011) 701–706, https://doi.org/10.1038/clpt.2011.186.

[13] N.S. Ferder, C.S. Eby, E. Deych, J.K. Harris, P.M. Ridker, P.E. Milligan, S. Z. Goldhaber, C.R. King, T. Giri, H.L. McLeod, R.J. Glynn, B.F. Gage, Ability of VKORC1 and CYP2C9 to predict therapeutic warfarin dose during the initial weeks of therapy, J. Thromb. Haemost.: JTH 8 (1) (2010) 95–100, https://doi.org/ 10.1111/j.1538-7836.2009.03677.x.

[14] U.S. Foods and Drug Administration (FDA), Coumadin (warfarin sodium) tablets label – FDA. Full prescribing information. ⟨https://www.accessdata.fda.gov/drugsatfda_docs/label/2011/009218s107lbl.pdf⟩ , 2011 (Accessed 5 August 2023).

[15] A.K. Hamberg, M. Wadelius, L.E. Friberg, T.T. Biss, F. Kamali, E.N. Jonsson, Characterizing variability in warfarin dose requirements in children using modelling and simulation, Br. J. Clin. Pharmacol. 78 (1) (2014) 158–169, https:// doi.org/10.1111/bcp.12308.

[16] A.K. Hamberg, L.E. Friberg, K. Hans'eus, B.M. Ekman-Joelsson, J. Sunnegårdh, A. Jonzon, B. Lundell, E.N. Jonsson, M. Wadelius, Warfarin dose prediction in children using

pharmacometric bridging–comparison with published pharmacogenetic dosing algorithms, Eur. J. Clin. Pharmacol. 69 (6) (2013) 1275–1283, https://doi.org/10.1007/s00228-012-1466-4.

[17] A.K. Hamberg, M.L. Dahl, M. Barban, M.G. Scordo, M. Wadelius, V. Pengo, R. Padrini, E.N. Jonsson, A PK-PD model for predicting the impact of age, CYP2C9, and VKORC1 genotype on individualization of warfarin therapy, Clin. Pharmacol. Ther. 81 (4) (2007) 529–538, https://doi.org/10.1038/sj.clpt.6100084.

[18] U. Falkenhagen, J. Kn¨ochel, C. Kloft, W. Huisinga, Deriving mechanism-based pharmacodynamic models by reducing quantitative systems pharmacology models: an application to warfarin, CPT: Pharmacomet. Syst. Pharmacol. 12 (4) (2023) 432–443, https://doi.org/10.1002/psp4.12903.

[19] J. Deng, V. Vozmediano, M. Rodriguez, L.H. Cavallari, S. Schmidt, Genotype-guided dosing of warfarin through modeling and simulation, Eur. J. Pharm. Sci. Off. J. Eur. Fed. Pharm. Sci. 109s (2017) S9–s14, https://doi.org/10.1016/j. ejps.2017.05.017.

[20] S. Reyes-Gonz'alez, C. de Las Barreras, G. Reynaldo, L. Rodríguez-Vera, C. Vlaar, V. L. Mejias, J.M. Monbaliu, T. Stelzer, V. Mangas, J. Duconge, Genotype-driven pharmacokinetic simulations of warfarin levels in Puerto Ricans, Drug Metab. Pers. Ther. (2020), https://doi.org/10.1515/dmdi-2020-0135.

[21] E. Comets, K. Brendel, F. Mentr'e, Computing normalised prediction distribution errors to evaluate nonlinear mixed-effect models: the npde add-on package for R, Comput. Methods Prog. Biomed. 90 (2) (2008) 154–166, https://doi.org/10.1016/ j.cmpb.2007.12.002.

[22] M. Bergstrand, A.C. Hooker, J.E. Wallin, M.O. Karlsson, Prediction-corrected visual predictive checks for diagnosing nonlinear mixed-effects models, AAPS J. 13 (2) (2011) 143–151, https://doi.org/10.1208/s12248-011-9255-z.

[23] L. Lindbom, P. Pihlgren, E.N. Jonsson, PsN-Toolkit–a collection of computer intensive statistical methods for non-linear mixed effect modeling using NONMEM, Comput. Methods Prog. Biomed. 79 (3) (2005) 241–257, https://doi.org/10.1016/ j.cmpb.2005.04.005.

[24] E.M. Hylek, S. Regan, A.S. Go, R.A. Hughes, D.E. Singer, S.J. Skates, Clinical predictors of prolonged delay in return of the

international normalized ratio to within the therapeutic range after excessive anticoagulation with warfarin, Ann. Intern. Med. 135 (6) (2001) 393–400, https://doi.org/10.7326/0003-4819-135-6- 200109180-00008.

[25] S.M. Saffian, S.B. Duffull, R.L. Roberts, R.C. Tait, L. Black, K.A. Lund, A. H. Thomson, D.F. Wright, Influence of Genotype on Warfarin Maintenance Dose Predictions Produced Using a Bayesian Dose Individualization Tool, Ther. Drug Monit. 38 (6) (2016) 677–683, https://doi.org/10.1097/ftd.0000000000000347.

[26] D.F. Hernandez-Suarez, K. Claudio-Campos, J.E. Mirabal-Arroyo, B.A. Torres- Hern'andez, A. L'opez-Candales, K. Melin, J. Duconge, Potential of a pharmacogenetic-guided algorithm to predict optimal warfarin dosing in a high-risk Hispanic patient: role of a novel NQO1*2 Polymorphism, J. Invest. Med. High. Impact Case Rep. 4 (4) (2016), 2324709616682049, https://doi.org/10.1177/2324709616682049.

[27] N. El Rouby, L. Rodrigues Marcatto, K. Claudio, L. Camargo Tavares, H. Steiner, M. R. Botton, S.A. Lubitz, E.N. Fallon, K. Yee, J. Kaye, S.A. Scott, J. Karnes, P. Caleb Junior de Lima Santos, J. Duconge, L.H. Cavallari, Multi-site Investigation of Genetic Determinants of Warfarin Dose Variability in Latinos, Clin. Transl. Sci. 14 (1) (2021) 268–276, https://doi.org/10.1111/cts.12854.

[28] PharmGKB website, Warfarin Pathway Pharmacodynamics. 〈https://www.pharm gkb.org/pathway/PA145011114〉, (Accessed 5 August 2023).

[29] PAGE. Abstracts of the Annual Meeting of the Population Approach Group in Europe. ISSN 1871–6032 Reference: PAGE 31 (2023) Abstr 10711 [www.pag e-meeting.org/?abstract=10711].

[30] Hirsh, J. Dalen, D.R. Anderson, et al., Oral anticoagulants: mechanism of action, clinical effectiveness, and optimal therapeutic range, Chest 119 (1_suppl) (2001) 8S–21S.

[31] A.E. Rettie, L.C. Wienkers, F.J. Gonzalez, W.F. Trager, K.R. Korzekwa, Impaired (S)-warfarin metabolism catalysed by the R144C allelic variant of CYP2C9, Pharmacogenetics 4 (1) (1994) 39–42.

Chapter 4: Model-Informed Precision Dosing for Personalized Ustekinumab Treatment in Plaque Psoriasis

Karine Rodríguez-Fernández [1,2,†], Javier Zarzoso-Foj [1,2,†], Marina Saez-Bello [3], Almudena Mateu-Puchades [4], Antonio Martorell-Calatayud [5], Matilde Merino-Sanjuan [1,2], Elena Gras-Colomer [6], Monica Climente-Martí [3] and Victor Mangas-Sanjuan [1,2]

Authors Affiliation: [1]Department of Pharmacy and Pharmaceutical Technology and Parasitology, University of Valencia, Valencia, 46100, Spain; [2]Interuniversity Research Institute for Molecular Recognition and Technological Development, Polytechnic University of Valencia-University of Valencia, Valencia, 46100, Spain;[3]Pharmacy Service, Doctor Peset University Hospital, Foundation for the Promotion of Health and Biomedical Research in the Valencian Region (FISABIO), Valencia, 46017, Spain; [4] Dermatology Service, Doctor Peset University Hospital, Foundation for the Promotion of Health and Biomedical Research in the Valencian Region (FISABIO), Valencia, 46017, Spain; [5]Dermatology Service, Hospital Manises of Valencia, Valencia, 46940, Spain; [6]Pharmacy Service, Hospital Manises of Valencia, Valencia, 46940, Spain; [†]These authors contributed equally to this work.

Pharmaceutics. 2024 Oct 4;16(10):1295

1. INTRODUCTION

The management of psoriasis, a chronic immune-mediated condition, has been revolutionized with the introduction of monoclonal antibody (mAb), with ustekinumab (UTK constituting one of the available treatment choices [1,2]. UTK targets with high specificity and affinity the shared p40 subunit of IL-12 and IL-23 [3,4]. Both cytokines play an important role in the immune cascade that leads to psoriasis, particularly in modulating the differentiation of naïve T-cells into Th1 and Th17 cells [5–7].

Under the brand name Stelara® (Janssen Biotech, Inc, Horsham, PA, the USA) UTK is available in solution for injection and can be administered subcutaneously. The latter formulation offers flexibility in administration, autoinjectors being the most recent [8]. The clinical development programs for UTK have been the most extensive for a biologic agent. Phase III clinical trials [9–12] for UTK in psoriasis have specified a significant decrease in Psoriasis Area and Severity Index (PASI) scores, supporting considerable improvements in the severity of the disease. Additionally, UTK has been directly compared to the tumor necrosis factor inhibitor etanercept [13], representing the first-ever head-to-head comparison of biological agents in psoriasis treatment. UTK is dosed according to body weight, as indicated in summary of product characteristics (SmPC) [8]. For individuals weighing ≤100 kg and those weighing >100 kg, a 45 and 90 mg dose is given, respectively, at weeks 0 and 4 (induction period), followed by subsequent doses every 12 weeks (the maintenance period). UTK typically reaches a steady state within approximately 28 weeks of regular dosing.

A population PK modeling approach was developed for UTK in clinical trial adult patients with moderate to severe plaque psoriasis [14] and psoriatic arthritis [15] and in real-world data patients [16], using a one-compartment model with first-order absorption and first-order-elimination, demonstrating a comparable PK between adult patients from clinical trials and real-world data. The same model was developed in clinical trial pediatric patients with moderate to severe plaque psoriasis [17]. In addition, an integrated population PK analysis was performed to describe the PK behavior of UTK in healthy subjects and individuals with psoriasis, psoriatic arthritis, Crohn's disease, and ulcerative colitis [18]. The chosen structural PK model for UTK was a two-compartment open model incorporating first-order absorption and elimination kinetics. Notably, parameters such as CL and the V_d

were found to increase nonlinearly with body weight. This model effectively incorporates the PK characteristics of UTK across all approved inflammatory conditions and in healthy individuals, providing a consistent framework for understanding UTK's PK profile in diverse patient populations. The relationship between serum concentration–time data with longitudinal measures of the PASI in patients with moderate to severe plaque psoriasis was described via an indirect response model in a clinical trial and real-world patient data [16,17,19,20]. The contribution of the UTK effect to the inhibition of the formation rate of psoriatic skin lesions was described by a maximum inhibition drug effect (I_{max}) model [21].

Dermatologists often follow labeled dosing recommendations for initial treatment with UTK, which may not be optimal or safe for every patient [22]. Due to variable psoriasis disease progression in individual patients and the variability in response, they perform changes in the dosing regimen of UTK during the maintenance period of treatment. These changes in routine clinical practice are called optimizations and intensifications of SmPC dosage regimens. Dose regimen optimization involves maintaining the dose but extending the dosing interval or decreasing the dose while maintaining the dosing interval. On the contrary, dose regimen intensification implies maintaining the dose but decreasing the dosing interval or increasing the dose while maintaining the dosing interval. With this approach, the risk of adverse events increases due to drug concentrations that are either supratherapeutic or subtherapeutic because of the lack of a model-informed decision-making process [23]. Additionally, the methods for individualization commonly used in standard clinical practice, such as those based on clinical response and TDM, demand strict adherence to the sampling schedule. Intervention typically occurs only after the drug has reached a steady state, and adjustments are made by comparing the patient's exposure to a target range. If the exposure falls outside this range, the dose is adjusted under the assumption of dose-exposure proportionality at steady state or based on clinical experience [24–27].

Consequently, dermatologists require a flexible approach for psoriasis treatment that considers non-labeled dosing regimens and transitions between different therapeutic modalities of psoriasis to select the optimal treatment for each patient and to solve the cases of suboptimal response, the loss of efficacy over time, or the emergence of adverse effects. These challenges highlight the critical importance of transitioning MIPD strategies guided by population PK/PD models.

With MIPD, any timed sample can be utilized, allowing interventions at any point, from before the first dose to when a steady state is reached. The intervention method involves calculating a dose that achieves a predefined PK/PD target [27–32]. Implementing PK/PD models in dosing decisions for psoriasis management improves precision dosing and addresses the IIV observed in psoriasis treatment responses, enhancing therapeutic outcomes and patient safety [14,17,19,33]. Therefore, the objective of this study was to propose a methodology capable of individualizing dosing strategies of UTK in patients with moderate to severe chronic plaque psoriasis based on the uncertainty of the individual parameters of a population PK/PD model.

2. MATERIALS AND METHODS

2.1. Study Design

A post-authorization, prospective, and observational clinical practice follow-up study was conducted on Spanish patients with moderate to severe chronic plaque psoriasis from Manises Hospital of Valencia. The authors affirm that all procedures undertaken in this study adhere to the ethical standards established by the pertinent national and institutional committees overseeing human experimentation. Furthermore, they ensure compliance with the Helsinki Declaration of 1975, with revisions made in 2008. The study received approval from the Ethics Committee of La Fe University and Polytechnic Hospital (protocol code VMS-UTK-2020-01 EPA-SP). All participants provided written informed consent. The enrollment period spanned from February 2021 to December 2022, encompassing individuals who had received at least one dose of UTK (Stelara®) and who were under treatment at the time of inclusion. The patients included in the study were receiving dosage regimens individualized (optimized/intensified or not) and authorized by the dermatologist based on their clinical response. Exclusion criteria included individuals below 18 years of age, pregnant individuals, and those with cognitive impairment. Treatment-related variables such as dosage regimen, time, and line of treatment were collected for each patient. Moreover, demographic data were extracted from the hospital's electronic clinical records, including age, sex, weight, and height.

2.2. Blood Sampling and Analytical Quantification of Samples

Patients were administered UTK via subcutaneous injection in the abdomen or upper thigh. The patients received the following dosage regimen as a current treatment: 45 or 90 mg of UTK every 12, 14, and 16 weeks (q12w, q14w, and q16w), 45 mg of UTK every 18 weeks (q18w), and 90 mg of UTK every 8, 10, and 15 weeks (q8w, q10w, q15w). Blood samples for PK analysis were collected using plain red vacutainer tubes immediately before UTK administration and approximately 2, 6, 10, 12, 14, 16, and 18 weeks afterward. After centrifugation, serum samples were transferred to separate tubes and frozen at temperatures between -20 and -80 °C until processing. Serum concentrations of UTK were measured in the laboratory of Manises Hospital using an enzyme-linked immunosorbent assay (ELISA; Promonitor-UTK assay, Progenika Biopharma, Grifols®, Spain). The Promonitor-UTK quantifies concentrations of UTK in the range of 0.63–20 μg/mL.

2.3. Psoriasis Area and Severity Index Score Measurement

In the dermatology service from Manises Hospital, patients initiating UTK therapy undergo PASI assessments every 3 months during the first year of treatment. Following the initial year, PASI evaluations occur every 6 months. Baseline PASI values, recorded at the onset of UTK therapy, were extracted from patient clinical records. All available PASI scores documented in patient clinal records during the approximately 1.5-year follow-up period were collected.

2.4. Modeling Data Analysis

Figure 1 summarizes the modeling strategy performed. The data analysis was initiated by simulation using the population PK parameters of the 7 reference PK models published for UTK [14–18,34]. This aided in identifying the model that most accurately represented our data. Subsequently, we applied the chosen model along with the individual UTK serum concentrations gathered during TDM to estimate individual PK parameters.

A previously published indirect response model with PASI synthesis inhibition [16] was considered to describe the PK/PD relationship between UTK serum concentrations and the PASI (Figure 2). The ordinary differential equations of the PK/PD model can be found in the Supplementary Material. This model structure was also previously

applied to other mAbs designed for the treatment of psoriasis ([19,35–38]). Linear, I_{max}, and sigmoid drug effects functions were evaluated [21].

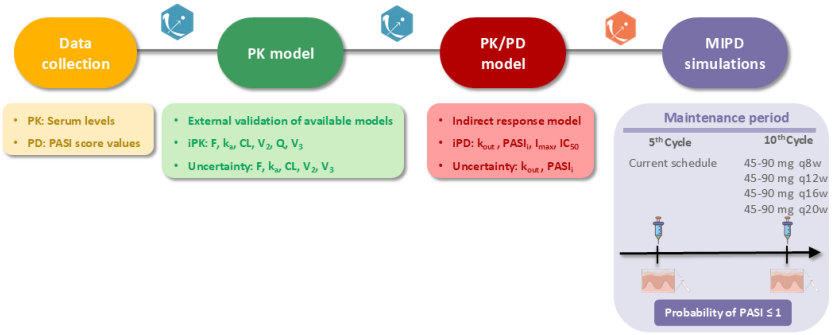

Figure 1. Modeling workflow. PK: pharmacokinetic; PD: pharmacodynamic; PASI: Psoriasis Area and Severity Index; iPK: individual pharmacokinetic parameter; iPD: individual pharmacodynamic parameter; F: bioavailability; k_a: absorption rate constant; CL: clearance; Q: intercompartmental transfer clearance; V_2: central volume of distribution; V_3: peripheral volume of distribution; k_{out}: first-order remission constant rate of psoriatic skin lesion; I_{max}: maximum inhibition drug effect model; $PASI_i$: estimated baseline levels of PASI response; IC_{50}: concentration of the drug needed to inhibit 50% of the response; MIPD: model-informed precision dosing; q8w: once every 8 weeks, q12w: once every 12 weeks; q16w: once every 16 weeks; q20w: once every 20 weeks.

Baseline levels of PASI response ($PASI_i$) were estimated using the B2 method [39], where $PASI_i$ represents the individual predicted baseline level of the PASI, $PASI_{i,o}$ is the individual observed baseline and $\boldsymbol{\eta}_{i,RV}$ is the estimated individual random component accounting for the difference between $PASI_i$ and $PASI_{i,o}$. This variable has a mean equal to zero and, during parameter estimation, is restricted to having the same variance as the RUV (Equation (1)). Consequently, we assumed that the variability observed in the rest of the data also applies to the baseline data.

$$PASI_i = PASI_{i,0} \cdot e^{\eta_{i,RV}} \quad (1)$$

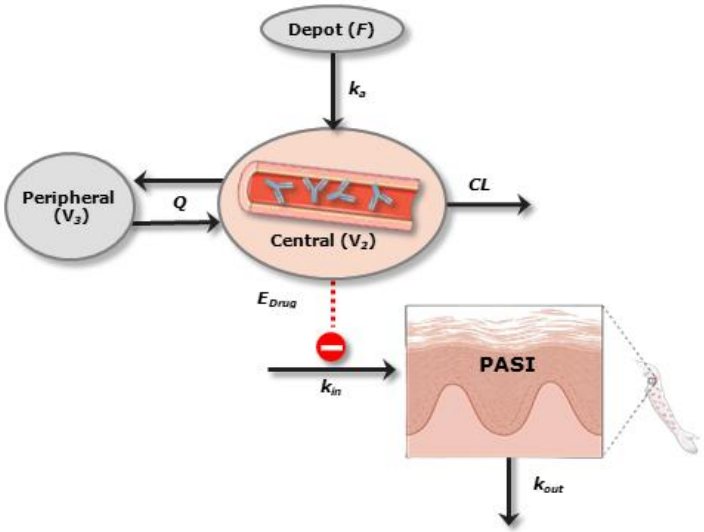

Figure 2. Schematic representation of the final PK/PD model. E_{Drug}: effect of the drug; k_{in}: zero-order progression constant rate of psoriatic skin lesion.

The selection of the PK/PD model was based on the comparison of the OFV, a visual exploration of GOF plots and the precision of model parameters stated in the standard errors. An evaluation of the selected PK/PD models was performed through simulation-based diagnostics pc-VPCs) [40,41]. All data analyses were performed based on the population approach with the software Monolix 2024R1 (Lixoft SAS, a Simulations Plus company, California, USA.) [42]. For graphical and statistical analysis, R software (http://cran.r-project.org, version 4.4.1, accessed on 30th September 2024) was employed [43,44].

2.5. Individual Dosing Regimen Strategy

To explore the performance of the final PK/PD model and its impact on clinical practice, the optimal MIPD regimen in each patient was determined, for which the PK and PD individual parameters and their uncertainties were considered. The individual conditional distributions of PK/PD parameters were estimated in Monolix, which represented the PK and PD individual parameter estimates and their corresponding uncertainty [45]. Uncertainty refers to the degree of accuracy with which PK and PD individual parameters can be determined based on the observed data and covariate value for that individual, considering that the individual belongs to the population for which the typical

parameter value (fixed effects) and the variability (standard deviation of the random effects) were previously estimated [45,46].

The determination of individual conditional distributions ($p(\psi_i|y_i)$, with ψ_i being the individual parameters for individual *i* and y_i the data observations for individual *i*), was performed with a MCMC procedure called the Metropolis–Hastings algorithm that samples parameter values from these distributions, using the following expression:

$$p(\psi_i|y_i) = \frac{p(y_i|\psi_i) \cdot p(\psi_i)}{p(y_i)} \quad (2)$$

where $p(y_i|\psi_i)$ is the conditional density function of the data when knowing the individual parameter values, $p(\psi_i)$ is the density function for the individual parameters and $p(y_i)$ is a constant that represents the likelihood.

With individual conditional distributions, one hundred clones per patient were generated and were imputed to Simulx 2024R1 (Lixoft SAS, a Simulations Plus company) [47] to predict through stochastic simulations, and the PASI levels expected at the 5th and 10th cycle (maintenance period) of treatment with UTK were as follows:

- 5th cycle: individual simulations of dosing regimens were generated considering 5 cycles of UTK (steady-state conditions) administration with the administered dosage regimen of each patient.
- 10th cycle: following the 5th cycle, we simulated the combination of alternative dose levels (45 and 90 mg) with different posology (q8w, q12w, q16w, and q20w) for each patient during 5 more cycles of treatment with UTK.

For each patient, the probabilities of achieving the response target (a PASI score ≤ 1) with each simulated dose regimen were calculated in cycle 5 and 10 using the following formula:

$$Probability = \frac{n_{PASI}}{T_{PASI}} \times 100 \quad (3)$$

where n_{PASI} represent the amount of simulated PASI score values that reach the response target (a PASI score ≤ 1), and T_{PASI} represent the total amount of simulated PASI score values (100 clones). In the 10th

cycle, the regimen with which the patient achieved a probability ≥ 90% (i.e., ≥ 90 virtual patients) was selected as the final dosage regimen. In case the patient achieved the response target with more than one dosage regimen, the optimized dosing regimen was selected as the final regimen, which represented a maintenance of the dose over a wider dosing interval or a decrease in the dose within the same dosing interval. The dosage regimen selected in the 10th cycle was compared with the current dosage regimen from the clinical practice of each patient to determine if the patients continued with their current regimen or required a change (optimization or intensification) in the dosage regimen.

3. RESULTS

3.1. Study Population

The modeling dataset consisted of 23 patients including 75 observations in serum samples (PK), a baseline PASI ($PASI_{i,0}$). for each patient, and 117 individual PASI (PD). Table 1 summarizes the characteristics of the study, including demographic data, comorbidities, TDM data, and treatment characteristics that describe the current dosage regimen from the clinical practice of the subjects enrolled.

3.2. Population PK Model

A two-compartment model with first-order absorption and linear disposition processes, previously published by Shao et al. [18], was considered as the population PK model (Figure 2). Then, the statistical significance of covariates included in the reference model was tested with the available information and patient population collected. Only the effect of body weight was maintained on CL, intercompartmental transfer clearance (Q), the V_d, and the peripheral volume of distribution. Therefore, body weight was the only covariate that influenced the determination of individual PK parameter values. The results from the model evaluation exercise indicate that the model could capture the individual PK profiles with adequate accuracy since most of the observations were aligned to the identity line (Figure 3). The pc-VPC of the PK model is shown in Supplementary Figure S1.

Table 1. Summary of patients'characteristics and PK/PD experimental data collected during TDM

	Mean ± SD	Range	n (%)
Demographic data			
Age (years)	62 ± 8.19	45–76	
Body weight (kg)	92 ± 18.4	70–135	
Height (m)	1.67 ± 0.06	1.54–1.83	
BMI (kg/m^2)	32.3 ± 6.8	24–50.19	
Gender (male)			14 (64)
Treatment period (years)	5.43 ± 3.3	0.304–11.4	
Biological "naive"			20 (87)
Comorbidities			
AHT			2 (9)
Dyslipidemia			2(9)
Diabetes			1 (4)
Obesity			4 (16)
Psoriatic arthropathy			2 (9)
Non-alcoholic fatty liver			2 (9)
Anxious–depressive disorder			2 (9)
Others			4 (16)
TDM data			
Total of patients			23
UTK concentration (mg/L)	4.1 ± 3.06	0.27–12.7	
Total of UTK concentrations			75
PASI (no units)	1.096 ± 2.13	0–12	
Total of PASIs			117
PASI $_{i,0}$	14.4 ± 6.23	5–31.9	

Current treatment characteristics							
SmPC		**Optimized**		**Intensified**		**Summary**	
45 mg q12w	1	45 mg q14w	1	90 mg q10w	1	SmPC	9 (40%)
90 mg q12w	8	45 mg q16w	3	90 mg q8w	2	Optimized	11 (48%)
		45 mg q18w	1			Intensified	3 (12%)
		90 mg q14w	1				
		90 mg q15w	2				
		90 mg q16w	3				

SD: standard deviation; BMI: body mass index; AHT: arterial hypertension; TDM: therapeutic drug monitoring; UTK: ustekinumab; PASI: Psoriasis Area and Severity Index; $PASI_{i,o}$: individual observed baseline; SmPC: summary of product characteristics; q8w: once every 8 weeks; q10w: once every 10 weeks; q12w: once every 12 weeks; q14w: once every 14 weeks; q15w: once every 15 weeks; q16w: once every 16 weeks; q18w: once every 18 weeks.

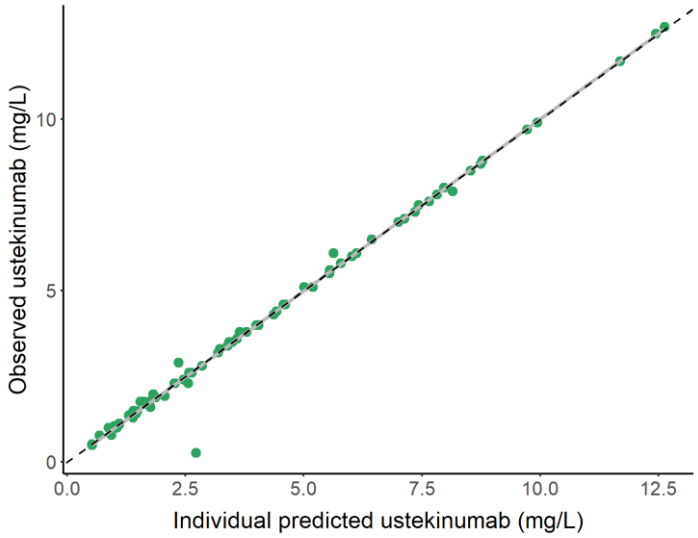

Figure 3. Individual predicted vs. the observed concentrations of UTK in patients with chronic plaque psoriasis.

3.3. Population PK/PD Model

The relationship between UTK concentration and PASI observations was described by an indirect response [48] in which UTK inhibited the zero-order progression constant rate of psoriatic skin lesion (k_{in}) through an I_{max} model. The first-order remission constant rate of psoriatic skin lesion (k_{out}) and the baseline PASI levels using the B2 method were estimated. The IC_{50} was fixed to a published value [16]. Longitudinal individual PK and PD profiles are shown in Figure 4. Overall, the PK/PD model can characterize the longitudinal behavior of the PASI at the individual level, suggesting that the current framework considers properly the combined drug effect and PASI turnover. The pc-VPC of the PK/PD model is shown in Supplementary Figure S2. Parameter estimates of the final population PK/PD model are summarized in Table 2. The mean and standard deviation of individual PK/PD parameters are summarized in Supplementary Tables S1 and S2, respectively.

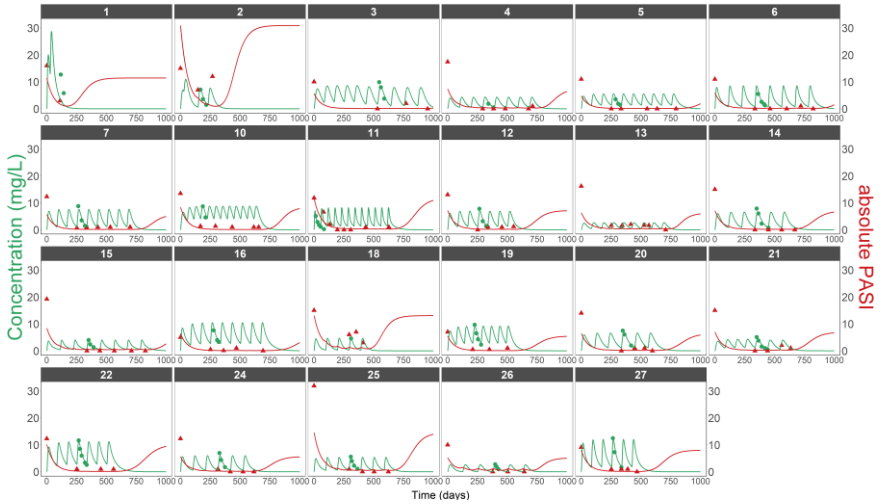

Figure 4. Individual predicted and observed UTK serum concentrations (green) and PASI (red) after UTK administration in patients with chronic plaque psoriasis. The line represents the individual prediction, and the green and red dots represent the UTK and PASI observations, respectively.

Table 2. Population PK/PD estimates after administration of UTK in patients with psoriasis

Parameter (Units)	Value	RSE (%)
Fixed effect		
k_{out} (d^{-1})	0.016	22
I_{max}	0.97	0.7
IC_{50} (mg/L)	0.07 FIX	
Interindividual variability		
k_{out} (%)	55.87	38.9
Residual unexplained variability		
Error (%)	0.86	9.95

k_{out}: first-order remission constant rate of psoriatic skin lesion; I_{max}: maximum inhibition drug effect; IC_{50}: concentration of the drug needed to inhibit 50% of the response.

3.4. Individual Dosing Regimen Evaluation

Probabilities across the cycles of treatment evaluated per patient are represented in Supplementary Figure S3. The MIPD strategy predicted that 8/23 (35%) and 6/23 (26%) of patients would require an optimized and intensified dosage regimen, respectively, compared with the current regimen received in clinical practice for the maintenance period. A change to the approved regimen of 45 mg q12w is proposed

in 3/23 (13%), representing 38% (3/8) of the total optimized patients. Also, in the optimized patients, non-labeled dosing regimens of 45 mg q16w and 45 mg q8w are suggested in 2/8 (24%) and 3/8 (38%) of patients, respectively. Regarding the patients with intensified dosage regimens, a change to 90 mg q8w (3/6) and 45 mg q8w (3/6), respectively, is recommended. No change in the dosing regimen was predicted in 5/23 (22%) patients. This MIPD strategy additionally allowed us to identify that 4/23 (17%) patients would not achieve the efficacy endpoint selected (a 90% probability of a PASI ≤ 1), contributing to the early identification of patients with therapeutic failure (Figure 5).

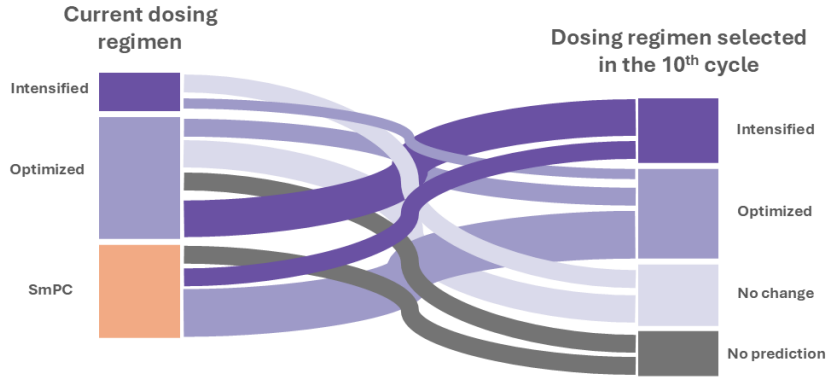

Figure 5. Sankey diagram to indicate the main flows of changes in the individual dose regimen from the current dosage regimen of clinical practice to the predicted dosage regimen in the maintenance period of treatment with UTK (cycle 10). SmPC: summary of product characteristics.

PK and PD simulations with the current dosage regimen from the clinical practice of each subject and the individual optimal dosing regimen established in the 10th cycle are depicted in Supplementary Figure S4. Figure 6 represents the relationship between the absolute PASI and a trough concentration at a steady state ($C_{trough\text{-}ss}$) for each patient, with all dosage regimens tested. Overall, the results suggest a non-linear relationship, indicating that the range of concentration 1.6-1.8 mg/L allows to achieve 90% of patients with a PASI ≤ 1.

4. DISCUSSION

In this study, we developed a procedure capable of individualizing dosing strategies of UTK in clinical practice Spanish patients with moderate to severe chronic plaque psoriasis based on the uncertainty

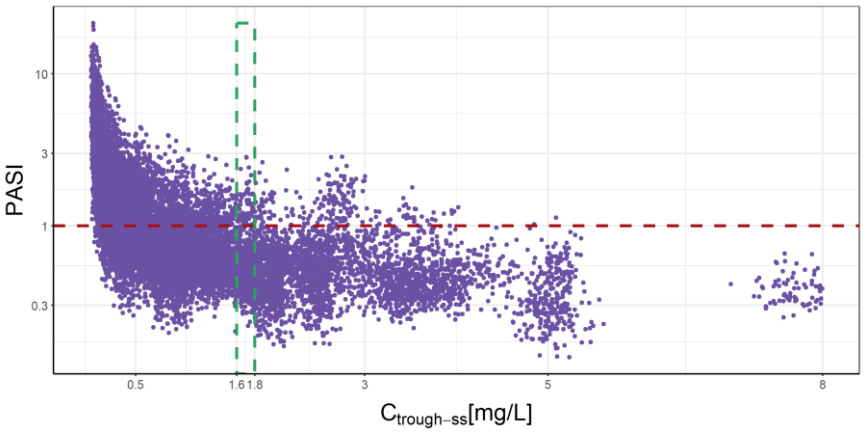

Figure 6. Simulated absolute PASI and trough concentration for each patient after 10 cycles of UTK administration using labeled and non-labeled dosing schemes. $C_{trough\text{-}ss}$: trough concentration at steady state.

of the individual parameter estimates of a population PK/PD model. Additionally, the inclusion of the uncertainty during the simulation step for a personalized dosing regimen selection facilitates the evaluation of the degree of certainty in model-informed predictions in the clinical setting, providing a probabilistic framework for the MIPD of UTK.

Of the total number of patients who need a dosage regimen modification, 35% would be oriented towards an optimized dosage regimen. In 22% of patients, this optimization is proposed to be performed using a non-labeled dosage regimen. This represents a reduction of one dose per year, meaning that patients, instead of receiving five doses of UTK in the first year of treatment with SmPC dosing regimens and four from the second year onwards, would receive four doses and three doses, respectively. According to the database of health information on medicines and parapharmacy products [49] the price of Stelara® 45 mg solution for injection in a pre-filled syringe is EUR 2915.4. Assuming the reduction in dosage, this will entail an annual cost per patient of EUR 11,661.6, which will represent a saving of 25%. In addition to fewer expenses related to the purchase of medication, with the lower number of administrations, there is less risk of the occurrence of injection site reactions due to SmPC. The previous fact includes patients who are to receive 45 mg q16w and also those who are to receive 45 mg q8w because the latter take much more intensive dosage regimens during clinical practice, for example, 90 mg q10w.

From our pool of patients, an intensification of the dosage regimen in comparison with the one received in clinical practice is proposed in 26% of the patients. In these patients, individual CL values higher than the typical value are observed; hence, this type of patient will require higher levels of UTK to achieve a successful therapeutic response. It should be taken into consideration that after performing our strategy for MIPD in UTK, dosage regimen optimization is recommended for most of the patients. As a result, an improvement in patient well-being and health system management can be achieved because, in the end, the patients would always be in an optimal therapeutic response range.

The MIPD strategy did not allow us to reach the efficacy endpoint (a 90% probability of a PASI $\leq$ 1) in 17% of patients. This strategy represents an advantage in identifying non-responding patients at the early stages of treatment, improving the effectiveness in the management of psoriasis for those patients, and avoiding the cost of treating these patients during successive cycles. A more in-depth analysis of these patients reveals CL or k_{out} values higher and lower, respectively, than the population average (Supplementary Figure S3), which could serve as a threshold to characterize patients with a low probability of optimal response to UTK.

For the estimation of individual PK/PD parameters, all the PASI and UTK concentration values available at the time of recruitment were used. To implement the proposed MIPD strategy, an adaptive procedure might be implemented. This procedure would involve re-estimating the individual parameters as additional data points become available to ensure the model remains accurate and reflective of the patient's evolving condition. On the other hand, this analysis confirms the need to collect PASI samples from patients during the first weeks of treatment (the induction phase), which enhances the characterization of PK and PD processes and increases the number of observations per patient, leading to a precise and accurate estimation of their individual PD parameters. The non-linear relationship between the PASI score and trough concentration levels of UTK (Figure 6) demonstrates both the impact of the PK and PD parameters to guarantee satisfactory treatment efficacy. Therefore, although it is possible to establish global exposure values for a PASI value, the individualization of treatment through this MIPD strategy allows for the achievement of a greater number of patients with effective therapeutic regimens, reducing therapeutic failure only for non-responding patients. In our study, a $C_{trough\text{-}ss}$ range of 1.6-1.8 mg/L was

able to help 90% of patients achieve a PASI ≤ 1. Even though the $C_{trough\text{-}ss}$ range obtained in a previous population PK/PD study [17] was 0.0914-0.978 mg/L, it should be noted that this range is representative only for patients weighing 60 to 100 kg with a dosing regimen of 45 mg q12w. Correspondingly, it was generated from the simulated data of patients who were exclusively starting treatment with UTK in pivotal phase III clinical trials, with the efficacy objective of PASI 75 in week 12. However, the range of our study represents a more demanding PD endpoint (PASI ≤ 1 or PASI 99), and it is representative of patients with no body weight limit (92 ± 18.4 [70-135] kg) receiving eight dosage regimens used in clinical practice (45 or 90 mg q8, 12, 16 and 20w) under steady-state UTK therapy conditions. Furthermore, this range provides target $C_{trough\text{-}ss}$ values that are associated with an optimal response in line with current clinical guideline recommendations (PASI ≤1) intended to maximize both clinical outcomes and the quality of life of patients with psoriasis [50,51].

Our work is based on previously published PK /PD models, thus recycling data and using previously developed knowledge, but in addition to our model, we have taken a step forward in the characterization of the relationship between UTK concentrations and response through the PASI observed in real-world clinical data. But also, this study is an example of individual-level precision dosing, which involves a more comprehensive and effective use of precision dosing strategies by recognizing, characterizing, and quantifying the various sources of variability in drug response through PK/PD modeling [23,33]. Such studies are particularly valuable for drugs like UTK that are used to treat heterogeneous conditions like psoriasis, where response variability is significant. While improving our understanding of PK/PD relationships within specific patient subgroups during clinical trials can enhance the identification of precise dosing targets, real-world patients remain significantly more diverse than those in controlled trial settings. Therefore, robust post-marketing surveillance is essential to explore unique precision dosing targets [52]. Advances in data collection and analysis methods from real-world patients offer opportunities to identify new precision dosing algorithms and refine existing ones established in clinical trials. These methods enable the continuous updating and extension of dosing strategies to better meet the individualized needs of patients [33,53]. Thus, our strategy based on MIPD in real-world clinical data could be the first attempt to ensure the most precise individual dosing of patients with plaque psoriasis treated with UTK.

Similar to any real-world study cohort, notable challenges involve the lack of patients (a small patient sample size), a few points available per patient, and therefore the presence of missing data. Due to the study design conditions, many PK/PD observations were taken very spaced out in time, without a continuous characterization (sparse data). For this reason, some unquantified changes in physiology or the progression of the psoriasis disease could directly impact the obtained results. In the future, similar models could be implemented into a conditional distribution dashboard system [54,55]. This would allow for real-time predictions of treatment response, aiding in informed decisions regarding dosing adjustments and treatment transitions for UTK. In this way, as suggested by Mould and Upton in their recently published review [56], options for alternative dosing strategies based on MIPD and/or TDM could be included in the SmPC of UTK.

5. CONCLUSIONS

In conclusion, this study proposes a methodology to individualize UTK dosing strategies considering the uncertainty of individual parameters within a population PK/PD model to optimize the probability of achieving targeted clinical outcomes in patients with moderate to severe chronic plaque psoriasis. This represents an initial step towards performing MIPD for biologics that act on the IL pathways of psoriasis, which has been explored very little. Future studies should implement our proposal in a greater cohort of real-world patients.

6. SUPPLEMENTARY MATERIALS

The following supporting information can be downloaded at: http://www.mdpi.com/xxx/s1 , Ordinary differential equations for the PK/PD model of UTK and PASI; Figure S1: Prediction-corrected visual predictive check obtained from one thousand simulated studies using the selected population PK model; Figure S2: Prediction-corrected visual predictive check obtained from one thousand simulated studies using the selected population PK/PD model; Table S1: Mean of the individual PK/PD parameters drawn from the conditional distribution task in Monolix; Table S2: Standard deviation of the individual PK/PD parameters drawn from the conditional distribution task in Monolix; Figure S3: Bar plot of 100 simulated absolute PASI for each patient after UTK administration at cycles 5 and 10, using the individual parameters from the final population PK/PD model and their uncertainties; Figure S4: PK and PD

simulations with the current dosage regimen from clinical practice and the individual optimal dosing regimen established after simulations in 10th cycle for each patient.

7. AUTHOR CONTRIBUTIONS

Conceptualization, M.M.-S., E.G.-C., M.C.-M., and V.M.-S.; methodology, K.R.-F., J.Z.-F., M.M.-S., E.G.-C., M.C.-M., and V.M.-S.; software, K.R.-F., J.Z.-F., and V.M.-S.; validation, K.R.-F., J.Z.-F., M.S.-B., M.M.-S., A.M.-P., A.M.-C., E.G.-C., M.C.-M., and V.M.-S.; formal analysis, K.R.-F., J.Z.-F., and V.M.-S.; investigation, K.R.-F., J.Z.-F., and V.M.-S.; resources, A.M.-P., A.M.-C., E.G.-C., and M.C.-M.; data curation, K.R.-F.; writing—original draft preparation, K.R.-F., J.Z.-F., and V.M.-S.; writing—review and editing, K.R.-F., J.Z.-F., M.S.-B., M.M.-S., A.M.-P., A.M.-C., E.G.-C., M.C.-M., and V.M.-S.; visualization, K.R.-F. and J.Z.-F. ; supervision, E.G.-C., M.C.-M., and V.M.-S.; project administration, E.G.-C., M.C.-M., and V.M.-S.; funding acquisition, A.M.-P., E.G.-C., and M.C.-M. All authors have read and agreed to the published version of the manuscript.

8. FUNDING

This research received no external funding.

9. INSTITUTIONAL REVIEW BOARD STATEMENT

The study was conducted following the Declaration of Helsinki and approved by the Ethics Committee of La Fe University and Polytechnic Hospital (protocol code: VMS-UTK-2020-01 and date of approval: 27 January 2021).

10. INFORMED CONSENT STATEMENT

Informed consent was obtained from all subjects involved in the study.

11. DATA AVAILABILITY STATEMENT

The data presented in this study are available on request from the corresponding author due to ethical and legal restrictions.

12. CONFLICTS OF INTEREST

The authors declare no conflicts of interest.

13. REFERENCES

1. Schadler, E.D.; Ortel, B.; Mehlis, S.L. Biologics for the primary care physician: Review and treatment of psoriasis. *Dis. A Mon.* 2018, *65*, 51–90. https://doi.org/10.1016/j.disamonth.2018.06.001.
2. Rendon, A.; Schäkel, K. Psoriasis Pathogenesis and Treatment. *Int. J. Mol. Sci.* 2019, *20*, 1475. https://doi.org/10.3390/ijms20061475.
3. Koutruba, N.; Emer, J.; Lebwohl, M. Review of ustekinumab, an interleukin-12 and interleukin-23 inhibitor used for the treatment of plaque psoriasis. *Ther. Clin. Risk Manag.* 2010, *6*, 123–141. https://doi.org/10.2147/tcrm.s5599.
4. Weber, J.; Keam, S.J. Ustekinumab. *Bio. Drugs Clin. Immunother. Biopharm. Gene Ther.* 2009, *23*, 53–61. https://doi.org/10.2165/00063030-200923010-00006.
5. Mahil, S.K.; Capon, F.; Barker, J.N. Update on psoriasis immunopathogenesis and targeted immunotherapy. *Semin. Immunopathol.* 2016, *38*, 11–27. https://doi.org/10.1007/s00281-015-0539-8.
6. Murphy, K.M.; Reiner, S.L. The lineage decisions of helper T cells. *Nat. Rev. Immunol.* 2002, *2*, 933–944. https://doi.org/10.1038/nri954.
7. Tesmer, L.A.; Lundy, S.K.; Sarkar, S.; Fox, D.A. Th17 cells in human disease. *Immunol. Rev.* 2008, *223*, 87–113. https://doi.org/10.1111/j.1600-065X.2008.00628.x.
8. FDA. Approved Drug Products: STELARA (Ustekinumab) Injection, for Subcutaneous or Intravenous Use. March 2024. Available online: https://www.accessdata.fda.gov/drugsatfda_docs/label/2024/761044s013lbl.pdf (accessed on 6 August 2024).
9. Leonardi, C.L.; Kimball, A.B.; Papp, K.A.; Yeilding, N.; Guzzo, C.; Wang, Y.; Li, S.; Dooley, L.T.; Gordon, K.B. Efficacy and safety of ustekinumab, a human interleukin-12/23 monoclonal antibody, in patients with psoriasis: 76-week results from a randomised, double-blind, placebo-controlled trial (PHOENIX 1). *Lancet* 2008, *371*, 1665–1674. https://doi.org/10.1016/s0140-6736(08)60725-4.
10. Papp, K.A.; Langley, R.G.; Lebwohl, M.; Krueger, G.G.; Szapary, P.; Yeilding, N.; Guzzo, C.; Hsu, M.C.; Wang, Y.; Li, S.; et al. Efficacy and safety of ustekinumab, a human

interleukin-12/23 monoclonal antibody, in patients with psoriasis: 52-week results from a randomised, double-blind, placebo-controlled trial (PHOENIX 2). *Lancet* 2008, *371*, 1675–1684. https://doi.org/10.1016/s0140-6736(08)60726-6.

11. Thein, D.; Rosenø, N.A.L.; Maul, J.T.; Wu, J.J.; Skov, L.; Bryld, L.E.; Rasmussen, M.K.; Ajgeiy, K.K.; Thomsen, S.F.; Thyssen, J.P.; et al. Drug Survival of Adalimumab, Secukinumab, and Ustekinumab in Psoriasis as Determined by Either Dose Escalation or Drug Discontinuation during the First 3 Years of Treatment–a Nationwide Cohort Study. *J. Investig. Dermatol.* 2023, *143*, 2211–2218.e2214. https://doi.org/10.1016/j.jid.2023.04.009.
12. Yiu, Z.Z.N.; Mason, K.J.; Hampton, P.J.; Reynolds, N.J.; Smith, C.H.; Lunt, M.; Griffiths, C.E.M.; Warren, R.B. Drug survival of adalimumab, ustekinumab and secukinumab in patients with psoriasis: A prospective cohort study from the British Association of Dermatologists Biologics and Immunomodulators Register (BADBIR). *Br. J. Dermatol.* 2020, *183*, 294–302. https://doi.org/10.1111/bjd.18981.
13. Young, M.S.; Horn, E.J.; Cather, J.C. The ACCEPT study: Ustekinumab versus etanercept in moderate-to-severe psoriasis patients. *Expert. Rev. Clin. Immunol.* 2011, *7*, 9–13. https://doi.org/10.1586/eci.10.92.
14. Zhu, Y.; Hu, C.; Lu, M.; Liao, S.; Marini, J.C.; Yohrling, J.; Yeilding, N.; Davis, H.M.; Zhou, H. Population pharmacokinetic modeling of ustekinumab, a human monoclonal antibody targeting IL-12/23p40, in patients with moderate to severe plaque psoriasis. *J. Clin. Pharmacol.* 2009, *49*, 162–175. https://doi.org/10.1177/0091270008329556.
15. Zhu, Y.W.; Mendelsohn, A.; Pendley, C.; Davis, H.M.; Zhou, H. Population pharmacokinetics of ustekinumab in patients with active psoriatic arthritis. *Int. J. Clin. Pharmacol. Ther.* 2010, *48*, 830–846. https://doi.org/10.5414/cpp48830.
16. Pan, S.; Tsakok, T.; Dand, N.; Lonsdale, D.O.; Loeff, F.C.; Bloem, K.; de Vries, A.; Baudry, D.; Duckworth, M.; Mahil, S.; et al. Using Real-World Data to Guide Ustekinumab Dosing Strategies for Psoriasis: A Prospective

Pharmacokinetic-Pharmacodynamic Study. *Clin. Transl. Sci.* 2020, *13*, 400–409. https://doi.org/10.1111/cts.12725.

17. Zhou, W.; Hu, C.; Zhu, Y.; Randazzo, B.; Song, M.; Sharma, A.; Xu, Z.; Zhou, H. Extrapolating Pharmacodynamic Effects from Adults to Pediatrics: A Case Study of Ustekinumab in Pediatric Patients With Moderate to Severe Plaque Psoriasis. *Clin. Pharmacol. Ther.* 2020, *109*, 131–139. https://doi.org/10.1002/cpt.2033.
18. Shao, J.; Xu, Z.; Xu, Y. Integrated Population Pharmacokinetic Analysis of Ustekinumab Across Multiple Immune-Mediated Inflammatory Disease Populations and Healthy Subjects. *Eur. J. Drug Metab. Pharmacokinet.* 2022, *47*, 537–548. https://doi.org/10.1007/s13318-022-00768-7.
19. Zhou, H.; Hu, C.; Zhu, Y.; Lu, M.; Liao, S.; Yeilding, N.; Davis, H.M. Population-based exposure-efficacy modeling of ustekinumab in patients with moderate to severe plaque psoriasis. *J. Clin. Pharmacol.* 2010, *50*, 257–267. https://doi.org/10.1177/0091270009343695.
20. Rodríguez-Fernández, K.; Mangas-Sanjuán, V.; Merino-Sanjuán, M.; Martorell-Calatayud, A.; Mateu-Puchades, A.; Climente-Martí, M.; Gras-Colomer, E. Impact of Pharmacokinetic and Pharmacodynamic Properties of Monoclonal Antibodies in the Management of Psoriasis. *Pharmaceutics* 2022, *14*, 654. https://doi.org/10.3390/pharmaceutics14030654.
21. Felmlee, M.A.; Morris, M.E.; Mager, D.E. Mechanism-based pharmacodynamic modeling. *Methods Mol. Biol.* 2012, *929*, 583–600. https://doi.org/10.1007/978-1-62703-050-2_21.
22. Notario, J.; Bordas, X. Practical management of ustekinumab in moderate-severe psoriasis. *Actas Dermo-Sifiliográficas* 2012, *103*, 52–58. https://doi.org/10.1016/S0001-7310(12)70009-1.
23. Tyson, R.J.; Park, C.C.; Powell, J.R.; Patterson, J.H.; Weiner, D.; Watkins, P.B.; Gonzalez, D. Precision Dosing Priority Criteria: Drug, Disease, and Patient Population Variables. *Front. Pharmacol.* 2020, *11*, 420. https://doi.org/10.3389/fphar.2020.00420.
24. Syversen, S.W.; Goll, G.L.; Jørgensen, K.K.; Sandanger, Ø.; Sexton, J.; Olsen, I.C.; Gehin, J.E.; Warren, D.J.; Brun, M.K.; Klaasen, R.A.; et al. Effect of Therapeutic Drug

Monitoring vs Standard Therapy During Infliximab Induction on Disease Remission in Patients With Chronic Immune-Mediated Inflammatory Diseases: A Randomized Clinical Trial. *Jama* 2021, *325*, 1744–1754. https://doi.org/10.1001/jama.2021.4172.

25. Albader, F.; Golovics, P.A.; Gonczi, L.; Bessissow, T.; Afif, W.; Lakatos, P.L. Therapeutic drug monitoring in inflammatory bowel disease: The dawn of reactive monitoring. *World J. Gastroenterol.* 2021, *27*, 6231–6247. https://doi.org/10.3748/wjg.v27.i37.6231.
26. D'Haens, G.R.; Sandborn, W.J.; Loftus, E.V., Jr.; Hanauer, S.B.; Schreiber, S.; Peyrin-Biroulet, L.; Panaccione, R.; Panés, J.; Baert, F.; Colombel, J.F.; et al. Higher vs Standard Adalimumab Induction Dosing Regimens and Two Maintenance Strategies: Randomized SERENE CD Trial Results. *Gastroenterology* 2022, *162*, 1876–1890. https://doi.org/10.1053/j.gastro.2022.01.044.
27. Minichmayr, I.K.; Dreesen, E.; Centanni, M.; Wang, Z.; Hoffert, Y.; Friberg, L.E.; Wicha, S.G. Model-informed precision dosing: State of the art and future perspectives. *Adv. Drug Deliv. Rev.* 2024, *2024*, 115421. https://doi.org/10.1016/j.addr.2024.115421.
28. Olivier, B.G.; Swat, M.J.; Moné, M.J. Modeling and Simulation Tools: From Systems Biology to Systems Medicine. *Methods Mol. Biol.* 2016, *1386*, 441–463. https://doi.org/10.1007/978-1-4939-3283-2_19.
29. Darwich, A.S.; Polasek, T.M.; Aronson, J.K.; Ogungbenro, K.; Wright, D.F.B.; Achour, B.; Reny, J.L.; Daali, Y.; Eiermann, B.; Cook, J.; et al. Model-Informed Precision Dosing: Background, Requirements, Validation, Implementation, and Forward Trajectory of Individualizing Drug Therapy. *Annu. Rev. Pharmacol. Toxicol.* 2021, *61*, 225–245. https://doi.org/10.1146/annurev-pharmtox-033020-113257.
30. Minichmayr, I.K.; Mizuno, T.; Goswami, S.; Peck, R.W.; Polasek, T.M.; Pharmacology, t.A.S.o.C.; Community, T.P.D. Recent Advances Addressing the Challenges of Precision Dosing. *Clin. Pharmacol. Ther.* 2024, *116*, 527–530. https://doi.org/10.1002/cpt.3365.
31. Bandín-Vilar, E.; Toja-Camba, F.J.; Vidal-Millares, M.; Durán-Maseda, M.J.; Pou-Álvarez, M.; Castro-Balado, A.; Maroñas, O.; Gil-Rodríguez, A.; Carracedo, Á.; Zarra-

Ferro, I.; et al. Towards precision medicine of long-acting aripiprazole through population pharmacokinetic modelling. *Psychiatry Res.* 2024, *333*, 115721. https://doi.org/10.1016/j.psychres.2024.115721.

32. Rodríguez-Fernández, K.; Reynaldo-Fernández, G.; Reyes-González, S.; de Las Barreras, C.; Rodríguez-Vera, L.; Vlaar, C.; Monbaliu, J.M.; Stelzer, T.; Duconge, J.; Mangas-Sanjuan, V. New insights into the role of VKORC1 polymorphisms for optimal warfarin dose selection in Caribbean Hispanic patients through an external validation of a population PK/PD model. *Biomed. Pharmacother. Biomed. Pharmacother.* 2024, *170*, 115977. https://doi.org/10.1016/j.biopha.2023.115977.
33. Polasek, T.M.; Peck, R.W. Beyond Population-Level Targets for Drug Concentrations: Precision Dosing Needs Individual-Level Targets that Include Superior Biomarkers of Drug Responses. *Clin. Pharmacol. Ther.* 2024, *116*, 602–612. https://doi.org/10.1002/cpt.3197.
34. Hu, C.; Szapary, P.O.; Mendelsohn, A.M.; Zhou, H. Latent variable indirect response joint modeling of a continuous and a categorical clinical endpoint. *J. Pharmacokinet. Pharmacodyn.* 2014, *41*, 335–349. https://doi.org/10.1007/s10928-014-9366-0.
35. Salinger, D.H.; Endres, C.J.; Martin, D.A.; Gibbs, M.A. A semi-mechanistic model to characterize the pharmacokinetics and pharmacodynamics of brodalumab in healthy volunteers and subjects with psoriasis in a first-in-human single ascending dose study. *Clin. Pharmacol. Drug Dev.* 2014, *3*, 276–283. https://doi.org/10.1002/cpdd.103.
36. Chigutsa, E.; Velez de Mendizabal, N.; Chua, L.; Heathman, M.; Friedrich, S.; Jackson, K.; Reich, K. Exposure-Response Modeling to Characterize the Relationship Between Ixekizumab Serum Drug Concentrations and Efficacy Responses at Week 12 in Patients with Moderate to Severe Plaque Psoriasis. *J. Clin. Pharmacol.* 2018, *58*, 1489–1500. https://doi.org/10.1002/jcph.1268.
37. Hu, C.; Yao, Z.; Chen, Y.; Randazzo, B.; Zhang, L.; Xu, Z.; Sharma, A.; Zhou, H. A comprehensive evaluation of exposure-response relationships in clinical trials: Application to support guselkumab dose selection for

patients with psoriasis. *J. Pharmacokinet. Pharmacodyn.* 2018, *45*, 523–535. https://doi.org/10.1007/s10928-018-9581-1.
38. van Huizen, A.; Bank, P.; van der Kraaij, G.; Musters, A.; Busard, C.; Menting, S.; Rispens, T.; de Vries, A.; van Doorn, M.; Prens, E.; et al. Quantifying the Effect of Methotrexate on Adalimumab Response in Psoriasis by Pharmacokinetic-Pharmacodynamic Modeling. *J. Investig. Dermatol.* 2024, *144*, 794–801.e796. https://doi.org/10.1016/j.jid.2023.10.022.
39. Dansirikul, C.; Silber, H.E.; Karlsson, M.O. Approaches to handling pharmacodynamic baseline responses. *J. Pharmacokinet. Pharmacodyn.* 2008, *35*, 269–283. https://doi.org/10.1007/s10928-008-9088-2.
40. Bergstrand, M.; Hooker, A.C.; Wallin, J.E.; Karlsson, M.O. Prediction-corrected visual predictive checks for diagnosing nonlinear mixed-effects models. *AAPS J.* 2011, *13*, 143–151.
41. Upton, R.N.; Mould, D.R. Basic concepts in population modeling, simulation, and model-based drug development: Part 3-introduction to pharmacodynamic modeling methods. *CPT Pharmacomet. Syst. Pharmacol.* 2014, *3*, e88. https://doi.org/10.1038/psp.2013.71.
42. Lixoft. Monolix Suite 2024R1. 2024. Available online: https://lixoft.com/products/monolix/ (accessed on 25 July 2024).
43. Ito, K.; Murphy, D. Application of ggplot2 to Pharmacometric Graphics. *CPT Pharmacomet. Syst. Pharmacol.* 2013, *2*, e79. https://doi.org/10.1038/psp.2013.56.
44. R Core Team. *R: A Language and Environment for Statistical Computing*; R Foundation for Statistical Computing: Vienna, Austria. Available online: http://www.R-project.org/ (accessed on 30 July 2024).
45. Monolix 2024R1 User Guide. Available online: https://monolix.lixoft.com/single-page/ (accessed on 25 January 2024).
46. Kümmel, A.; Bonate, P.L.; Dingemanse, J.; Krause, A. Confidence and Prediction Intervals for Pharmacometric Models. *CPT Pharmacomet. Syst. Pharmacol.* 2018, *7*, 360–373. https://doi.org/10.1002/psp4.12286.
47. Lixoft. Simulx 2024R1. 2024. Available online: https://simulx.lixoft.com/ (accessed on 25 July 2024).

48. Dayneka, N.L.; Garg, V.; Jusko, W.J. Comparison of four basic models of indirect pharmacodynamic responses. *J. Pharmacokinet. Biopharm.* 1993, *21*, 457–478. https://doi.org/10.1007/bf01061691.
49. BOT PLUS. Available online: https://botplusweb.farmaceuticos.com/ (accessed on 29 August 2024).
50. Torres, T.; Puig, L. Treatment goals for psoriasis: Should PASI 90 become the standard of care? *Actas Dermo-Sifiliográficas* 2015, *106*, 155–157. https://doi.org/10.1016/j.ad.2014.10.001.
51. Nast, A.; Smith, C.; Spuls, P.I.; Avila Valle, G.; Bata-Csörgö, Z.; Boonen, H.; De Jong, E.; Garcia-Doval, I.; Gisondi, P.; Kaur-Knudsen, D.; et al. EuroGuiDerm Guideline on the systemic treatment of Psoriasis vulgaris–Part 1: Treatment and monitoring recommendations. *J. Eur. Acad. Dermatol. Venereol.* 2020, *34*, 2461–2498. https://doi.org/10.1111/jdv.16915.
52. Kamal, M.A.; Ganguly, S.; Kadambi, A.; Smith, P.F. Extended Model-Informed Drug Development: Beyond Clinical Trials and Regulatory Approval. *Clin. Pharmacol. Ther.* 2024, *116*, 518–521. https://doi.org/10.1002/cpt.3357.
53. Darwich, A.S.; Ogungbenro, K.; Vinks, A.A.; Powell, J.R.; Reny, J.L.; Marsousi, N.; Daali, Y.; Fairman, D.; Cook, J.; Lesko, L.J.; et al. Why has model-informed precision dosing not yet become common clinical reality? lessons from the past and a roadmap for the future. *Clin. Pharmacol. Ther.* 2017, *101*, 646–656. https://doi.org/10.1002/cpt.659.
54. Dolan, J.G.; Veazie, P.J.; Russ, A.J. Development and initial evaluation of a treatment decision dashboard. *BMC Med. Inform. Decis. Mak.* 2013, *13*, 51. https://doi.org/10.1186/1472-6947-13-51.
55. Mould, D.R.; Upton, R.N.; Wojciechowski, J. Dashboard systems: Implementing pharmacometrics from bench to bedside. *AAPS J.* 2014, *16*, 925–937. https://doi.org/10.1208/s12248-014-9632-5.
56. Mould, D.R.; Upton, R.N. "Getting the Dose Right"-Revisiting the Topic with Focus on Biologic Agents. *Clin. Pharmacol. Ther.* 2024, *116*, 613–618. https://doi.org/10.1002/cpt.3285.

Chapter 5: Personalized Secukinumab Treatment in Patients with Plaque Psoriasis Using Model-Informed Precision Dosing

Karine Rodríguez-Fernández [1,2,†], Javier Zarzoso-Foj [1,2,†], Marina Saez-Bello [3], Almudena Mateu-Puchades [4], Antonio Martorell-Calatayud [5], Matilde Merino-Sanjuan [1,2], Elena Gras-Colomer [6], Monica Climente-Martí [3] and Victor Mangas-Sanjuan [1,2]

Authors Affiliation: [1]Department of Pharmacy and Pharmaceutical Technology and Parasitology, University of Valencia, Valencia, 46100, Spain; [2]Interuniversity Research Institute for Molecular Recognition and Technological Development, Polytechnic University of Valencia-University of Valencia, Valencia, 46100, Spain;[3]Pharmacy Service, Doctor Peset University Hospital, Foundation for the Promotion of Health and Biomedical Research in the Valencian Region (FISABIO), Valencia, 46017, Spain; [4] Dermatology Service, Doctor Peset University Hospital, Foundation for the Promotion of Health and Biomedical Research in the Valencian Region (FISABIO), Valencia, 46017, Spain; [5]Dermatology Service, Hospital Manises of Valencia, Valencia, 46940, Spain; [6]Pharmacy Service, Hospital Manises of Valencia, Valencia, 46940, Spain; [†]These authors contributed equally to this work.

Pharmaceutics. 2024 Dec 10;16(12):1576.

1. INTRODUCTION

Secukinumab (SCK) is a fully human immunoglobulin G1k (IgG1k) mAb designated for the treatment of psoriasis [1,2], a chronic autoimmune skin disorder characterized by pro-inflammatory cytokines and keratinocyte hyperproliferation [3–5]. Psoriasis disease is partially explained by an elevation of proinflammatory IL-17A, which binds to the IL-17 receptor present in keratinocytes, triggering the signaling pathway associated with inflammatory processes [6,7]. The pharmacological mechanism of action of SCK consists in selective binding to IL-17A, which diminishes its interaction with the IL-17 receptor, and therefore, reduces the inflammatory cascade [8].

Currently, SCK (Cosentyx®) is approved as an injection for subcutaneous use for treating plaque psoriasis, also called psoriasis vulgaris, from moderate to severe modality in adults. As indicated in the SmPC [9], SCK should be administered in a dose of 300 mg in weeks 0, 1, 2, 3, and 4 (induction period), and then every 4 weeks (maintenance period). For patients with a body weight of 90 kg or more, a maintenance dose of 300 mg every 2 weeks may provide additional benefit [10]. Clinical trials evaluating the efficacy of SCK in psoriasis have reported notable reductions in PASI scores, reflecting a substantial improvement in disease severity [11–17].

The population PK properties of SCK have been characterized using pooled results from six clinical trials: one phase I, three phase II, and two phase III studies in patients with psoriasis [11–13,18–20]. A two-compartment PK model with first-order absorption for SC administration and with zero-order infusion for IV administration successfully characterized its longitudinal PK behavior in patients with moderate to severe psoriasis [21,22]. SCK shows a terminal half-life of 27 days and slow CL (0.19 L/day). Low central (3.61 L) and peripheral (2.87 L) volumes of distribution were estimated. An allometric relationship between body weight and CL and V_d characterized the influence of body weight on PK disposition parameters of SCK. A disease progression model incorporating a symptomatic drug effect was recently developed for SCK [23]. In this model, the proportion of patients achieving PASI 75 and PASI 90 reported in clinical trials was used as the efficacy index.

The initial treatment with SCK is indicated by dermatologists following the labeled dosing recommendations. This procedure may not be the most favorable or harmless for all patients [24]. When the patient is in

the maintenance phase of treatment with SCK because of the variable psoriasis disease progression and the fluctuation in individual response, modifications in SmPC dosage regimens become necessary. These modifications in the routine clinical practice of a dermatology service are called intensifications and optimizations. The goal of dosage regimen optimization is to either decrease the dose while keeping the dosing interval the same or retain the dose whereas the dosing interval is expanded. In contrast, dosage regimen intensification results in keeping the dose but cutting the dosing interval or increasing the dose but keeping the dosing interval. Due to the lack of a model-informed decision-making process, this strategy raises the likelihood of adverse outcomes caused by the emergence of subtherapeutic or supratherapeutic drug concentrations [25]. Furthermore, rigorous adherence to the sample schedule is required by the individualization techniques that are frequently employed in conventional clinical practice, like those related to TDM and clinical response. During these techniques, the drug's exposure in patients is compared to an objective range to make modifications, and intervention usually happens only after the medication has achieved a steady state. In cases when the exposure deviates from this range, the dosage is modified based on either clinical experience or the hypothesis of proportionality in dose exposure at a steady state [26–29].

For dosage selection in a patient, the ideal treatment and addressing events of insufficient response, gradual depletion of efficacy, or the advent of side effects, dermatologists must adopt an adaptable approach for treating chronic psoriasis vulgaris that contemplates dosage regimens not included in the SmPC (non-labeled) and transitions between various therapeutic alternatives of the disease. These obstacles underline how crucial it is to switch in the direction of MIPD techniques based on population PK/PD models. Because MIPD allows for the use of any timed sample, interventions can be carried out before the initial dosage or until a steady state is attained. The procedure of intervention determines a dosage that meets a predetermined target for PK/PD [29–34]. Therapeutic results and patient safety are improved when PK/PD models are used in dosage selection for the control of chronic plaque psoriasis since they address IIV in therapy responses and increase precision dosing [35-37]. Therefore, this study aims to suggest a strategy for individualizing dosage regimens of SCK in patients with moderate to severe long-lasting psoriasis vulgaris reflecting the uncertainty associated with individual parameters obtained from a population PK/PD model.

2. MATERIALS AND METHODS

2.1. Research Design

A prospective, observational, post-authorization clinical practice follow-up study was carried out at Dr. Peset University Hospital of Valencia on Spanish patients with chronic psoriasis vulgaris from moderate to severe modality. The study's authors certify that the methods used in the investigation comply with the moral guidelines set out by relevant institutional and national bodies that regulate the use of human subjects in research. Additionally, they guarantee adherence to the 1975 Helsinki Declaration, which underwent amendments in 2008. The Dr. Peset University Hospital Ethics Committee approved the study (protocol code VMS-SCK-2020-01 EPA-SP). Prior to beginning any study procedures, the patients' written informed consent was obtained. The time frame for the study was July 2020–December 2022. Patients who were receiving therapy at the time of registration and had received at least one dose of SCK (Cosentyx®) were eligible to participate. Personalized (optimized/intensified) dose regimens were prescribed to the study participants by the dermatologist, considering their clinical responses. Pregnant women, those under the age of 18, and people with cognitive impairments were all excluded. For every patient, therapy-related information including time, dose, and treatment line were gathered. Demographic information, such as weight, sex, height, and age, were also obtained from the hospital's electronic medical records.

2.2. Blood Collection and Sample Analytical Quantification

The patients received 150 or 300 mg of SCK by SC injection (abdomen or upper thigh) every 4, 5 and 6 weeks (q4w, q5w and q6w). Blood samples for PK analysis were collected using plain red vacutainer tubes immediately before SCK administration and approximately 2, 7, 14, 22, 30, and 40 days afterwards. The collected blood samples were centrifuged for 10 to 15 min at 3500–4000 rpm, and subsequently, the remaining was transferred to another tube and frozen until processing. Concentrations of SCK in serum were measured by A. Menarini Diagnostics (08918 Badalona, Barcelona, Spain) using an ISO 15189 [38] validated enzyme-linked immunosorbent assay (ELISA) in a freedom Evolyzer Tecan. The concentration range of the calibration curve was 0.2 μg/mL to 225 μg/mL.

2.3. Assessment of Psoriasis Area and Severity Index Score

Patients which began SCK therapy at Dr. Peset University Hospital's dermatological service received PASI evaluations between weeks 5 and 6 and weeks 16 and 24 after the induction period. Following this, PASI measurements were performed every 6 months. All the PASI scores that were available and registered in patients'clinical records through the almost 1.5-year follow-up period were used for this investigation. Medical records of the patients were additionally examined to extract the baseline PASI values registered at the beginning of the SCK therapy.

2.4. Modeling Data Analysis

A summary of the modeling approach used is shown in Figure 1. The population PK parameters of the published reference model for SCK [21] were employed for simulation to determine if the available model was able to accurately represent our data. A two-compartment model with an absorption compartment through linear processes (Figure 2) represents the structural PK model. Then, a population PK/PD model was developed to characterize the time course of PASI response [39,40]. Several structural PK/PD models were proposed to characterize the time delay between PK and PD observations. Linear, maximum inhibition (I_{max}), and functions for sigmoid drug effects were assessed [41]. The first section of the Supplementary Materials provides the ordinary differential equations of the PK/PD model.

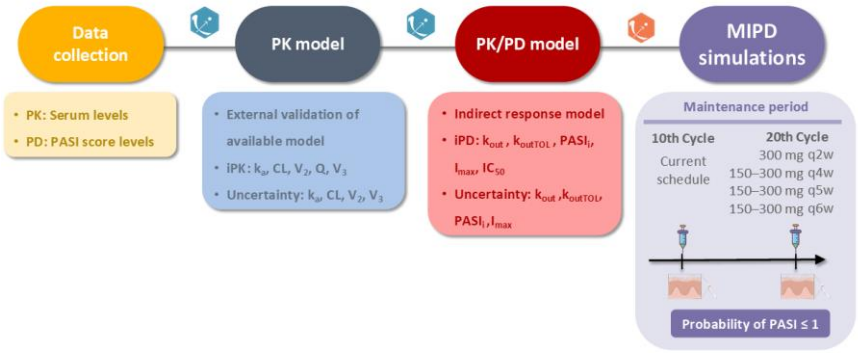

Figure 1. Workflow of the modeling process. PASI: Psoriasis Area and Severity Index; PD: pharmacodynamic; PK: pharmacokinetic; iPK: individual pharmacokinetic parameters; k_a: absorption rate constant; CL: clearance; Q: intercompartmental transfer clearance; V_2: central volume of distribution; V_3: peripheral volume of distribution; iPD:

individual pharmacodynamic parameters; k_{out}: first-order reduction constant rate of psoriatic skin lesion; $k_{outTOLt}$: first-order remission constant rate of tolerance; $PASI_i$: estimated baseline levels of PASI response; I_{max}: maximum inhibition drug effect model; IC_{50}: concentration of the drug needed to inhibit 50% of the response; MIPD: model-informed precision dosing; q2w: once every 2 weeks, q4w: once every 4 weeks, q5w: once every 5 weeks, q6w: once every 6 weeks.

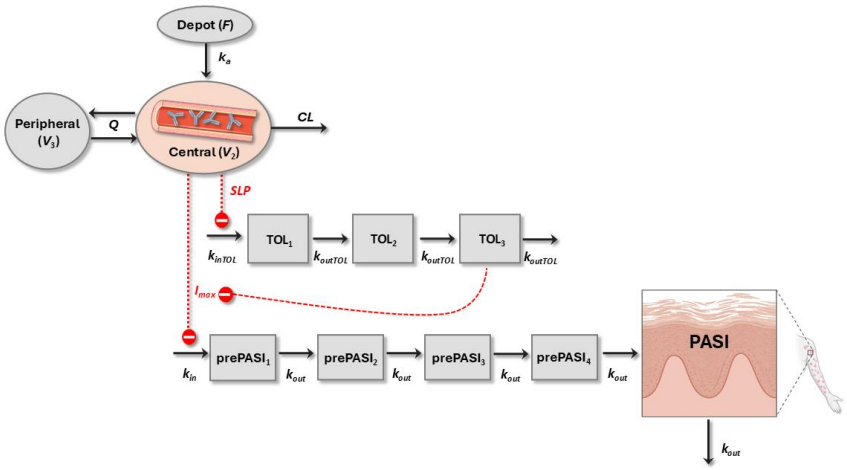

Figure 2. Final PK/PD model representation. F: bioavailability; k_{in}: zero-order evolution constant rate of psoriatic skin lesion; k_{inTOL}: zero-order progression constant rate of tolerance; SLP: linear drug effect model.

The B2 method [42] was applied to estimate baseline levels of PASI response, where $PASI_i$ characterizes the individual predicted baseline level of PASI, the individual observed baseline are represented by $PASI_{i,0}$, and the distinguishing features between $PASI_i$ and $PASI_{i,0}$ are incorporated in the estimated individual random component $\eta_{i,RV}$. The mean of this random component is equal to zero, and its variance is constrained to have the same value as the RUV (Equation (1)). Hence, we expected that the baseline data would likewise exhibit the variability seen in the remaining data.

$$PASI_i = PASI_{i,0} \cdot e^{\eta_{i,RV}} \quad (1)$$

A comparison of the OFV, a visual examination of GOF plots, and the accuracy of model parameters as indicated by the RSE were the basis for selecting the PK/PD model. By applying simulation-based

diagnostics called pc-VPC, the evaluation of the elected PK/PD models was completed [40,43]. The data analyses were conducted via the population approach established in the software Monolix 2024R1 (Lixoft SAS, a Simulations Plus company, Lancaster, CA, USA) [44]. The R software (version 4.4.1; http://cran.r-project.org, accessed on 15 November 2024) [45,46] was used for statistical and graphical analysis.

2.5. Individual Dosage Regimen Approach

The most appropriate MIPD regimen for each patient was found by simulation analysis incorporating the PK and PD individual parameters and their uncertainties, in order to investigate the performance of the final PK/PD model and its influence on clinical practice. The PK and PD individual parameter estimates and their corresponding uncertainty were obtained by computing the individual conditional distributions of PK/PD parameters in Monolix 2024R1 [47]. The degree to which PK and PD individual parameters can be accurately obtained based on the observed data and covariate value for that individual, reflecting that the individual is a member of the population for which the typical parameter value (fixed effects) and the variability (standard deviation of the random effects) were previously estimated, is known as uncertainty [47,48].

A MCMC process known as Metropolis–Hastings algorithms was used to determine individual conditional distributions ($p(\psi_i|y_i)$, where $\psi_i$indicates the individual parameters for individual *i* and y_i symbolizes the data observations for individual i. The following expression was used to sample parameter values from these distributions:

$$p(\psi_i|y_i) = \frac{p(y_i|\psi_i) \cdot p(\psi_i)}{p(y_i)} \quad (4)$$

where the constant that denotes the likelihood is $p(y_i)$, the density function for the individual parameters is referred as $p(\psi_i)$, and $p(y_i|\psi_i)$ reflects the conditional density function of the data when the individual parameter values are known.

In order to predict, via stochastic simulations, the PASI levels and trough concentrations at steady state ($C_{trough\text{-}ss}$) expected at the 10th and 20th cycle (maintenance period) of treatment with SCK, one hundred clones per patient were created applying individual conditional distributions and later imputed to Simulx 2024R1 (Lixoft SAS, a

Simulations Plus company) [49]. Simulations were performed as follows:

- 10th cycle: using each patient's prescribed dosage regimen, simulations of individual dosage regimens were generated considering 10 cycles of SCK (steady-state conditions) administration
- 20th cycle: once 10 cycles were applied, 10 more cycles of SCK treatment for each patient were implemented additionally, to simulate the combination of alternative dose levels (150 and 300 mg) with different posology (q2w, q4w, q5w, and q6w) (Figure 1).

The probabilities of reaching the response aim (PASI score ≤ 1) in the 10th and 20th cycle for each patient, with each simulated dosage regimen, were calculated applying the following expression:

$$Probability = \frac{n_{PASI}}{T_{PASI}} \times 100 \quad (5)$$

The total quantity of simulated PASI score values (100 clones) corresponds to T_{PASI}, whereas n_{PASI} is the number of simulated PASI score values that accomplish the response target (PASI score ≤ 1). The regimen with a probability ≥ 90% (i.e., ≥90 virtual patients) in the 20th cycle was chosen as the final dosage regimen. For methodological reasons, intensified dosing regimens were tested at the 20th cycle; a successful response was achieved even at the 10th cycle. When the response target was reached by the patient with several dosage regimens, it was selected as the final regimen, the one that was the most optimized among all. The most optimized dosage regimen stands for a lower dose while maintaining the dosing interval or equally a larger dosing interval but keeping the dose. After selecting a dosage regimen in the 20th cycle, it was compared with the clinical practice dosing regimen in each patient to determine if it was optimized or intensified, if the patients maintained their current regimen, or if it had not been possible to make a prediction for the patient.

3. RESULTS

3.1. Research Subjects

A total of 22 patients were included in the study. The modeling dataset consisted of 85 concentrations of SCK in samples of serum (PK), 106 individual values of PASI score (PD) and for each patient a baseline

PASI ($PASI_{i,0}$). Comorbidities, demographic and TDM data are presented in Table 1. Moreover, the current dosage regimens of the subjects who participated in the study are described as treatment characteristics in Table 1.

Table 1. Overview of the PK/PD experimental data and patient characteristics gathered within TDM.

	Mean ± SD	Range	n (%)
Demographic data			
Body weight (kg)	74.5 ± 15	46–97	
Height (m)	1.7 ± 0.09	1.54–1.85	
BMI (kg/m²)	25.5 ± 4.9	16–41	
Age (years)	50.07 ± 13.4	28–76	
Gender (male)			14 (64)
Treatment period (years)	2 ± 1.7	0.005–5.1	
Biological "naive"			19 (86)
Comorbidities			
AHT			5 (23)
Dyslipidemia			7 (32)
Diabetes			3 (14)
Obesity			2 (9.1)
Psoriatic arthropathy			5 (23)
Non-alcoholic fatty liver			1 (4.5)
Anxious–depressive disorder			2 (9.1)
Others			11 (50)
TDM data			
Total of patients			22
SCK concentration (mg/L)	48.2 ± 18.5	7.4–89	85
PASI (no units)	1 ± 1.7	0–12.3	106
$PASI_{i,0}$	11.6 ± 5.8	2–27.5	22

Clinical practice treatment characteristics					
SmPC		**Optimized**		**Summary**	
300 mg q4w	18	150 mg q4w	2	SmPC	18 (82%)
		300 mg q5w	1	Optimized	4 (18%)
		300 mg q6w	1	Intensified	none

SD: standard deviation; BMI: body mass index; AHT: arterial hypertension; TDM: therapeutic drug monitoring; SCK: secukinumab; PASI: Psoriasis Area and Severity Index; SmPC: summary of product characteristics; q4w: once every 4 weeks; q5w: once every 5 weeks; q6w: once every 6 weeks.

3.2. Population PK Model

The population PK model was a two-compartment model with first-order absorption and linear disposition processes that had been formerly issued by Bruin et al. [21]. The available data and patient population were then used to examine the statistical significance of the

covariates enclosed in the original paper. Only body weight on CL (0.8) and V_d (1) were maintained through an allometric relationship. Given that most of the observations were in line with the identity line, individual characterization of the individual PK profiles was confirmed (Supplementary Figure S1).

3.3. Population PK/PD Model

An indirect response [50] was selected to describe the relationship between SCK concentration and PASI observations in which SCK inhibits the zero-order evolution constant rate of psoriatic skin lesion (k_{in}). The inhibition of kin through an Imax model provided a statistically significant reduction in the OFV (p-value < 0.01). Other mAbs intended to treat moderate to severe chronic psoriasis vulgaris have previously used this model structure [51–56]. To capture the delay between SCK administration and observable effects, an additional chain of four turnover prePASI compartments was added, each representing a step in the disease progression (Figure 2).

The $PASI_i$ was estimated using the B2 method. Also, the value of first-order reduction constant rate of psoriatic skin lesion (k_{out}) was computed. Due to difficulties during the minimization and convergence processes, the IC_{50} could not be estimated and was fixed to a published value (9.35 mg/L) [23]. A tolerance mechanism was incorporated to account for the increase in PASI score over time during the administration of SCK in four patients (ID: 5, 10, 13, and 16). Tolerance and desensitization phenomena have been previously modeled in preclinical data for proinflammatory cytokines that determine the triggering of plaque psoriasis [57]. A turn-over mechanism including three mediator-like compartments was proposed, where the rate of progression of tolerance (k_{inTOL}) is triggered by drug effects incorporated as a linear function (SLP) of the predicted levels of SCK in serum.

Individual PK and PD profiles across time are reproduced in Figure 3. According to the PK/PD model, the current framework appropriately takes into account the combined action of SCK and PASI turnover, since it can describe the longitudinal behavior of PASI at the individual level. Individual predicted vs. the observed PASI in patients with chronic plaque psoriasis and the pcVPC of the PK/PD model are shown in Supplementary Figures S2 and S3, respectively. Table 2 provides a summary of parameter estimates for the final population PK/PD model. Supplementary Tables S1 and S2 include an overview

of the mean and standard deviation of the PK/PD parameters in each patient, respectively.

Table 2. Population PK/PD estimates in patients with chronic plaque psoriasis after administration of SCK

Parameter (Units)	Value	RSE (%)
Fixed-effect		
k_{out} (day^{-1})	0.11	26.1
k_{outTOL} (day^{-1})	0.003	106
I_{max}	1.19	1.88
IC_{50} (mg/L)	9.35 FIX	
Interindividual variability		
k_{out} (%)	91.3	20
k_{outTOL} (%)	37.15	431
I_{max} (%)	7.63	18
Residual unexplained variability		
Error (%)	0.76	9.2

RSE: relative standard error; k_{out}: first-order reduction constant rate of psoriatic skin lesion; I_{max}: maximum inhibition drug effect; $k_{outTOLt}$: first-order remission constant rate of tolerance; IC_{50}: concentration of the drug needed to inhibit 50% of the response.

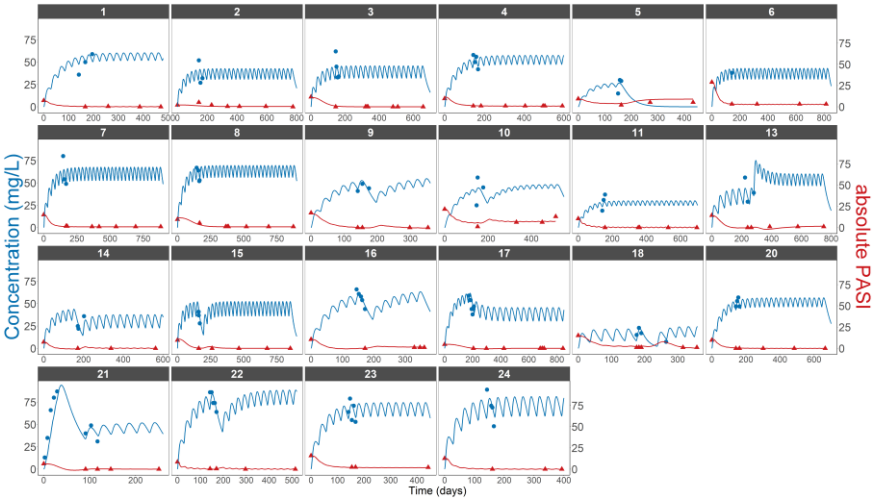

Figure 3. Predicted and observed PASI score (red) and SCK concentrations (blue) after the administration of SCK in patients with long-lasting psoriasis vulgaris. Individual predictions are represented by lines, and the SCK and PASI observations are represented by blue and red dots, respectively.

3.4. Individual Dosage Regimen Evaluation

Supplementary Figure S4 illustrates the probabilities across treatment cycles for each patient. The MIPD strategy indicated that 50% (11/22) of patients would require an optimized dose regimen, while 14% (3/22) would need an intensified regimen compared to the clinical practice regimen used during the maintenance period of treatment with SCK. The optimized patients are suggested to follow non-standard dosage regimens: 150 mg q4w for 9% (1/11), 150 mg q5w for 9% (1/11), 150 mg q6w for 18% (2/11), 300 mg q5w for 45% (5/11), and 300 mg q6w for 18% (2/11) of patients. In patients requiring intensified regimens, switching to 300 mg q2w is advised for all. For 18% (4/22) of patients, no changes to their current regimen were predicted. Furthermore, this MIPD strategy helped identify 18% (4/22) of patients who would not reach the efficacy target (90% probability of PASI ≤ 1), enabling early recognition of those at risk of therapeutic failure. Figure 4 specifies the changes from the dose regimen in clinical practice to the predicted regimen during the maintenance phase of therapy with SCK (cycle 20).

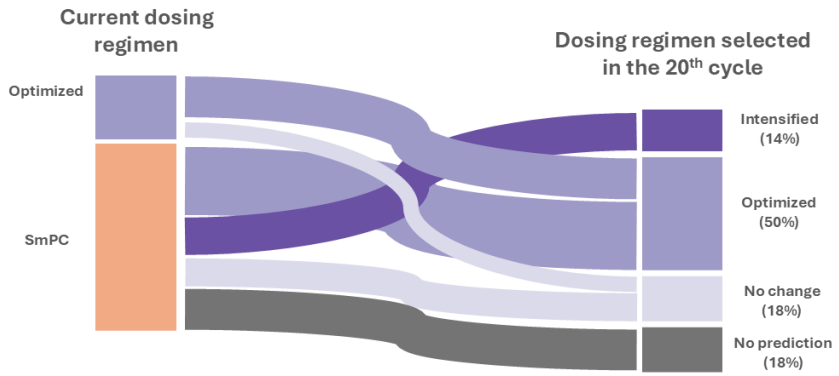

Figure 4. Sankey diagram of the shifts in individual dosage regimens. SmPC: summary of product characteristics.

Supplementary Figure S5 depicts the PK and PD simulations for each patient, comparing the current clinical practice regimen with the optimized dosing regimen determined by the 20th cycle. Figure 5 highlights the connection between absolute PASI scores and steady-state $C_{trough\text{-}ss}$ under all tested regimens. The general findings show a non-linear association, establishing that a $C_{trough\text{-}ss}$ varying from 64.2 to 69.3 mg/L allows a PASI score ≤ 1 in 90% of patients.

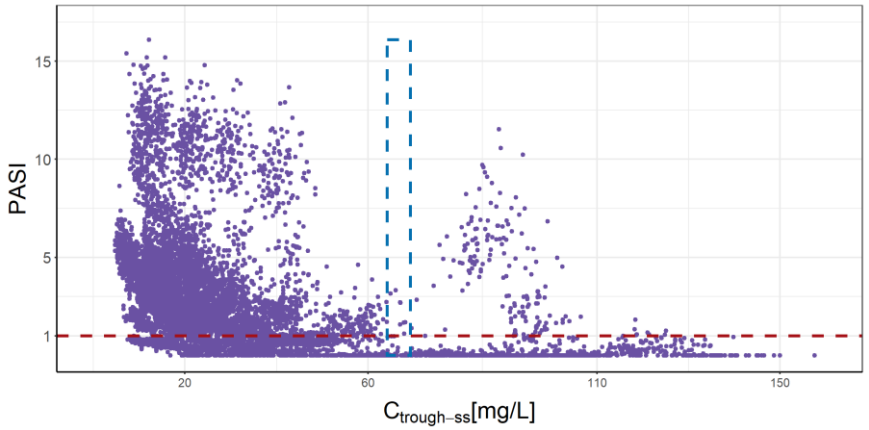

Figure 5. Simulated trough level and absolute PASI score for all subjects after receiving 150 mg q4w, q5w, and q6w; and 300 mg q2w, q4w, q5w and q6w of SCK SC administration in the 20th cycle. The purple dots represent the simulated PASI score and their corresponding $C_{trough-ss}$. The blue dashed box represents the $C_{trough-ss}$ (64.2–69.3 mg/L) that allows a PASI score ≤ 1 in 90% of patients. The red dashed line represents the PASI value of 1. $C_{trough-ss}$: trough concentration at steady state.

4. DISCUSSION

In this study, an exposure-response model was developed for PASI, the most employed endpoint for efficacy in clinical practice patients with persistent psoriasis vulgaris. An indirect response model was evaluated to characterize the effects of SCK, incorporating an additional series of turnover compartments for prePASI and a tolerance mechanism. This approach was based on the expectation of a time lag between the peak concentrations of SCK and the maximum drug effect on psoriatic lesions, represented by PASI scores. Since SCK inhibits the IL-17A, the exposure-efficacy model represented SCK as having an inhibitory pharmacological effect on the development of psoriatic lesions following drug administration. However, we are aware of the drawbacks in the developed PK/PD model reflected in the low precision in parameter estimation of the tolerance mechanism (RSE of k_{outTOL} and RSE of k_{outTOL} IIV), which is only activated in four patients (5, 10, 13, and 16).

The cornerstone of this study was the development of a procedure for tailoring dosing approaches of SCK in Spanish patients with moderate to severe long-lasting psoriasis vulgaris, based on the uncertainty

surrounding individual parameter estimates from a population PK/PD model. Moreover, by integrating uncertainty into the simulation stage designed for personalized dosing regimen choice, it becomes possible to assess the confidence level of model-informed forecasts in clinical practice, offering an approach with probabilistic character for MIPD of SCK. Among the patients needing a modification to their dosage regimen, an optimized dosage regimen is suggested in 50% of them. In almost all optimized patients (91%), the optimization should be to a non-labeled dosage regimen, with 300 mg q5w being recommended in 45% of patients. This adjustment would lead to a decrease of 3 doses for each year, meaning that as an alternative to receiving 14 doses in the following years after the first year of treatment with SKC according to the SmPC dosing guidelines, patients would receive 11 doses. Corresponding to the health information database for medicines and pharmacy products [58], the cost of Cosentyx® 300 mg injection in a pre-filled syringe is EUR 1246.98. With the optimization of SCK therapy, the annual cost per patient would amount to EUR 13717, resulting in savings of 21%. Additionally, fewer medication purchases and a smaller quantity of administrations would decrease the threat of injection site reactions.

In contrast to the clinical practice's dose regimen schedule, intensification was recommended in 14% of the subjects. Because in these patients the I_{max} values were lower (1.06–1.13) than the typical value (1.19), a higher level of SCK dose would be required to achieve a successful therapeutic response. Note that most of the included patients required a dose regimen optimization following the implementation of our MIPD method in SCK. Consequently, since patients are more likely to be within the appropriate treatment response range, it is possible to enhance patient welfare and health system administration. In 18% of subjects, the efficacy endpoint (90% probability of PASI $\leq$ 1) was not obtained. Therefore, the MIPD strategy proposed in this investigation implies a benefit for identifying patients who are not responding to treatment in the beginning. In this way, the management of plaque psoriasis can be enhanced in these individuals, and unnecessary costs associated with treating them in subsequent cycles could be avoided. Furthermore, their k_{out} values are lower (0.07) than the typically observed (0.11), which might be used as a cutoff point for distinguishing patients who are unlikely to respond optimally to SCK.

The full data of SCK concentrations and PASI scores that were acquirable in each patient included in this study were applied to estimate the individual PK/PD parameters. An adaptable process might be employed to apply the suggested MIPD approach into practice. To make sure the model continues to be accurate and still represents the patient's progressing state, this approach would involve a refining process of the individual parameters as novel data points appear. In this study, the importance of collecting samples of absolute PASI from patients throughout the initial weeks of treatment to accurately determine their individual PD parameters is highlighted. The significance of both PK and PD parameters in ensuring effective treatment outcomes is demonstrated by the non-linear relationship between the simulated absolute PASI and $C_{trough\text{-}ss}$ of SCK (Figure 5). While it is feasible to set general exposure values corresponding to an absolute PASI, the use of this MIPD approach to personalize treatment can lead to a higher proportion of patients reaching efficient dosage regimens, thereby minimizing treatment failure among non-responders.

A more exigent $C_{trough\text{-}ss}$ range (64.2-69.3 mg/L) was proposed in this study to accomplish in 90% of patients an absolute PASI ≤ 1. A previously reported $C_{trough\text{-}ss}$ range (12.9-62.9 mg/L) was established in a prior population PK modeling investigation [21], which included individuals on a 300 mg q4w dosage regimen, and it was produced using simulated data from clinical trials in patients who were only beginning therapy with SCK, in which the efficacy objective was to achieve in week 12 the PASI 75. Conversely, the $C_{trough\text{-}ss}$ range found in this research stand for a more rigorous PD endpoint (PASI ≤ 1 or PASI 99) from patients in routine clinical practice. Also, the proposed $C_{trough\text{-}ss}$ range aligns with optimal response criteria consistent with current clinical guidelines (PASI ≤ 1), intended to enhance the quality of life and clinical results for those with persistent psoriasis vulgaris [59,60].

This research is based on PK/PD models previously reported. Nevertheless, our work is an example of how to effectively use established knowledge. However, we have gone one step further in the description of the relationship among SCK concentrations and patient responses measured by absolute PASI under real-world circumstances. In addition, this investigation exemplifies individualized precision dosing, representing a more thorough and effective application of precision dosing approaches by identifying, characterizing, and quantifying the different causes of variability in drug response via

PK/PD modeling [25,35]. While gaining a deeper comprehension of PK/PD interrelation in particular patient populations during clinical studies can aid in identifying precise dosing objectives, patients from clinical practice are often much more distinct than those in supervised study environments. As a result, efficient post-marketing monitoring is crucial for investigating distinctive precision-dosing aims [61]. Improvements in methods for gathering and analyzing data from real-world patients present chances to discover novel precision-dosing procedures and improve those confirmed in clinical trials. These techniques facilitate the ongoing renewing and enhancement of dosing strategies to more effectively address patient requirements [35,62]. That is why our approach, which is based on MIPD under real-world circumstances, may be a first effort to guarantee the most accurate individual dosage for patients with psoriasis vulgaris receiving SCK.

Some limitations have been played against our investigation. Firstly, as a consequence of the study design conditions, there was a small patient sample size. Secondly, many PK/PD observations were either missing or were captured very distant in time (sparse data), resulting in a small number of points per patient. Because of that, the progression of psoriasis vulgaris or unmeasured physiological transformations may have straightforwardly affected the outcomes obtained. Looking ahead, similar models could be incorporated into a provisional distribution dashboard system for enhanced analysis [63,64]. Regarding the proposed optimization with the unlabeled dosage regimen of 300 mg q5w, and despite its advantages in terms of efficiency and safety, sometimes such optimizations may not be carried out because it would mean extending the frequency of administration by one more week. Changing the dosage could cause some confusion in, for example, elderly patients, patients who are seriously ill at the start of SCK therapy, and patients who have been heavily pretreated with multi-resistant forms. Furthermore, we incorporated tolerance mechanisms because we first developed a PK/PD model with all the experimental evidence and then conducted an MIPD approach to evaluate the optimal dosing regimen. Therefore, the tolerance mechanisms could not be anticipated in a traditional TDM approach for prospective prediction without measured PK and PD levels.

The results of this study confirm the recommendations already formulated by other authors, who propose incorporating alternatives for different dosing schemes based on MIPD and/or TDM into the SmPC [65]. This proposal could enhance treatment management in chronic diseases, such as plaque psoriasis, and could facilitate real-time

predictions of treatment responses, helping healthcare providers make informed decisions regarding dosing modifications and therapy transitions for SCK.

5. CONCLUSIONS

In conclusion, this study represents a significant initial step for biologists to implement MIPD that targets the IL routes in long-lasting psoriasis vulgaris, an area that has been largely understudied. We propose a methodology to personalize dosing strategies for SCK, which considers the uncertainty of individual parameters within a population PK/PD model to enhance the likelihood of succeeding targeted clinical effects in patients with psoriasis vulgaris from moderate to severe modality. Future research should focus on applying our approach to a larger group of real-world patients and validating the proposed dosing strategies.

6. SUPPLEMENTARY MATERIALS

The following supporting information can be downloaded at: **https://www.mdpi.com/article/10.3390/pharmaceutics16121576/s1**,Ordinary differential equations for the PK/PD model of SCK and absolute PASI; Figure S1: Individually predicted vs. the observed concentrations of SCK in patients with chronic psoriasis vulgaris; Figure S2: Individually predicted vs. the observed PASI in patients with chronic psoriasis vulgaris; Figure S3: Prediction-corrected visual predictive check obtained from one thousand simulated studies using the selected population PK/PD model; Table S1: Means of the individual PK/PD parameters drawn from the conditional distribution task in Monolix; Table S2: Standard deviation of the individual PK/PD parameters drawn from the conditional distribution task in Monolix; Figure S4: Bar plot of 100 simulated absolute PASI for each patient after SCK administration at cycles 10 and 20, using the individual parameters from the final population PK/PD model and their uncertainties; Figure S5: PK and PD simulations with the current dosage regimen from clinical practice and the individual optimal dosing regimen established after simulations in 20th cycle for each patient.

7. AUTHOR CONTRIBUTIONS

Conceptualization, M.M.-S., E.G.-C., M.C.-M. and V.M.-S.; methodology, K.R.-F., J.Z.-F., M.M.-S., E.G.-C., M.C.-M. and V.M.-S.; software, K.R.-F., J.Z.-F. and V.M.-S.; validation, K.R.-F., J.Z.-F., M.S.-B., M.M.-S., A.M.-P., A.M.-C., E.G.-C., M.C.-M. and V.M.-S.;

formal analysis, K.R.-F., J.Z.-F. and V.M.-S.; investigation, K.R.-F., J.Z.-F. and V.M.-S.; resources, A.M.-P., A.M.-C., E.G.-C. and M.C.-M.; data curation, K.R.-F.; writing—original draft preparation, K.R.-F., J.Z.-F. and V.M.-S.; writing—review and editing, K.R.-F., J.Z.-F., M.S.-B., M.M.-S., A.M.-P., A.M.-C., E.G.-C., M.C.-M. and V.M.-S.; visualization, K.R.-F. and J.Z.-F.; supervision, E.G.-C., M.C.-M. and V.M.-S.; project administration, E.G.-C., M.C.-M. and V.M.-S.; funding acquisition, A.M.-P., E.G.-C. and M.C.-M. All authors have read and agreed to the published version of the manuscript.

8. FUNDING

This research received no external funding.

9. INSTITUTIONAL REVIEW BOARD STATEMENT

This study was conducted following the Declaration of Helsinki and approved by the Ethics Committee of Dr. Peset University Hospital (protocol code: VMS-SCK-2020-01 and date of approval: 30 March 2020).

10. INFORMED CONSENT STATEMENT

Informed consent was obtained from all subjects involved in the study.

11. DATA AVAILABILITY STATEMENT

The data presented in this study are available on request from the corresponding author due to ethical and legal restrictions.

12. CONFLICTS OF INTEREST

The authors declare no conflicts of interest.

11. REFERENCES

1. Frieder, J.; Kivelevitch, D.; Menter, A. Secukinumab: A review of the anti-IL-17A biologic for the treatment of psoriasis. Ther. Adv. Chronic Dis. 2018, 9, 5-21. [CrossRef] [PubMed]
2. Garnock-Jones, K.P. Secukinumab: A review in moderate to severe plaque psoriasis. Am. J. Clin. Dermatol. 2015, 16, 323-330. [CrossRef] [PubMed]
3. Nestle, F.O.; Kaplan, D.H.; Barker, J. Psoriasis. N. Engl. J. Med. 2009, 361, 496-509. [CrossRef]

4. Schadler, E.D.; Ortel, B.; Mehlis, S.L. Biologics for the primary care physician: Review and treatment of psoriasis. Disease-a-Month 2018, 65, 51‑90. [CrossRef] [PubMed]
5. Rendon, A.; Schakel, K. Psoriasis Pathogenesis and Treatment. Int. J. Mol. Sci. 2019, 20, 1475. [CrossRef] [PubMed]
6. Patel, D.D.; Lee, D.M.; Kolbinger, F.; Antoni, C. Effect of IL-17A blockade with secukinumab in autoimmune diseases. Ann. Rheum. Dis. 2012, 72 (Suppl. 2), ii116‑ii1123. [CrossRef]
7. Mahil, S.K.; Capon, F.; Barker, J.N. Update on psoriasis immunopathogenesis and targeted immunotherapy. Semin. Immunopathol. 2016, 38, 11‑27. [CrossRef]
8. Lynde, C.W.; Poulin, Y.; Vender, R.; Bourcier, M.; Khalil, S. Interleukin 17A: Toward a new understanding of psoriasis pathogenesis. J. Am. Acad. Dermatol. 2014, 71, 141‑150. [CrossRef]
9. EMA: COSENTYX-EPAR-product information. Available online: https://www.ema.europa.eu/en/documents/productinformation/cosentyx-epar-product-information_en.pdf (accessed on 17 September 2024).
10. Phung, M.; Ighani, A.; Georgakopoulos, J.R.; Vender, R.; Giroux, L.; Lansang, P.; Yeung, J. Off-Label High-Dose Secukinumab for the Treatment of Moderate-to-Severe Psoriasis. J. Cutan. Med. Surg. 2019, 23, 391‑393. [CrossRef]
11. Rich, P.; Sigurgeirsson, B.; Thaci, D.; Ortonne, J.P.; Paul, C.; Schopf, R.E.; Morita, A.; Roseau, K.; Harfst, E.; Guettner, A.; et al. Secukinumab induction and maintenance therapy in moderate-to-severe plaque psoriasis: A randomized, double-blind, placebo-controlled, phase II regimen-finding study. Br. J. Dermatol. 2013, 168, 402‑411. [CrossRef]
12. Papp, K.A.; Langley, R.G.; Sigurgeirsson, B.; Abe, M.; Baker, D.R.; Konno, P.; Haemmerle, S.; Thurston, H.J.; Papavassilis, C.; Richards, H.B. Efficacy and safety of secukinumab in the treatment of moderate-to-severe plaque psoriasis: A randomized, double-blind, placebo-controlled phase II dose-ranging study. Br. J. Dermatol. 2013, 168, 412‑421. [CrossRef] [PubMed]
13. Langley, R.G.; Elewski, B.E.; Lebwohl, M.; Reich, K.; Griffiths, C.E.; Papp, K.; Puig, L.; Nakagawa, H.; Spelman, L.; Sigurgeirsson, B.; et al. Secukinumab in plaque psoriasis--

results of two phase 3 trials. N. Engl. J. Med. 2014, 371, 326-338.[CrossRef]

14. Augustin, M.; Jullien, D.; Martin, A.; Peralta, C. Real-world evidence of secukinumab in psoriasis treatment−A meta-analysis of 43 studies. J. Eur. Acad. Dermatol. Venereol. JEADV 2020, 34, 1174-1185. [CrossRef] [PubMed]
15. Yiu, Z.Z.N.; Mason, K.J.; Hampton, P.J.; Reynolds, N.J.; Smith, C.H.; Lunt, M.; Griffiths, C.E.M.;Warren, R.B. Drug survival of adalimumab, ustekinumab and secukinumab in patients with psoriasis: A prospective cohort study from the British Association of Dermatologists Biologics and Immunomodulators Register (BADBIR). Br. J. Dermatol. 2020, 183, 294-302. [CrossRef]
16. Leonardi, C.; Zhu, B.; Malatestinic, W.N.; Eastman, W.J.; Guo, J.; Murage, M.J.; Choong, C.K.; Burge, R.; Blauvelt, A. Real-World Biologic Adherence, Persistence, and Monotherapy Comparisons in US Patients with Psoriasis: Results from IBM MarketScan(R) Databases. Adv. Ther. 2022, 39, 3214-3224. [CrossRef]
17. Thein, D.; Roseno, N.A.L.; Maul, J.T.;Wu, J.J.; Skov, L.; Bryld, L.E.; Rasmussen, M.K.; Ajgeiy, K.K.; Thomsen, S.F.; Thyssen, J.P.; et al. Drug Survival of Adalimumab, Secukinumab, and Ustekinumab in Psoriasis as Determined by Either Dose Escalation or Drug Discontinuation during the First 3 Years of Treatment−A Nationwide Cohort Study. J. Investig. Dermatol. 2023, 143, 2211-2218.e2214. [CrossRef] [PubMed]
18. Hueber,W.; Patel, D.D.; Dryja, T.;Wright, A.M.; Koroleva, I.; Bruin, G.; Antoni, C.; Draelos, Z.; Gold, M.H.; Psoriasis Study Group; et al. Effects of AIN457, a Fully Human Antibody to Interleukin-17A, on Psoriasis, Rheumatoid Arthritis, and Uveitis. Sci. Transl. Med. 2010, 2, 52ra72. [CrossRef]
19. Reich, K.; Papp, K.A.; Matheson, R.T.; Tu, J.H.; Bissonnette, R.; Bourcier, M.; Gratton, D.; Kunynetz, R.A.; Poulin, Y.; Rosoph, L.A.; et al. Evidence that a neutrophil-keratinocyte crosstalk is an early target of IL-17A inhibition in psoriasis. Exp. Dermatol. 2015, 24, 529-535. [CrossRef]
20. Paul, C.; Lacour, J.P.; Tedremets, L.; Kreutzer, K.; Jazayeri, S.; Adams, S.; Guindon, C.; You, R.; Papavassilis, C. Efficacy, safety and usability of secukinumab administration by autoinjector/pen in psoriasis: A randomized, controlled trial

(JUNCTURE). J. Eur. Acad. Dermatol. Venereol. JEADV 2015, 29, 1082‑1090. [CrossRef]
21. Bruin, G.; Loesche, C.; Nyirady, J.; Sander, O. Population pharmacokinetic modeling of secukinumab in patients with moderate to severe psoriasis. J. Clin. Pharmacol. 2017, 57, 876‑885. [CrossRef]
22. Rodríguez-Fernández, K.; Mangas-Sanjuán, V.; Merino-Sanjuán, M.; Martorell-Calatayud, A.; Mateu-Puchades, A.; Climente- Martí, M.; Gras-Colomer, E. Impact of Pharmacokinetic and Pharmacodynamic Properties of Monoclonal Antibodies in the Management of Psoriasis. Pharmaceutics 2022, 14, 654. [CrossRef] [PubMed]
23. Liu, Y.; Xu, L.; Wang, X.; Wu, L.; Cai, R.; Li, L.; Zheng, Q. Optimization of secukinumab dose regimens in patients with moderate-to-severe plaque psoriasis via exposure-response modeling. Expert Rev. Clin. Pharmacol. 2023, 16, 999‑1008. [CrossRef]
24. Notario, J.; Bordas, X. Practical management of ustekinumab in moderate-severe psoriasis. Actas Dermo-Sifiliogr. 2012, 103, 52‑58. [CrossRef]
25. Tyson, R.J.; Park, C.C.; Powell, J.R.; Patterson, J.H.; Weiner, D.; Watkins, P.B.; Gonzalez, D. Precision Dosing Priority Criteria: Drug, Disease, and Patient Population Variables. Front. Pharmacol. 2020, 11, 420. [CrossRef] [PubMed]
26. Syversen, S.W.; Goll, G.L.; Jorgensen, K.K.; Sandanger, O.; Sexton, J.; Olsen, I.C.; Gehin, J.E.;Warren, D.J.; Brun, M.K.; Klaasen, R.A.; et al. Effect of Therapeutic Drug Monitoring vs Standard Therapy During Infliximab Induction on Disease Remission in Patients with Chronic Immune-Mediated Inflammatory Diseases: A Randomized Clinical Trial. JAMA 2021, 325, 1744‑1754. [CrossRef] [PubMed]
27. Albader, F.; Golovics, P.A.; Gonczi, L.; Bessissow, T.; Afif,W.; Lakatos, P.L. Therapeutic drug monitoring in inflammatory bowel disease: The dawn of reactive monitoring. World J. Gastroenterol. 2021, 27, 6231‑6247. [CrossRef]
28. D'Haens, G.R.; Sandborn, W.J.; Loftus, E.V., Jr.; Hanauer, S.B.; Schreiber, S.; Peyrin-Biroulet, L.; Panaccione, R.; Panés, J.; Baert, F.; Colombel, J.F.; et al. Higher vs Standard Adalimumab Induction Dosing Regimens and Two Maintenance Strategies: Randomized SERENE CD Trial Results. Gastroenterology 2022, 162, 1876‑1890. [CrossRef]

29. Minichmayr, I.K.; Dreesen, E.; Centanni, M.;Wang, Z.; Hoffert, Y.; Friberg, L.E.;Wicha, S.G. Model-informed precision dosing: State of the art and future perspectives. Adv. Drug Deliv. Rev. 2024, 215, 115421. [CrossRef]
30. Olivier, B.G.; Swat, M.J.; Moné, M.J. Modeling and Simulation Tools: From Systems Biology to Systems Medicine. In Systems Medicine; Schmitz, U., Wolkenhauer, O., Eds.; Methods in Molecular Biology; Humana Press: New York, NY, USA, 2016; Volume 1386, pp. 441‑463. [CrossRef]
31. Darwich, A.S.; Polasek, T.M.; Aronson, J.K.; Ogungbenro, K.; Wright, D.F.B.; Achour, B.; Reny, J.L.; Daali, Y.; Eiermann, B.; Cook, J.; et al. Model-Informed Precision Dosing: Background, Requirements, Validation, Implementation, and Forward Trajectory of Individualizing Drug Therapy. Annu. Rev. Pharmacol. Toxicol. 2021, 61, 225‑245. [CrossRef]
32. Minichmayr, I.K.; Mizuno, T.; Goswami, S.; Peck, R.W.; Polasek, T.M.; American Society of Clinical Pharmacology; Therapeutics Precision Dosing Community. Recent Advances Addressing the Challenges of Precision Dosing. Clin. Pharmacol. Ther. 2024, 116, 527‑530. [CrossRef]
33. Bandín-Vilar, E.; Toja-Camba, F.J.; Vidal-Millares, M.; Durán-Maseda, M.J.; Pou-Álvarez, M.; Castro-Balado, A.; Maronas, O.; Gil-Rodríguez, A.; Carracedo, Á.; Zarra-Ferro, I.; et al. Towards precision medicine of long-acting aripiprazole through population pharmacokinetic modelling. Psychiatry Res. 2024, 333, 115721. [CrossRef] [PubMed]
34. Rodríguez-Fernández, K.; Reynaldo-Fernández, G.; Reyes-González, S.; de Las Barreras, C.; Rodríguez-Vera, L.; Vlaar, C.; Monbaliu, J.M.; Stelzer, T.; Duconge, J.; Mangas-Sanjuan, V. New insights into the role of VKORC1 polymorphisms for optimal warfarin dose selection in Caribbean Hispanic patients through an external validation of a population PK/PD model. Biomed. Pharmacother.=Biomed. Pharmacother. 2024, 170, 115977. [CrossRef] [PubMed]
35. Polasek, T.M.; Peck, R.W. Beyond Population-Level Targets for Drug Concentrations: Precision Dosing Needs Individual-Level Targets that Include Superior Biomarkers of Drug Responses. Clin. Pharmacol. Ther. 2024, 116, 602‑612. [CrossRef]
36. Zhu, Y.; Hu, C.; Lu, M.; Liao, S.; Marini, J.C.; Yohrling, J.; Yeilding, N.; Davis, H.M.; Zhou, H. Population

pharmacokinetic modeling of ustekinumab, a human monoclonal antibody targeting IL-12/23p40, in patients with moderate to severe plaque psoriasis. J. Clin. Pharmacol. 2009, 49, 162‑175. [CrossRef] [PubMed]
37. Zhou, W.; Hu, C.; Zhu, Y.; Randazzo, B.; Song, M.; Sharma, A.; Xu, Z.; Zhou, H. Extrapolating Pharmacodynamic Effects From Adults to Pediatrics: A Case Study of Ustekinumab in Pediatric PatientsWith Moderate to Severe Plaque Psoriasis. Clin. Pharmacol. Ther. 2020, 109, 131‑139. [CrossRef]
38. ISO 15189; Medical Laboratories—Requirements for Quality and Competence. International Organization for Standardization: Geneva, Switzerland, 2022.
39. Mould, D.R.; Upton, R.N. Basic concepts in population modeling, simulation, and model-based drug development. CPT Pharmacomet. Syst. Pharmacol. 2012, 1, e6. [CrossRef]
40. Upton, R.N.; Mould, D.R. Basic concepts in population modeling, simulation, and model-based drug development: Part 3-introduction to pharmacodynamic modeling methods. CPT Pharmacomet. Syst. Pharmacol. 2014, 3, e88. [CrossRef]
41. Felmlee, M.A.; Morris, M.E.; Mager, D.E. Mechanism-based pharmacodynamic modeling. In Computational Toxicology; Reisfeld, B., Mayeno, A., Eds.; Methods in Molecular Biology; Humana Press: Totowa, NJ, USA, 2012; Volume 929, pp. 583‑600. [CrossRef]
42. Dansirikul, C.; Silber, H.E.; Karlsson, M.O. Approaches to handling pharmacodynamic baseline responses. J. Pharmacokinet. Pharmacodyn. 2008, 35, 269‑283. [CrossRef]
43. Bergstrand, M.; Hooker, A.C.; Wallin, J.E.; Karlsson, M.O. Prediction-corrected visual predictive checks for diagnosing nonlinear mixed-effects models. AAPS J. 2011, 13, 143‑151. [CrossRef]
44. Lixoft. Monolix Suite 2024R1 (2024). Available online: https://lixoft.com/products/monolix/ (accessed on 25 July 2024).
45. Ito, K.; Murphy, D. Application of ggplot2 to Pharmacometric Graphics. CPT Pharmacomet. Syst. Pharmacol. 2013, 2, e79. [CrossRef]
46. R Core Team. R: A Language and Environment for Statistical Computing; R Foundation for Statistical Computing: Vienna, Austria, 1999‑2024; Available online: http://www.R-project.org/ (accessed on 30 July 2024).

47. Monolix 2024R1 User Guide. Available online: https://monolix.lixoft.com/single-page/ (accessed on 25 January 2024).
48. Kummel, A.; Bonate, P.L.; Dingemanse, J.; Krause, A. Confidence and Prediction Intervals for Pharmacometric Models. CPT Pharmacomet. Syst. Pharmacol. 2018, 7, 360‐373. [CrossRef] [PubMed]
49. Lixoft. Simulx 2024R1 (2024). Available online: https://simulx.lixoft.com/ (accessed on 25 July 2024).
50. Dayneka, N.L.; Garg, V.; Jusko, W.J. Comparison of four basic models of indirect pharmacodynamic responses. J. Pharmacokinet. Biopharm. 1993, 21, 457‐478. [CrossRef]
51. Zhou, H.; Hu, C.; Zhu, Y.; Lu, M.; Liao, S.; Yeilding, N.; Davis, H.M. Population-based exposure-efficacy modeling of ustekinumab in patients with moderate to severe plaque psoriasis. J. Clin. Pharmacol. 2010, 50, 257‐267. [CrossRef] [PubMed]
52. Salinger, D.H.; Endres, C.J.; Martin, D.A.; Gibbs, M.A. A semi-mechanistic model to characterize the pharmacokinetics and pharmacodynamics of brodalumab in healthy volunteers and subjects with psoriasis in a first-in-human single ascending dose study. Clin. Pharmacol. Drug Dev. 2014, 3, 276‐283. [CrossRef]
53. Tham, L.-S.; Tang, C.-C.; Choi, S.-L.; Satterwhite, J.H.; Cameron, G.S.; Banerjee, S. Population exposure-response model to support dosing evaluation of ixekizumab in patients with chronic plaque psoriasis. J. Clin. Pharmacol. 2014, 54, 1117‐1124. [CrossRef] [PubMed]
54. Pan, S.; Tsakok, T.; Dand, N.; Lonsdale, D.O.; Loeff, F.C.; Bloem, K.; de Vries, A.; Baudry, D.; Duckworth, M.; Mahil, S.; et al. Using Real-World Data to Guide Ustekinumab Dosing Strategies for Psoriasis: A Prospective Pharmacokinetic-Pharmacodynamic Study. Clin. Transl. Sci. 2020, 13, 400‐409. [CrossRef]
55. Kerbusch, T.; Li, H.; Wada, R.; Jauslin, P.M.; Wenning, L. Exposure-response characterisation of tildrakizumab in chronic plaque psoriasis: Pooled analysis of 3 randomised controlled trials. Br. J. Clin. Pharmacol. 2020, 86, 1795‐1806. [CrossRef]
56. Rodríguez-Fernández, K.; Zarzoso-Foj, J.; Saez-Bello, M.; Mateu-Puchades, A.; Martorell-Calatayud, A.; Merino-Sanjuan,

M.; Gras-Colomer, E.; Climente-Martí, M.; Mangas-Sanjuan, V. Model-Informed Precision Dosing for Personalized Ustekinumab Treatment in Plaque Psoriasis. Pharmaceutics 2024, 16, 1295. [CrossRef]
57. DeBonis, J.; Veiseh, O.; Igoshin, O.A. Uncovering the interleukin-12 pharmacokinetic desensitization mechanism and its consequences with mathematical modeling. CPT Pharmacomet. Syst. Pharmacol. 2024. [CrossRef]
58. BOT PLUS. Available online: https://botplusweb.farmaceuticos.com/ (accessed on 29 August 2024).
59. Torres, T.; Puig, L. Treatment goals for psoriasis: Should PASI 90 become the standard of care? Actas Dermo-Sifiliogr. 2015, 106, 155-157. [CrossRef]
60. Nast, A.; Smith, C.; Spuls, P.I.; Avila Valle, G.; Bata-Csorgo, Z.; Boonen, H.; De Jong, E.; Garcia-Doval, I.; Gisondi, P.; Kaur-Knudsen, D.; et al. EuroGuiDerm Guideline on the systemic treatment of Psoriasis vulgaris−Part 1: Treatment and monitoring recommendations. J. Eur. Acad. Dermatol. Venereol. JEADV 2020, 34, 2461-2498. [CrossRef] [PubMed]
61. Kamal, M.A.; Ganguly, S.; Kadambi, A.; Smith, P.F. Extended Model-Informed Drug Development: Beyond Clinical Trials and Regulatory Approval. Clin. Pharmacol. Ther. 2024, 116, 518-521. [CrossRef] [PubMed]
62. Darwich, A.S.; Ogungbenro, K.; Vinks, A.A.; Powell, J.R.; Reny, J.L.; Marsousi, N.; Daali, Y.; Fairman, D.; Cook, J.; Lesko, L.J.; et al. Why has model-informed precision dosing not yet become common clinical reality? lessons from the past and a roadmap for the future. Clin. Pharmacol. Ther. 2017, 101, 646-656. [CrossRef]
63. Dolan, J.G.; Veazie, P.J.; Russ, A.J. Development and initial evaluation of a treatment decision dashboard. BMC Med. Inform. Decis. Mak. 2013, 13, 51. [CrossRef] [PubMed]
64. Mould, D.R.; Upton, R.N.; Wojciechowski, J. Dashboard systems: Implementing pharmacometrics from bench to bedside. AAPS J.2014, 16, 925-937. [CrossRef]
65. Mould, D.R.; Upton, R.N. "Getting the Dose Right" − Revisiting the Topic with Focus on Biologic Agents. Clin. Pharmacol. Ther. 2024, 116, 613-618. [CrossRef]

Results and Discussion

Results and Discussion

Part 1: In-silico Prediction of Food Effects on the Bioavailability of Orally Administered Drugs

This section summarizes the main findings of the research work described in Chapter 1.

Food can significantly alter the PK of orally administered drugs by modifying the rate and extent of drug absorption, thereby impacting both their therapeutic efficacy and safety [46]. Conventional PBPK models are increasingly used to predict FE, but PBPK model parameterization is challenged by IVIV disconnect and/or parameter non-identifiability. To overcome these issues a novel method has been proposed capable of establishing a quantitative framework for the early prediction of FE by estimating a range (the SR) from the interplay of solubility of the drug in a biorelevant medium and the dose.

The characterization of *in vitro* solubility in FaSSIF medium is often considered to adequately mimic *in vivo* conditions of orally administered drugs. However, the measured solubility may still be conservative as *in vitro* settings may not adequately capture the *in vivo* sink conditions and transit kinetics [48]. Thus, not all BCS II/IV drugs classified based on measured solubility exhibit positive FE. The determination of FaSSIF/D provides a drug-independent determinant of OR drug absorption *in vivo*. A conservative setting for FE prediction was ensured by choosing an upper and lower limit of conservative SR of FaSSIF/D based on a determination of FaSSIF in the Boehringer Ingelheim laboratory for 26 compounds. If the compound FaSSIF/D values were less than $3x10^{-5}$ 1/ml (below SR), it is likely to present FE. If FaSSIF/D was greater than $1x10^{-3}$ 1/ml (above SR), it is likely to exhibit no FE (Figure 4). If the FaSSIF/D value is in the SR area, then SLA determination with PBPK simulations can help to predict if the drug is likely to have FE or not, if the drug is not extensively metabolized in the gut. The inclusion of the 25 additional compounds with literature-reported FaSSIF data provided comparable SR limits to those derived from our laboratory data, despite the FaSSIF values found in the literature being derived from different laboratories and unreported conditions of measurements. Therefore, with this study, it was demonstrated that FaSSIF/D can indeed discriminate between drugs with or without FE, as long as the drugs are outside the SR. Extension of this work in the future to cover all compounds within SR will serve

to further enhance confidence in the use of SLA to identify drugs that are likely to exhibit positive FE.

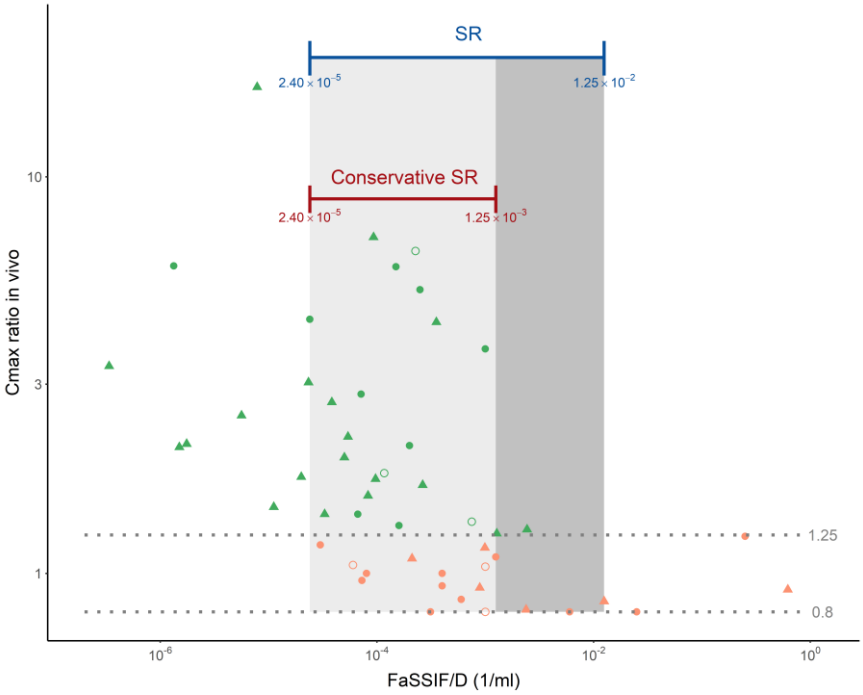

Figure 4. Conservative SR with experimental FaSSIF data and SR with experimental FaSSIF data plus literature FaSSIF data. The shadow grey area represents the SR. Grey dotted lines represent the limits for FE categorization, green filled circles represent the compounds with FE positive and FaSSIF measured experimentally, green filled triangles represent the compounds with FE positive and FaSSIF from literature, orange filled circles represent the compounds with no FE and FaSSIF measured experimentally, orange filled triangles represent the compounds with no FE and FaSSIF from literature, non-filled circles present the compounds with FE positive (green) and no FE (orange) within conservative SR and SR with FaSSIF measured experimentally and selected for PBPK simulations of SLA.

For SLA determination, as dose-adjusted solubility is decreased from a hypothetically high value, the corresponding simulated OR drug absorption is constant at 100% and high, until a critical threshold, below which OR drug absorption starts to decrease. A drug with a dose-adjusted solubility below this critical threshold is said to have SLA. The *in vivo* solubility of such a drug may be enhanced by food via its influence on one or more factors (gastric pH, gastric emptying rate,

as well as drug and bile salt concentrations). This approach is not valid for compounds with high intestinal metabolism nor substrates of intestinal transporters; both felodipine and clopidogrel are high CL drugs (Table 1) with extensive CYP3A4-mediated intestinal metabolism. Consequently, the bioavailability of these drugs is limited by metabolism to a much larger extent than limited by solubility. Extensive gut metabolism is likely for very high CL CYP3A4 or UGT substrates and can be identified in the PBPK model when simulated C_{max} with FaSSIF solubility is greater than the observed C_{max} (since it is unlikely that FaSSIF solubility is greater than *in vivo* solubility). However, even when C_{max} with FaSSIF solubility is less than the observed C_{max}, gut metabolism cannot be excluded for CYP3A4 and UGT substrates. The individual contributions of solubility and gut metabolism in limiting drug absorption are non-identifiable since model optimization against observed plasma drug concentrations can resolve uncertainty only in one parameter. Thus, for drugs with gut metabolism, the resulting masking will provide conservative estimates of FE prediction, if it is possible to apply the proposed approach (C_{max} simulated with FaSSIF < C_{max} observed). Unfortunately, a reliable quantitative prediction of gut metabolism is not easy even for CYP3A substrates [102-104]. However, since most high CL drugs are screened out during lead optimization, and low CL drugs are not likely to be impacted by gut metabolism, the proportion of drugs for which FE cannot be reliably predicted by the method proposed by this work is expected to be low.

Difficulty in verifying underlying mechanisms of the multiple processes such as dissolution, precipitation and solubilization included in conventional PBPK models [44,45,105,106], leads to a model with many assumptions that may fit the observed data but cannot reliably predict an untested scenario (e.g., FE). The parameterization of these models relies on *in vitro* data that are generally under-predictive and cannot be optimized against the observed concentration-time profile due to non-identifiability. Therefore, FE predictions with PBPK models in the traditional setting tend to be conservative and uncertain resulting in unnecessary clinical FE studies [49]. This implies that pilot FE studies would be conducted even for drugs that may not have SLA or FE *in vivo* (e.g., a drug like mefenamic acid).

Table 1. SLA for the prediction of FE using the PBPK modeling approach

* The value could not be determined.

Compound		Clopidogrel	Felodipine	Mefenamic acid	Digoxin	Efavirenz	Carbamazepine
Solubility	**FaSSIF**	0.017	0.01	0.015	0.001	0.07	0.3
	Optimize	0.06	0.012	0.5	0.055	0.068	0.85
	Maximum	*	*	0.5	0.055	0.22	1.8
AUC ratio	**Observed**	9.2	1.53	0.97	0.98	1.28	1.12
	Predicted	*	*	1	1	1.44	1.08
C_{max} ratio	**Observed**	6.5	1.04	1.05	0.8	1.79	1.35
	Predicted	*	*	1	1	1.87	1.21
Positive FE *in vivo*		yes	no	no	no	yes	yes
Positive FE predicted by		*	*	no	no	yes	yes
CYP3A4 or UGT		CYP3A4	CYP3A4	no	no	CYP3A4	CYP3A4, UGT
CL (L/h)		84[110]	90[109]	21.23(po)[108]	5.28[108]	9.4 (po)[108]	2.7[107]

AUC: area under the curve; C_{max}: maximum blood/plasma concentration; CL: total body clearance value; CYP3A4: Cytochrome P450 3A4; FaSSIF: fasted state simulated intestinal fluid solubility; Maximum solubility: PBPK model hypothetical solubility that exceeds the optimized solubility that helps to identify SLA; Optimized solubility: PBPK model hypothetical solubility beyond which there were no further changes between predicted and observed profile; PBPK: physiologically based pharmacokinetic model; SLA: solubility-limited absorption; UGT: uridine diphosphate glucuronosyltransferase.

We have proposed a basic framework to assess FE prediction based on a simplified model, where the SLA is the surrogate for FE. This allows the only parameter that impacts FE (solubility) to be optimized against observed data for drugs that are not extensively metabolized/effluxed in the gut, thereby resulting in a more reliable FE prediction. However, this is only a retrospective study. In the future, this approach can be applied to prospective predictions. A reliable binary prediction of FE (yes/no) in a conservative setting (no false negatives) using the method proposed in this work is more valuable for making timely decisions on the need for a pilot FE study and the timing of a pivotal FE study compared to quantitative prediction by a PBPK in the traditional setting based on several assumptions and uncertain parameters.

Part 2: Preclinical Characterization of Entero-Hepatic Circulation Processes of Amiodarone

This part summarizes the main findings of the research work described in Chapter 2.

The drug AM has a lipophilic character and a distinct PK profile that shows a relationship between OR maintenance dose and plasma levels. Although AM effectively controls arrhythmias, higher dosages also can raise the possibility of drug toxicity [111]. Thus, it is more beneficial to verify total cumulative doses rather than plasma AM levels. Gaining knowledge of AM's PK can help enhance dosage modification and decrease variability. Furthermore, the authorized IV formulation is not recommended for use in newborns or children younger than three years old because it includes benzyl alcohol. Consequently, it is essential to create OR formulations to increase AM's bioavailability [112,113]. Complex PK processes may generate unprecise model predictions; thus, a quantitative modeling framework should consider biological complexity in experimental data for valid drug development decision-making.

The study involved 96 male Wistar rats of 20 weeks, 250-320 g body weight, with 985 AM observations in plasma (n = 901) and bile (n = 84). IV and OR routes of administration of AM at dose levels from 10 to 25 mg were evaluated, including single and multiple dosing regimens. IV formulation was the commercial injectable of AM chlorhydrate (Trangorex®, 50 mg/ml). Three OR formulations of AM were evaluated, including the IV injectable (Trangorex®, Solution I, 50 mg/ml), a suspension from Trangorex® tablets (Tablet, 200 mg), and a solution with 5% Polysorbate 80 (Solution II, 5 mg/ml).

A population PK model has been successfully applied to characterize the absorption and EHR processes of three OR formulations of AM (Solution I, Tablet and Solution II) by adapting a previous population PK model [80] that accounted for the non-linear and linear distribution processes of AM after IV administration (Figure 5).

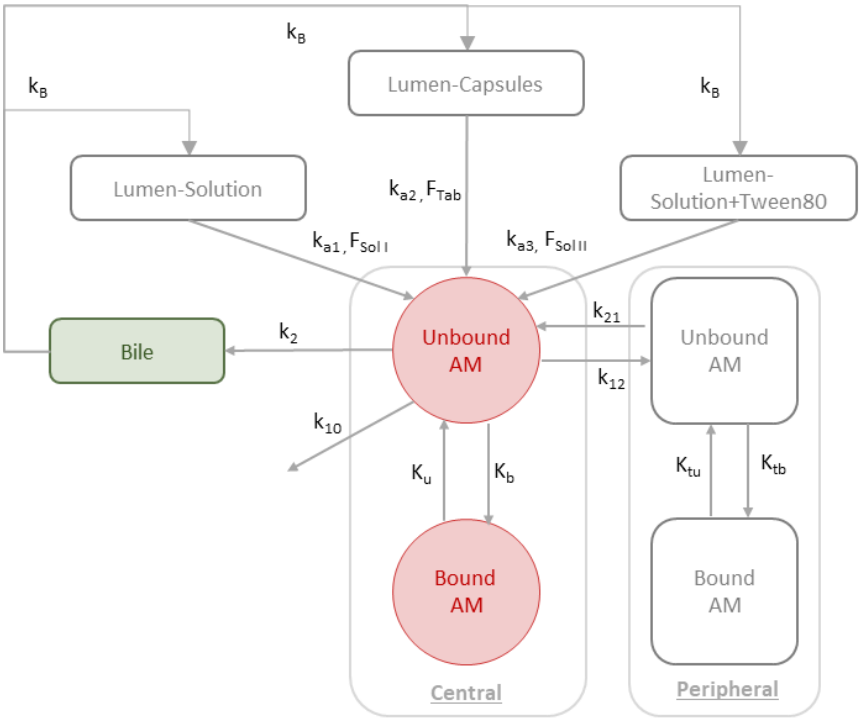

Figure 5. Schematic representation of the final PK model developed. k_B: first-order rate constant from bile, k_{a1}: first-order absorption rate constant of Solution I formulation, $F_{Sol\,I}$: OR bioavailability of Solution I formulation, k_{a2}: first-order absorption rate constant of Tablet formulation, F_{Tab}: OR bioavailability of Tablet formulation, k_{a3}: first-order absorption rate constant of Solution II formulation, $F_{Sol\,II}$: OR

bioavailability of Solution II formulation, k_{10}: first-order elimination rate constant, k_2: first-order distribution constant, K_u: rate constant of unbinding in central compartment, K_b: rate constant of binding in central compartment, K_{tu}: rate constant of unbinding in peripheral compartment, K_{tb}: rate constant of binding in peripheral compartment, k_{21}: first-order distribution constant from central to peripheral compartment, k_{12}: first-order rate constant from peripheral to central compartment.

The EHR represents the distribution of free AM from the central compartment into the bile and then, into the lumen based on the evidence collected in continuous enterohepatic cycle (CC group) and non-continuous enterohepatic cycle (NC group). The population PK model quantifies the fraction (12.3%) of AM that suffers EHR and the respective fraction of AM that is metabolized. This result confirms the significant contribution of EHR in the disposition of AM, although due to the absence of experimental observations in the lumen, the fraction excreted via feces could not be estimated. Following the model evaluation results, the model was able to accurately represent the longitudinal profiles of the median and the data distribution based on the standard GOF plots (Figure 6).

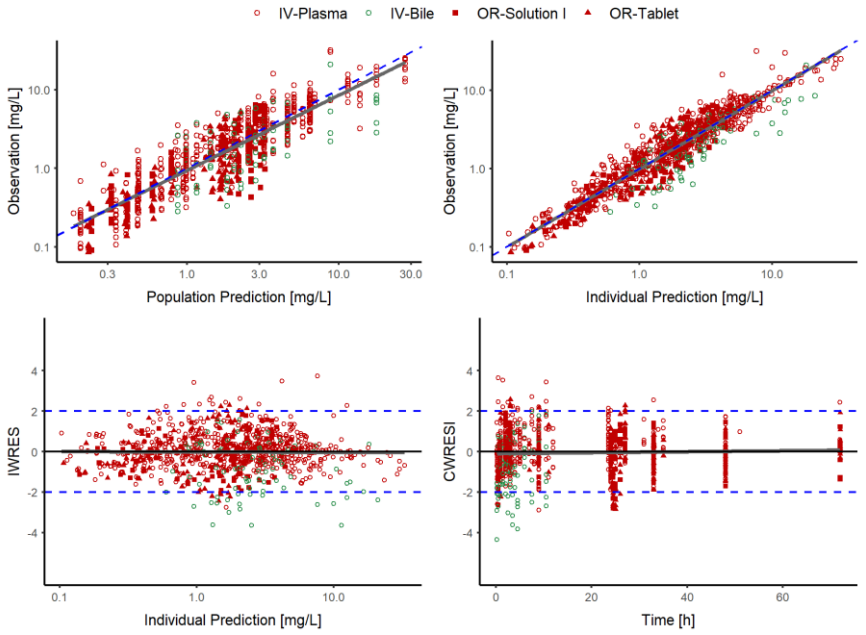

Figure 6. GOF plots of the final population PK model of AM in rats for each OR formulation. The grey solid line represents the non-linear

regression, and the blue dotted line represents the line of identity. IWRES: individual weighted residuals, CWRESI: conditional weighted residuals.

The ability to determine from a very simplistic perspective to a more detailed and complex manner the mechanisms involved in the time course of a drug contributes to a more efficient and rational decision-making process. Thus, the re-utilization of PK models and their integration into new experimental evidence enhances the potential impact and recognition from adjoining areas. The population PK model externally validates the disposition PK model previously proposed for AM in rats [80] to quantify the contribution of OR formulations and EHR of AM. Similar final parameter estimates were observed between both approaches, demonstrating the adequacy of the population PK model of AM in rats.

The final population PK model assumes a different k_a for each formulation ($k_{a1}=1.33\bullet10^{-1}$ h^{-1}, $k_{a2}=8.20\bullet10^{-2}$ h^{-1} and $k_{a3}= 2.05\bullet10^{-1}$ h^{-1}) showing a k_a of AM from Solution II and Solution I increased by 2.5- and 1.62-fold compared to Tablet formulation. Furthermore, the bioavailability of AM from Tablet, Solution I, and Solution II was 37%, 40%, and 50%, respectively. The overall results demonstrate the contribution of supramicellar concentrations of surfactant (Polysorbate 80) in the OR absorption improvement of AM. With the performed simulation-based analysis of unbound/bound fractions of AM, an eightfold dose increase (from 12.5 to 100 mg) suggests that the ratio of unbound/bound fractions of AM is only modified by 3%. For that reason, at typical concentrations, protein plasma binding is unlikely to be saturated. In this regard, novel formulations that improve AM bioavailability are unlikely to significantly alter the fractions of free AM in plasma or the time required to achieve equilibrium between the free and bound fractions.

Part 3: Precision Dosing for Optimal Dosage Regimen Selection in Small Molecules and Monoclonal Antibodies

This section summarizes the main findings of the research work described in Chapter 3, Chapter 4 and Chapter 5.

Warfarin Dose Range in Caribbean Hispanic Patients

Warfarin is an OR anticoagulant that has been used for decades to prevent thromboembolic events. It works by inhibiting the synthesis of vitamin K-dependent clotting factors in the liver, thus reducing the production of blood clots [114]. However, warfarin therapy is associated with several challenges, including a narrow therapeutic window, a high risk of bleeding, and significant interpatient variability in response. Several investigations have studied the effects of genetic polymorphisms on warfarin response, especially for two important pharmacogenes: the *VKORC1* gene encodes the catalytic subunit 1 of the vitamin K epoxide reductase complex enzyme, and the *CYP2C9* gene encodes the cytochrome P450 isoform 2C9, an enzyme belonging to cytochrome P450 superfamily [115,116]. Warfarin administration creates significant therapeutic gaps since there are currently no clinical guidelines assessing the effects of distinct *CYP2C9* and *VKORC1* genotypes on routine INR values (efficacy surrogate endpoint) in the Caribbean Hispanic population. Consequently, according to individual INR values, patients show sub-optimal clinical response rates. To address this, we have adapted a population PK/PD model of warfarin from individual data and dose records over 2 years in Caribbean Hispanic elderly patients from a local anticoagulation clinic to optimize the dosing regimens in this population.

A total of 138 Caribbean Hispanic individuals (mean age: 68 years, mean weight: 83 kg), with 1033 INR observations were included in the study. All the patients received long-term warfarin anticoagulant therapy for different thromboembolic disorders in total weekly doses ranging from 7 to 82 mg, depending on the 24- or 48-hour dosing intervals. Eight different *CYP2C9* alleles (*1/*2, *1/*3, *1/*5, *1/*8, *2/*2, *2/*3, *2/*5) and three *VKORC1* haplotypes (G/A, G/G, A/A) were present in the included patients. By performing an external validation of PK and PK/PD models previously published [117,118], it can be confidently extrapolating findings from the model to real-

world patient scenarios such as the Hispanic Caribbean population, for collecting their behavior which is different from that used in previous studies.

As previously reported [118], the final population PK/PD model includes the body weight on V_d and *CYP2C9* on CL as covariates. Additionally, *VKORC1* polymorphisms are included as a statistically significant covariate for the PD parameters INR_{base} and IC_{50}. By taking into consideration the effects of particular alleles (G and A), the influence of *VKORC1* haplotypes on IC_{50} was modeled, offering a more reliable estimate in rare genotypes. One of the most surprising results of this study is the IC_{50} values obtained for each of the *VKORC1* haplotypes were higher (9.22–11.76 mg/L) than those earlier reported in other populations (1.56–3.11 mg/L) [12,119]. This is consistent with the therapeutic gaps observed in this underrepresented population and suggests increased resistance of Caribbean Hispanic patients to warfarin, who may require more intensive dosing regimens to achieve similar target INR responses. This phenomenon may be the consequence of a longer longitudinal evaluation than in previous studies (>2000 d), as well as a slightly higher distribution of G/G and G/A polymorphisms that may be partially affecting the point estimate.

On the other hand, when considering the INR_{base} across different *VKORC1* haplotypes, we observed higher measures in A/A carriers (2.18) compared to those in patients with haplotypes containing the G allele (1.78 and 1.84, respectively). This could be explained by a more prolonged prothrombin time and lower levels of functional (active) prothrombin-dependent coagulation factors in carriers of the *VKORC1*-A allele due to their reduced expression of the hepatic VKORC1 enzyme, which plays a pivotal role in the vitamin K cycle in the liver. As a result, the prothrombin time will be prolonged, and the INR level will rise accordingly. This would open the door to hypothesize that *VKORC1* polymorphisms not only affect the potency of warfarin but also influence basal INR levels, partially explaining the excessive IIV in INR_{base}. After the covariate analysis, the IIV on INR_{base} and IC_{50} were reduced to 23% and 34%, respectively. A satisfactory agreement between the observed data and model predictions for the median (50th percentile) and the variability (2.5th and 97.5th percentiles) was suggested by the examination of the pc-VPC (Figure 7).

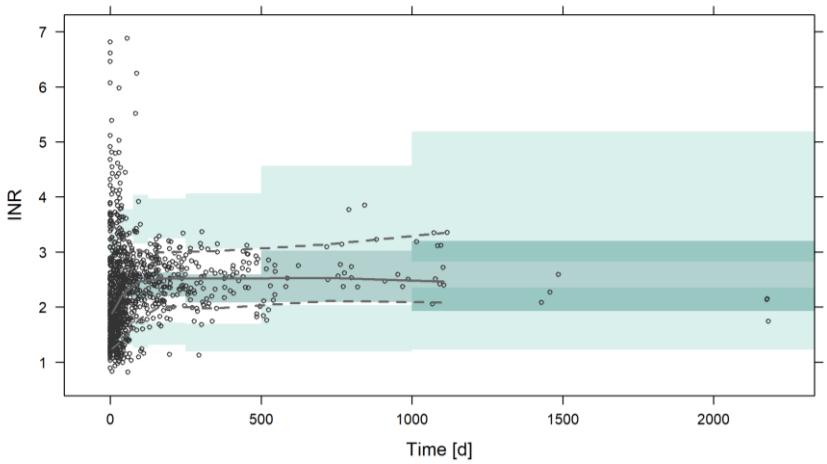

Figure 7. Prediction-corrected visual predictive checks of the final population PD model. Grey lines represent the 2.5th, 50th and 97.5th experimental percentiles. Green shaded areas represent the 95% prediction interval of the 2.5th, 50th and 97.5th percentiles. Empty grey dots represent experimental INR observations. INR: international normalized ratio.

A MIPD for dosage regimen selection has been conducted based on simulations to calculate the probability of ensuring therapeutic INR levels (2-3) in a virtual population using the fixed and random parameters from the final population PK/PD model for different daily regimens of warfarin. The different sub-populations considered are the result of the combination of *CYP2C9* and *VKORC1* polymorphisms. In this regard, 3-5 mg of daily warfarin would achieve therapeutic INR levels in most of the scenarios considered (Figure 8). The sub-group of patients with * 2/* 2-, * 2/* 3- and * 2/* 5-A/A would require only 1 mg daily of warfarin to achieve therapeutic INR levels at steady-state conditions. Our findings support the significance and clinical relevance of using a population PK/PD approach in elucidating the role of genetic polymorphisms (e.g., *CYP2C9* and *VKORC1* haplotypes) for the optimal design of warfarin dosing schemes in Caribbean Hispanic patients. The simulations provided a comprehensive understanding of how a broader range of *CYP2C9* variants and, specifically, the *VKORC1*-1636 A allele influences the PK and PD of warfarin, as well as baseline INR measures, within this diverse population and shed light on potential underlying mechanisms linked to increased IC_{50} values.

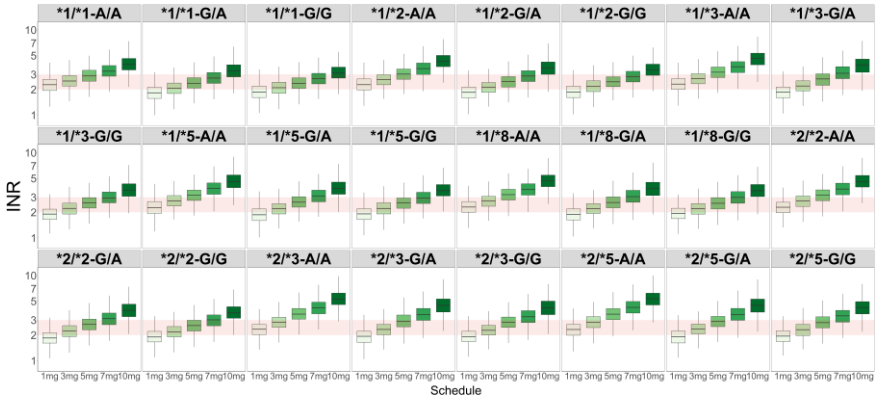

Figure 8. Stochastic simulations (n = 10,000) of INR levels using the final population PK/PD model assuming different daily dosing regimens for each sub-population of *CYP2C9* and *VKORC1* polymorphisms. The red band represents the therapeutic INR interval (2-3). INR: international normalized ratio.

This MIPD approach is expected to minimize the risk of adverse events linked to inaccurate warfarin dosing due to genetic differences at the individual level and enhance therapeutic outcomes. In addition, it will ultimately foster safer and more effective clinical management of personalized anticoagulation therapy in this specific patient subgroup, which is often underrepresented in clinical studies.

Individualized Ustekinumab and Secukinumab Treatment in Patients with Plaque Psoriasis

Psoriasis is a chronic (long-lasting) disease in which the immune system becomes overactive, causing keratinocyte hyperproliferation. Key mediators in the disease process include infiltration of Th17 cells and overproduction of pro-inflammatory IL such as IL-12, IL-23, and IL-17A[14]. These ILs can be specifically targeted by mAbs for instance, UTK and SCK, as a part of the available biological therapies for psoriasis. UTK acts directed against the common p40 IL-12 and IL-23 subunit. At the same time, SCK selectively binds to IL-17A and diminishes its interaction with the IL-17 receptor, and therefore, both mAbs reduce the inflammatory cascade of psoriasis [120,121].

A post-authorization, prospective, multicentre, and observational clinical practice follow-up study was conducted on patients with plaque psoriasis undergoing UTK and SCK treatment. A total of 75 plasma samples and 117 PASI measures (efficacy surrogate endpoint) were

available from the 23 patients (mean age: 62 years [standard deviation (SD) =8.19 %], mean weight: 92 kg [SD=18.4 %]) included in the study of UTK. Regarding the investigation of SCK, a total of 22 patients (mean age: 50 years [SD=13.4%], mean weight: 74.5 kg [SD=15%]), with 85 plasma samples and 106 PASI observations were included.

Population PK/PD Models

The relationship between UTK concentration and PASI observations was described using the same structure of the indirect response reference model previously published for UTK [122], where UTK inhibited the zero-order progression constant rate of psoriatic skin lesion (k_{in}) through an I_{max} model. This indirect response model [123] was also selected to describe the relationship between SCK concentration and PASI. To capture the delay between SCK administration and observable effects, an additional chain of 4 turnover prePASI compartments was added, each representing a step in disease progression. A tolerance mechanism was incorporated to account for the increase in PASI score over time during the administration of SCK in four patients. Tolerance and desensitization phenomena have been previously modeled in preclinical data for proinflammatory cytokines that determine the triggering of plaque psoriasis [124]. A turn-over mechanism including three mediator-like compartments was proposed, where the rate of progression of tolerance (k_{inTOL}) is triggered by drug effects incorporated as a linear function (SLP) of the predicted levels of SCK in serum.

The first-order remission constant rate of psoriatic skin lesion (k_{out}) and the baseline PASI levels using the B2 method were estimated for both mAbs [125]. Due to difficulties during the minimization and convergence processes, the IC_{50} could not be estimated and were fixed to published values for UTK (0.07 mg/L) [122] and SCK (9.35 mg/L) [126]. Figure 9 depicts the PK/PD models for UTK and SCK respectively.

Personalized Dosage Regimen Approach

The off-label individualization dosing of UTK and SCK, with optimizations and intensifications, is frequently applied in clinical practice to improve the individual benefit/risk balance. In this part, it was developed a procedure capable of individualizing dosing strategies of UTK and SCK in clinical practice Spanish patients with moderate to

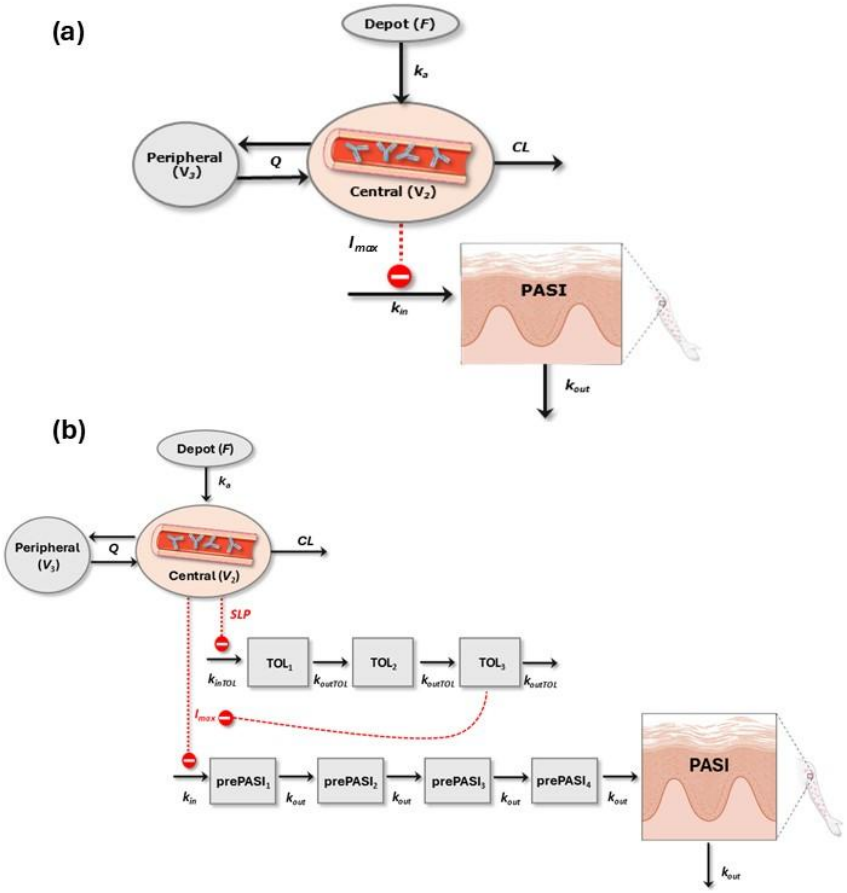

Figure 9. Schematic representation of the final PK/PD model for UTK (a) and SCK (b).F: bioavailability; k_a: absorption rate constant; CL: clearance; Q: intercompartmental transfer clearance; V_2: central volume of distribution; V_3: peripheral volume of distribution; I_{max}: maximum inhibition drug effect model; k_{in}: zero-order progression constant rate of psoriatic skin lesion; k_{out}: first-order remission constant rate of psoriatic skin lesion; SLP: linear drug effect model; k_{inTOL}: zero-order progression constant rate of tolerance; $k_{outTOLt}$: first-order remission constant rate of tolerance.

severe chronic plaque psoriasis based on the uncertainty of the individual parameter estimates of a population PK/PD model. Additionally, the inclusion of the uncertainty during the simulation step for a personalized dosing regimen selection facilitates the evaluation of the degree of certainty in model-informed predictions in the clinical setting, providing a probabilistic framework for the MIPD of UTK and SCK.

Of the total number of patients treated with UTK who need a dosage regimen modification, 35% (8/23) would be oriented toward an optimized dosage regimen. In 22% (5/23) of patients, this optimization is proposed to be performed using a non-labeled dosage regimen. This represents a reduction of one dose per year and therefore a decrease in drug spending. Also, with the lower number of administrations, there is less risk of an occurrence of injection site reactions due to the SmPC.

An intensification of the dosage regimen compared to the one received in clinical practice is proposed in 26% (6/23) of the patients. In these patients, individual CL values higher than the typical value are observed; hence, this type of patient will require higher levels of UTK to achieve a successful therapeutic response. Among the patients treated with SCK who need a modification to their dosage regimen, it is suggested an optimized regimen for 50% (11/22) of them. This optimization should be to a non-labeled dosage regimen in almost all optimized patients (91%). This adjustment would lead to a decrease of 3 doses per year. In comparison with the dosage regimen received in clinical practice, an intensification of SCK is proposed in 14% (3/22) of the patients. Because individual I_{max} values in these patients were lower (1.06 –1.13) than the typical value (1.19), a higher level of SCK dose would be required to achieve a successful therapeutic response. In general optimizations or intensifications of UTK and SCK dosage in clinical practice, related to the ones described in the SmPC, can take into consideration the recommendations obtained through the proposed MIPD along with other factors related to the patient, lifestyle, etc., and the usage policy defined in hospital centers with interdisciplinary consensus.

The MIPD strategy did not allow to reach the efficacy endpoint (a 90% probability of a PASI ≤ 1) in a comparable percent of patients treated with UTK (17%) and SCK (18%). Therefore, the MIPD strategy proposed for UTK and SCK implies an advantage in recognizing non-responding patients at the early stages of treatment. In this way, the management of psoriasis can be enhanced for these patients and the unnecessary costs associated with treating them in subsequent cycles could be avoided. A more in-depth analysis of these patients reveals k_{out} values lower (0.011 and 0.07 d^{-1}) than the population average (0.016 and 0.11d^{-1}) for UTK and SCK respectively. This could serve as a threshold to characterize patients with a low probability of optimal response to UTK. The main changes in the individual dose regimen of

UTK and SCK from the current to the predicted via the MIPD approach are represented in Figure 10.

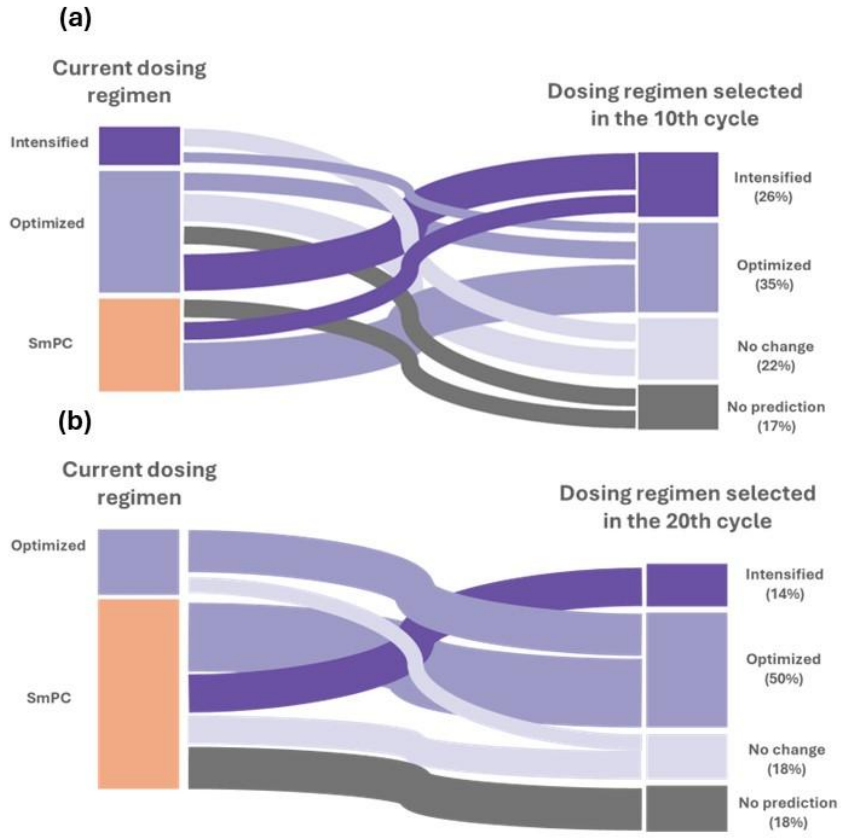

Figure 10. Sankey diagram to indicate the main flows of changes in the individual dose regimen from the current dosage regimen of clinical practice to the predicted dosage regimen in the maintenance period of treatment with UTK in cycle 10 (a) and SCK in cycle 20 (b).

For the estimation of individual PK/PD parameters, all the PASI, UTK and SCK concentration values available at the time of recruitment were used. To implement the proposed MIPD strategy, an adaptive procedure might be implemented. This procedure would involve re-estimating the individual parameters as additional data points become available to ensure the model remains accurate and reflective of the evolving condition of the patient. On the other hand, this analysis confirms the need to collect PASI samples from patients

during the first weeks of treatment (the induction phase), which enhances the characterization of PK and PD processes and increases the number of observations per patient, leading to a precise and accurate estimation of their individual PD parameters.

By identifying, characterizing, and quantifying the different sources of variability in drug response through PK/PD modeling, this study exemplifies individual-level precision dosing using real-world clinical data, which entails a more thorough and efficient use of precision dosing strategies [88,127]. For medications like UTK and SCK that are used to treat diverse chronic inflammatory diseases like psoriasis, where response variability is substantial, such trials are very helpful. Enhancements in the gathering and evaluation of data from actual patients can aid in the discovery of novel precision dosing algorithms and the improvement of current ones, allowing for the ongoing extension and modification of dosing plans to better suit the unique requirements of each patient [85,127]. Thus, our strategy based on MIPD in real-world clinical data could be the first attempt to ensure the most precise individual dosing of patients with plaque psoriasis treated with UTK and SCK.

Like any real-world study cohort, the small patient sample size, the limited number of points accessible per patient, and consequently the existence of missing data are significant obstacles. The study's design conditions resulted in a large number of PK/PD observations that were taken at extremely different times and lacked continuous characterization (sparse data). Because of this, some unmeasured alterations in physiology or the course of psoriasis may have a direct effect on the outcomes. Despite the limitations, similar models could be implemented into a conditional distribution dashboard system in the future, similar models could be implemented into a conditional distribution dashboard system [128,129]. This would enable real-time treatment response predictions, supporting well-informed decisions about UTK and SCK therapy transitions and dosage modifications. In this manner, the SmPC of UTK and SCK could incorporate alternatives for MIPD-based dosing techniques, as proposed by Mould and Upton in their recently published review [130].

Conclusions

Conclusions

1. The selection of the sensitivity range of dose-adjusted solubility in a biorelevant medium and identification of solubility-limited absorption by the PBPK model allows for reliable prediction of food effect to enable decisions on the need for pilot and timing of pivotal food effect studies.

2. The population PK model of amiodarone demonstrated the contribution of entero-hepatic circulation to the overall disposition and the absorption enhancement when amiodarone is formulated with supramicellar concentrations of Polysorbate 80 (Solution II) compared to commercially available OR formulation (Tablet). This may contribute to developing suitable and alternative OR solution formulations for patients with swallowing difficulties that could improve the benefit/risk balance of amiodarone.

3. Tailored and precise warfarin dosing recommendations of 1 and from 3 to 5 mg for guiding anticoagulant therapy in Caribbean Hispanic individuals were proposed based on the predictive capacity of the population PK/PD modeling approach.

4. The proposed methodology to individualize UTK and SCK dosing strategies considering a PK/PD model with the uncertainty of individual parameters, allows optimizing the probability of achieving target clinical outcomes in patients with moderate to severe chronic plaque psoriasis and represents an initial and underexplored step towards performing MIPD for biologics acting on interleukin pathways, to increase effectiveness, safety and efficiency of the treatment.

5. Overall, the pharmacometrics model-informed strategies implemented in this Thesis have demonstrated their relevance for characterizing the PK/PD properties of small molecules and biologic drugs in the preclinical and clinical setting, aiming to guide individualized optimal treatment for patients and better healthcare outcomes.

References

References

1. Lalonde, R.L.; Kowalski, K.G.; Hutmacher, M.M.; Ewy, W.; Nichols, D.J.; Milligan, P.A.; Corrigan, B.W.; Lockwood, P.A.; Marshall, S.A.; Benincosa, L.J.; et al. Model-based drug development. *Clinical pharmacology and therapeutics* **2007**, *82*, 21-32, doi:10.1038/sj.clpt.6100235.
2. Milligan, P.A.; Brown, M.J.; Marchant, B.; Martin, S.W.; van der Graaf, P.H.; Benson, N.; Nucci, G.; Nichols, D.J.; Boyd, R.A.; Mandema, J.W.; et al. Model-Based Drug Development: A Rational Approach to Efficiently Accelerate Drug Development. *Clinical Pharmacology & Therapeutics* **2013**, *93*, 502-514, doi:https://doi.org/10.1038/clpt.2013.54.
3. Williams, P.; Ette, E., (Eds.) *Pharmacometrics: impacting drug developement and Pharmacotherapy* John Wiley and Sns, Inc.: Hoboken, New Jersey, 2007.
4. Sheiner, L.B. Learning versus confirming in clinical drug development. *Clinical pharmacology and therapeutics* **1997**, *61*, 275-291, doi:10.1016/s0009-9236(97)90160-0.
5. Madabushi, R.; Seo, P.; Zhao, L.; Tegenge, M.; Zhu, H. Review: Role of Model-Informed Drug Development Approaches in the Lifecycle of Drug Development and Regulatory Decision-Making. *Pharmaceutical Research* **2022**, *39*, 1669-1680, doi:10.1007/s11095-022-03288-w.
6. Reigner, B.G.; Williams, P.E.; Patel, I.H.; Steimer, J.L.; Peck, C.; van Brummelen, P. An evaluation of the integration of pharmacokinetic and pharmacodynamic principles in clinical drug development. Experience within Hoffmann La Roche. *Clinical pharmacokinetics* **1997**, *33*, 142-152, doi:10.2165/00003088-199733020-00005.
7. Gieschke, R.; Steimer, J.L. Pharmacometrics: modelling and simulation tools to improve decision making in clinical drug development. *European journal of drug metabolism and pharmacokinetics* **2000**, *25*, 49-58, doi:10.1007/bf03190058.
8. Gobburu, J.V.S. Pharmacometrics 2020. *The Journal of Clinical Pharmacology* **2010**, *50*, 151S-157S, doi:https://doi.org/10.1177/0091270010376977.
9. Lee, J.Y.; Garnett, C.E.; Gobburu, J.V.; Bhattaram, V.A.; Brar, S.; Earp, J.C.; Jadhav, P.R.; Krudys, K.; Lesko, L.J.; Li, F.; et al. Impact of pharmacometric analyses on new drug approval and labelling decisions: a review of 198 submissions between 2000

and 2008. *Clinical pharmacokinetics* **2011**, *50*, 627-635, doi:10.2165/11593210-000000000-00000.

10. Dunn, A.; Gobburu, J.V.S. The trajectory of pharmacometrics to support drug licensing and labelling. *British journal of clinical pharmacology* **2023**, doi:10.1111/bcp.15728.
11. U.S. Food and Drug Administration. Physiologically Based Pharmacokinetic Analyses — Format and Content Guidance for Industry. September 2018. Available online: https://www.fda.gov/regulatory-information/search-fda-guidance-documents/physiologically-based-pharmacokinetic-analyses-format-and-content-guidance-industry (accessed on 18 January 2025).
12. Hamberg, A.-K.; Wadelius, M.; Lindh, J.D.; Dahl, M.L.; Padrini, R.; Deloukas, P.; Rane, A.; Jonsson, E.N. A Pharmacometric Model Describing the Relationship Between Warfarin Dose and INR Response With Respect to Variations in CYP2C9, VKORC1, and Age. *Clinical Pharmacology & Therapeutics* **2010**, *87*, 727-734, doi:https://doi.org/10.1038/clpt.2010.37.
13. U.S. Food and Drug Administration. Population Pharmacokinetics Guidance for Industry. February 2022. Available online: https://www.fda.gov/regulatory-information/search-fda-guidance-documents/population-pharmacokinetics (accessed on 18 January 2025).
14. Schadler, E.D.; Ortel, B.; Mehlis, S.L. Biologics for the primary care physician: Review and treatment of psoriasis. *Disease-a-month : DM* **2019**, *65*, 51-90, doi:10.1016/j.disamonth.2018.06.001.
15. U.S. Food and Drug Administration. Exposure-Response Relationships — Study Design, Data Analysis, and Regulatory Applications. April 2003. Available online: https://www.fda.gov/media/71277/download (accessed on 18 January 2025).
16. Darwich, A.S.; Polasek, T.M.; Aronson, J.K.; Ogungbenro, K.; Wright, D.F.B.; Achour, B.; Reny, J.L.; Daali, Y.; Eiermann, B.; Cook, J.; et al. Model-Informed Precision Dosing: Background, Requirements, Validation, Implementation, and Forward Trajectory of Individualizing Drug Therapy. *Annual review of pharmacology and toxicology* **2021**, *61*, 225-245, doi:10.1146/annurev-pharmtox-033020-113257.
17. Wicha, S.G.; Kees, M.G.; Solms, A.; Minichmayr, I.K.; Kratzer, A.; Kloft, C. TDMx: a novel web-based open-access support

tool for optimising antimicrobial dosing regimens in clinical routine. *International journal of antimicrobial agents* **2015**, *45*, 442-444, doi:10.1016/j.ijantimicag.2014.12.010.

18. Chatelut, E.; Hendrikx, J.J.M.A.; Martin, J.; Ciccolini, J.; Moes, D.J.A.R. Unraveling the complexity of therapeutic drug monitoring for monoclonal antibody therapies to individualize dose in oncology. *Pharmacology Research & Perspectives* **2021**, *9*, e00757, doi:https://doi.org/10.1002/prp2.757.
19. Papamichael, K.; Afif, W.; Drobne, D.; Dubinsky, M.C.; Ferrante, M.; Irving, P.M.; Kamperidis, N.; Kobayashi, T.; Kotze, P.G.; Lambert, J.; et al. Therapeutic drug monitoring of biologics in inflammatory bowel disease: unmet needs and future perspectives. *The Lancet Gastroenterology & Hepatology* **2022**, *7*, 171-185, doi:10.1016/S2468-1253(21)00223-5.
20. Minichmayr, I.K.; Mizuno, T.; Goswami, S.; Peck, R.W.; Polasek, T.M.; Pharmacology, t.A.S.o.C.; Community, T.P.D. Recent Advances Addressing the Challenges of Precision Dosing. *Clinical Pharmacology & Therapeutics* **2024**, *116*, 527-530, doi:https://doi.org/10.1002/cpt.3365.
21. Sheiner, L.B. Computer-aided long-term anticoagulation therapy. *Computers and biomedical research, an international journal* **1969**, *2*, 507-518, doi:10.1016/0010-4809(69)90030-5.
22. Jelliffe, R.W. Administration of digoxin. *Diseases of the chest* **1969**, *56*, 56-60, doi:10.1378/chest.56.1.56.
23. Tsamandouras, N.; Rostami-Hodjegan, A.; Aarons, L. Combining the 'bottom up' and 'top down' approaches in pharmacokinetic modelling: fitting PBPK models to observed clinical data. *British journal of clinical pharmacology* **2015**, *79*, 48-55, doi:https://doi.org/10.1111/bcp.12234.
24. Sheiner, L.B.; Steimer, J.-L. Pharmacokinetic/Pharmacodynamic Modeling in Drug Development. *Annual review of pharmacology and toxicology* **2000**, *40*, 67-95, doi:https://doi.org/10.1146/annurev.pharmtox.40.1.67.
25. Dahl, S.G.; Aarons, L.; Gundert-Remy, U.; Karlsson, M.O.; Schneider, Y.J.; Steimer, J.L.; Trocóniz, I.F. Incorporating physiological and biochemical mechanisms into pharmacokinetic-pharmacodynamic models: a conceptual framework. *Basic & clinical pharmacology & toxicology* **2010**, *106*, 2-12, doi:10.1111/j.1742-7843.2009.00456.x.
26. Mould, D.R.; Upton, R.N. Basic concepts in population modeling, simulation, and model-based drug development-part

2: introduction to pharmacokinetic modeling methods. *CPT: pharmacometrics & systems pharmacology* **2013**, *2*, e38, doi:10.1038/psp.2013.14.

27. Upton, R.N.; Mould, D.R. Basic concepts in population modeling, simulation, and model-based drug development: part 3-introduction to pharmacodynamic modeling methods. *CPT: pharmacometrics & systems pharmacology* **2014**, *3*, e88, doi:10.1038/psp.2013.71.
28. Doménech, J.; Martínez, J.; Peraire, C. Capítulo 1: Fundamentos de la Biofarmacia y la Farmacocinética. In *Tratado general de Biofarmacia y Farmacocinética. Volumen I. LADME. Análisis farmacocinético. Biodisponibilidad y bioequivalencia*; Editorial Síntesis S.A.: Vallehermoso, 34. 28015 Madrid, 2013; Volume Volumen I, pp. 35-49.
29. Holford, N.; Yim, D.-S. Clearance. *Translational and Clinical Pharmacology* **2015**, *23*, 42, doi:10.12793/tcp.2015.23.2.42.
30. Holford, N.; Yim, D.-S. Volume of Distribution. *Translational and Clinical Pharmacology* **2016**, *24*, 74, doi:10.12793/tcp.2016.24.2.74.
31. Doménech, J.; Martínez, J.; Peraire, C. Capítulo 3: Distribución de Fármacos en el Organismo. In *Tratado general de Biofarmacia y Farmacocinética. Volumen I. LADME. Análisis farmacocinético. Biodisponibilidad y bioequivalencia*; Editorial Síntesis S.A.: Vallehermoso, 34. 28015 Madrid, 2013; Volume Volumen I, pp. 77-109.
32. Doménech, J.; Martínez, J.; Peraire, C. Capítulo 6: Aclaramiento. In *Tratado general de Biofarmacia y Farmacocinética. Volumen I. LADME. Análisis farmacocinético. Biodisponibilidad y bioequivalencia*; Editorial Síntesis S.A.: Vallehermoso, 34. 28015 Madrid, 2013; Volume Volumen I, pp. 187-210.
33. Rowland, M.; Peck, C.; Tucker, G. Physiologically-based pharmacokinetics in drug development and regulatory science. *Annual review of pharmacology and toxicology* **2011**, *51*, 45-73, doi:10.1146/annurev-pharmtox-010510-100540.
34. Rostami-Hodjegan, A. Reverse Translation in PBPK and QSP: Going Backwards in Order to Go Forward With Confidence. *Clinical Pharmacology & Therapeutics* **2018**, *103*, 224-232, doi:https://doi.org/10.1002/cpt.904.
35. Ibarra, M.; Schiavo, A.; Lesko, L.J. Physiologically Based Pharmacokinetic Modeling: Definition and History. In *The ADME Encyclopedia: A Comprehensive Guide on Biopharmacy and*

Pharmacokinetics, Talevi, A., Ed.; Springer International Publishing: Cham, 2022; pp. 1004-1013.

36. Jones, H.M.; Gardner, I.B.; Watson, K.J. Modelling and PBPK Simulation in Drug Discovery. *The AAPS Journal* **2009**, *11*, 155-166, doi:10.1208/s12248-009-9088-1.
37. Peters, S.A.; Ungell, A.L.; Dolgos, H. Physiologically based pharmacokinetic (PBPK) modeling and simulation: applications in lead optimization. *Current opinion in drug discovery & development* **2009**, *12*, 509-518.
38. Sager, J.E.; Yu, J.; Ragueneau-Majlessi, I.; Isoherranen, N. Physiologically Based Pharmacokinetic (PBPK) Modeling and Simulation Approaches: A Systematic Review of Published Models, Applications, and Model Verification. *Drug metabolism and disposition: the biological fate of chemicals* **2015**, *43*, 1823-1837, doi:10.1124/dmd.115.065920.
39. Jones, H.M.; Parrott, N.; Jorga, K.; Lavé, T. A Novel Strategy for Physiologically Based Predictions of Human Pharmacokinetics. *Clinical pharmacokinetics* **2006**, *45*, 511-542, doi:10.2165/00003088-200645050-00006.
40. Marsousi, N.; Desmeules, J.A.; Rudaz, S.; Daali, Y. Usefulness of PBPK Modeling in Incorporation of Clinical Conditions in Personalized Medicine. *Journal of pharmaceutical sciences* **2017**, *106*, 2380-2391, doi:10.1016/j.xphs.2017.04.035.
41. Khalil, F.; Läer, S. Physiologically Based Pharmacokinetic Modeling: Methodology, Applications, and Limitations with a Focus on Its Role in Pediatric Drug Development. *BioMed Research International* **2011**, *2011*, 907461, doi:https://doi.org/10.1155/2011/907461.
42. Leong, R.; Vieira, M.L.; Zhao, P.; Mulugeta, Y.; Lee, C.S.; Huang, S.M.; Burckart, G.J. Regulatory experience with physiologically based pharmacokinetic modeling for pediatric drug trials. *Clinical pharmacology and therapeutics* **2012**, *91*, 926-931, doi:10.1038/clpt.2012.19.
43. Zhang, H.; Xia, B.; Sheng, J.; Heimbach, T.; Lin, T.-H.; He, H.; Wang, Y.; Novick, S.; Comfort, A. Application of Physiologically Based Absorption Modeling to Formulation Development of a Low Solubility, Low Permeability Weak Base: Mechanistic Investigation of Food Effect. *AAPS PharmSciTech* **2014**, *15*, 400-406, doi:10.1208/s12249-014-0075-1.
44. Tistaert, C.; Heimbach, T.; Xia, B.; Parrott, N.; Samant, T.S.; Kesisoglou, F. Food Effect Projections via Physiologically

Based Pharmacokinetic Modeling: Predictive Case Studies. *Journal of pharmaceutical sciences* **2019**, *108*, 592-602, doi:10.1016/j.xphs.2018.05.024.

45. Cheng, L.; Wong, H. Food Effects on Oral Drug Absorption: Application of Physiologically-Based Pharmacokinetic Modeling as a Predictive Tool. *Pharmaceutics* **2020**, *12*, doi:10.3390/pharmaceutics12070672.
46. O'Shea, J.P.; Holm, R.; O'Driscoll, C.M.; Griffin, B.T. Food for thought: formulating away the food effect – a PEARRL review. *Journal of Pharmacy and Pharmacology* **2019**, *71*, 510-535, doi:10.1111/jphp.12957.
47. US. Food and Drug Administration. Assessing the Effects of Food on Drugs in INDs and NDAs – Clinical Pharmacology Considerations Guidance for Industry, June 2022. Available online: https://www.fda.gov/media/121313/download (accessed on 11 April).
48. Vinarov, Z.; Butler, J.; Kesisoglou, F.; Koziolek, M.; Augustijns, P. Assessment of food effects during clinical development. *International Journal of Pharmaceutics* **2023**, *635*, 122758, doi:10.1016/j.ijpharm.2023.122758.
49. Kesisoglou, F.; Basu, S.; Belubbi, T.; Bransford, P.; Chung, J.; Dodd, S.; Dolton, M.; Heimbach, T.; Kulkarni, P.; Lin, W.; et al. Streamlining Food Effect Assessment - Are Repeated Food Effect Studies Needed? An IQ Analysis. *The AAPS Journal* **2023**, *25*, 60, doi:10.1208/s12248-023-00822-5.
50. Tylutki, Z.; Polak, S.; Wiśniowska, B. Top-down, Bottom-up and Middle-out Strategies for Drug Cardiac Safety Assessment via Modeling and Simulations. *Current pharmacology reports* **2016**, *2*, 171-177, doi:10.1007/s40495-016-0060-3.
51. Sancho-Araiz, A.; Mangas-Sanjuan, V.; Trocóniz, I.F. The Role of Mathematical Models in Immuno-Oncology: Challenges and Future Perspectives. *Pharmaceutics* **2021**, *13*, doi:10.3390/pharmaceutics13071016.
52. Mi, K.; Zhou, K.; Sun, L.; Hou, Y.; Ma, W.; Xu, X.; Huo, M.; Liu, Z.; Huang, L. Application of Semi-Mechanistic Pharmacokinetic and Pharmacodynamic Model in Antimicrobial Resistance. *Pharmaceutics* **2022**, *14*, doi:10.3390/pharmaceutics14020246.
53. Nielsen, E.I.; Friberg, L.E. Pharmacokinetic-pharmacodynamic modeling of antibacterial drugs. *Pharmacological reviews* **2013**, *65*, 1053-1090, doi:10.1124/pr.111.005769.

54. Brill, M.J.E.; Kristoffersson, A.N.; Zhao, C.; Nielsen, E.I.; Friberg, L.E. Semi-mechanistic pharmacokinetic–pharmacodynamic modelling of antibiotic drug combinations. *Clinical Microbiology and Infection* **2018**, *24*, 697-706, doi:10.1016/j.cmi.2017.11.023.
55. Sasaki, T.; Takane, H.; Ogawa, K.; Isagawa, S.; Hirota, T.; Higuchi, S.; Horii, T.; Otsubo, K.; Ieiri, I. Population pharmacokinetic and pharmacodynamic analysis of linezolid and a hematologic side effect, thrombocytopenia, in Japanese patients. *Antimicrobial agents and chemotherapy* **2011**, *55*, 1867-1873, doi:10.1128/aac.01185-10.
56. Gupta, P.; Friberg, L.E.; Karlsson, M.O.; Krishnaswami, S.; French, J. A semi-mechanistic model of CP-690,550-induced reduction in neutrophil counts in patients with rheumatoid arthritis. *Journal of clinical pharmacology* **2010**, *50*, 679-687, doi:10.1177/0091270009346060.
57. Friberg, L.E.; Henningsson, A.; Maas, H.; Nguyen, L.; Karlsson, M.O. Model of chemotherapy-induced myelosuppression with parameter consistency across drugs. *Journal of clinical oncology : official journal of the American Society of Clinical Oncology* **2002**, *20*, 4713-4721, doi:10.1200/jco.2002.02.140.
58. Reynaldo-Fernández, G.; Solozábal, J.; Amaro, D.; Fernández-Sánchez, E.M.; Rodríguez-Vera, L.; Bermejo, M.; Mangas-Sanjuan, V.; Troconiz, I.F. Semi-mechanistic Pharmacokinetic/Pharmacodynamic model of three pegylated rHuEPO and ior®EPOCIM in New Zealand rabbits. *European Journal of Pharmaceutical Sciences* **2018**, *120*, 123-132, doi:https://doi.org/10.1016/j.ejps.2018.04.047.
59. Mangas-Sanjuan, V.; Navarro-Fontestad, C.; García-Arieta, A.; Trocóniz, I.F.; Bermejo, M. Computer simulations for bioequivalence trials: Selection of analyte in BCS class II and IV drugs with first-pass metabolism, two metabolic pathways and intestinal efflux transporter. *European Journal of Pharmaceutical Sciences* **2018**, *117*, 193-203, doi:https://doi.org/10.1016/j.ejps.2018.02.014.
60. Kirschner, D.; Panetta, J.C. Modeling immunotherapy of the tumor – immune interaction. *Journal of Mathematical Biology* **1998**, *37*, 235-252, doi:10.1007/s002850050127.
61. de Pillis, L.G.; Radunskaya, A.E.; Wiseman, C.L. A validated mathematical model of cell-mediated immune response to

tumor growth. *Cancer research* **2005**, *65*, 7950-7958, doi:10.1158/0008-5472.can-05-0564.

62. Doménech, J.; Martínez, J.; Peraire, C. Capítulo 11: Farmacocinética Poblacional. In *Tratado general de Biofarmacia y Farmacocinética. Volumen II. Vias de administración de fámacos: aspectos biofarmacéuticos. Farmacocinética no lineal y clínica*; Editorial Síntesis S.A.: Vallehermoso, 34. 28015 Madrid, 2013; Volume Volumen I, pp. 319-363.
63. Bonate, P.L.; Steimer, J.-L. Nonlinear Mixed Effects Models: Theory. In *Pharmacokinetic-pharmacodynamic modeling and simulation*; Springer; 2nd ed.: 2011; pp. 205-265.
64. Karlsson, M.O.; Sheiner, L.B. The importance of modeling interoccasion variability in population pharmacokinetic analyses. *Journal of pharmacokinetics and biopharmaceutics* **1993**, *21*, 735-750, doi:10.1007/bf01113502.
65. Kümmel, A.; Bonate, P.L.; Dingemanse, J.; Krause, A. Confidence and Prediction Intervals for Pharmacometric Models. *CPT: pharmacometrics & systems pharmacology* **2018**, *7*, 360-373, doi:10.1002/psp4.12286.
66. Monolix 2024R1 User guide. Available online: https://monolix.lixoft.com/single-page/ (accessed on 25 January 2024).
67. Peters, S.A. Chapter 9 Uncertainty and Population Variability. In *Physiologically based pharmacokinetic (PBPK) modeling and simulations: principles, methods, and applications in the pharmaceutical industry*, Second Edition ed.; John Wiley & Sons, Inc.: 2022; pp. 263-285.
68. Karlsson, M.O.; Savic, R.M. Diagnosing model diagnostics. *Clinical pharmacology and therapeutics* **2007**, *82*, 17-20, doi:10.1038/sj.clpt.6100241.
69. Nguyen, T.H.; Mouksassi, M.S.; Holford, N.; Al-Huniti, N.; Freedman, I.; Hooker, A.C.; John, J.; Karlsson, M.O.; Mould, D.R.; Pérez Ruixo, J.J.; et al. Model Evaluation of Continuous Data Pharmacometric Models: Metrics and Graphics. *CPT: pharmacometrics & systems pharmacology* **2017**, *6*, 87-109, doi:10.1002/psp4.12161.
70. Wählby, U.; Jonsson, E.N.; Karlsson, M.O. Assessment of actual significance levels for covariate effects in NONMEM. *Journal of pharmacokinetics and pharmacodynamics* **2001**, *28*, 231-252, doi:10.1023/a:1011527125570.
71. Ette, E.I. Comparing non-hierarchical models: Application to non-linear mixed effects modeling. *Computers in Biology and*

Medicine **1996**, *26*, 505-512, doi:https://doi.org/10.1016/S0010-4825(96)00031-5.

72. Bergstrand, M.; Hooker, A.C.; Wallin, J.E.; Karlsson, M.O. Prediction-corrected visual predictive checks for diagnosing nonlinear mixed-effects models. *Aaps j* **2011**, *13*, 143-151, doi:10.1208/s12248-011-9255-z.
73. Irurzun-Arana, I.; Rackauckas, C.; McDonald, T.O.; Trocóniz, I.F. Beyond Deterministic Models in Drug Discovery and Development. *Trends in Pharmacological Sciences* **2020**, *41*, 882-895, doi:https://doi.org/10.1016/j.tips.2020.09.005.
74. Chaikin, P.; Rhodes, G.R.; Bruno, R.; Rohatagi, S.; Natarajan, C. Pharmacokinetics/pharmacodynamics in drug development: an industrial perspective. *Journal of clinical pharmacology* **2000**, *40*, 1428-1438.
75. Bandeira, L.C.; Pinto, L.; Carneiro, C.M. Pharmacometrics: The Already-Present Future of Precision Pharmacology. *Therapeutic innovation & regulatory science* **2023**, *57*, 57-69, doi:10.1007/s43441-022-00439-4.
76. Workgroup, E.M.; Marshall, S.; Burghaus, R.; Cosson, V.; Cheung, S.; Chenel, M.; DellaPasqua, O.; Frey, N.; Hamrén, B.; Harnisch, L.; et al. Good Practices in Model-Informed Drug Discovery and Development: Practice, Application, and Documentation. *CPT: pharmacometrics & systems pharmacology* **2016**, *5*, 93-122, doi:https://doi.org/10.1002/psp4.12049.
77. Kimko, H.C.; Duffull, S.B. *Simulation for designing clinical trials*; Marcel Dekker Incorporated: 2002.
78. Peck, C.C.; Kimko, H.H.C. *Clinical Trial Simulations : Applications and Trends*, 1. Aufl. ed.; Springer New York: New York, NY, 2011; Volume 1.
79. Ibarra, M.; Lorier, M.; Trocóniz, I.F. Pharmacometrics: Definition and History. In *The ADME Encyclopedia: A Comprehensive Guide on Biopharmacy and Pharmacokinetics*, Talevi, A., Ed.; Springer International Publishing: Cham, 2022; pp. 933-939.
80. Campos Moreno, E.; Merino Sanjuán, M.; Merino, V.; Nácher, A.; Martín Algarra, R.V.; Casabó, V.G. Population modelling to describe pharmacokinetics of amiodarone in rats: Relevance of plasma protein and tissue depot binding. *European Journal of Pharmaceutical Sciences* **2007**, *30*, 190-197, doi:https://doi.org/10.1016/j.ejps.2006.11.006.
81. Hamberg, A.-K.; Wadelius, M.; Friberg, L.E.; Biss, T.T.; Kamali, F.; Jonsson, E.N. Characterizing variability in warfarin

dose requirements in children using modelling and simulation. *British journal of clinical pharmacology* **2014**, *78*, 158-169, doi:https://doi.org/10.1111/bcp.12308.

82. Salinger, D.H.; Shen, D.D.; Thummel, K.; Wittkowsky, A.K.; Vicini, P.; Veenstra, D.L. Pharmacogenomic trial design: use of a PK/PD model to explore warfarin dosing interventions through clinical trial simulation. *Pharmacogenetics and genomics* **2009**, *19*, 965-971, doi:10.1097/FPC.0b013e3283333b80.
83. Polasek, T.M.; Rayner, C.R.; Peck, R.W.; Rowland, A.; Kimko, H.; Rostami-Hodjegan, A. Toward Dynamic Prescribing Information: Codevelopment of Companion Model-Informed Precision Dosing Tools in Drug Development. *Clinical pharmacology in drug development* **2019**, *8*, 418-425, doi:10.1002/cpdd.638.
84. Gonzalez, D.; Rao, G.G.; Bailey, S.C.; Brouwer, K.L.R.; Cao, Y.; Crona, D.J.; Kashuba, A.D.M.; Lee, C.R.; Morbitzer, K.; Patterson, J.H.; et al. Precision Dosing: Public Health Need, Proposed Framework, and Anticipated Impact. *Clinical and Translational Science* **2017**, *10*, 443-454, doi:https://doi.org/10.1111/cts.12490.
85. Darwich, A.S.; Ogungbenro, K.; Vinks, A.A.; Powell, J.R.; Reny, J.L.; Marsousi, N.; Daali, Y.; Fairman, D.; Cook, J.; Lesko, L.J.; et al. Why has model-informed precision dosing not yet become common clinical reality? lessons from the past and a roadmap for the future. *Clinical pharmacology and therapeutics* **2017**, *101*, 646-656, doi:10.1002/cpt.659.
86. Eichler, H.G.; Abadie, E.; Breckenridge, A.; Flamion, B.; Gustafsson, L.L.; Leufkens, H.; Rowland, M.; Schneider, C.K.; Bloechl-Daum, B. Bridging the efficacy-effectiveness gap: a regulator's perspective on addressing variability of drug response. *Nature reviews. Drug discovery* **2011**, *10*, 495-506, doi:10.1038/nrd3501.
87. Minichmayr, I.K.; Dreesen, E.; Centanni, M.; Wang, Z.; Hoffert, Y.; Friberg, L.E.; Wicha, S.G. Model-informed precision dosing: State of the art and future perspectives. *Advanced Drug Delivery Reviews* **2024**, 115421, doi:https://doi.org/10.1016/j.addr.2024.115421.
88. Tyson, R.J.; Park, C.C.; Powell, J.R.; Patterson, J.H.; Weiner, D.; Watkins, P.B.; Gonzalez, D. Precision Dosing Priority Criteria: Drug, Disease, and Patient Population Variables. *Frontiers in pharmacology* **2020**, *11*, 420, doi:10.3389/fphar.2020.00420.

89. El Hassani, M.; Marsot, A. External Evaluation of Population Pharmacokinetic Models for Precision Dosing: Current State and Knowledge Gaps. *Clinical pharmacokinetics* **2023**, *62*, 533-540, doi:10.1007/s40262-023-01233-7.
90. Olivier, B.G.; Swat, M.J.; Moné, M.J. Modeling and Simulation Tools: From Systems Biology to Systems Medicine. *Methods in molecular biology (Clifton, N.J.)* **2016**, *1386*, 441-463, doi:10.1007/978-1-4939-3283-2_19.
91. Wicha, S.G.; Märtson, A.-G.; Nielsen, E.I.; Koch, B.C.P.; Friberg, L.E.; Alffenaar, J.-W.; Minichmayr, I.K.; the International Society of Anti-Infective Pharmacology , t.P.P.s.g.o.t.E.S.o.C.M., Infectious Diseases. From Therapeutic Drug Monitoring to Model-Informed Precision Dosing for Antibiotics. *Clinical Pharmacology & Therapeutics* **2021**, *109*, 928-941, doi:https://doi.org/10.1002/cpt.2202.
92. Neely, M.; Margol, A.; Fu, X.; van Guilder, M.; Bayard, D.; Schumitzky, A.; Orbach, R.; Liu, S.; Louie, S.; Hope, W. Achieving target voriconazole concentrations more accurately in children and adolescents. *Antimicrobial agents and chemotherapy* **2015**, *59*, 3090-3097, doi:10.1128/aac.00032-15.
93. Neely, M.; Philippe, M.; Rushing, T.; Fu, X.; van Guilder, M.; Bayard, D.; Schumitzky, A.; Bleyzac, N.; Goutelle, S. Accurately Achieving Target Busulfan Exposure in Children and Adolescents With Very Limited Sampling and the BestDose Software. *Therapeutic drug monitoring* **2016**, *38*, 332-342, doi:10.1097/ftd.0000000000000276.
94. Staatz, C.E.; Tett, S.E. Maximum a posteriori Bayesian estimation of mycophenolic Acid area under the concentration-time curve: is this clinically useful for dosage prediction yet? *Clinical pharmacokinetics* **2011**, *50*, 759-772, doi:10.2165/11596380-000000000-00000.
95. Darwich, A.S.; Ogungbenro, K.; Hatley, O.J.; Rostami-Hodjegan, A. Role of pharmacokinetic modeling and simulation in precision dosing of anticancer drugs. *Translational Cancer Research* **2017**, S1512-S1529.
96. Maier, C.; de Wiljes, J.; Hartung, N.; Kloft, C.; Huisinga, W. A continued learning approach for model-informed precision dosing: Updating models in clinical practice. *CPT: pharmacometrics & systems pharmacology* **2022**, *11*, 185-198, doi:https://doi.org/10.1002/psp4.12745.
97. Le Louedec, F.; Leenhardt, F.; Marin, C.; Chatelut, É.; Evrard, A.; Ciccolini, J. Cancer Immunotherapy Dosing: A

Pharmacokinetic/Pharmacodynamic Perspective. *Vaccines* **2020**, *8*, 632.

98. Wright, D.F.; Duffull, S.B. Development of a bayesian forecasting method for warfarin dose individualization. *Pharm Res* **2011**, *28*, 1100-1111, doi:10.1007/s11095-011-0369-x.
99. Wright, D.F.; Duffull, S.B. A Bayesian dose-individualization method for warfarin. *Clinical pharmacokinetics* **2013**, *52*, 59-68, doi:10.1007/s40262-012-0017-6.
100. Strik, A.S.; Löwenberg, M.; Mould, D.R.; Berends, S.E.; Ponsioen, C.I.; van den Brande, J.M.H.; Jansen, J.M.; Hoekman, D.R.; Brandse, J.F.; Duijvestein, M.; et al. Efficacy of dashboard driven dosing of infliximab in inflammatory bowel disease patients; a randomized controlled trial. *Scandinavian Journal of Gastroenterology* **2021**, *56*, 145-154, doi:10.1080/00365521.2020.1856405.
101. Santacana Juncosa, E.; Rodríguez-Alonso, L.; Padullés Zamora, A.; Guardiola, J.; Rodríguez-Moranta, F.; Serra Nilsson, K.; Bas Minguet, J.; Morandeira Rego, F.; Colom Codina, H.; Padullés Zamora, N. Bayes-based dosing of infliximab in inflammatory bowel diseases: Short-term efficacy. *British journal of clinical pharmacology* **2021**, *87*, 494-505, doi:https://doi.org/10.1111/bcp.14410.
102. Fagerholm, U. Prediction of human pharmacokinetics--gut-wall metabolism. *The Journal of pharmacy and pharmacology* **2007**, *59*, 1335-1343, doi:10.1211/jpp.59.10.0002.
103. Peters, S.A.; Jones, C.R.; Ungell, A.L.; Hatley, O.J. Predicting Drug Extraction in the Human Gut Wall: Assessing Contributions from Drug Metabolizing Enzymes and Transporter Proteins using Preclinical Models. *Clinical pharmacokinetics* **2016**, *55*, 673-696, doi:10.1007/s40262-015-0351-6.
104. Davies, M.; Peramuhendige, P.; King, L.; Golding, M.; Kotian, A.; Penney, M.; Shah, S.; Manevski, N. Evaluation of In Vitro Models for Assessment of Human Intestinal Metabolism in Drug Discovery. *Drug metabolism and disposition: the biological fate of chemicals* **2020**, *48*, 1169-1182, doi:10.1124/dmd.120.000111.
105. Jones, H.M.; Chen, Y.; Gibson, C.; Heimbach, T.; Parrott, N.; Peters, S.A.; Snoeys, J.; Upreti, V.V.; Zheng, M.; Hall, S.D. Physiologically based pharmacokinetic modeling in drug discovery and development: a pharmaceutical industry perspective. *Clinical pharmacology and therapeutics* **2015**, *97*, 247-262, doi:10.1002/cpt.37.

106. Riedmaier, A.E.; DeMent, K.; Huckle, J.; Bransford, P.; Stillhart, C.; Lloyd, R.; Alluri, R.; Basu, S.; Chen, Y.; Dhamankar, V.; et al. Use of Physiologically Based Pharmacokinetic (PBPK) Modeling for Predicting Drug-Food Interactions: an Industry Perspective. *The AAPS Journal* **2020**, *22*, 123, doi:10.1208/s12248-020-00508-2.
107. Marino, S.E.; Birnbaum, A.K.; Leppik, I.E.; Conway, J.M.; Musib, L.C.; Brundage, R.C.; Ramsay, R.E.; Pennell, P.B.; White, J.R.; Gross, C.R.; et al. Steady-state carbamazepine pharmacokinetics following oral and stable-labeled intravenous administration in epilepsy patients: effects of race and sex. *Clinical pharmacology and therapeutics* **2012**, *91*, 483-488, doi:10.1038/clpt.2011.251.
108. Knox, C.; Wilson, M.; Klinger, C.M.; Franklin, M.; Oler, E.; Wilson, A.; Pon, A.; Cox, J.; Chin, N.E.L.; Strawbridge, S.A.; et al. DrugBank 6.0: the DrugBank Knowledgebase for 2024. *Nucleic acids research* **2024**, *52*, D1265-d1275, doi:10.1093/nar/gkad976.
109. Edgar, B.; Lundborg, P.; Regårdh, C.G. Clinical pharmacokinetics of felodipine. A summary. *Drugs* **1987**, *34 Suppl 3*, 16-27, doi:10.2165/00003495-198700343-00005.
110. Duong, J.K.; Nand, R.A.; Patel, A.; Della Pasqua, O.; Gross, A.S. A physiologically based pharmacokinetic model of clopidogrel in populations of European and Japanese ancestry: An evaluation of CYP2C19 activity. *Pharmacol Res Perspect* **2022**, *10*, e00946, doi:10.1002/prp2.946.
111. Cahoon Jr, W.; Flattery, M.P.; Hess, M.L. Amiodarone: Development, Clinical Indications, and Safety. *Progress in Cardiovascular Nursing* **2007**, *22*, 173-176, doi:https://doi.org/10.1111/j.0889-7204.2007.07398.x.
112. Creţeanu, A.; Tàntaru, G.; Vieriu, M.; Panainte, A.D.; Ochiuz, L. OPTIMIZATION OF THE PREPARATION OF KOLLIDON SR-BASED AMIODARONE HYDROCHLORIDE TABLETS WITH SUSTAINED RELEASE. *Revista medico-chirurgicală a Societăţii de Medici şi Naturalişti din Iaşi* **2015**, *119*, 1161-1165.
113. Wang, D.; Chen, G.; Ren, L. Preparation and Characterization of the Sulfobutylether-β-Cyclodextrin Inclusion Complex of Amiodarone Hydrochloride with Enhanced Oral Bioavailability in Fasted State. *AAPS PharmSciTech* **2017**, *18*, 1526-1535, doi:10.1208/s12249-016-0646-4.

114. Wallin, R.; Hutson, S.M. Warfarin and the Vitamin K-Dependent γ-Carboxylation System. *Trends in Molecular Medicine* **2004**, *10*, 299-302, doi:10.1016/j.molmed.2004.05.003.
115. Liu, R.; Li, X.; Zhang, W.; Zhou, H.-H. Comparison of Nine Statistical Model Based Warfarin Pharmacogenetic Dosing Algorithms Using the Racially Diverse International Warfarin Pharmacogenetic Consortium Cohort Database. *PLOS ONE* **2015**, *10*, e0135784, doi:10.1371/journal.pone.0135784.
116. Asiimwe, I.G.; Pirmohamed, M. Ethnic Diversity and Warfarin Pharmacogenomics. *Frontiers in pharmacology* **2022**, *13*, doi:10.3389/fphar.2022.866058.
117. Hamberg, A.K.; Dahl, M.L.; Barban, M.; Scordo, M.G.; Wadelius, M.; Pengo, V.; Padrini, R.; Jonsson, E.N. A PK-PD model for predicting the impact of age, CYP2C9, and VKORC1 genotype on individualization of warfarin therapy. *Clinical pharmacology and therapeutics* **2007**, *81*, 529-538, doi:10.1038/sj.clpt.6100084.
118. Reyes-González, S.; de Las Barreras, C.; Reynaldo, G.; Rodríguez-Vera, L.; Vlaar, C.; Mejias, V.L.; Monbaliu, J.M.; Stelzer, T.; Mangas, V.; Duconge, J. Genotype-driven pharmacokinetic simulations of warfarin levels in Puerto Ricans. *Drug metabolism and personalized therapy* **2020**, doi:10.1515/dmdi-2020-0135.
119. Hamberg, A.-K.; Dahl, M.-L.; Barban, M.; Scordo, M.G.; Wadelius, M.; Pengo, V.; Padrini, R.; Jonsson, E.N. A PK–PD Model for Predicting the Impact of Age, CYP2C9, and VKORC1 Genotype on Individualization of Warfarin Therapy. *Clinical Pharmacology & Therapeutics* **2007**, *81*, 529-538, doi:https://doi.org/10.1038/sj.clpt.6100084.
120. Weber, J.; Keam, S.J. Ustekinumab. *BioDrugs : clinical immunotherapeutics, biopharmaceuticals and gene therapy* **2009**, *23*, 53-61, doi:10.2165/00063030-200923010-00006.
121. Patel, D.D.; Lee, D.M.; Kolbinger, F.; Antoni, C. Effect of IL-17A blockade with secukinumab in autoimmune diseases. *Annals of the Rheumatic Diseases* **2013**, *72*, iii116-iii123, doi:10.1136/annrheumdis-2012-202371.
122. Pan, S.; Tsakok, T.; Dand, N.; Lonsdale, D.O.; Loeff, F.C.; Bloem, K.; de Vries, A.; Baudry, D.; Duckworth, M.; Mahil, S.; et al. Using Real-World Data to Guide Ustekinumab Dosing Strategies for Psoriasis: A Prospective Pharmacokinetic-Pharmacodynamic Study. *Clinical and Translational Science* **2020**, *13*, 400-409, doi:https://doi.org/10.1111/cts.12725.

123. Dayneka, N.L.; Garg, V.; Jusko, W.J. Comparison of four basic models of indirect pharmacodynamic responses. *Journal of pharmacokinetics and biopharmaceutics* **1993**, *21*, 457-478, doi:10.1007/bf01061691.
124. DeBonis, J.; Veiseh, O.; Igoshin, O.A. Uncovering the interleukin-12 pharmacokinetic desensitization mechanism and its consequences with mathematical modeling. *CPT: pharmacometrics & systems pharmacology* **2024**, *n/a*, doi:https://doi.org/10.1002/psp4.13258.
125. Dansirikul, C.; Silber, H.E.; Karlsson, M.O. Approaches to handling pharmacodynamic baseline responses. *Journal of pharmacokinetics and pharmacodynamics* **2008**, *35*, 269-283, doi:10.1007/s10928-008-9088-2.
126. Liu, Y.; Xu, L.; Wang, X.; Wu, L.; Cai, R.; Li, L.; Zheng, Q. Optimization of secukinumab dose regimens in patients with moderate-to-severe plaque psoriasis via exposure-response modeling. *Expert Review of Clinical Pharmacology* **2023**, *16*, 999-1008, doi:10.1080/17512433.2023.2259300.
127. Polasek, T.M.; Peck, R.W. Beyond Population-Level Targets for Drug Concentrations: Precision Dosing Needs Individual-Level Targets that Include Superior Biomarkers of Drug Responses. *Clinical pharmacology and therapeutics* **2024**, doi:10.1002/cpt.3197.
128. Dolan, J.G.; Veazie, P.J.; Russ, A.J. Development and initial evaluation of a treatment decision dashboard. *BMC Medical Informatics and Decision Making* **2013**, *13*, 51, doi:10.1186/1472-6947-13-51.
129. Mould, D.R.; Upton, R.N.; Wojciechowski, J. Dashboard systems: implementing pharmacometrics from bench to bedside. *Aaps j* **2014**, *16*, 925-937, doi:10.1208/s12248-014-9632-5.
130. Mould, D.R.; Upton, R.N. "Getting the Dose Right"—Revisiting the Topic With Focus on Biologic Agents. *Clinical Pharmacology & Therapeutics* **2024**, *116*, 613-618, doi:https://doi.org/10.1002/cpt.3285.

Annexes

Annex 1: Evaluation of Solubility-Limited Absorption as a Surrogate to Predicting Positive Food Effect of BCS II/IV Drugs

Clinical Pharmacokinetics
https://doi.org/10.1007/s40262-025-01473-9

ORIGINAL RESEARCH ARTICLE

Evaluation of Solubility-Limited Absorption as a Surrogate to Predicting Positive Food Effect of BCS II/IV Drugs

Karine Rodriguez-Fernandez[1,2] · José David Gómez-Mantilla[3] · Suneet Shukla[3] · Peter Stopfer[3] · Peter Sieger[4] · Victor Mangas-Sanjuán[1,2] · Sheila Annie Peters[3]

Accepted: 31 December 2024

Abstract

Introduction and Objective Physiologically based pharmacokinetic (PBPK) models are increasingly used to predict food effect (FE) but model parameterization is challenged by in vitro–in vivo (IVIV) disconnect and/or parameter nonidentifiability. To overcome these issues, we propose a simplified PBPK model, in which all solubility-driven processes are lumped into a single parameter, solubility, which is optimized against observed concentration–time data.

Methods A set of commercially available biopharmaceutical classification system (BCS) II/IV compounds was selected to measure the solubility in a fasted state simulated intestinal fluid (FaSSIF) medium. The compounds were ranked from the lowest to the highest dose-adjusted FaSSIF solubility (FaSSIF/D) value and subdivided into three areas based on an upper and a lower limit: drugs with FaSSIF/D > upper limit having no FE, drugs with FaSSIF/D < lower limit having FE, and drugs between the limits said to be in the sensitivity range (SR), for which we tested the hypothesis that solubility-limited absorption (SLA) identified by simplified PBPK model can reliably predict positive FE if their exposures are not impacted by gut efflux or gut metabolism.

Results We demonstrate, using a subset of drugs within SR for which PBPK models were available, that drugs with SLA exhibited a positive FE, while those with no SLA did not show FE.

Conclusions This proposal allows for a reliable binary prediction of FE to enable timely decisions on the need for pilot FE studies as well as the timing of pivotal FE studies.

✉ Sheila Annie Peters
sheila.peters@boehringer-ingelheim.com

1 Department of Pharmacy and Pharmaceutical Technology and Parasitology, University of Valencia, Valencia, Spain

2 Interuniversity Research Institute for Molecular Recognition and Technological Development, Polytechnic University of Valencia-University of Valencia, Valencia, Spain

3 Translational Medicine and Clinical Pharmacology, Boehringer Ingelheim Pharma GmbH & Co. KG, Binger Straße 173, 55216 Ingelheim am Rhein, Germany

4 Drug Discovery Sciences, Boehringer Ingelheim Pharma GmbH & Co. KG, 88397 Biberach a.d. Riss, Germany

Published online: 03 February 2025

Graphical Abstract

Clinical Pharmacokinetics

PEER-REVIEWED FEATURE

Evaluation of solubility-limited absorption as a surrogate to predicting positive food effect of BCS II/IV drugs

Karine Rodriguez-Fernandez, José David Gómez-Mantilla, Suneet Shukla, Peter Stopfer, Peter Sieger, Victor Mangas-Sanjuán and Sheila Annie Peters

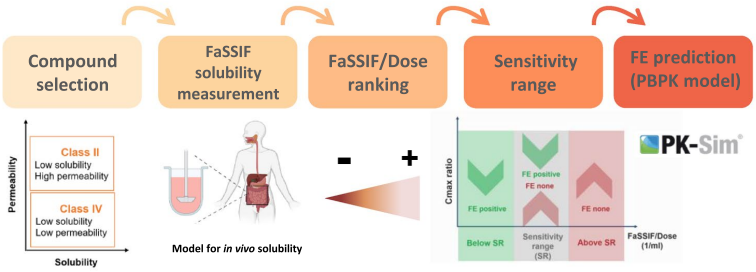

FaSSIF fasted state simulated intestinal fluid, *FE* food effect, *Cmax* maximum blood/plasma concentration, *PBPK* physiologically based pharmacokinetic.

Key Points

A methodology has been proposed for the in silico prediction of positive food effect based on determining a sensitivity range of dose-adjusted fasted state simulated intestinal fluid solubility for BCS II/IV compounds.

Dose-adjusted fasted state simulated intestinal fluid solubility can be used to distinguish drugs with food effect from those with no food effect outside the sensitivity range.

Within the sensitivity range, where dose-adjusted fasted state simulated intestinal fluid solubility cannot discriminate drugs based on food effect, solubility-limited absorption can serve as a good surrogate for binary prediction of food effect.

1 Introduction

The effect of food on oral drug absorption is a complex phenomenon that has long captivated the attention of pharmaceutical researchers and clinicians [1]. Food can significantly alter the pharmacokinetics (PK) of orally administered drugs by modifying the rate and extent of drug absorption, thereby impacting both their therapeutic efficacy and safety [2]. Food-induced physiological changes affecting absorption include changes in gastric emptying, gastric pH, luminal drug concentrations, bile secretion, and splanchnic blood flow [3]. Understanding the effect of food on the systemic exposure of an orally administered drug is a critical aspect of drug development, regulatory requirements, and clinical practice. During drug development, a pilot food effect (FE) study is often conducted as part of a phase I clinical trial for drugs that are expected to have low bioavailability to inform dosing with or without food in subsequent trials. Later, a pivotal FE study must be conducted with the final dose and formulation of the drug to inform drug labeling in support

of new drug application (NDA) submission [4, 5], unless the investigational drug is a biopharmaceutical classification system (BCS) class I drug with an oral bioavailability ≥ 85%. Predictions of FE can significantly streamline drug development by guiding formulation strategies, optimizing clinical trial designs, and informing dosing recommendations. In early clinical development, decisions on the need to conduct a time- and resource-consuming FE study in phase I require a binary (yes/no) prediction with high confidence rather than a quantitative prediction. A reliable, conservative prediction of a lack of FE for the drug of interest can help avert pilot FE studies, as well as delay the pivotal FE study until later in the drug development process when there is more certainty about the drug's market potential.

Current methods to predict human FE during drug development include in vitro and in silico tools [6]. In vitro methods include simple solubility- and permeability-based models such as BCS classification [7], predictions based on physicochemical properties such as dose number and maximum absorbable dose [8, 9], and compendial dissolution methods using fasted and fed state simulated intestinal fluid (FaSSIF/FeSSIF), as well as complex in vitro tools such as TIM and dynamic gastric model (DGM) systems [10]. There is a growing interest in the application of in silico physiologically based pharmacokinetic (PBPK) models (e.g., SimCYP, GastroPlus, OSP Suite) that incorporate various factors influencing oral drug absorption for quantitative prediction of FE [11–18]. However, both in vitro and in silico tools have some limitations in predicting FE on drug absorption. In vitro studies often simplify gastrointestinal environments and operate under static environments leading to in vitro–in vivo (IVIV) disconnect and resulting in a systematic underprediction of in vivo drug absorption. Methods employing dose number assume a luminal fluid volume of 250 ml [19], whose relevance in vivo is not verifiable. PBPK models describe oral drug absorption with processes such as dissolution, precipitation, solubilization, etc., each with its own set of parameters [20, 21]. The downside of this complexity is that model verification and parameterization are often hindered by the IVIV disconnect and parameter nonidentifiability in "middle out" approaches—too many parameters with uncertainty and too few observed data (concentration–time data) adversely affecting confidence in model predictions [22–25].

Nonidentifiability issues in a PBPK model may be overcome through model simplification/lumping [26]. In an accompanying article in this issue [22], we proposed a simplified PBPK model in which drug solubility represents all solubility-driven processes (dissolution, precipitation, solubilization, etc.). For a poorly soluble BCS II drug that is not a substrate of cytochrome P450 3A (CYP3A) or intestinal transporters, the in vitro solubility employed in the model then becomes the sole parameter associated with uncertainty, which can be readily optimized against observed plasma drug concentrations. The aim of this work is to explore a novel approach to predict positive FE of BCS II/IV drugs using the proposed simplified PBPK model, recognizing solubility limited absorption as the sole driver of positive FE for BCS II/IV drugs. Through a comprehensive analysis, we test the hypothesis that a binary FE prediction using solubility-limited absorption (SLA) identified by a simplified PBPK model in a conservative setting can reliably predict positive FE for BCS II drugs that are not extensively metabolized or effluxed in the gut.

2 Materials and Methods

2.1 Compound Selection

A systematic literature search was performed in databases in the field of Health Sciences—Embase, MEDLINE (via PubMed), and Scopus—to find BCS class II and/or IV compounds with a FE clinical study available or at least with information on changes in exposure parameters in the product label after food intake. When more than one clinical FE study was available, the one carried out on healthy individuals with high-fat meals was selected. The categorization of FE type was determined by evaluating the ratio of maximum blood/plasma concentration (C_{max}) of fed to fasted states using the bioequivalence criteria. If the C_{max} was higher in the fed state compared with the fasted state (ratio > 1.25), it was categorized as a positive FE. Conversely, if C_{max} was greater in the fasted state than in the fed state (ratio < 0.80), it was considered a negative FE. If there was no significant difference in C_{max} when taken with or without food (ratio within 0.8–1.25), it was classified as no FE. The compounds with negative FE were not considered for this investigation. In general, the negative FE observed for a few weak, basic BCS II/IV compounds is attributed to drug precipitation in small intestine due to higher prevailing pH, relative to gastric pH. Although demonstrated in vitro, drug precipitation is unlikely under in vivo sink conditions. In drugs showing negative FE, the effect sizes are generally small and not linked to safety risks. Therefore, negative FE prediction is generally not considered critical in drug development [22]. In addition to BCS class and FE in vivo (positive or none), other information collected from the literature included physical–chemical properties, solubility in FaSSIF, and dose of the drug product.

2.2 FaSSIF Solubility Measurement

The solubility in the FaSSIF medium for a subset of drugs was experimentally measured. The FaSSIF medium was the commercially available product from Biorelevant (www.

biorelevant.com). The drug subset was selected based on the availability of the raw materials from Boehringer Ingelheim Pharma: nintedanib, mefenamic acid, phenytoin, ibrutinib, dabigatran etexilate, flibanserin, spironolactone, clopidogrel, progesterone, telmisartan, nefazodone HCl, nevirapine, carbamazepine, amiodarone HCl, digoxin, ibuprofen, meloxicam, and repaglinide were available. Albendazole, crizotinib, efavirenz, felodipine, gefitinib, nelfinavir mesylate, telaprevir, and tizanidine were purchased from Sigma-Aldrich Chemie GmbH. Purity for all drug substance batches was at least 98% or greater and was tested by high-performance liquid chromatography (HPLC) before usage. The determination of the equilibrium solubility in FaSSIF medium was performed at 37 ± 1 °C by using an in-house-built robotic system. Saturated solutions were prepared in well plates by adding an appropriate volume of FaSSIF medium (typically in the range of 0.5–1.0 ml) into each well that contains a known quantity of solid drug substance (typically in the range of 1–2 mg). The well plates were shaken for 24 h and then filtered using PTFE filters with 0.45 µm pore size. Filter absorption was avoided by discarding the first few drops of filtrate. The amount of dissolved drug substance was determined by UV spectroscopy against a reference solution. In addition, the pH of the aqueous saturated solution was measured using a glass-electrode pH meter. The pH in the final medium was close to 6.5.

2.3 Dose-Adjusted FaSSIF Solubility Estimation

The dose-adjusted FaSSIF solubility (FaSSIF/D) was calculated as the ratio between the solubility in FaSSIF conditions gathered from literature data or measured experimentally and the dose from the in vivo FE study for each compound. The compounds were then ranked from the lowest to the highest FaSSIF/D values.

2.4 Sensitivity Range Determination

On the basis of the FaSSIF/D ranking, compounds were subdivided into three categories: (i) drugs with no FE, (ii) drugs with positive FE, and (iii) drugs with positive FE/no FE. The lower and upper limits of the sensitivity range (SR), which included drugs with positive FE/no FE, were established based on the FaSSIF/D values from the upper limit of the drugs with positive FE (below the SR) and the lower limit of the drugs with no FE (above the SR) (Fig. 1). The SR was established via two sets of FaSSIF data. The first was the conservative SR determined only for compounds with FaSSIF solubility measured experimentally in this study under the same conditions. The second SR was defined also with the compounds of the conservative SR, as well as using other compounds with literature-reported FaSSIF solubility values assessed under unknown and uncontrolled conditions.

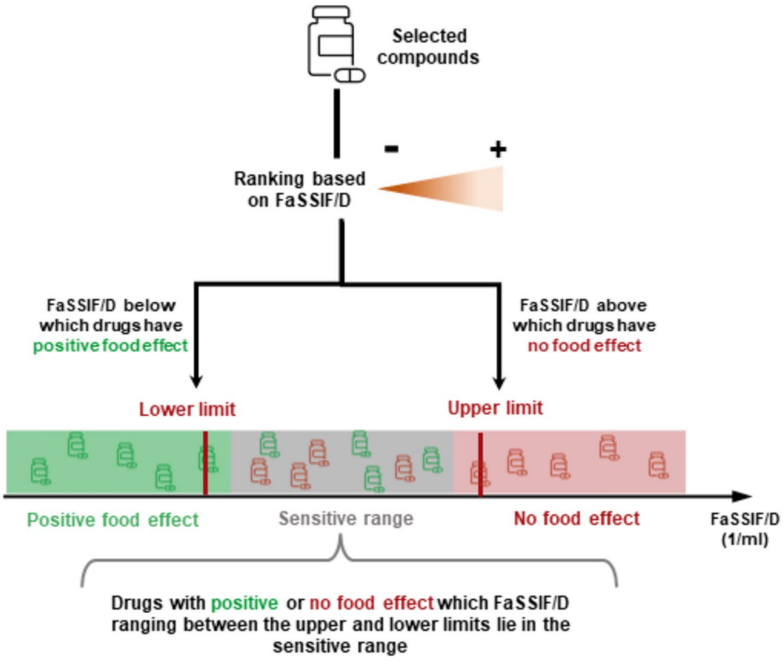

Fig. 1 Workflow for SR determination for BCS class II and IV compounds. *D* dose, *FaSSIF* fasted state simulated intestinal fluid, *FaSSIF/D* dose-adjusted FaSSIF solubility, *SR* sensitivity range

2.5 FE Prediction Through SLA Absorption with PBPK Modeling

The in vivo SLA was explored as a surrogate for FE prediction for drugs within the SR for which PBPK models were already available in PK-Sim (Open Systems Pharmacology Suite 11.2, www.open-systems-pharmacology.org, 2023). In these models, the model parameters related to systemic disposition (clearance and volume of distribution) were already optimized against observed clinical PK data. The steps for determining SLA are shown in Fig. 2. The model-simulated oral PK profile considering the measured FaSSIF solubility was compared with the oral PK profile observed in fasted state. If no relevant differences between the simulated and observed C_{max} were seen, the experimental FaSSIF solubility was considered adequate to describe drug absorption. When simulated area under the curve (AUC) and C_{max} were less than the observed parameter values, the measured FaSSIF solubility is said to underpredict in vivo drug absorption due to IVIV disconnect. In this case (Fig. 2, Scenario 1), the solubility value in the model was increased (optimized solubility) until the simulated AUC and C_{max} matched the observed data. This optimized solubility is referred to as the "at least" in vivo solubility [21], since the actual in vivo solubility could be even higher than the optimized value if the drug absorption in vivo is not limited by solubility. To confirm that absorption of the drug is not limited by solubility in vivo, the model solubility value was hypothetically increased beyond the best-fit solubility. Depending on the cases described above, the best-fit solubility could be the measured FaSSIF solubility itself or the optimized solubility. A lack of C_{max} and AUC sensitivity to increases beyond best-fit solubility confirms that in vivo drug absorption is not limited by solubility. If a stepwise increase in model value of solubility lead to increases in simulated C_{max} and AUC, the in vivo drug absorption is said to be limited by solubility. The value of hypothetically high solubility beyond which there are no changes to simulated AUC and C_{max} is referred to as maximum solubility. If AUC and C_{max} ratios resulting from simulated exposure with maximum solubility and optimized or FaSSIF solubility was > 1, in vivo oral drug absorption is solubility limited and suggests a high probability of positive FE. If the ratios are close to 1, then the in vivo drug absorption is not limited by solubility [21]. When model-simulated C_{max} was greater than the observed C_{max}, gut metabolism- or efflux-limited absorption are assumed to be the driving factors (Fig. 2, Scenario 2). This conclusion is justified since the models are already optimized for systemic drug disposition due to clearance and volume of distribution using intravenous PK data. For drugs for which the simulated C_{max} was greater than the observed, it is not possible to apply the proposed method for positive FE prediction.

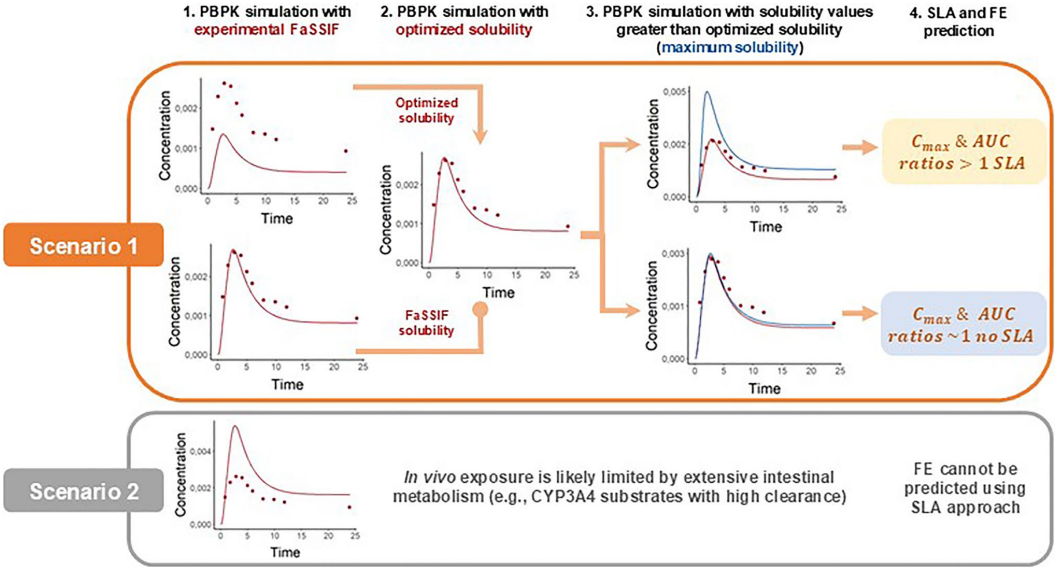

Fig. 2 Schematic diagram of the PBPK modeling approach to identify SLA and FE for a drug within the SR. C_{max} maximum blood/plasma concentration, *FaSSIF* fasted state simulated intestinal fluid solubility, *FE* food effect, *PBPK* physiologically based pharmacokinetic model, *SLA* solubility-limited absorption, *SR* sensitivity range

Graphical and numerical analyses were performed using R programming language version 4.3.1 (The R Foundation for Statistical Computing, Vienna, Austria, 2023) and R studio.

3 Results

3.1 Compound Selection

A clinical in vivo FE study was reported for 51 compounds showing positive (61%) or no FE (39%), of which 65%, 8%, and 27% were BCS class II, II/IV, and IV drugs, respectively. Literature-reported solubility in FaSSIF medium was available for 25 compounds, showing positive (76%) or no FE (24%), for which 44%, 8%, and 48% were BCS class II, II/IV, and IV drugs, respectively (Supplementary Table S1).

3.2 FaSSIF Solubility Measurement

FaSSIF solubility was measured for 26 compounds with positive FE (46%) and no FE (54%) (Table 1), of which 22 belonged to BCS class II. It is noteworthy that 55% of the BCS class II drugs showed no FE in vivo. A comparison between experimentally determined FaSSIF values and those from the literature is shown in Fig. 3. To quantify the bias in the measurement of FaSSIF, we calculated the average-fold error, which resulted in 0.14, therefore we can affirm that the FaSSIF solubility measured in our laboratory was generally lower compared with literature FaSSIF data.

Table 1 Selected compounds for determination of FaSSIF solubility and the conservative SR

Compound	BCS	C_{max} ratio *in vivo*	FE *in vivo*	Dose (mg)	Measured FaSSIF (mg/ml)	FaSSIF/D (1/ml)
Telaprevir	II	5.96	positive[16]	750	0.001	$1.33x10^{-06}$
Nelfinavir mesylate	II/IV	4.37	positive[16]	1250	0.03	**$2.40x10^{-05}$**
Nintedanib	II	1.18	none[a]	100	0.003	$3.00x10^{-05}$
Mefenamic acid	II	1.05	none[33]	250	0.015	$6.60x10^{-05}$
Phenytoin	II	1.41	positive[34]	300	0.02	$6.67x10^{-05}$
Ibrutinib	II	2.83	positive[35]	420	0.03	$7.14x10^{-05}$
Dabigatran etexilate	II	0.96	none[a]	110	0.008	$7.27x10^{-05}$
Flibanserin	II	1	none[a]	100	0.008	$8.00x10^{-05}$
Efavirenz	II	1.79	positive[36]	600	0.07	$1.17x10^{-04}$
Albendazole	II/IV	5.93	positive[37]	400	0.06	$1.50x10^{-04}$
Gefitinib	II	1.32	positive[38]	250	0.04	$1.60x10^{-04}$
Spironolactone	II	2.1	positive[39]	200	0.04	$2.00x10^{-04}$
Clopidogrel	II	6.5	positive[40]	75	0.017	$2.27x10^{-04}$
Progesterone	II	5.19	positive[41]	200	0.05	$2.50x10^{-04}$
Telmisartan	II	0.8	none[a]	160	0.05	$3.13x10^{-04}$
Nefazodone HCl	II	0.93	none[42]	200	0.08	$4.00x10^{-04}$
Nevirapine	II	1	none[a]	200	0.08	$4.00x10^{-04}$
Crizotinib	IV	0.86	none[43]	250	0.15	$6.00x10^{-04}$
Carbamazepine	II	1.35	positive[44]	400	0.3	$7.50x10^{-04}$
Amiodarone HCl	II	3.68	positive[45]	600	0.6	$1.00x10^{-03}$
Digoxin	IV	0.8	none[46]	1	0.001	$1.00x10^{-03}$
Felodipine	II	1.04	none[47]	10	0.01	$1.00x10^{-03}$
Ibuprofen	II	1.1	none[48]	800	1	**$1.25x10^{-03}$**
Meloxicam	II	0.8	none[a]	15	0.09	$6.00x10^{-03}$
Repaglinide	II	0.8	none[a]	2	0.05	$2.50x10^{-02}$
Tizanidine	II	1.24	none[49]	8	1	$1.25x10^{-01}$

The italics FaSSIF/D area represents the conservative SR, and the bold FaSSIF/D values represent the upper and lower limits of the conservative SR

BCS biopharmaceutical classification system, C_{max} maximum blood/plasma concentration, *D* dose, *FaSSIF* fasted state simulated intestinal fluid solubility, *FaSSIF/D* dose-adjusted *FaSSIF*, *SR* sensitivity range

[a]Food effect information was provided by Boehringer Ingelheim Pharma

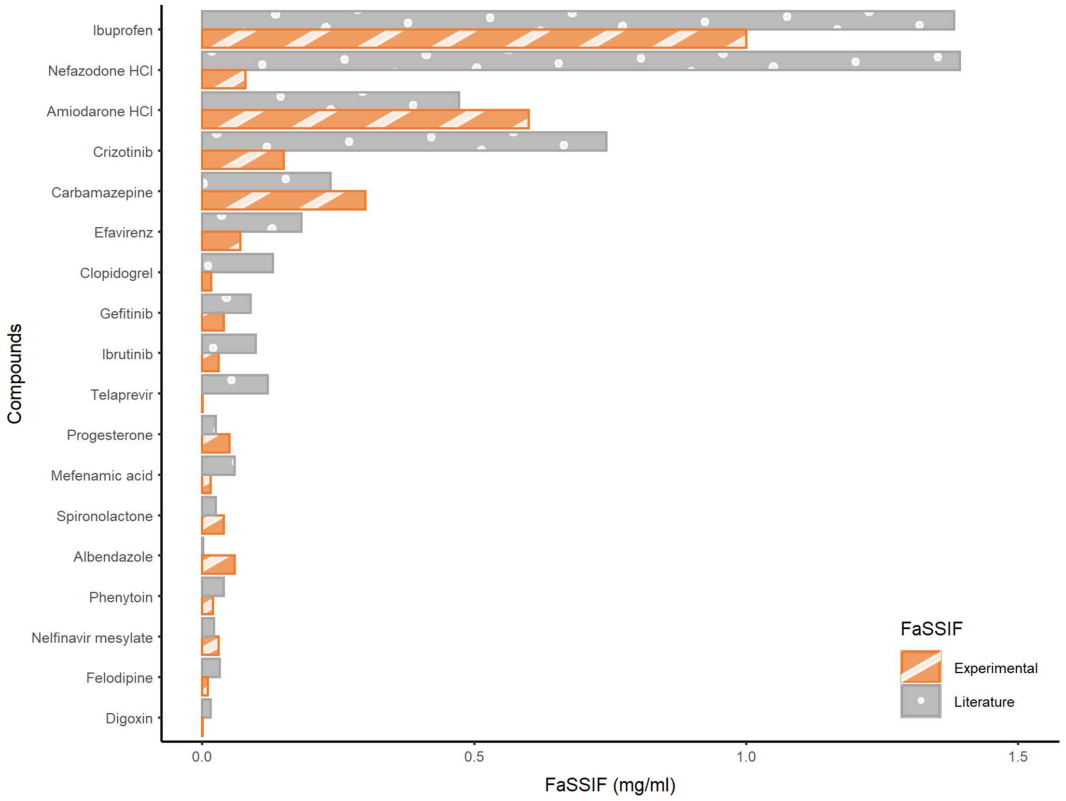

Fig. 3 Comparison of experimentally determined and literature-reported FaSSIF values. *FaSSIF* fasted state simulated intestinal fluid solubility

3.3 Sensitivity Range

First, a conservative SR was assessed using the FaSSIF/D values (Table 1) from the 26 compounds with experimental FaSSIF solubility measured. A total of 20 compounds lay within the conservative SR area (Fig. 4). All compounds with FaSSIF/D values less than 3×10^{-5} 1/ml showed only a positive FE while all compounds with FaSSIF/D greater than 1×10^{-3} 1/ml demonstrated no associated FE. Since the FaSSIF solubility measured in our laboratory was generally lower compared with literature FaSSIF data (Fig. 3), a second SR was also developed including 25 compounds with FaSSIF solubility from the literature (Supplementary Table S1). The SR with a total dataset of 51 compounds included 10 compounds (all positive FE) with FaSSIF/D lower than the lower limit of the SR, 37 compounds (21 with positive FE and 16 with no FE) within the SR, and 4 compounds (all no FE) with FaSSIF/D values higher than the upper limit of the SR. Overall, the SR showed good agreement with the previous conservative SR, since an equal lower limit was achieved and a slightly higher upper limit of the conservative SR was established (Fig. 4).

3.4 PBPK Simulations for SLA Prediction for Drugs within Conservative SR

PBPK models were available in PK-Sim for 6 out of 20 drugs with a FaSSIF/D ratio within conservative SR. The model parameters impacting absorption, metabolism, distribution, and elimination for these six drugs are presented in Supplementary Table S2. The PBPK simulations of PK profiles of a representative drug with SLA (efavirenz) and another representative drug without SLA (digoxin) are shown in Fig. 5. The PBPK simulations of PK profiles of the rest of the compounds are shown in Supplementary Figs. S1 and S2. The values of optimized and maximum solubility for the predicted and observed exposure ratios and in vivo and predicted FE from PBPK simulations of all six drugs are presented in Table 2.

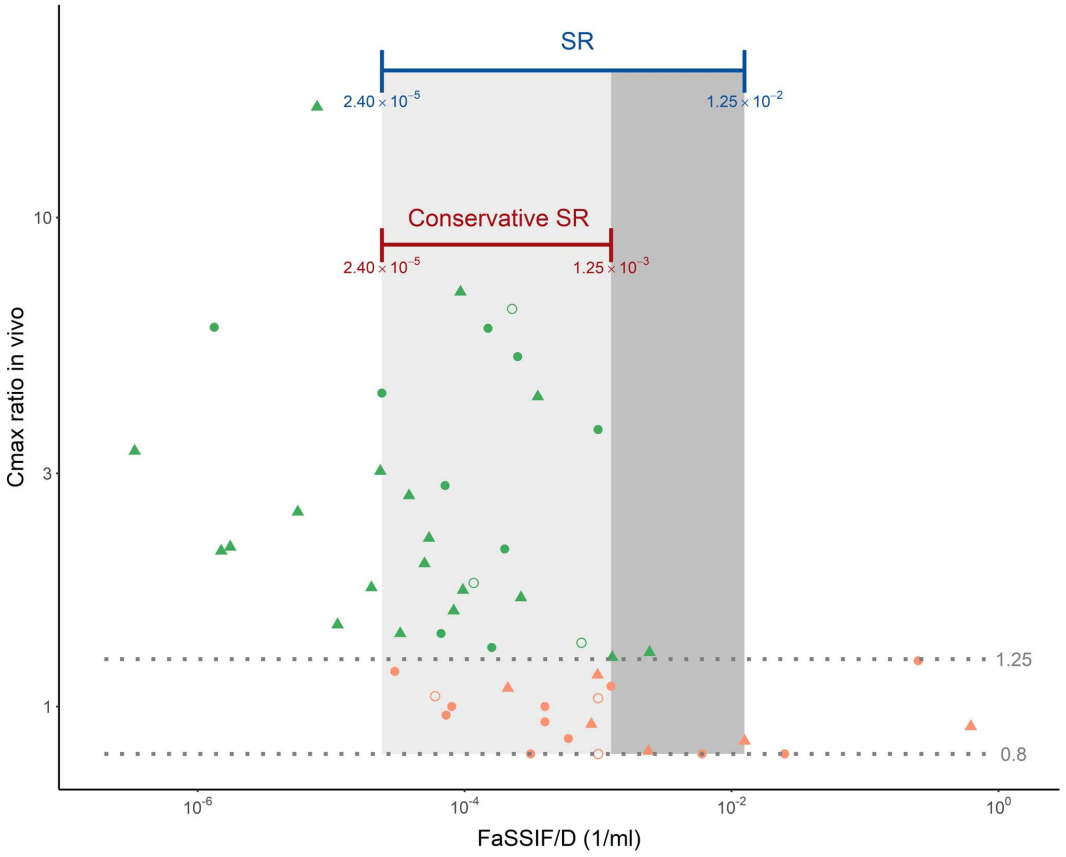

Fig. 4 Conservative SR with experimental FaSSIF data and SR with experimental FaSSIF data plus literature FaSSIF data. The shadow grey area represents the SR. Grey dotted lines represent the limits for FE categorization, green filled circles represent the compounds with FE positive and FaSSIF measured experimentally, green filled triangles represent the compounds with FE positive and FaSSIF from literature, orange filled circles represent the compounds with no FE and FaSSIF measured experimentally, orange filled triangles represent the compounds with no FE and FaSSIF from literature, non-filled circles present the compounds with FE positive (green) and no FE (orange) within conservative SR and SR with FaSSIF measured experimentally and selected for PBPK simulations of SLA. *D* dose, *FaSSIF* fasted state simulated intestinal fluid, *FaSSIF/D* dose-adjusted FaSSIF solubility, *SR* sensitivity range

For carbamazepine, the first compound in scenario 1 (Supplementary Fig. S1), the solubility was optimized to a value almost three times higher than that obtained experimentally and the maximum solubility in this case was greater than the optimized one. Efavirenz is the second case of scenario 1 (Fig. 5) where the FaSSIF solubility is very similar to the optimized one, consequently, the experimental FaSSIF solubility was predictive of the observed. Furthermore, we were able to modify up to a maximum solubility greater than the optimized one, which is why efavirenz is a compound sensitive to increasing solubility. Both efavirenz and carbamazepine had C_{max} ratios significantly greater than 1, which represent SLA and support the positive FE observed in vivo. The following cases correspond to digoxin and mefenamic where the FaSSIF solubility did not describe the observed behavior. Therefore, the FaSSIF solubility was optimized for these compounds. For both compounds, the oral exposure was not sensitive to an increase in the input solubility beyond the best-fit solubility. Hence, the predicted C_{max} ratios were 1, representing a non-SLA and also predicted no FE in silico, which was in agreement with the observed behavior in vivo. The in silico/in vivo ratios of the FE were very close to 1 in all the previous cases. The compounds in the second scenario, clopidogrel, and felodipine (Supplementary Fig. S2) did show in vivo positive FE or no FE, respectively, but it was not possible to describe the

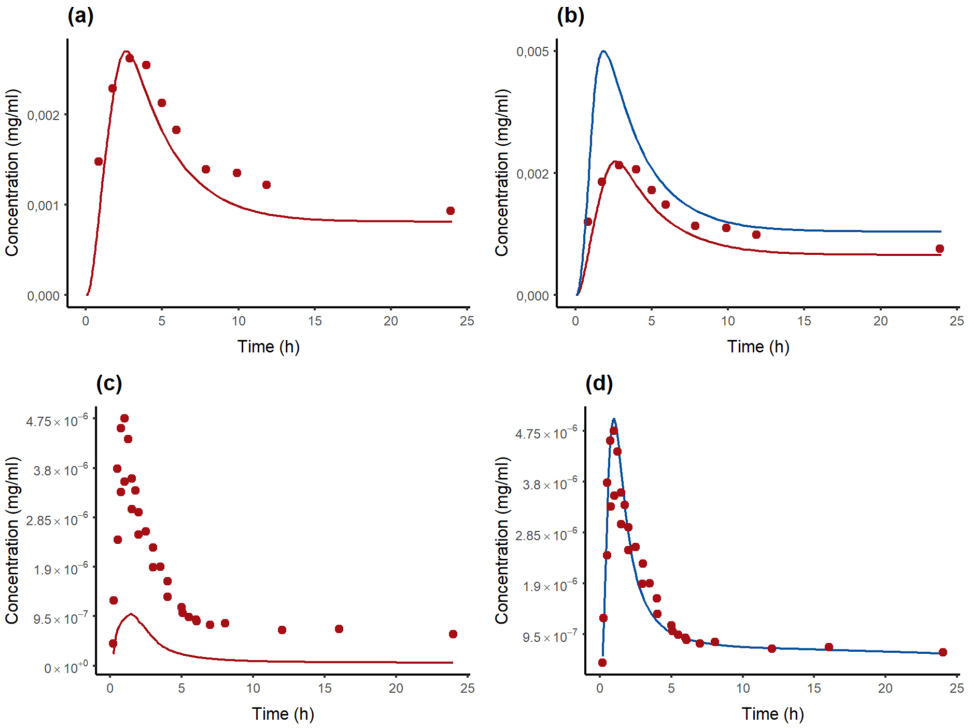

Fig. 5 PBPK simulations of fasted PK profiles of efavirenz (**a**, **b**) and digoxin (**c**, **d**). **a** Efavirenz 600 mg oral administration simulated with measured FaSSIF solubility. **b** Efavirenz 600 mg oral administration simulated with optimized (red line) and maximum solubility (blue line). **c** Digoxin 1 mg oral administration simulated with measured FaSSIF solubility. **d** Digoxin 1 mg oral administration simulated with optimized (red line) and maximum solubility (blue line), in this case, overlapped. *FaSSIF* fasted state simulated intestinal fluid.

change in the observed C_{max} either with the experimental FaSSIF solubility or with a hypothetical increase in solubility, indicating that the exposure of these drugs is limited by gut metabolism/efflux. Therefore, it was not possible to identify SLA.

4 Discussion

A novel method has been proposed capable of establishing a quantitative framework for the early prediction of FE by estimating a SR range from the interplay of solubility of the drug in biorelevant medium and the dose. This method aims to establish a conservative prediction, with zero uncertainty for both positive FE and non-FE conditions, which enables confident and timely decisions during drug development. Furthermore, it precisely establishes the scope of uncertainty about the impact of food on drug exposure (SR), allowing for simple but informative risk assessment. Although FE impacts the time to reach the maximum blood/plasma concentration (T_{max}), C_{max}, and AUC, compound selection was based on the C_{max} ratio. This is because, C_{max} is likely to be more sensitive to food-induced changes in exposure compared to AUC, while FE changes in T_{max} are likely to be confounded by gastric emptying. The characterization of in vitro solubility in physiological pH or FaSSIF and FeSSIF medium are often considered to adequately mimic in vivo conditions of orally administered drugs. However, these measured solubilities may still be conservative as in vitro settings may not adequately capture the in vivo sink conditions and transit kinetics [10]. Thus, not all BCS II/IV drugs classified based on measured solubility exhibit positive FE. According to a recent publication [18], only 36% of the 111 BCS II/IV approved drugs (25/68 BCS II, 6/25 BCS IV, 9/18 BCS II/IV) exhibit a positive FE, while 60% had no FE and 6% had negative FE. Out of the BCS II drugs exhibiting positive FE, only 15 had FE with significantly increased exposure (AUC ratio $\geq$ 2.0) [27]. All 15 were drugs with log$P$ > 3 for which enhanced bile solubilization

Table 2 SLA for the prediction of FE using the PBPK modeling approach

Compound	Solubility			AUC ratio		C_{max} ratio		Positive FE in vivo	Positive FE predicted by SLA	CYP3A4 or UGT substrate?	CL (l/h)
	FaSSIF (mg/ml)	Optimized (mg/ml)	Maximum (mg/ml)	Observed	Predicted	Observed	Predicted				
Carbamazepine	0.3	0.85	1.8	1.12	1.08	1.35	1.21	Yes	Yes	CYP3A4, UGT	2.7 [50]
Efavirenz	0.07	0.068	0.22	1.28	1.44	1.79	1.87	Yes	Yes	CYP3A4	9.4 (po) [51]
Digoxin	0.001	0.055	0.055	0.98	1	0.8	1	No	No	No	5.28 [51]
Mefenamic acid	0.015	0.5	0.5	0.97	1	1.05	1	No	No	No	21.23 (po) [51]
Felodipine	0.01	0.012	*	1.53	*	1.04	*	No	*	CYP3A4	90 [47]
Clopidogrel	0.017	0.06	*	9.2	*	6.5	*	Yes	*	CYP3A4	84 [52]

AUC area under the curve, C_{max} maximum blood/plasma concentration, *CL* total body clearance value, *CYP3A4* Cytochrome P450 3A4, *FaSSIF* fasted state simulated intestinal fluid solubility, *Maximum solubility* PBPK model hypothetical solubility that exceeds the optimized solubility that helps to identify SLA, *Optimized solubility* PBPK model hypothetical solubility beyond which there were no further changes between predicted and observed profile, *PBPK* physiologically based pharmacokinetic model, *SLA* solubility-limited absorption, *UGT* uridine diphosphate glucuronosyltransferase

*The value could not be determined

can play an important role in increasing in vivo solubility and therefore absorption, supporting that poor solubility is a plausible predictor of positive FE for BCS II drugs. The lack of FE for 60% of BCS II drugs can be explained by a possible misclassification of BCS I drugs as BCS II, based on conservative in vitro measures of solubility disconnected from the real in vivo solubility. In the previous research article by Owens et al. [27], the authors also showed that negative FEs are mostly seen in BCS III drugs (28% of the 28 drugs) and only 3 of these showed an AUC ratio of < 2.0-fold. Given the weak correlation of FE with BCS classes, the authors concluded that multiple physiological mechanisms impact FE [27]. However, since none of the 25 BCS I drugs in their study showed a positive FE (as expected from this class), it follows that high absorption resulting from high solubility and permeability does guarantee a lack of FE. This implies that mechanisms of FE not mediated by solubility and permeability (food–drug complexation, lower luminal drug concentration in fed state leading to increased susceptibility of substrates to intestinal efflux and inhibition of CYP3A and/or efflux transporters in gastrointestinal tract) are rare, even if theoretically possible. The absence of positive FE for BCS I drugs also suggests that it is very unlikely for measured solubility to over-predict in vivo solubility and misclassify a BCS II as BCS I.

Dose-adjusted solubility provides a drug-independent determinant of oral drug absorption in vivo. As dose-adjusted solubility is decreased from a hypothetically high value, the corresponding simulated oral drug absorption is constant at 100% and high, until a critical threshold, below which oral drug absorption starts to decrease. A drug with a dose-adjusted solubility below this critical threshold is said to have SLA (Supplementary Fig. S3). The in vivo solubility of such a drug may be enhanced by food via its influence on one or more factors (gastric pH and gastric emptying rate, as well as drug and bile salt concentrations). The information provided in Table 1 can aid in early clinical development, if the compound FaSSIF/D values are less than 3×10^{-5} 1/ml (below SR), it is likely to present FE. If FaSSIF/D is greater than 1×10^{-3} 1/ml (above SR), it is likely to exhibit no FE. If the FaSSIF/D value is within the SR area, then SLA determination with PBPK simulations can help to predict if the drug is likely to have FE or not, if the drug is not extensively metabolized in the gut. As can be appreciated, FaSSIF/D can indeed discriminate between drugs with or without FE, under the term that drugs are outside the SR area (Fig. 4). A conservative setting for FE prediction was ensured by choosing an upper and lower limit of conservative SR based on a determination of FaSSIF in our laboratory for 26 compounds. The FaSSIF values found in the literature are derived from different laboratories and unreported conditions of measurements. However, despite

these limitations, the inclusion of the additional compounds with literature-reported FaSSIF data provided comparable SR limits to those derived from in-house data (Fig. 4).

As previously mentioned, this approach is not valid for compounds with high intestinal metabolism nor substrates of intestinal transporters; both felodipine and clopidogrel are high clearance drugs (see Table 2) with extensive CYP3A4-mediated intestinal metabolism. Consequently, the bioavailability of these drugs is limited by metabolism to a much larger extent than limited by solubility. Extensive gut metabolism is likely for very high clearance CYP3A4 or uridine diphosphate lucuronosyltransferase (UGT) substrates and can be identified in the PBPK model when the simulated C_{max} with FaSSIF solubility is greater than the observed C_{max} (since it is unlikely that FaSSIF solubility is greater than in vivo solubility). However, even when the C_{max} with FaSSIF solubility is lesser than the observed C_{max}, gut metabolism cannot be excluded for CYP3A4 and UGT substrates. The individual contributions of solubility and gut metabolism in limiting drug absorption are nonidentifiable since model optimization against observed plasma drug concentrations can resolve uncertainty only in one parameter. Thus, for drugs with gut metabolism, the resulting masking will provide conservative estimates of FE prediction, if it is possible to apply the proposed approach (C_{max} simulated with FaSSIF < C_{max} observed). Unfortunately, a reliable quantitative prediction of gut metabolism is not easy even for CYP3A substrates [28–30]. However, since most high-clearance drugs are screened out during lead optimization, and low-clearance drugs are not likely to be impacted by gut metabolism, the proportion of drugs for which FE cannot be reliably predicted by the method proposed by our work is expected to be low. It is noteworthy that felodipine has no FE despite extensive metabolism by CYP3A4 in the gut, which seems to suggest that the standard high-fat food recommended for FE studies does not impact CYP3A4-driven gut metabolism. This is also consistent with the absence of FE for BCS I drugs [27], many of which are CYP3A4 substrates. However, certain other foods such as grapefruit juice have been shown to selectively inhibit intestinal metabolism [31].

Conventional PBPK models [13, 15–17] that are used for FE predictions include multiple unverifiable processes such as dissolution, precipitation, and solubilization, thus introducing a large array of parameters in the models. Difficulty in verifying underlying mechanisms leads to a model with many assumptions that may fit the observed data but cannot reliably predict an untested scenario (e.g., FE). The parameterization of these models relies on in vitro data that are generally under-predictive and cannot be optimized against observed concentration–time profile due to nonidentifiability. Therefore, FE predictions with PBPK models in the traditional setting tend to be conservative and uncertain resulting in unnecessary clinical FE studies [32]. This implies that pilot FE studies would be conducted even for drugs that may not have SLA or FE in vivo (e.g., a drug such as mefenamic acid). We propose here a basic framework to assess FE prediction based on a simplified model, where SLA is the surrogate for FE. This allows the only parameter that impacts FE (solubility) to be optimized against observed data for drugs that are not extensively metabolized/effluxed in the gut, thereby resulting in a more reliable binary FE prediction. However, this is only a retrospective study. In the future, this approach can be applied for prospective predictions. A reliable binary prediction of FE (yes/no) in a conservative setting (no false negatives) using the method proposed in this work is more valuable for making timely decisions on the need for a pilot FE study and timing of a pivotal FE study compared with quantitative prediction by a PBPK in the traditional setting based on several assumptions and uncertain parameters.

5 Conclusions

The results from this work have demonstrated that dose-adjusted FaSSIF solubility can be used to discriminate drugs with positive FE from those with no FE outside SR. Within SR, drugs with SLA identified by PBPK are likely to have FE. Comparable SR limits, with or without the addition of drugs with literature-reported FaSSIF data to drugs with FaSSIF solubility measured in-house, despite interlaboratory differences in the FaSSIF values, show that the SR limits are not too sensitive to these differences and that the SR limits established in this work can be applied to drugs with FaSSIF solubility measured elsewhere. The selection of SR based on conservative, in-house FaSSIF measurements on 26 drugs, and identification of SLA by PBPK allows for reliable prediction of FE to enable decisions on the need for pilot FE study and timing of pivotal FE study. It is important to note that this approach cannot be applied to drugs with extensive gut metabolism or transporter-mediated elimination. The reliability of positive FE prediction using SLA was tested with six compounds within SR, for which PK-Sim models were available. The simplified PBPK model proposed here combines all nonidentifiable parameters into a single identifiable parameter for the purpose of FE prediction, although this may compromise quantitative prediction accuracy. Our work shows that the binary prediction accuracy, which is critical for decision-making in clinical development, is not compromised. Extension of this work in the future to cover all compounds within SR will serve to further enhance confidence in the use of SLA to identify drugs that are likely to exhibit positive FE.

Supplementary Information The online version contains supplementary material available at https://doi.org/10.1007/s40262-025-01473-9.

Acknowledgments The authors acknowledge the leaderships of the Boehringer Ingelheim Pharma departments, especially Translational Medicine & Clinical Pharmacology (TMCP) and Biopharmaceutical Working Group for providing the framework and funding for this research. The authors also thank Ghazal Montaseri from the TMCP Data Science department and Jelisaveta Ignjatović from the Drug Metabolism and Pharmacokinetics DMPK department for all the support to make possible this study.

Declarations

Funding This study was funded by Boehringer Ingelheim Pharma GmbH & Co.

Conflicts of Interest José David Gómez-Mantilla, Suneet Shukla, Peter Stopfer, Peter Sieger,and Sheila Annie Peters, are paid employees of Boehringer Ingelheim Pharma GmbH & Co. The authors declare that they do not possess any identifiable financial interests or personal associations that might have appeared to exert an influence on the research presented in this paper.

Availability of Data and Material Data will be made available on request.

Author Contributions Investigation, data curation, formal analysis, methodology, visualization, writing—original draft, writing—review and editing: Karine Rodriguez-Fernandez. Investigation, formal analysis, methodology, project administration, supervision, visualization, writing—review and editing: José David Gómez-Mantilla. Investigation, methodology, supervision, visualization, writing—review and editing: Shukla Suneet. Conceptualization, funding acquisition, resources, writing—review and editing: Peter Stopfer. Investigation, formal analysis, writing—review and editing: Peter Sieger. Formal analysis, supervision, visualization, writing—original draft, writing—review and editing: Victor Mangas-Sanjuan. Investigation, conceptualization, formal analysis, methodology, project administration, supervision, visualization, writing—original draft, writing—review and editing: Sheila-Annie Peters.

Ethical Approval Not applicable.

Code Availability Not applicable.

Consent to Participate Not applicable.

Consent for Publication Not applicable.

References

1. Welling PG. Influence of food and diet on gastrointestinal drug absorption: a review. J Pharmacokinet Biopharm. 1977. https://doi.org/10.1007/bf01061694.
2. O'Shea JP, Holm R, O'Driscoll CM, et al. Food for thought: formulating away the food effect—a PEARRL review. J Pharm Pharmacol. 2019. https://doi.org/10.1111/jphp.12957.
3. Deng J, Zhu X, Chen Z, et al. A review of food-drug interactions on oral drug absorption. Drugs. 2017. https://doi.org/10.1007/s40265-017-0832-z.
4. Eur. European Medicines Agency (EMA) 21 June 2012 CPMP/EWP/560/95/Rev. 1 Corr. 2**, Committee for Human Medicinal Products(CHMP). Guideline on the investigation of drug interactions. https://www.ema.europa.eu/en/documents/scientific-guideline/guideline-investigation-drug-interactions-revision-1_en.pdf. Accessed 11 Arp 2024.
5. US. Food and Drug Administration. Assessing the Effects of Food on Drugs in INDs and NDAs – Clinical Pharmacology Considerations Guidance for Industry, June 2022. https://www.fda.gov/media/121313/download. Accessed 11 Apr 2024.
6. Lentz KA. Current methods for predicting human food effect. AAPS J. 2008. https://doi.org/10.1208/s12248-008-9025-8.
7. Amidon GL, Lennernäs H, Shah VP, et al. A theoretical basis for a biopharmaceutic drug classification: the correlation of in vitro drug product dissolution and in vivo bioavailability. Pharm Res. 1995. https://doi.org/10.1023/a:1016212804288.
8. Gu CH, Li H, Levons J, et al. Predicting effect of food on extent of drug absorption based on physicochemical properties. Pharm Res. 2007. https://doi.org/10.1007/s11095-007-9236-1.
9. Sugano K, Okazaki A, Sugimoto S, et al. Solubility and dissolution profile assessment in drug discovery. Drug Metab Pharmacokinet. 2007. https://doi.org/10.2133/dmpk.22.225.
10. Vinarov Z, Butler J, Kesisoglou F, et al. Assessment of food effects during clinical development. Int J Pharm. 2023. https://doi.org/10.1016/j.ijpharm.2023.122758.
11. Willmann S, Lippert J, Sevestre M, et al. PK-Sim®: a physiologically based pharmacokinetic "whole-body" model. Biosilico. 2003. https://doi.org/10.1016/S1478-5382(03)02342-4.
12. Jones HM, Parrott N, Ohlenbusch G, et al. mcPredicting pharmacokinetic food effects using biorelevant solubility media and physiologically based modelling. Clin Pharmacokinet. 2006. https://doi.org/10.2165/00003088-200645120-00006.
13. Jones HM, Chen Y, Gibson C, et al. Physiologically based pharmacokinetic modeling in drug discovery and development: a pharmaceutical industry perspective. Clin Pharmacol Ther. 2015;97(3):247–62.
14. GP. Simulations Plus, Manual GastroPlus™, California, EUA; 2010.
15. Tistaert C, Heimbach T, Xia B, et al. Food effect projections via physiologically based pharmacokinetic modeling: predictive case studies. J Pharm Sci. 2019. https://doi.org/10.1016/j.xphs.2018.05.024.
16. Riedmaier AE, DeMent K, Huckle J, et al. Use of physiologically based pharmacokinetic (PBPK) modeling for predicting drug-food interactions: an industry perspective. AAPS J. 2020. https://doi.org/10.1208/s12248-020-00508-2.
17. Cheng L, Wong H. Food effects on oral drug absorption: application of physiologically-based pharmacokinetic modeling as a predictive tool. Pharmaceutics. 2020. https://doi.org/10.3390/pharmaceutics12070672.
18. Ezuruike U, Zhang M, Pansari A, et al. Guide to development of compound files for PBPK modeling in the Simcyp population-based simulator. CPT Pharmacometrics Syst Pharmacol. 2022. https://doi.org/10.1002/psp4.12791.

19. Wuelfing WP, El Marrouni A, Lipert MP, et al. Dose number as a tool to guide lead optimization for orally bioavailable compounds in drug discovery. J Med Chem. 2022. https://doi.org/10.1021/acs.jmedchem.1c01687.
20. Shono Y, Jantratid E, Dressman JB. Precipitation in the small intestine may play a more important role in the in vivo performance of poorly soluble weak bases in the fasted state: case example nelfinavir. Eur J Pharm Biopharm. 2011. https://doi.org/10.1016/j.ejpb.2011.04.005.
21. Fink C, Sun D, Wagner K, et al. Evaluating the role of solubility in oral absorption of poorly water-soluble drugs using physiologically-based pharmacokinetic modeling. Clin Pharmacol Ther. 2019. https://doi.org/10.1002/cpt.1672.
22. Rodriguez-Fernandez K, Gómez-Mantilla J, Shukla S, et al. Solubility-limited absorption identified by a simplified PBPK model for the prediction of positive food effect of BCS II/IV drugs. Clin Pharmacokinet 2024. https://doi.org/10.1007/s40262-025-01472-w.
23. Li M, Zhao P, Pan Y, et al. Predictive performance of physiologically based pharmacokinetic models for the effect of food on oral drug absorption: current status. CPT Pharmacometrics Syst Pharmacol. 2018. https://doi.org/10.1002/psp4.12260.
24. Peters SA, Dolgos H. Requirements to establishing confidence in physiologically based pharmacokinetic (PBPK) models and overcoming some of the challenges to meeting them. Clin Pharmacokinet. 2019. https://doi.org/10.1007/s40262-019-00790-0.
25. Kesisoglou F. Can PBPK modeling streamline food effect assessments? J Clin Pharmacol. 2020. https://doi.org/10.1002/jcph.1678.
26. Okino MS, Mavrovouniotis ML. Simplification of mathematical models of chemical reaction systems. Chem Rev. 1998. https://doi.org/10.1021/cr9502231.
27. Owens K, Argon S, Yu J, et al. Exploring the relationship of drug BCS classification, food effect, and gastric pH-Dependent Drug Interactions. AAPS J. 2021. https://doi.org/10.1208/s12248-021-00667-w.
28. Peters SA, Jones CR, Ungell AL, et al. Predicting drug extraction in the human gut wall: assessing contributions from drug metabolizing enzymes and transporter proteins using preclinical models. Clin Pharmacokinet. 2016. https://doi.org/10.1007/s40262-015-0351-6.
29. Fagerholm U. Prediction of human pharmacokinetics–gut-wall metabolism. J Pharm Pharmacol. 2007. https://doi.org/10.1211/jpp.59.10.0002.
30. Davies M, Peramuhendige P, King L, et al. Evaluation of in vitro models for assessment of human intestinal metabolism in drug discovery. Drug Metab Dispos. 2020. https://doi.org/10.1124/dmd.120.000111.
31. Bailey DG, Malcolm J, Arnold O, et al. Grapefruit juice-drug interactions. Br J Clin Pharmacol. 1998. https://doi.org/10.1046/j.1365-2125.1998.00764.x.
32. Kesisoglou F, Basu S, Belubbi T, et al. Streamlining food effect assessment - are repeated food effect studies needed? An IQ analysis. AAPS J. 2023. https://doi.org/10.1208/s12248-023-00822-5.
33. Hamaguchi T, Shinkuma D, Yamanaka Y, et al. Bioavailability of mefenamic acid: influence of food and water intake. J Pharm Sci. 1986. https://doi.org/10.1002/jps.2600750914.
34. Melander A, Brante G, Johansson O, et al. Influence of food on the absorption of phenytoin in man. Eur J Clin Pharmacol. 1979. https://doi.org/10.1007/bf00618516.
35. de Jong J, Sukbuntherng J, Skee D, et al. The effect of food on the pharmacokinetics of oral ibrutinib in healthy participants and patients with chronic lymphocytic leukemia. Cancer Chemother Pharmacol. 2015. https://doi.org/10.1007/s00280-015-2708-9.
36. Kaul S, Ji P, Lu M, et al. Bioavailability in healthy adults of efavirenz capsule contents mixed with a small amount of food. Am J Health Syst Pharm. 2010. https://doi.org/10.2146/ajhp090327.
37. Lange H, Eggers R, Bircher J. Increased systemic availability of albendazole when taken with a fatty meal. Eur J Clin Pharmacol. 1988. https://doi.org/10.1007/bf00540964.
38. Swaisland HC, Smith RP, Laight A, et al. Single-dose clinical pharmacokinetic studies of gefitinib. Clin Pharmacokinet. 2005. https://doi.org/10.2165/00003088-200544110-00004.
39. Overdiek HWPM, Merkus FWHM. Influence of food on the bioavailability of spironolactone. Clin Pharmacol Ther. 1986. https://doi.org/10.1038/clpt.1986.219.
40. Nirogi RV, Kandikere VN, Mudigonda K. Effect of food on bioavailability of a single oral dose of clopidogrel in healthy male subjects. Arzneimittelforschung. 2006. https://doi.org/10.1055/s-0031-1296783.
41. Rangaraj N, Sampathi S, Junnuthula V, et al. Fast-fed variability: insights into drug delivery, molecular manifestations, and regulatory aspects. Pharmaceutics. 2022. https://doi.org/10.3390/pharmaceutics14091807.
42. Dockens RC, Greene DS, Barbhaiya RH. The lack effect of food on the bioavailability of nefazodone tablets. Biopharm Drug Dispos. 1996. https://doi.org/10.1002/(sici)1099-081x(199603)17:2%3c135::aid-bdd947%3e3.0.co;2-k.
43. Xu H, O'Gorman M, Boutros T, et al. Evaluation of crizotinib absolute bioavailability, the bioequivalence of three oral formulations, and the effect of food on crizotinib pharmacokinetics in healthy subjects. J Clin Pharmacol. 2015. https://doi.org/10.1002/jcph.356.
44. McLean A, Browne S, Zhang Y, et al. The influence of food on the bioavailability of a twice-daily controlled release carbamazepine formulation. J Clin Pharmacol. 2001. https://doi.org/10.1177/009127001220100005.
45. Meng X, Mojaverian P, Doedée M, et al. Bioavailability of amiodarone tablets administered with and without food in healthy subjects. Am J Cardiol. 2001. https://doi.org/10.1016/s0002-9149(00)01396-5.
46. Johnson BF, O'Grady J, Sabey GA, et al. Effect of a standard breakfast on digoxin absorption in normal subjects. Clin Pharmacol Ther. 1978. https://doi.org/10.1002/cpt1978233315.
47. Edgar B, Lundborg P, Regårdh CG. Clinical pharmacokinetics of felodipine. A summary. Drugs. 1987. https://doi.org/10.2165/00003495-198700343-00005.
48. Pargal A, Kelkar MG, Nayak PJ. The effect of food on the bioavailability of ibuprofen and flurbiprofen from sustained release formulations. Biopharm Drug Dispos. 1996. https://doi.org/10.1002/(sici)1099-081x(199608)17:6%3c511::aid-bdd969%3e3.0.co;2-y.
49. Shah J, Wesnes KA, Kovelesky RA, et al. Effects of food on the single-dose pharmacokinetics/pharmacodynamics of tizanidine capsules and tablets in healthy volunteers. Clin Ther. 2006. https://doi.org/10.1016/j.clinthera.2006.09.014.
50. Marino SE, Birnbaum AK, Leppik IE, et al. Steady-state carbamazepine pharmacokinetics following oral and stable-labeled intravenous administration in epilepsy patients: effects of race and sex. Clin Pharmacol Ther. 2012. https://doi.org/10.1038/clpt.2011.251.
51. Knox C, Wilson M, Klinger CM, et al. DrugBank 6.0: the drug bank knowledge base for 2024. Nucleic Acids Res. 2024. https://doi.org/10.1093/nar/gkad976.
52. Duong JK, Nand RA, Patel A, et al. A physiologically based pharmacokinetic model of clopidogrel in populations of European and Japanese ancestry: an evaluation of CYP2C19 activity. Pharmacol Res Perspect. 2022. https://doi.org/10.1002/prp2.946.

Supplementary Information

Article title: Evaluation of solubility-limited absorption as a surrogate to predicting positive food effect of BCS II/IV drugs

Journal: Clinical Pharmacokinetics

Authors: Karine Rodriguez-Fernandez[1,2], José David Gómez-Mantilla[3], Suneet Shukla[3], Peter Stopfer[3], Peter Sieger[4], Victor Mangas-Sanjuán [1,2] and Sheila-Annie Peters[3*]

Affiliation:

[1]Department of Pharmacy and Pharmaceutical Technology and Parasitology, University of Valencia. Valencia, Spain.

[2]Interuniversity Research Institute for Molecular Recognition and Technological Development, Polytechnic University of Valencia-University of Valencia, Valencia, Spain.

[3]Translational Medicine & Clinical Pharmacology, Boehringer Ingelheim Pharma GmbH & Co. KG, 55216 Ingelheim, Germany.

[4]Drug Discovery Sciences, Boehringer Ingelheim Pharma GmbH & Co. KG, 88397 Biberach a.d. Riss, Germany.

***Corresponding author:** Sheila-Annie Peters

E-mail: sheila.peters@boehringer-ingelheim.com.

Telephone: +49 (6132) 77-171433

Address: Translational Medicine & Clinical Pharmacology, Boehringer Ingelheim Pharma GmbH & Co. KG, Binger Straße 173, 55216, Ingelheim am Rhein, Germany.

Table S1 Selected compounds for determination of the SR

Compound	BCS	Clinical formulation	C_{max} ratio *in vivo*	FE *in vivo*	Dose (mg)	Literature FaSSIF (mg/ml)	Measured FaSSIF (mg/ml)	FaSSIF/D (1/ml)
Venetoclax	IV	Tablet	3.33	positive[1]	100	0.0000337[2]		$3.37x10^{-07}$
Telaprevir	II	Unknow*	5.96	positive[2]	750	0.12[2]	0.001	$1.33x10^{-06}$
Pazopanib HCl	II	Tablet	2.08	positive[3]	800	0.0012[4]		$1.50x10^{-06}$
Nilotinib	IV	Capsule	2.12	positive[5]	200	0.0003504[5]		$1.75x10^{-06}$
Vemurafenib	IV	Tablet	2.5	positive[6]	960	0.0054[4]		$5.63x10^{-06}$
Abiraterone	IV	Unknow*	16.83	positive[7]	1000	0.007831[5]		$7.83x10^{-06}$
Ceritinib	IV	Capsule	1.47	positive[8]	500	0.0055814[5]		$1.12x10^{-05}$
Vismodegib	II	Capsule	1.75	positive[9]	150	0.003[10]		$2.00x10^{-05}$
Lapatinib ditosylate	IV	Tablet	3.03	positive[11]	1500	0.035[4]		$2.33x10^{-05}$
Nelfinavir mesylate	II/IV	Tablet	4.37	positive[2]	1250	0.022[2]	0.03	**$2.40x10^{-05}$**
Nintedanib	II	Capsule	1.18	none**	100		0.003	$3.00x10^{-05}$
Bosutinib	IV	Unknow *	1.41	positive[12]	400	0.01316[5]		$3.29x10^{-05}$
Alectinib	IV	Capsule	2.7	positive[13]	600	0.023[2]		$3.83x10^{-05}$
Ziprasidone HCl	II	Capsule	1.96	positive[14]	80	0.004[2]		$5.00x10^{-05}$
Aprepitant	II/IV	Micronized	2.21	positive[2]	100	0.0054[15]		$5.40x10^{-05}$
Mefenamic acid	II	Capsule	1.05	none[16]	250	0.06[17]	0.015	$6.00x10^{-05}$
Phenytoin	II	Unknow*	1.41	positive[18]	300	0.0396[2]	0.02	$6.67x10^{-05}$
Ibrutinib	II	Unknow *	2.83	positive[19]	420	0.098235[5]	0.03	$7.14x10^{-05}$
Dabigatran etexilate	II	Capsule	0.96	none**	110		0.008	$7.27x10^{-05}$
Flibanserin	II	Tablet	1	none**	100		0.008	$8.00x10^{-05}$
Erlotinib	II	Tablet	1.57	positive[20]	150	0.0124[4]		$8.27x10^{-05}$
Bexarotene	II	Unknow *	7.04	positive[5]	75	0.00697[5]		$9.29x10^{-05}$
Regorafenib	IV	Unknow *	1.73	positive[5]	160	0.0156[5]		$9.70x10^{-05}$
Efavirenz	II	Capsule	1.79	positive[21]	600	0.182[22]	0.07	$1.17x10^{-04}$
Albendazole	II/IV	Unknow*	5.93	positive[23]	400	0.002[24]	0.06	$1.50x10^{-04}$
Gefitinib	II	Tablet	1.32	positive[25]	250	0.0887[4]	0.04	$1.60x10^{-04}$

The shadow FaSSIF/D represent the SR., the blue FaSSIF/D values represent the upper and lower limit of the SR. SR: sensitivity range; BCS: biopharmaceutical classification system; C_{max}: maximum blood/plasma concentration; FaSSIF: fasted state simulated intestinal fluid solubility; D: dose; FaSSIF/D: dose-adjusted FaSSIF. The parameter FaSSIF/D was calculated with the measured FaSSIF in the compounds in which it was available. * Oral forms but the reference does not specify which formulation was used. **Food effect information was provided by Boehringer Ingelheim Pharma.

Table S1 Continuation

Compound	BCS	Clinical formulation	C_{max} ratio *in vivo*	FE *in vivo*	Dose (mg)	Literature FaSSIF (mg/ml)	Measured FaSSIF (mg/ml)	FaSSIF/D (1/ml)
Spironolactone	II	Tablet	2.1	positive[26]	200	0.024996[27]	0.04	$2.00x10^{-04}$
Sunitinib	IV	Capsule	1.09	none[28]	50	0.01054[29]		$2.11x10^{-04}$
Clopidogrel	II	Tablet	6.5	positive[30]	75	0.13[31]	0.017	$2.27x10^{-04}$
Progesterone	II	Capsule	5.19	positive[32]	200	0.02547[27]	0.05	$2.50x10^{-04}$
Clarithromycim	II	Tablet	1.67	positive[33]	500	0.132[2]		$2.64x10^{-04}$
Telmisartan	II	Tablet	0.8	none**	160		0.05	$3.13x10^{-04}$
Ivacaftor	II/IV	Unknow*	4.3	positive[2]	150	0.053[2]		$3.53x10^{-04}$
Nefazodone HCl	II	Tablet	0.93	none[34]	200	1.393[2]	0.08	$4.00x10^{-04}$
Nevirapine	II	Tablet	1	none**	200		0.08	$4.00x10^{-04}$
Crizotinib	IV	Capsule	0.86	none[35]	250	0.743[4]	0.15	$6.00x10^{-04}$
Isotretinoin	II	Tablet	2.4	positive[36]	80	0.05107[27]		$6.38x10^{-04}$
Carbamazepine	II	Capsule	1.35	positive[37]	400	0.2363[27]	0.3	$7.50x10^{-04}$
Glibenclamide	II	Unknow*	0.92	none[38]	5	0.004446[27]		$8.89x10^{-04}$
Rivaroxaban	II	Tablet	1.16	none[39]	10	0.0099[24]		$9.90x10^{-04}$
Amiodarone HCl	II	Tablet	3.68	positive[40]	600	0.472[2]	0.6	$1.00x10^{-03}$
Digoxin	IV	Tablet	0.8	none[41]	1	0.01562[27]	0.001	$1.00x10^{-03}$
Felodipine	II	Tablet	1.04	none[42]	10	0.0318[43]	0.01	$1.00x10^{-03}$
Ibuprofen	II	Tablet	1.1	none[44]	800	1.38221[27]	1	$1.25x10^{-03}$
Tezacaftor	II	Unknow*	0.81	none[2]	50	0.119[2]		$2.38x10^{-03}$
Tepotinib	IV	Unknow*	1.29	positive[4]	30	0.0728[4]		$2.43x10^{-03}$
Meloxicam	II	Capsule	0.8	none**	15		0.09	$6.00x10^{-03}$
Imatinib mesylate	II	Tablet	0.85	none[2]	400	5[4]		**$1.25x10^{-02}$**
Repaglinide	II	Tablet	0.8	none**	2		0.05	$2.50x10^{-02}$
Tizanidine	II	Capsule	1.24	none[45]	4		1	$1.25x10^{-01}$
Vorinostat	IV	Unknow*	0.91	none[46]	400	248[5]		$6.20x10^{-01}$

The shadow FaSSIF/D represent the SR., the blue FaSSIF/D values represent the upper and lower limit of the SR. SR: sensitivity range; BCS: biopharmaceutical classification system; C_{max}: maximum blood/plasma concentration; FaSSIF: fasted state simulated intestinal fluid solubility; D: dose; FaSSIF/D: dose-adjusted FaSSIF. The parameter FaSSIF/D was calculated with the measured FaSSIF in the compounds in which it was available. * Oral forms but the reference does not specify which formulation was used. **Food effect information was provided by Boehringer Ingelheim Pharma.

Table S2 PBPK model input parameters from PK-Sim® for the compounds using for SLA prediction

	Carbamazepine	Efavirenz	Digoxin	Mefenamic acid	Felodipine	Clopidogrel
Physicochemical properties						
Molecular weight, g/mol	236.7	315.68	780.93	241.29	384.25	321.82
Compound type	acid	acid	neutral	acid	neutral	base
LogP	2.01	3.44	1.4	5.03	4.51	3.23
pKa	11.83	10.1		4.2		4.66
Formulation	Extended release capsule	Hard capsule	Solution	Hard gelatin capsule	Inmediated release tablet	Film coated tablet
System-drug parameters						
f_u, %	0.243	0.00596	0.71	1.9	0.0036	2
B/P	0.75	0.64	0.86	12.9	1.20	0.74
Particle disolution and solubility						
Solubility, mg/ml (source)	0.54602 (fitted)	0.03992 (fitted)	0.0648 (aqueous)	0.08095 (optimized)	12 (FaSSIF II)	0.06 (optimized)
Ref pH	6.70	0	7	5.50	6.50	7.40
Aqueous difusion coefficient, cm/min	0.000373	0.000326	0.000215	0.000369	0.0002977	0.0003231
Dissolution time, min (50%dissolved)	315.24	60		1	46.50	15.16
Dissolution shape	1.23	0.27		10	0.89	1.16
Density, g/cm3	1	1	1	1	1	1
ADME						
Partition coefficients calculation	Rodgers and Rowland	Schmitt	Rodgers and Rowland	Rodgers and Rowland	Rodgers and Rowland	Rodgers and Rowland
Cellular permeabilities calculation	PK-Sim Standard	PK-Sim Standard	PK-Sim Standard	PK-Sim Standard	PK-Sim Standard	PK-Sim Standard
Intestinal permeability, cm/seg	$5.63*10^{-7}$	$4.95*10^{-7}$	$4.6*10^{-9}$	$2.35*10^{-7}$	$3.46*10^{-5}$	$2.5*10^{-6}$
Organ permeability, cm/seg	0.0003	0.0065	$1.68*10^{-7}$	0.26	0.01	0.001
Protein binding	no	no	ATP1A2	no	no	no
koff, 1/min			0.00098			
Kd, nmol/l			25.6			
Metabolizing enzymes	CYP2B6, CYP3A4, UGT2B7	CYP1A2, CYP2B6, CYP2A6, CYP3A4, CYP3A5	none	none	CYP3A4	CYP2A6, CYP3A4, CES1, CES2

Table S2 Continuation

	Carbamazepine	Efavirenz	Digoxin	Mefenamic acid	Felodipine	Clopidogrel
ADME						
Vmax in vitro, pmol/min/mg						
CYP1A2		0.6				
CYP2B6	49	3.5				
CYP2C19						7.52
CYP2A6		1				
CYP3A4	726	0.16			163	266
CYP3A5		0.6				
CES1						3558
CES2						357
UGT2B7	3.5					
CYP1A2		0.6				
Km, umol/l						
CYP1A2		8.3				
CYP2B6	235	6.4				
CYP2C19						0.05
CYP2A6		7.7				
CYP3A4	808	23.5			2.81	2.07
CYP3A5		19.1				
CES1						46.4
CES2						14.08
UGT2B7	234					
kcat, 1/min						
CYP1A2		0.19				
CYP2B6	0.94	1.6				
CYP2C19						14.26
CYP2A6		0.32				
CYP3A4	5.01	0.05			204.7	55.36
CYP3A5		0.19				
CES1						2.51
CES2						4960.15
UGT2B7	0.071					
Specific clearance, 1/min			0.04	9.5	12.8	
Transport proteins			ABCB1			
Vmax in vitro, pmol/ml/min			8.67			
Km, umol/l			177			
kcat, 1/min			71.16			
GFR fraction, %	0.02	1	1			1

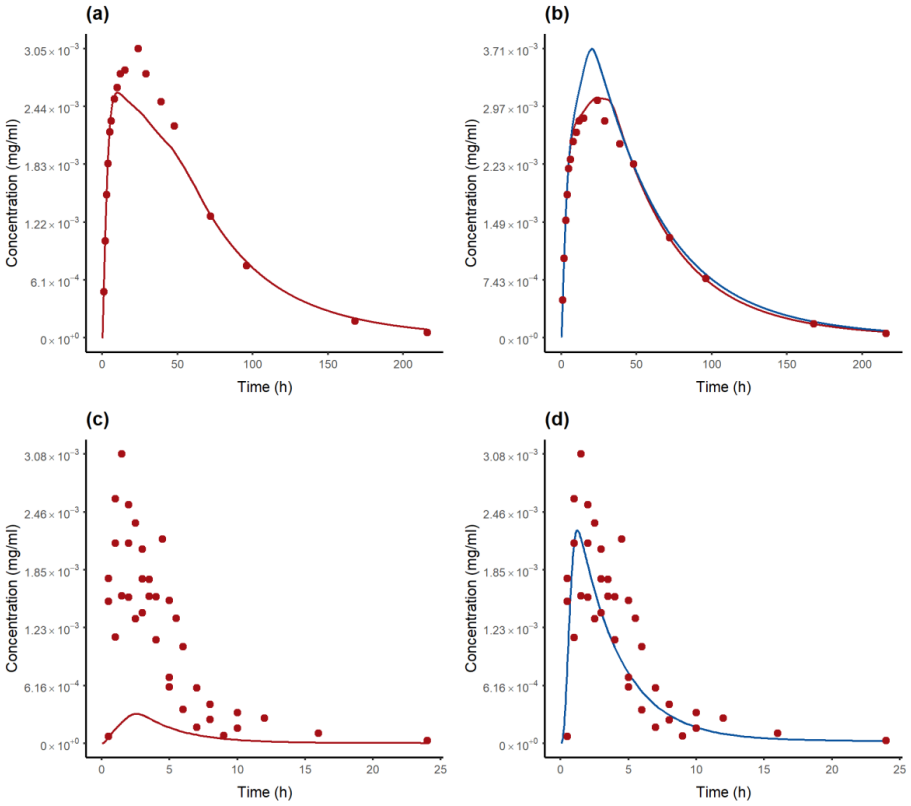

Fig. S1 PBPK simulations of fasted PK profiles of carbamazepine (a, b), and mefenamic acid (c, d). (a) Carbamazepine 400 mg oral administration simulated with measured FaSSIF solubility. (b) Carbamazepine 400 mg oral administration simulated with optimized (red line) and maximum solubility (blue line). (c) Mefenamic 250 mg oral administration simulated with in measured FaSSIF solubility (d) Mefenamic 250 mg oral administration simulated with optimized (red line) and maximum solubility (blue line), in this case overlapped. FaSSIF: fasted state simulated intestinal fluid

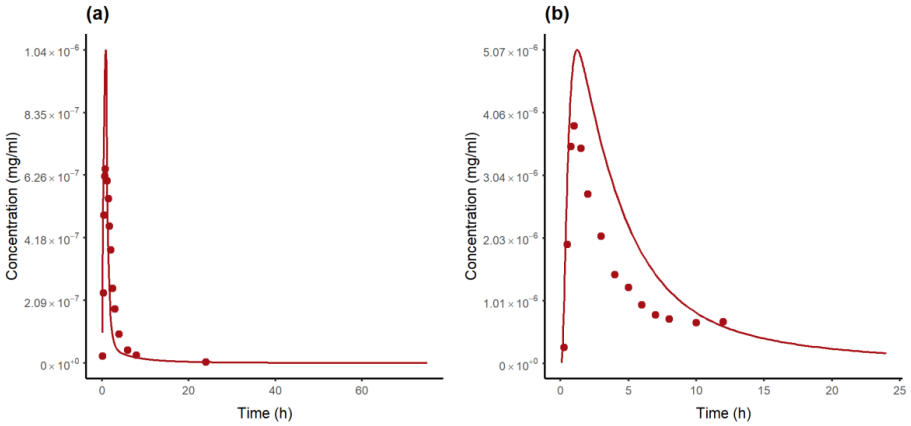

Fig. S2 PBPK simulations of PK profiles of CYP3A4 substrates. (a) Clopidogrel 75mg oral administration simulated with measured FaSSIF solubility. (b) Felodipine 10 mg oral administration simulated with in vitro FaSSIF solubility. In these compounds the food effect cannot be predicted using solubility limited absorption approach.

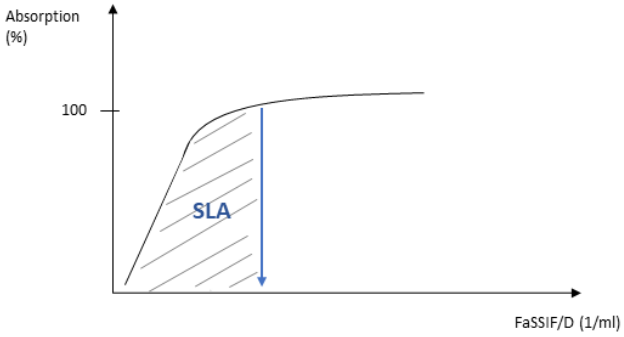

Fig. S3 Schematic representation of critical solubility limited absorption threshold

References

[1] Salem AH, Agarwal SK, Dunbar M, et al. Effect of Low- and High-Fat Meals on the Pharmacokinetics of Venetoclax, a Selective First-in-Class BCL-2 Inhibitor. J Clin Pharmacol. 2016; https://doi.org/10.1002/jcph.741

[2] Riedmaier AE, DeMent K, Huckle J, et al. Use of Physiologically Based Pharmacokinetic (PBPK) Modeling for Predicting Drug-Food Interactions: an Industry Perspective. The AAPS Journal. 2020; https://doi.org/10.1208/s12248-020-00508-2

[3] Heath EI, Chiorean EG, Sweeney CJ, et al. A phase I study of the pharmacokinetic and safety profiles of oral pazopanib with a high-fat or low-fat meal in patients with advanced solid tumors. Clin Pharmacol Ther. 2010; https://doi.org/10.1038/clpt.2010.199

[4] Fink C, Sun D, Wagner K, et al. Evaluating the Role of Solubility in Oral Absorption of Poorly Water-Soluble Drugs Using Physiologically-Based Pharmacokinetic Modeling. Clin Pharmacol Ther. 2020; https://doi.org/10.1002/cpt.1672

[5] Omachi F, Kaneko M, Iijima R, et al. Relationship between the effects of food on the pharmacokinetics of oral antineoplastic drugs and their physicochemical properties. Journal of Pharmaceutical Health Care and Sciences. 2019; https://doi.org/10.1186/s40780-019-0155-1

[6] Ribas A, Zhang W, Chang I, et al. The effects of a high-fat meal on single-dose vemurafenib pharmacokinetics. J Clin Pharmacol. 2014; https://doi.org/10.1002/jcph.255

[7] Chi KN, Spratlin J, Kollmannsberger C, et al. Food effects on abiraterone pharmacokinetics in healthy subjects and patients with metastatic castration-resistant prostate cancer. J Clin Pharmacol. 2015; https://doi.org/10.1002/jcph.564

[8] Lau YY, Gu W, Lin T, et al. Effects of meal type on the oral bioavailability of the ALK inhibitor ceritinib in healthy adult subjects. J Clin Pharmacol. 2016; https://doi.org/10.1002/jcph.619

[9] Sharma MR, Karrison TG, Kell B, et al. Evaluation of food effect on pharmacokinetics of vismodegib in advanced solid tumor patients. Clin Cancer Res. 2013; https://doi.org/10.1158/1078-0432.ccr-12-3829

[10] Lin L, Wright MR, Hop C, et al. Physiologically Based Pharmacokinetic Models Can Be Used to Predict the Unique Nonlinear Absorption Profiles of Vismodegib. Drug Metabolism and Disposition. 2022; https://doi.org/10.1124/dmd.122.000885

[11] Koch KM, Reddy NJ, Cohen RB, et al. Effects of food on the relative bioavailability of lapatinib in cancer patients. J Clin Oncol. 2009; https://doi.org/10.1200/jco.2008.18.3285

[12] Abbas R, Hug BA, Leister C, et al. A phase I ascending single-dose study of the safety, tolerability, and pharmacokinetics of bosutinib (SKI-606) in healthy adult subjects. Cancer Chemother Pharmacol. 2012; https://doi.org/10.1007/s00280-011-1688-7

[13] Morcos PN, Guerini E, Parrott N, et al. Effect of Food and Esomeprazole on the Pharmacokinetics of Alectinib, a Highly Selective ALK Inhibitor, in Healthy Subjects. Clin Pharmacol Drug Dev. 2017; https://doi.org/10.1002/cpdd.296

[14] Miceli JJ, Glue P, Alderman J, et al. The effect of food on the absorption of oral ziprasidone. Psychopharmacol Bull. 2007; 40 (3):58–68.

[15] Shono Y, Jantratid E, Kesisoglou F, et al. Forecasting in vivo oral absorption and food effect of micronized and nanosized aprepitant formulations in humans. Eur J Pharm Biopharm. 2010; https://doi.org/10.1016/j.ejpb.2010.05.009

[16] Hamaguchi T, Shinkuma D, Yamanaka Y, et al. Bioavailability of mefenamic acid: influence of food and water intake. J Pharm Sci. 1986; https://doi.org/10.1002/jps.2600750914

[17] Nurhikmah W, Sumirtapura YC, Pamudji JS. Dissolution Profile of Mefenamic Acid Solid Dosage Forms in Two Compendial and Biorelevant (FaSSIF) Media. Sci Pharm. 2016; https://doi.org/10.3797/scipharm.ISP.2015.09

[18] Melander A, Brante G, Johansson O, et al. Influence of food on the absorption of phenytoin in man. Eur J Clin Pharmacol. 1979; https://doi.org/10.1007/bf00618516

[19] de Jong J, Sukbuntherng J, Skee D, et al. The effect of food on the pharmacokinetics of oral ibrutinib in healthy participants and patients with chronic lymphocytic leukemia. Cancer Chemother Pharmacol. 2015; https://doi.org/10.1007/s00280-015-2708-9

[20] Ling J, Fettner S, Lum BL, et al. Effect of food on the pharmacokinetics of erlotinib, an orally active epidermal growth factor receptor tyrosine-kinase inhibitor, in healthy individuals. Anticancer Drugs. 2008; https://doi.org/10.1097/CAD.0b013e3282f2d8e4

[21] Kaul S, Ji P, Lu M, et al. Bioavailability in healthy adults of efavirenz capsule contents mixed with a small amount of food. Am J Health Syst Pharm. 2010; https://doi.org/10.2146/ajhp090327

[22] Silva TMD, Honorio TDS, Chaves M, et al. In silico bioavailability for BCS class II efavirenz tablets using biorelevant dissolution media for IVIVR and simulation of formulation changes. Drug Dev Ind Pharm. 2021; https://doi.org/10.1080/03639045.2021.1991368

[23] Lange H, Eggers R, Bircher J. Increased systemic availability of albendazole when taken with a fatty meal. Eur J Clin Pharmacol. 1988; https://doi.org/10.1007/bf00540964
[24] Ramasubramanian H, Castleberry S. Biopharmaceutical Modeling of Food Effect─Exploring the Role of Dietary Fat. Molecular Pharmaceutics. 2023; https://doi.org/10.1021/acs.molpharmaceut.3c00170
[25] Swaisland HC, Smith RP, Laight A, et al. Single-dose clinical pharmacokinetic studies of gefitinib. Clin Pharmacokinet. 2005; https://doi.org/10.2165/00003088-200544110-00004
[26] Overdiek HWPM, Merkus FWHM. Influence of food on the bioavailability of spironolactone. Clinical Pharmacology & Therapeutics. 1986; https://doi.org/10.1038/clpt.1986.219
[27] Fagerberg JH, Karlsson E, Ulander J, et al. Computational prediction of drug solubility in fasted simulated and aspirated human intestinal fluid. Pharm Res. 2015; https://doi.org/10.1007/s11095-014-1487-z
[28] Bello CL, Sherman L, Zhou J, et al. Effect of food on the pharmacokinetics of sunitinib malate (SU11248), a multi-targeted receptor tyrosine kinase inhibitor: results from a phase I study in healthy subjects. Anticancer Drugs. 2006; https://doi.org/10.1097/00001813-200603000-00015
[29] Summary Public Assessment Report. Sunitinib Viasana 12.5 mg, 25 mg, 50 mg hard capsules (Sunitinib hydrochloride) LT/H/0160/001-003/DC, 2022.
[30] Nirogi RV, Kandikere VN, Mudigonda K. Effect of food on bioavailability of a single oral dose of clopidogrel in healthy male subjects. Arzneimittelforschung. 2006; https://doi.org/10.1055/s-0031-1296783
[31] Jankovsky C, Tsinman O, Thakral NK. Food effect risk assessment in preformulation stage using material sparing μFLUX methodology. Admet dmpk. 2022; https://doi.org/10.5599/admet.1476
[32] Rangaraj N, Sampathi S, Junnuthula V, et al. Fast-Fed Variability: Insights into Drug Delivery, Molecular Manifestations, and Regulatory Aspects. Pharmaceutics. 2022; https://doi.org/10.3390/pharmaceutics14091807
[33] Guay DR, Gustavson LE, Devcich KJ, et al. Pharmacokinetics and tolerability of extended-release clarithromycin. Clin Ther. 2001; https://doi.org/10.1016/s0149-2918(01)80060-6
[34] Dockens RC, Greene DS, Barbhaiya RH. The lack effect of food on the bioavailability of nefazodone tablets. Biopharm Drug Dispos. 1996; https://doi.org/10.1002/(sici)1099-081x(199603)17:2<135::aid-bdd947>3.0.co;2-k
[35] Xu H, O'Gorman M, Boutros T, et al. Evaluation of crizotinib absolute bioavailability, the bioequivalence of three oral formulations, and the effect of food on crizotinib pharmacokinetics in healthy subjects. J Clin Pharmacol. 2015; https://doi.org/10.1002/jcph.356
[36] Colburn WA, Gibson DM, Wiens RE, et al. Food increases the bioavailability of isotretinoin. J Clin Pharmacol. 1983; https://doi.org/10.1002/j.1552-4604.1983.tb01800.x
[37] McLean A, Browne S, Zhang Y, et al. The influence of food on the bioavailability of a twice-daily controlled release carbamazepine formulation. J Clin Pharmacol. 2001; https://doi.org/10.1177/00912700122010005
[38] Sartor G, Melander A, Scherstén B, et al. Serum glibenclamide in diabetic patients, and influence of food on the kinetics and effects of glibenclamide. Diabetologia. 1980; https://doi.org/10.1007/bf01228296
[39] Mueck W, Stampfuss J, Kubitza D, et al. Clinical pharmacokinetic and pharmacodynamic profile of rivaroxaban. Clin Pharmacokinet. 2014; https://doi.org/10.1007/s40262-013-0100-7
[40] Meng X, Mojaverian P, Doedée M, et al. Bioavailability of amiodarone tablets administered with and without food in healthy subjects. Am J Cardiol. 2001; https://doi.org/10.1016/s0002-9149(00)01396-5
[41] Johnson BF, O'Grady J, Sabey GA, et al. Effect of a standard breakfast on digoxin absorption in normal subjects. Clin Pharmacol Ther. 1978; https://doi.org/10.1002/cpt1978233315
[42] Edgar B, Lundborg P, Regårdh CG. Clinical pharmacokinetics of felodipine. A summary. Drugs. 1987; https://doi.org/10.2165/00003495-198700343-00005
[43] Andersson SBE, Alvebratt C, Bergström CAS. Controlled Suspensions Enable Rapid Determinations of Intrinsic Dissolution Rate and Apparent Solubility of Poorly Water-Soluble Compounds. Pharm Res. 2017; https://doi.org/10.1007/s11095-017-2188-1
[44] Pargal A, Kelkar MG, Nayak PJ. The effect of food on the bioavailability of ibuprofen and flurbiprofen from sustained release formulations. Biopharm Drug Dispos. 1996; https://doi.org/10.1002/(sici)1099-081x(199608)17:6<511::aid-bdd969>3.0.co;2-y
[45] Shah J, Wesnes KA, Kovelesky RA, et al. Effects of food on the single-dose pharmacokinetics/pharmacodynamics of tizanidine capsules and tablets in healthy volunteers. Clin Ther. 2006; https://doi.org/10.1016/j.clinthera.2006.09.014
[46] Rubin EH, Agrawal NGB, Friedman EJ, et al. A Study to Determine the Effects of Food and Multiple Dosing on the Pharmacokinetics of Vorinostat Given Orally to Patients with Advanced Cancer. Clinical Cancer Research. 2006; https://doi.org/10.1158/1078-0432.ccr-06-1802

Annex 2: Pharmacometric characterization of entero-hepatic circulation processes of orally administered formulations of amiodarone under complex binding kinetics

European Journal of Pharmaceutical Sciences 174 (2022) 106198

Contents lists available at ScienceDirect

European Journal of Pharmaceutical Sciences

journal homepage: www.elsevier.com/locate/ejps

Pharmacometric characterization of entero-hepatic circulation processes of orally administered formulations of amiodarone under complex binding kinetics

Karine Rodríguez-Fernández [a], Elena Gras-Colomer [b], Mónica Climente-Martí [a,c,d], Victor Mangas-Sanjuán [a,e,*], Matilde Merino-Sanjuán [a,e]

[a] Department of Pharmacy and Pharmaceutical Technology and Parasitology, University of Valencia, Av Vicent András Estellés, s/n. 46100, Valencia, Burjassot, Valencia, Spain
[b] Department of Pharmacy, Hospital Manises of Valencia, Spain
[c] Department of Pharmacy, University Hospital Doctor Peset of Valencia, Spain
[d] Foundation for the Promotion of Healthcare and Biomedical Research in the Valencian Community (FISABIO), Valencia, Spain
[e] Interuniversity Research Institute for Molecular Recognition and Technological Development, Polytechnic University of Valencia-University of Valencia, Valencia, Spain

ARTICLE INFO

Keywords:
Amiodarone
Population pharmacokinetic modeling
Pharmacometrics
Enterohepatic recirculation
Oral formulation
Polysorbate 80
Protein binding

Abbreviations: -2ll, -2xlog(likelihood)
95%ci, confidence intervals 95%
Am, amiodarone
Her, entero-hepatic reabsorption
Gof, goodness of fit
Iv, intravenous
Iiv, inter-individual variability
OFV, objective function value
OR, oral
pc-VPC, prediction-corrected visual predictive checks
PK, pharmacokinetics
RUV, residual unexplained variability

ABSTRACT

Aims: The aims of this work are (i) to characterize the absorption properties of orally administered formulations at different dose levels, and (ii) to evaluate the impact of entero-hepatic circulation on the time-course of amiodarone (AM) in rats in order to optimize the development of new oral (OR) formulations.
Methods: Intravenous (IV) formulation consisted on a solution of a commercial injectable of AM chlorhydrate. OR formulations included the IV commercial formulation (Trangorex®) (Solution I), an aqueous supramicellar solution of AM chlorhydrate with Polysorbate at 5% (Solution II) and a suspension from Trangorex® tablets (Tablet). Data from 96 male Wistar rats, including 985 AM observations, were analyzed using NONMEM v7.4.
Results: The population pharmacokinetic (PK) model assumes linear absorption processes, showing k_a of AM from Solution II (Polysorbate 80, 5%) and Solution I increased by 2.5- and 1.62-fold compared to Tablet formulation. OR bioavailability of AM from Tablet, Solution I and Solution II was 37%, 40%, and 50%, respectively. The structural model of AM disposition was adapted from a previously population PK model and expanded by incorporating entero-hepatic reabsorption (EHR) processes, which estimated a 12.3% biliary excretion of AM and complete re-absorption from lumen.
Conclusions: The current population PK model of AM demonstrated the absorption rate enhancement when AM is formulated with supramicellar concentrations of Polysorbate 80. The study design allowed to characterize the EHR of AM and its contribution in the overall AM disposition.

1. Introduction

Amiodarone (AM), an iodine-rich benzofuran derivative, is a class III antiarrhythmic medication, which is indicated for the treatment of life-threatening ventricular arrhythmias, supraventricular arrhythmias and atrial fibrillation. Despite having demonstrated a high effectiveness as antiarrhythmic medication in clinical practice, long-term therapy can result in a wide variety of side effects affecting several organ systems, some of which can be life threatening (Cahoon et al., 2007; Mujović et al., 2020). Commercially available AM presentations include intravenous (IV) and oral (OR) formulations, being the latter indicated in patients with mild and moderate heart disease, whereas IV route of administration is preferred in hemodynamically destabilizing ventricular tachycardia or ventricular fibrillation or when patients are unable to

* Corresponding author at: Department of Pharmacy and Pharmaceutical Technology and Parasitology, University of Valencia, *Av* Vicent András Estellés, s/n. 46100, Valencia, Burjassot, Valencia, Spain.
E-mail address: victor.mangas@uv.es (V. Mangas-Sanjuán).

https://doi.org/10.1016/j.ejps.2022.106198
Received 12 November 2021; Received in revised form 19 March 2022; Accepted 28 April 2022
Available online 30 April 2022

Table 1
Summary of study design characteristics.

Route of administration	Schedule	Dose (mg)	Formulation	Sample	N° Animals	N° Observations
IV	SD	12.5	Solution I	Blood	16	231
			Solution I	Blood, Bile^{NC}	6	84
			Solution I	Blood, Bile^{CC}	6	82
OR	SD	10	Solution II	Blood	8	63
OR	SD	25	Tablet	Blood	8	68
OR	SD	25	Solution I	Blood	8	59
IV+IV	MD	12.5 + 12.5 (t = 24 h)	Solution *I*+ Solution I	Blood	8	93
IV+OR	MD	12.5 + 25 (t = 24 h)	Solution *I* +Tablet	Blood	8	102
IV+OR	MD	12.5 + 25 (t = 24 h)	Solution *I* +Solution I	Blood	8	103
IV+OR	MD	12.5 + 10 (t = 24 h)	Solution *I* +Solution II	Blood	8	100

Abbreviations: IV: intravenous; OR: oral; SD: single dose; MD: multiple doses, n: number.

take oral medications (Mujović et al., 2020). AM is given as a monotherapy or in combination with other drugs (e.g. β-adrenergic antagonists, calcium channel blocking agents or digoxin), showing its effectiveness in several clinical trials (Andrade et al., 2010; Cappelletto et al., 2021; Hamer et al., 1989; Kim et al., 2014; Lupercio et al., 2018; Mitchell et al., 2005; Mooss et al., 1990; Somberg and Molnar, 2016; Somberg et al., 2004). In addition, AM is one of the most effective pharmacological agents with extensive off-label use for the treatment of supraventricular arrhythmia in children (Etheridge et al., 2001; Moak, 2000; Saul et al., 2005). Despite of its outstanding pharmacological properties, the slow onset of its antiarrhythmic action, the presence of multiple drug-drug interactions and the several safety concerns, including ophthalmological, pulmonary, and neurological toxicity after its chronic administration has limited its use in clinical practice (Mujović et al., 2020).

AM according to the Biopharmaceutics Classification System (Amidon et al., 1995) is a class III drug, with low solubility (0.35 mg/mL) (Wang et al., 2017) and high permeability drug due to its high lipophilicity, which explains its large distribution into highly perfused and lipophilic tissues. Approved dosing schedules for maintenance regimens ranged from 200 to 400 mg/day (Siddoway, 2003). Slow and variable AM absorption has been reported, reaching a maximal plasma concentration between 3 and 7 h after oral administration and a moderate bioavailability (35–65%). High protein binding (>96%) has been reported (Lalloz et al., 1984; Veronese et al., 1988) predominately to albumin, but also to β-lipoprotein, and large accumulation of AM in liver, lung, adipose tissue, skeletal muscles and skin has been reported (Kodama et al., 1997; Plomp et al., 1987; Singh, 2006; Zimetbaum, 2012). Recently Hashimoto et al. (2021) found serum amiodarone concentrations increased in patients with hypertriglyceridemia state since as the concentration of LDL/VLDL increases, the fraction of drug bound increases restricting its distribution to other organs/tissues and hepatic metabolism of amiodarone. AM is metabolized primarily to desethylamiodarone through the cytochrome P450 enzyme CYP3A4, and by CYP2C8. The major route of elimination is hepatic excretion into bile with some degree of entero-hepatic recirculation and the renal excretion for AM is negligible in humans (Haffajee, 1987; Pollak et al., 2000; Somani, 1989). A therapeutic range of AM from 1.0 to 2.5 mg/L has been suggested (Haffajee et al., 1983; Rotmensch et al., 1984), and adverse reactions have been reported at amiodarone concentrations above 2.6 mg/L (Falik et al., 1987; Greenberg et al., 1987; Rotmensch et al., 1984). Complexity in AM pharmacokinetics properties, including the reduced and variable oral absorption, associated with the high inter-individual variability (IIV) in plasma levels, and its narrow therapeutic index due to the high risk of drug toxicity has limited the therapeutic usefulness of AM for its chronic administration. New OR formulations have been developed recently to improve the clinical use of AM focusing on the improvement of its water-solubility and bioavailability, demonstrating the need to improve the technological properties of OR formulations of AM for an optimal therapeutic use (Beig et al., 2015; Creţeanu et al., 2015; Elgart et al., 2013; Patel et al., 2015a; Wang et al., 2017).

Preclinical characterization of complex pharmacokinetic properties through model-informed approaches has been widely considered during the drug development process and has demonstrated its utility for an optimal selection of dosing regimens in first-time-in-humans studies (Biliouris et al., 2018; Choi et al., 2019; Dong et al., 2011; Kang et al., 2021; Kwak et al., 2021; Li et al., 2019; Luu et al., 2012; Nirogi et al., 2020; Song et al., 2020; Zou et al., 2012). The advantage of this strategy becomes even more evident when non-linear kinetic processes come into play, since the classical approaches for data analysis are unable to accurately determine the magnitude of the effects together. In this regard, non-linear mixed effects modeling allows to quantitatively characterize the central tendency of the experimental data and the different sources of variability in order to accurately describe the observed behavior (Bonate, 1999). Therefore, the aims of this pre-clinical study are (i) to characterize the absorption properties of different orally administered formulations and at different dose levels, and (ii) to evaluate the impact of entero-hepatic circulation on the time-course of AM in rats in order to optimize the development of new OR formulations of AM.

Table 2
Composition of oral formulations of Amiodarone administered.

Formulations	Composition	
Solution I	Amiodarone chlorhydrate	0.150 g
	Polysorbate 80	0.300 g
	Benzyl alcohol	0.060 g
	Bidistilled water q.s.	3 mL
Tablet	Amiodarone chlorhydrate	0.200 g
	Lactose	0.071 g
	Cornstarch	0.066 g
	Polividone	0.006 g
	Colloidal silica	0.0024 g
	Magnesium stearate	0.0046 g
Solution II	Amiodarone chlorhydrate Polysorbate 80	5 mg/mL 5%

2. Materials and methods

2.1. Study design

All pharmacokinetic studies reported here adhere to the Principles of Laboratory Animal Care and were approved by the Research Committee of Animal Use from the Faculty of Pharmacy from University of Valencia (Spain). Data were obtained from the doctoral theses presented by Pascual-Costa (1994) and Chicano-Piá (1998). The experimental dataset consisted of 96 male Wistar rats of 20-weeks, 250–320 g body weight, including 985 AM observations in plasma (n = 901) and bile (n = 84). Wistar rats were housed under pathogen-free conditions, on a 12 h light/dark cycle, with controlled temperature (22–24 °C) and humidity (25%). Food and water were given ad libitum. IV and OR routes of administration of AM at different dose levels were evaluated, including

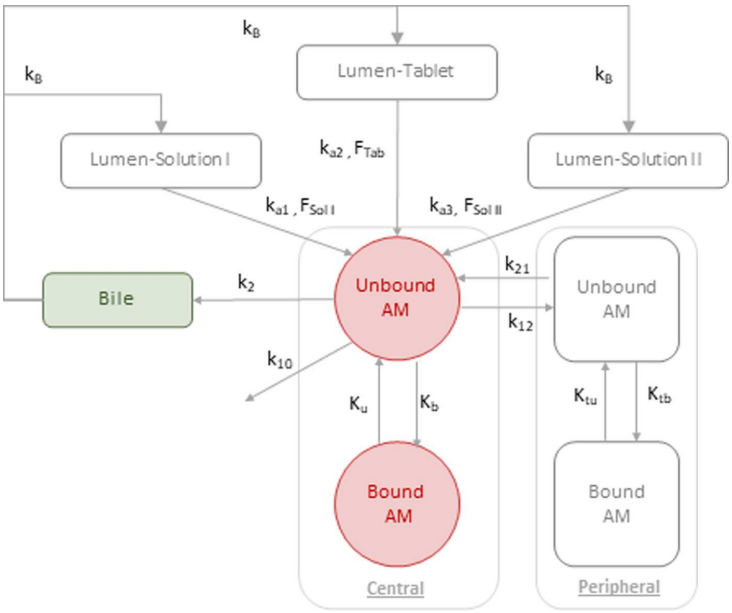

Fig. 1. Schematic representation of the final PK model developed.
k_B: first-order rate constant from bile, k_{a1}: first-order absorption rate constant of Solution I formulation, $F_{Sol\ I}$: oral bioavailability of Solution I formulation, k_{a2}: first-order absorption rate constant of Tablet formulation, F_{Tab}: oral bioavailability of Tablet formulation, k_{a3}: first-order absorption rate constant of Solution II formulation, $F_{Sol\ II}$: oral bioavailability of Solution II formulation, k_{10}: first-order elimination rate constant, k_2: first-order distribution constant, K_u: rate constant of unbinding in central compartment, K_b: rate constant of binding in central compartment, K_{tu}: rate constant of unbinding in peripheral compartment, K_{tb}: rate constant of binding in peripheral compartment, k_{21}: first-order distribution constant from central to peripheral compartment, k_{12}: first-order rate constant from peripheral to central compartment.

single and multiple dosing regimens. Different sampling strategies were considered based on the route of administration and schedule, but all samples were collected to ensure the characterization of the PK profile of each animal. Table 1 summarizes the characteristics of the study, including, dose of AM administered for each administration route and number of animals enrolled and samples available in each group.

IV formulation was the commercial injectable of AM chlorhydrate (Trangorex®, 50 mg/ml). Three OR formulations of AM were evaluated, including the IV injectable (Trangorex®, Solution I, 50 mg/ml), a suspension from Trangorex® tablets (Tablet, 200 mg) and a solution with 5% Polysorbate 80 (Solution II, 5 mg/ml). The composition of the formulations is detailed in Table 2.

2.2. Blood sampling and analytical methods

Twenty-four hours before the administration of AM, the jugular vein, and portions of the bile duct and the small intestine were channeled in the different groups of rats. Prior to the surgical intervention, a dose of 2.7 ml/kg of anesthesia solution was administered by an intraperitoneal injection. The anesthesia was prepared by mixing solutions of 5 mg/ml diazepam, 50 mg/ml ketamine and 1 mg/ml atropine. After surgery and until drug administration, animals were kept fasted overnight with water freely available.

Drug administration of the three OR formulations was performed through a gastric tube. Blood samples (0.5 ml) were withdrawn into heparinized syringes from the jugular vein cannula, then centrifuged at 3000 r.p.m. for 5 min and stored at −20 °C. Bile samples were collected from two groups of rats with continuous enterohepatic cycle (CC group) and non- continuous enterohepatic cycle (NC group). In the CC group, the enterohepatic cycle was maintained, and the flowing bile was collected for 5 min before and 5 min after the administration of AM, disconnecting the bridging tubes of the bile duct and small intestine. In the NC group, the enterohepatic cycle was interrupted as soon as AM was administered, disconnecting the bridging tube from the bile duct catheter. Bile samples were stored at 4–8 °C (Chicano-Piá, 1998; Pascual-Costa, 1994).

The quantification of AM in plasma and bile samples was performed through high performance liquid chromatography with spectrophotometric detection under ultraviolet light at a wavelength of 242 nm. The chromatographic method was validated following the recommendations of the International Conference on harmonisation (ICH, 1995) in terms of linearity, precision (intra- and interday), accuracy, limit of detection and quantification, specificity, interval and robustness. The limit of quantification was 0.1 μg/ml.

2.3. Pharmacokinetic model

The modeling strategy used a previously developed population PK model (Campos Moreno et al., 2007) in rats after IV administration, which contained a two-compartment model with saturable dynamic plasma protein and linear tissular depot binding in the peripheral compartment. Equal PK parametrization of the disposition of AM was assumed as described by Campos Moreno et al. (2007). Then, the model (Fig. 1) was adapted to describe the absorption kinetics of AM from the three OR formulations administered to the rats by assuming linear absorption kinetics. Non-linear absorption kinetics, absorption latency and complex absorption processes (parallel absorption, precipitation, transit compartments, etc.) were also evaluated. EHR of AM was modelled through linear kinetic processes of AM transition into and out of the bile compartment.

2.4. Data analysis

Plasma observations were logarithmically transformed. All data analyses were performed based on the population approach with the software NONMEM® (v7.4, ICON plc Development Solutions, Hanover, MD, USA). The population PK parameters were estimated using the Stochastic Approximation of the Expectation Maximization and the Importance Sampling Estimation method.

IIV associated to the PK model parameters was modeled exponentially preventing negative values for the individual estimates, and residual unexplained variability (RUV) was described with an additive

model on the logarithmic scale. The significance of the non-diagonal elements of the Ω variance-covariance matrix and subject specific RUV were also evaluated.

2.4.1. Model selection

Model selection was based on physiological and pharmacological rationale with the principle of parsimony (Wade et al., 1994). The minimum value of the objective function value (OFV) provided by NONMEM® and approximately equal to −2xlog (likelihood) (−2LL) was used together with the visual inspection of the goodness of fit (GOF) plots to perform model selection. A decrease in 6.63 points in −2LL value between two nested models differing in one parameter was considered significant at the 1% level.

2.4.2. Model evaluation

Model evaluation of the selected models was performed through prediction-corrected visual predictive checks (pc-VPC). Briefly, one thousand simulated datasets were simulated; the 2.5th, 50th, and 97.5th percentiles for every simulated study and sampling time-period were calculated. Then, the 95% prediction intervals of the percentiles were calculated and displayed graphically together with corresponding percentiles computed from raw data. In addition, the condition number, computed as the ratio of the largest eigenvalue to the smallest eigenvalue of the variance-covariance matrix, was calculated. A condition number less than 400 was targeted as it indicates good stability in the parameter estimates (Bonate, 1999). Precision of model parameter estimates, defined as the relative standard error (RSE), were calculated from the variance-covariance matrix (when possible) and from the analysis of one thousand simulated bootstrap datasets.

For graphical and statistical analysis, the R software (http://cran.r-project.org, version 4.0.3) was used. Pc-VPC and bootstrap analysis were performed using PsN.

3. Results

3.1. Pharmacokinetic model

The absorption process after the OR administration of three formulations of AM (Solution I, Tablet and Solution II) were described through a linear process using different first order absorption rate constants for each formulation (k_{a1-3}). The results suggest a major improvement in k_a when AM was administered as solution in the presence of 5% of Polysorbate 80 (Solution II: 250% increase) and 10% of Polysorbate 80 (Solution I: 62% increase) compared to Tablet formulation. Alternative mechanisms were also evaluated (i.e. zero-order absorption, non-linear kinetics, sequential/parallel first-and zero-order processes, transit compartment) but resulted in worse model performance ($p > 0.01$). AM showed a moderate OR bioavailability, which was parametrized independently for each formulation. Tablet showed less OR bioavailability (37%), compared to Solution I (40%) and Solution II (50%). These results reinforce the idea that OR bioavailability of AM could be enhanced by the presence of supramicellar concentration of surfactants that help to increase the AM solubility and dissolution process in the intestinal lumen (Elgart et al., 2013; Wang et al., 2017).

The structural model of AM disposition was adapted from a previous publication (Campos Moreno et al., 2007) in order to characterize PK longitudinal data of AM after IV and OR administration for new dose levels and dosing regimens (Table 1), which included a saturable and non-instantaneous plasma protein binding of AM (B_{max}, C_{50} and K_u) and linear tissue binding in the peripheral compartment (K_{tb} and K_{tu}). The first order binding rate constant (K_b) was derived as K_u/C_{50} and the binding saturation in plasma was modeled considering the available binding capacity. Peripheral distribution of AM occurred only between free fractions of the central and peripheral compartment through linear kinetics (k_{12}, k_{21}), suggesting a large distribution of AM into the peripheral compartment due to its high lipophilicity. The total protein binding in plasma was characterized through the B_{max} parameter, which was assumed as 5.05 mg based on the previous population PK model developed with IV data (Campos Moreno et al., 2007). A more detailed description of the equations governing the PK of AM have been previously published (Campos Moreno et al., 2007). The PK disposition model of AM was expanded by incorporating an EHR process of AM, which assumed a linear distribution process of AM from the unbound central compartment into the bile compartment and its transit into the lumen through a first-order rate constant (k_B=12.9 h^{-1}). The absence of a gallbladder in rats leads to a constant distribution of the bile content into the lumen, preventing the implementation of more complex EHR models

Table 3
Final population pharmacokinetic parameters after sub-cutaneous administration of reserpine in rats.

	Population PK model estimates		Bootstrap results	
Fixed-effect	Value	Shrinkage (%)	Median	95%CI
k_{a1} (h^{-1})	1.33 × 10^{-1}		1.34 × 10^{-1}	[1.16–1.49] x10^{-1}
k_{a2} (h^{-1})	8.20 × 10^{-2}		8.24 × 10^{-2}	[7.69–8.87] x10^{-2}
k_{a3} (h^{-1})	2.05 × 10^{-1}		2.02 × 10^{-1}	[1.67–2.51] x10^{-1}
$F_{Sol\ I}$ (%)	4.02 × 10^{1}		4.03 × 10^{1}	[3.71–4.26] x10^{1}
F_{Tab} (%)	3.71 × 10^{1}		3.75 × 10^{1}	[2.79–4.12] x10^{1}
$F_{Sol\ II}$ (%)	5.05 × 10^{1}		5.02 × 10^{1}	[4.21–6.19] x10^{1}
k_{12} (h^{-1})	7.17 × 10^{1} FIX		7.17 × 10^{1} FIX	
k_{21} (h^{-1})	4.64 × 10^{-1} FIX		4.64 × 10^{-1} FIX	
V_2 (L)	1.44 × 10^{-2} FIX		1.44 × 10^{-2} FIX	
B_{max} (mg)	5.05 × 10° FIX		5.05 × 10° FIX	
C_{50} (mg/L)	1.49 × 10^{1} FIX		1.49 × 10^{1} FIX	
K_u (h^{-1})	5.42 × 10° FIX		5.42 × 10° FIX	
K_{tb} (h^{-1})	1.63 × 10^{-1} FIX		1.63 × 10^{-1} FIX	
K_{tu} (h^{-1})	9.87 × 10^{-2} FIX		9.87 × 10^{-2} FIX	
k_B (h^{-1})	1.29 × 10^{1}		1.28 × 10^{1}	[1.07–1.42] x10^{1}
k_{10} (h^{-1})	2.98 × 10^{1} FIX		2.98 × 10^{1} FIX	
Inter-individual variability				
k_{a1} (%)	39	16	41	[31–56]
k_{a2-3} (%)	34	21	35	[27–41]
k_{12} (%)	24	32	27	[19–33]
V_2 (%)	46	26	42	[31–58]
K_u (%)	13	38	12	[9–15]
Residual unexplained variability				
Plasma (%)	46	7	45	[42–49]

k_{a1}: first-order absorption rate constant of Solution I formulation, $F_{Sol\ I}$: oral bioavailability of Solution I formulation, k_{a2}: first-order absorption rate constant of Tablet formulation, F_{Tab}: oral bioavailability of Tablet formulation, k_{a3}: first-order absorption rate constant of Solution II formulation, $F_{Sol\ II}$: oral bioavailability of Solution II formulation, k_{12}: first-order rate constant from peripheral to central compartment, k_{21}: first-order distribution constant from central to peripheral compartment, V_2: apparent central volume of the central compartment, B_{max}: maximal binding capacity, C_{50}: AM unbounded plasma concentration that produces a $B_{max}/2$, K_u: rate constant of unbinding in central compartment, K_{tu}: rate constant of unbinding in peripheral compartment, K_{tb}: rate constant of binding in peripheral compartment, k_B: first-order rate constant from bile, k_{10}: first-order elimination rate constant.

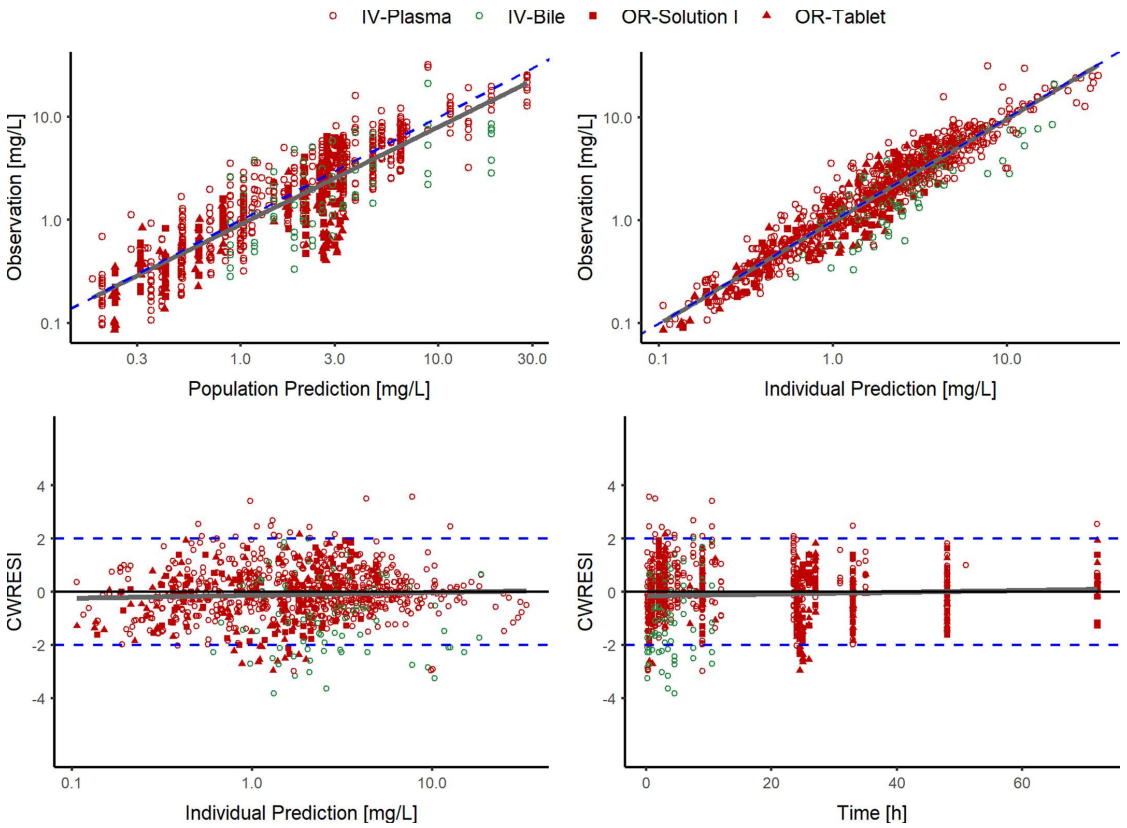

Fig. 2. Goodness-of-fit plots of the final population pharmacokinetic model of amiodarone in rats for each oral formulation.
The gray solid line represents the non-linear regression and the blue dotted line represents the line of identity. IWRES: individual weighted residuals, CWRESI: conditional weighted residuals (For interpretation of the references to color in this figure legend, the reader is referred to the web version of this article).

(Ibarra et al., 2021; Jain et al., 2011; Lehr et al., 2009; Okour et al., 2018). An alternative parametrization was evaluated, which included a k_B and a first-order constant into the lumen (k_7), but did not statistically improved the overall fit. The re-absorption intestinal process once the AM returns into the lumen due to the EHR was assumed to be equal to the initial intestinal absorption after oral AM administration (k_{a1}, k_{a2} and k_{a3}). A reduced fraction of the drug was distributed into the bile (F_{bile}=12.3%), which was calculated as follows (Lehr et al., 2009):

$$F_{bile} = \frac{k_B}{(k_B + k_{10} + k_{12} + K_b)}$$

Where k_B is 1.29×10^1 h^{-1}, k_{10} is 2.98×10^1 h^{-1}, k_{12} is 7.17×10^1 h^{-1} and K_b is 3.6×10^{-1} $Lh^{-1}mg^{-1}$

Inter-individual random effects were associated to V_2 (46%), k_{12} (24%), K_u (13%), k_{a1} (39%), and k_{a2-3} (34%), showing a moderate-to-high IIV of PK parameters. Non-diagonal elements were explored but did not statistically improved the model performance. The RUV was 46% using an additive error model for log-transformed observations.

3.2. Pharmacokinetic model evaluation

Table 3 lists the estimates of the PK model parameters together with their corresponding precision according the PK model developed (Fig. 1). All PK parameters were statistically significant as the 95% confidence intervals (95% CI) did not include the null value. The results from the model evaluation exercise indicate that the model was capable of capturing the longitudinal profiles of the median and the dispersion of the data based on the pc-VPC (Fig. 2) and the standard GOF plots (Fig. 3).

3.3. Simulation-based analysis of unbound/bound fractions of AM

The typical longitudinal ratios between the unbound and bound fraction of AM in the central and peripheral compartments of each OR formulation are depicted in Fig. 4, including dose levels evaluated in the current population PK analysis (12.5 and 25 mg) and extrapolated dose levels (50 and 100 mg) of AM. A rapid decrease in the unbound/bound ratio at both compartments is explained by the binding process of AM, achieving steady-state conditions around 24 h, showing the slow binding process of AM. These results show a slight increase in the unbound fraction with the dose level in the central compartment and irrespective of the OR formulation considered, as expected due to the non-linear binding kinetics of the population PK model. Due to the linear kinetic binding in the peripheral compartment, no differences were observed between the dose levels considered.

4. Discussion

AM is highly lipophylic drug, showing a unique pharmacokinetic

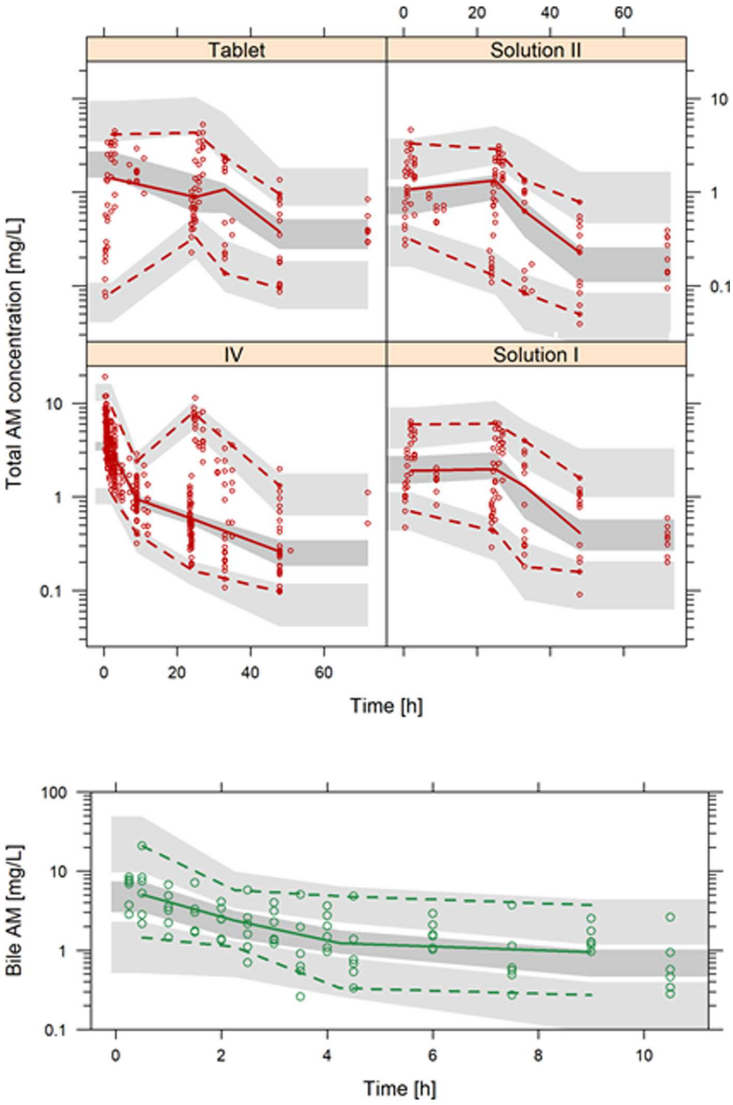

Fig. 3. Prediction-corrected visual predictive check of the final population PK model.
Shaded areas represent the 95% prediction intervals of the 2.5th, 50th and 97.5th percentiles of the simulated data. Circles represent amiodarone observations and lines represent the 2.5th, 50th and 97.5th percentiles of the raw data.

profile. There is a good correlation between plasma concentration of AM and its oral maintenance dose and higher plasma concentration of the drug provides a more effective arrhythmia suppression, but it is associated with a higher risk of drug toxicity. Therefore, in routine clinical practice the monitoring of total cumulative dose may be more useful than monitoring the plasma amiodarone levels. Hence, a better knowledge of the pharmacokinetics of AM, both in absorption and elimination, will reduce variability and improve dosage adjustment in patients. In addition, the approved IV formulation of AM contains benzyl alcohol, which is contraindicated in neonates and should be used with caution in infants and children up to 3 years old (Electronic Medicines Compendium, 2022). Therefore, the development of oral formulations able to increase the oral bioavailability of AM are highly needed.

Complex PK processes of drugs, which have not been properly characterized, may increase the IIV of PK parameters and generate unprecise model-predictions. In this sense, quantitative modeling framework should encompass the biological complexity observed in experimental data in order to serve as a valid tool in the decision-making process of the drug development. A population PK model has been successfully applied to characterize the absorption and EHR processes of different OR formulations of AM in rats by adapting a previously population PK model that accounted for the non-linear and linear distribution processes of AM after IV administration. The population PK model assumes different first-order absorption rate constant for each

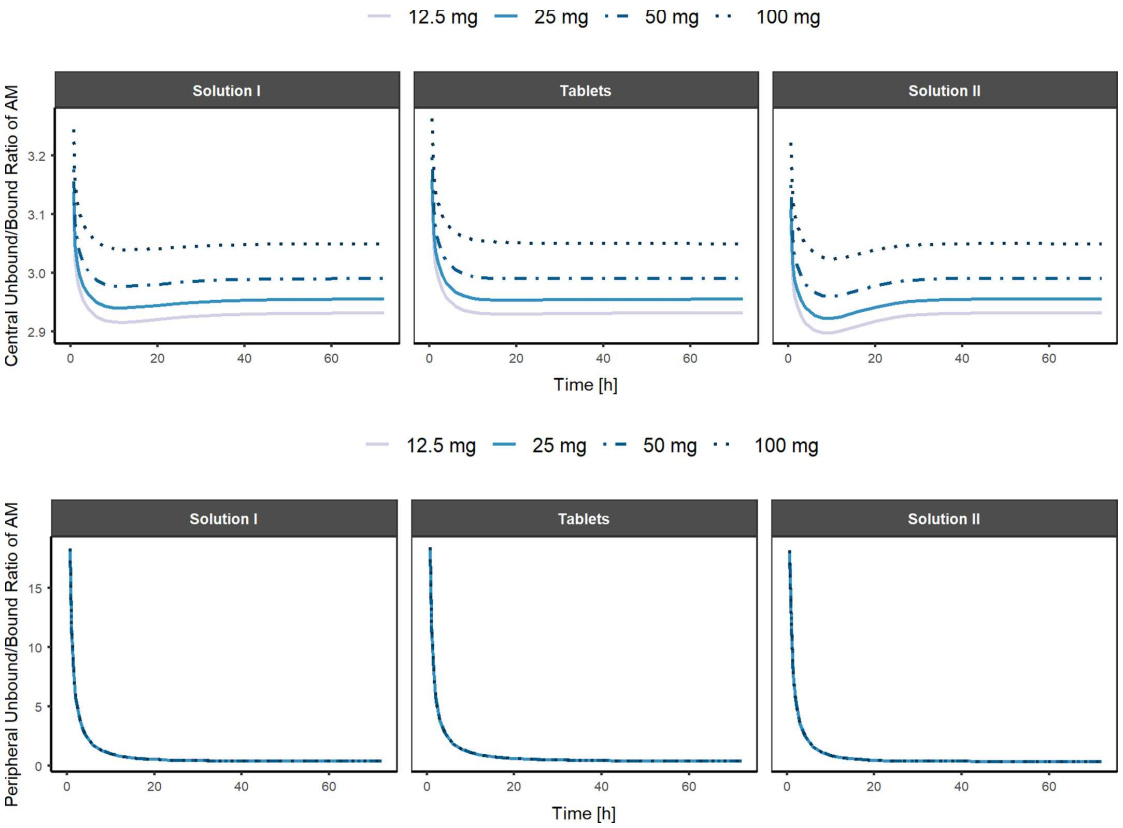

Fig. 4. Model predicted unbound/bound ratio of amiodarone in the central (upper) and peripheral (bottom) compartments for each oral formulation after single dose administration of four dose levels.

formulation, demonstrating the contribution of supramicellar concentrations of surfactant (Polysorbate 80) in the improvement of AM oral absorption (k_{a3}= 2.05•10^{-1} h^{-1}). Similar results were obtained for other lipophilic active principles when co-formulated with surfactants (Alqahtani et al., 2013; Chen et al., 2018; Patel et al., 2015b; Rahman et al., 2016). The current EHR represents the distribution of free AM from the central compartment into the bile and then, into the lumen based on the evidence collected in CC and NC groups. The lack of gallbladder in rats allows assume the continuous emptying of AM into the lumen, which limited the implementation of complex EHR models when the gallbladder exists (Ide et al., 2009; Lehr et al., 2009; Okour et al., 2018; Papathanasiou et al., 2016). The current population PK model quantifies the fraction (12.3%) of AM that suffers EHR and the respective fraction of AM that is metabolized. This result confirms the significant contribution of EHR in the disposition of AM, although due to the absence of experimental observations in the lumen, the fraction excreted via feces could not be estimated.

The development of oral formulations able to increase AM solubility and, ultimately, its absorption rate has been part of research activity recently (Creţeanu et al., 2015; Elgart et al., 2013; Wang et al., 2017). In this sense, an increase of absorption rate of drugs in oral formulation with Polysorbate 80 has been hypothesized to be related to the alteration of the intestinal mucus barrier and mucosal barrier, but these results require further clarification (Martin-Algarra et al., 1995; Zhu et al., 2021). On the other hand, the addition of 5% of Polysorbate 80 resulted in 2.50-fold increase on k_a and 35% increase in its bioavailability compared to Tablet formulation. However, higher concentrations (10%) of Polysorbate 80 in Solution I compared to Tablet formulation only improved by a 1.62-fold the k_a (and 8% its bioavailability), suggesting that increased concentrations of Polysorbate 80 in AM formulations may compromised the absorption process. This phenomenom may be explained by the lipophilic properties of AM and the intramicellar solubilization. Based on this study, 5% concentrations of Polysorbate improve the solubilization of AM in lumen. Higher concentrations of Polysorbate 80 (10%) lead to higher formation of micelles, affecting the release of AM out of the micelles, becoming the PK rate-limiting step process (Martin-Algarra et al., 1995).

Model-based approaches currently represent one of the most demanding and increasing areas in the drug discovery and development process. The ability to determine from a very simplistic perspective to a more detailed and complex manner the mechanisms involved in the time-course of a drug clearly contribute to a more efficient and rationale decision-making process. Thus, the re-use of PK models and its integration to new experimental evidence enhances the potential impact and recognition from adjoining areas. The population PK model externally validates the disposition PK model previously proposed for AM in rats (Campos Moreno et al., 2007) to quantify the contribution of OR formulations and EHR of AM. Similar final parameter estimates were observed between both approaches, demonstrating the adequacy of the population PK model of AM in rats.

Despite the study design characteristics, reduced number of treatment groups evaluated the PK properties of AM after multiple dose

regimens, which might be of relevance in order to better understand how the binding kinetics might be affected when complex and multiple dose levels are administered. Although all formulations contained a polysorbate 80 concentration higher than the CMC, the impact of polysorbate 80 on the AM metabolism could not be assessed due to the lack of hepatic microsomes measurements after its OR and IV administration and the absence of a formulation without polysorbate 80. The complexity of the surgical intervention to collect bile samples resulted in a limited number of observations helping to characterize the EHR process of AM. A 8-fold dose increase (from 12.5 to 100 mg) implies that the unbound/bound ratio of AM only changes by 3% (Fig. 4), indicating that at the usual doses the protein plasma binding is not likely to be saturated. In this sense, it is probable that new formulations that increase the bioavailability of AM do not significantly modify the fractions of free AM in plasma nor the time in which the equilibrium between the free and bound fraction is reached. Alternative preclinical models are encouraged in order to characterize the allometric relationship and the impact of gallbladder emptying that would help to establish accurate and reliable predictions in humans.

5. Conclusion

In conclusion, the current population PK model of AM demonstrated the absorption enhancement when AM is formulated with supramicellar concentrations of Polysorbate 80 (Solution II) compared to commercially available oral formulation (Tablet). The study design allowed to characterize the EHR of AM and its contribution in the overall AM disposition. The mathematical framework developed based on preclinical evidence on AM could help to optimize the development of new oral formulations able to increase the oral bioavailability of AM at the preclinical and clinical level and assess whether the impact of EHR processes is similar across different species. Furthermore, this study may contribute to the development of oral solution formulations of AM that could improve the benefit/risk balance of AM and its adherence in pediatric patients.

CRediT authorship contribution statement

Karine Rodríguez-Fernández: Methodology, Software, Formal analysis, Investigation, Writing – original draft, Writing – review & editing. **Elena Gras-Colomer:** Writing – original draft, Writing – review & editing. **Mónica Climente-Martí:** Supervision, Writing – original draft, Writing – review & editing. **Victor Mangas-Sanjuán:** Methodology, Software, Formal analysis, Writing – original draft, Writing – review & editing. **Matilde Merino-Sanjuán:** Conceptualization, Methodology, Writing – original draft, Writing – review & editing.

Declaration of Competing Interest

Authors declare no conflict of interest.

References

Alqahtani, S., Alayoubi, A., Nazzal, S., Sylvester, P.W., Kaddoumi, A., 2013. Nonlinear absorption kinetics of self-emulsifying drug delivery systems (SEDDS) containing tocotrienols as lipophilic molecules: *in vivo* and *in vitro* studies. AAPS J. 15, 684–695.

Amidon, G.L., Lennernäs, H., Shah, V.P., Crison, J.R., 1995. A theoretical basis for a biopharmaceutic drug classification: the correlation of *in vitro* drug product dissolution and *in vivo* bioavailability. Pharm. Res. 12, 413–420.

Andrade, J.G., Connolly, S.J., Dorian, P., Green, M., Humphries, K.H., Klein, G.J., Sheldon, R., Talajic, M., Kerr, C.R., 2010. Antiarrhythmic use from 1991 to 2007: insights from the Canadian registry of atrial fibrillation (CARAF I and II). Heart Rhythm. 7, 1171–1177.

Beig, A., Agbaria, R., Dahan, A., 2015. The use of captisol (SBE7-β-CD) in oral solubility-enabling formulations: comparison to HPβCD and the solubility-permeability interplay. Eur. J. Pharm. Sci. 77, 73–78.

Biliouris, K., Nestorov, I., Naik, H., Dai, D., Xiao, G., Wang, Q., Pellerin, A., Rabah, D., Lesko, L.J., Trame, M.N., 2018. A pre-clinical quantitative model predicts the pharmacokinetics/pharmacodynamics of an anti-BDCA2 monoclonal antibody in humans. J. Pharmacokinet. Pharmacodyn. 45, 817–827.

Bonate, P.L., 1999. The effect of collinearity on parameter estimates in nonlinear mixed effect models. Pharm. Res. 16, 709–717.

Cahoon, W., Flattery, M.P., Hess, M.L., 2007. Amiodarone: development, clinical indications, and safety. Prog. Cardiovasc. Nurs. 22, 173–176.

Campos Moreno, E., Merino Sanjuán, M., Merino, V., Nácher, A., Martín Algarra, R.V., Casabó, V.G., 2007. Population modelling to describe pharmacokinetics of amiodarone in rats: relevance of plasma protein and tissue depot binding. Eur. J. Pharm. Sci. 30, 190–197.

Cappelletto, C., Gregorio, C., Barbati, G., Romani, S., De Luca, A., Merlo, M., Mestroni, L., Stolfo, D., Sinagra, G., 2021. Antiarrhythmic therapy and risk of cumulative ventricular arrhythmias in arrhythmogenic right ventricle cardiomyopathy. Int. J. Cardiol.

Creţeanu, A., Tàntaru, G., Vieriu, M., Panainte, A.D., Ochiuz, L., 2015. Optimization of the preparation of kollidon SR-based amiodarone hydrochloride tablets with sustained release. Rev. Med. Chir. Soc. Med. Nat. Iasi 119, 1161–1165.

Chen, X.Q., Ziemba, T., Huang, C., Chang, M., Xu, C., Qiao, J.X., Wang, T.C., Finlay, H.J., Salvati, M.E., Adam, L.P., Gudmundsson, O., Hageman, M.J., 2018. Oral delivery of highly lipophilic, poorly water-soluble drugs: self-emulsifying drug delivery systems to improve oral absorption and enable high-dose toxicology studies of a cholesteryl ester transfer protein inhibitor in preclinical species. J. Pharm. Sci. 107, 1352–1360.

Chicano-Piá, P.V., 1998. Study of the first pass effect and the enterohepatic cycle of amiodarone in the rat. (Doctoral Thesis). University of Valencia, Valencia, Spain, p. 180.

Choi, S., Han, S., Jeon, S., Yim, D.S., 2019. Quantitative prediction of human pharmacokinetics and pharmacodynamics of CKD519, a potent inhibitor of cholesteryl ester transfer protein (CETP). Pharmaceutics 11.

Dong, J.Q., Salinger, D.H., Endres, C.J., Gibbs, J.P., Hsu, C.P., Stouch, B.J., Hurh, E., Gibbs, M.A., 2011. Quantitative prediction of human pharmacokinetics for monoclonal antibodies: retrospective analysis of monkey as a single species for first-in-human prediction. Clin. Pharmacokinet. 50, 131–142.

Electronic Medicines Compendium, 2022. Amiodarone hydrochloride 50mg/ml concentrate for solution for injection/infusion. SmPC. Available online: https://www.medicines.org.uk/emc/product/3940/smpc#gref (accessed 2022 March 13).

Elgart, A., Cherniakov, I., Aldouby, Y., Domb, A.J., Hoffman, A., 2013. Improved oral bioavailability of BCS class 2 compounds by self nano-emulsifying drug delivery systems (SNEDDS): the underlying mechanisms for amiodarone and talinolol. Pharm. Res. 30, 3029–3044.

Etheridge, S.P., Craig, J.E., Compton, S.J., 2001. Amiodarone is safe and highly effective therapy for supraventricular tachycardia in infants. Am. Heart J. 141, 105–110.

Falik, R., Flores, B.T., Shaw, L., Gibson, G.A., Josephson, M.E., Marchlinski, F.E., 1987. Relationship of steady-state serum concentrations of amiodarone and desethylamiodarone to therapeutic efficacy and adverse effects. Am. J. Med. 82, 1102–1108.

Greenberg, M.L., Lerman, B.B., Shipe, J.R., Kaiser, D.L., DiMarco, J.P., 1987. Relation between amiodarone and desethylamiodarone plasma concentrations and electrophysiologic effects, efficacy and toxicity. J. Am. Coll. Cardiol. 9, 1148–1155.

Haffajee, C.I., 1987. Clinical pharmacokinetics of amiodarone. Clin. Cardiol. 10, 16–19.

Haffajee, C.I., Love, J.C., Canada, A.T., Lesko, L.J., Asdourian, G., Alpert, J.S., 1983. Clinical pharmacokinetics and efficacy of amiodarone for refractory tachyarrhythmias. Circulation 67, 1347–1355.

Hamer, A.W., Arkles, L.B., Johns, J.A., 1989. Beneficial effects of low dose amiodarone in patients with congestive cardiac failure: a placebo-controlled trial. J. Am. Coll. Cardiol. 14, 1768–1774.

Hashimoto, N., Doki, K., Kawano, S., Aonuma, K., Ieda, M., Homma, M., 2021. Increased serum amiodarone concentration in hypertriglyceridemic patients: effects of drug distribution to serum lipoproteins. Clin. Transl. Sci.

Ibarra, M., Trocóniz, I.F., Fagiolino, P., 2021. Enteric reabsorption processes and their impact on drug pharmacokinetics. Sci. Rep. 11, 5794.

ICH, E.M.A., 1995. CPMP/ICH/381/95- ICH Topic Q2 (R1) validation of analytical procedures: text and methodology. Available online: https://www.ema.europa.eu/en/documents/scientific-guideline/ich-q-2-r1-validation-analytical-procedures-text-methodology-step-5_en.pdf (accessed 2022 March 10).

Ide, T., Sasaki, T., Maeda, K., Higuchi, S., Sugiyama, Y., Ieiri, I., 2009. Quantitative population pharmacokinetic analysis of pravastatin using an enterohepatic circulation model combined with pharmacogenomic Information on SLCO1B1 and ABCC2 polymorphisms. J. Clin. Pharmacol. 49, 1309–1317.

Jain, L., Woo, S., Gardner, E.R., Dahut, W.L., Kohn, E.C., Kummar, S., Mould, D.R., Giaccone, G., Yarchoan, R., Venitz, J., Figg, W.D., 2011. Population pharmacokinetic analysis of sorafenib in patients with solid tumours. Br. J. Clin. Pharmacol. 72, 294–305.

Kang, D.W., Ryu, C.H., Kim, J.H., Choi, G.W., Kim, S., Chon, C.H., Kim, J.H., Cho, H.Y., 2021. Pharmacokinetic-pharmacodynamic modeling approach for dose prediction of the optimal long-acting injectable formulation of finasteride. Int. J. Pharm. 601, 120527.

Kim, H.L., Seo, J.B., Chung, W.Y., Kim, S.H., Kim, M.A., Zo, J.H., 2014. The incidence and predictors of overall adverse effects caused by low dose amiodarone in real-world clinical practice. Korean J. Intern. Med. 29, 588–596.

Kodama, I., Kamiya, K., Toyama, J., 1997. Cellular electropharmacology of amiodarone. Cardiovasc. Res. 35, 13–29.

Kwak, E.Y., Kim, M.J., Park, J.H., Jung, H.W., Jung, M.E., 2021. Target-mediated drug disposition (TMDD) modeling of an anti-TFPI antibody (MG1113) in cynomolgus monkeys to predict human pharmacokinetics and pharmacodynamics. J. Thromb. Haemost. JTH.

Lalloz, M.R., Byfield, P.G., Greenwood, R.M., Himsworth, R.L., 1984. Binding of amiodarone by serum proteins and the effects of drugs, hormones and other interacting ligands. J. Pharm. Pharmacol. 36, 366–372.
Lehr, T., Staab, A., Tillmann, C., Trommeshauser, D., Schaefer, H.G., Kloft, C., 2009. A quantitative enterohepatic circulation model: development and evaluation with tesofensine and meloxicam. Clin. Pharmacokinet. 48, 529–542.
Li, C., Zhang, C., Deng, R., Leipold, D., Li, D., Latifi, B., Gao, Y., Zhang, C., Li, Z., Miles, D., Chen, S.C., Samineni, D., Wang, B., Agarwal, P., Lu, D., Prabhu, S., Girish, S., Kamath, A.V., 2019. Prediction of human pharmacokinetics of antibody-drug conjugates from nonclinical data. Clin. Transl. Sci. 12, 534–544.
Lupercio, F., Romero, J., Peltzer, B., Maraboto, C., Briceno, D., Villablanca, P., Ferrick, K., Gross, J.N., Kim, S., Fisher, J., Di Biase, L., Krumerman, A., 2018. Efficacy and safety outcomes of direct oral anticoagulants and amiodarone in patients with atrial fibrillation. Am. J. Med. 131, 573 e571-573.e578.
Luu, K.T., Bergqvist, S., Chen, E., Hu-Lowe, D., Kraynov, E., 2012. A model-based approach to predicting the human pharmacokinetics of a monoclonal antibody exhibiting target-mediated drug disposition. J. Pharmacol. Exp. Ther. 341, 702–708.
Martin-Algarra, R.V., Pascual-Costa, R.M., Merino, M., Casabó, V.G., 1995. Effects of polysorbate 80 on amiodarone intestinal absorption in the rat. Int. J. Pharm. 122, 1–8.
Mitchell, L.B., Exner, D.V., Wyse, D.G., Connolly, C.J., Prystai, G.D., Bayes, A.J., Kidd, W. T., Kieser, T., Burgess, J.J., Ferland, A., MacAdams, C.L., Maitland, A., 2005. Prophylactic oral amiodarone for the prevention of arrhythmias that begin early after revascularization, valve replacement, or repair: PAPABEAR: a randomized controlled trial. JAMA 294, 3093–3100.
Moak, J.P., 2000. Supraventricular tachycardia in the neonate and infant. Prog. Pediatr. Cardiol. 11, 25–38.
Mooss, A.N., Mohiuddin, S.M., Hee, T.T., Esterbrooks, D.J., Hilleman, D.E., Rovang, K.S., Sketch, M.H., 1990. Efficacy and tolerance of high-dose intravenous amiodarone for recurrent, refractory ventricular tachycardia. Am. J. Cardiol. 65, 609–614.
Mujović, N., Dobrev, D., Marinković, M., Russo, V., Potpara, T.S., 2020. The role of amiodarone in contemporary management of complex cardiac arrhythmias. Pharmacol. Res. 151, 104521.
Nirogi, R., Bhyrapuneni, G., Muddana, N.R., Manoharan, A., Shinde, A.K., Mohammed, A.R., Padala, N.P., Ajjala, D.R., Subramanian, R., Palacharla, V.R.C., 2020. Absorption, distribution, metabolism, excretion (ADME), drug-drug interaction potential and prediction of human pharmacokinetics of SUVN-G3031, a novel histamine 3 receptor (H(3)R) inverse agonist in clinical development for the treatment of narcolepsy. Eur. J. Pharm. Sci. 152, 105425.
Okour, M., Jacobson, P.A., Ahmed, M.A., Israni, A.K., Brundage, R.C., 2018. Mycophenolic acid and its metabolites in kidney transplant recipients: a semimechanistic enterohepatic circulation model to improve estimating exposure. J. Clin. Pharmacol. 58, 628–639.
Papathanasiou, T., Juul, R.V., Gabel-Jensen, C., Kreilgaard, M., Lund, T.M., 2016. Population pharmacokinetic modelling of morphine, gabapentin and their combination in the rat. Pharm. Res. 33, 2630–2643.
Pascual-Costa, R.M., 1994. Oral bioavailability of amiodarone in the rat. (Doctoral Thesis). University of Valencia, Valencia, Spain, p. 323.
Patel, A., Shelat, P., Lalwani, A., 2015a. Development and optimization of solid self nanoemulsifying drug delivery (S-SNEDDS) using d-optimal design for improvement of oral bioavailability of amiodarone hydrochloride. Curr. Drug Deliv. 12, 745–760.
Patel, A.R., Doddapaneni, R., Andey, T., Wilson, H., Safe, S., Singh, M., 2015b. Evaluation of self-emulsified DIM-14 in dogs for oral bioavailability and in Nu/nu mice bearing stem cell lung tumor models for anticancer activity. J. Controll. Release 213, 18–26 official journal of the Controlled Release Society.
Plomp, T.A., Wiersinga, W.M., Van Rossum, J.M., Maes, R.A., 1987. Pharmacokinetics and body distribution of amiodarone and desethylamiodarone in rats after oral administration. In Vivo 1, 265–279 (Brooklyn).
Pollak, P.T., Bouillon, T., Shafer, S.L., 2000. Population pharmacokinetics of long-term oral amiodarone therapy. Clin. Pharmacol. Ther. 67, 642–652.
Rahman, M.A., Mujahid, M., Hussain, A., 2016. Self-emulsifying pellets prepared by extrusion/spheronization: *in vitro/in vivo* evaluation. Recent Pat. Drug Deliv. Formul. 10, 245–252.
Rotmensch, H.H., Belhassen, B., Swanson, B.N., Shoshani, D., Spielman, S.R., Greenspon, A.J., Greenspan, A.M., Vlasses, P.H., Horowitz, L.N., 1984. Steady-state serum amiodarone concentrations: relationships with antiarrhythmic efficacy and toxicity. Ann. Intern. Med. 101, 462–469.
Saul, J.P., Scott, W.A., Brown, S., Marantz, P., Acevedo, V., Etheridge, S.P., Perry, J.C., Triedman, J.K., Burriss, S.W., Cargo, P., Graepel, J., Koskelo, E.K., Wang, R., 2005. Intravenous amiodarone for incessant tachyarrhythmias in children: a randomized, double-blind, antiarrhythmic drug trial. Circulation 112, 3470–3477.
Siddoway, L.A., 2003. Amiodarone: guidelines for use and monitoring. Am. Fam. Physician 68, 2189–2196.
Singh, B.N., 2006. Amiodarone: a multifaceted antiarrhythmic drug. Curr. Cardiol. Rep. 8, 349–355.
Somani, P., 1989. Basic and clinical pharmacology of amiodarone: relationship of antiarrhythmic effects, dose and drug concentrations to intracellular inclusion bodies. J. Clin. Pharmacol. 29, 405–412.
Somberg, J., Molnar, J., 2016. Sotalol versus amiodarone in treatment of atrial fibrillation. J. Atr. Fibrillation 8, 1359.
Somberg, J.C., Timar, S., Bailin, S.J., Lakatos, F., Haffajee, C.I., Tarjan, J., Paladino, W.P., Sarosi, I., Kerin, N.Z., Borbola, J., Bridges, D.E., Molnar, J., 2004. Lack of a hypotensive effect with rapid administration of a new aqueous formulation of intravenous amiodarone. Am. J. Cardiol. 93, 576–581.
Song, L., Yao, X., Liu, Y., Zhong, W., Jiang, J., Liu, H., Zhou, H., Shi, C., Zong, K., Wang, C., Ma, C., Liu, D., Hu, P., 2020. Translational prediction of first-in-human pharmacokinetics and pharmacodynamics of janagliflozin, a selective SGLT2 inhibitor, using allometric scaling, dedrick and PK/PD modeling methods. Eur. J. Pharm. Sci. 147, 105281.
Veronese, M.E., McLean, S., Hendriks, R., 1988. Plasma protein binding of amiodarone in a patient population: measurement by erythrocyte partitioning and a novel glass-binding method. Br. J. Clin. Pharmacol. 26, 721–731.
Wade, J.R., Beal, S.L., Sambol, N.C., 1994. Interaction between structural, statistical, and covariate models in population pharmacokinetic analysis. J. Pharmacokinet. Biopharm. 22, 165–177.
Wang, D., Chen, G., Ren, L., 2017. Preparation and characterization of the sulfobutylether-β-cyclodextrin inclusion complex of amiodarone hydrochloride with enhanced oral bioavailability in fasted state. AAPS PharmSciTech. 18, 1526–1535.
Zhu, Y.T., Yuan, Y.Z., Feng, Q.P., Hu, M.Y., Li, W.J., Wu, X., Xiang, S.Y., Yu, S.Q., 2021. Food emulsifier polysorbate 80 promotes the intestinal absorption of mono-2-ethylhexyl phthalate by disturbing intestinal barrier. Toxicol. Appl. Pharmacol. 414, 115411.
Zimetbaum, P., 2012. Antiarrhythmic drug therapy for atrial fibrillation. Circulation 125, 381–389.
Zou, P., Zheng, N., Yu, Y., Yu, S., Sun, W., McEachem, D., Yang, Y., Yu, L.X., Wang, S., Sun, D., 2012. Preclinical pharmacokinetics of MI-219, a novel human double minute 2 (HDM2) inhibitor and prediction of human pharmacokinetics. J. Pharm. Pharm. Sci. 15, 265–280 a publication of the Canadian Society for Pharmaceutical Sciences, Societe canadienne des sciences pharmaceutiques.

Annex 3: New insights into the role of VKORC1 polymorphisms for optimal warfarin dose selection in Caribbean Hispanic patients through an external validation of a population PK/PD model

Biomedicine & Pharmacotherapy 170 (2024) 115977

Contents lists available at ScienceDirect

Biomedicine & Pharmacotherapy

journal homepage: www.elsevier.com/locate/biopha

New insights into the role of *VKORC1* polymorphisms for optimal warfarin dose selection in Caribbean Hispanic patients through an external validation of a population PK/PD model

Karine Rodríguez-Fernández [a], Gledys Reynaldo-Fernández [b], Stephanie Reyes-González [c], Camila de las Barreras [b], Leyanis Rodríguez-Vera [d], Cornelis Vlaar [c], Jean-Christophe M. Monbaliu [e], Torsten Stelzer [c,f], Jorge Duconge [c,*], Victor Mangas-Sanjuan [a,g]

[a] *Department of Pharmacy and Pharmaceutical Technology and Parasitology, University of Valencia, Valencia, Spain*
[b] *Institute of Pharmacy and Foods, University of Havana, Havana 11300, Cuba*
[c] *Department of Pharmaceutical Sciences, School of Pharmacy, University of Puerto Rico - Medical Sciences Campus, San Juan 00936, PR, USA*
[d] *Center for Pharmacometrics and System Pharmacology at Lake Nona (Orlando), Department of Pharmaceutics, College of Pharmacy, University of Florida, Orlando, FL 32827, USA*
[e] *Center for Integrated Technology and Organic Synthesis, MolSys Research Unit, University of Liège, B-4000 Liège (Sart Tilman), Liège, Belgium*
[f] *Crystallization Design Institute, Molecular Sciences Research Center, University of Puerto Rico, San Juan 00926, PR, USA*
[g] *Interuniversity Research Institute for Molecular Recognition and Technological Development, Polytechnic University of Valencia-University of Valencia, Valencia, Spain*

ARTICLE INFO

Keywords:
Warfarin
Pharmacokinetic/pharmacodynamic
VKORC1
CYP2C9
Hispanic Caribbean

ABSTRACT

Warfarin, an oral anticoagulant, has been used for decades to prevent thromboembolic events. The complex interplay between *CYP2C9* and *VKORC1* genotypes on warfarin PK and PD properties is not fully understood in special sub-groups of patients. This study aimed to externally validate a population pharmacokinetic/pharmacodynamic (PK/PD) model for the effect of warfarin on international normalized ratio (INR) and to evaluate optimal dosing strategies based on the selected covariates in Caribbean Hispanic patients. INR, and *CYP2C9* and *VKORC1* genotypes from 138 patients were used to develop a population PK/PD model in NONMEM. The structural definition of a previously published PD model for INR was implemented. A numerical evaluation of the parameter-covariate relationship was performed. Simulations were conducted to determine optimal dosing strategies for each genotype combinations, focusing on achieving therapeutic INR levels. Findings revealed elevated IC_{50} for G/G, G/A, and A/A *VKORC1* haplotypes (11.76, 10.49, and 9.22 mg/L, respectively), in this population compared to previous reports. The model-guided dosing analysis recommended daily warfarin doses of 3–5 mg for most genotypes to maintain desired INR levels, although subjects with combination of *CYP2C9* and *VKORC1* genotypes * 2/* 2-, * 2/* 3- and * 2/* 5-A/A would require only 1 mg daily. This research underscores the potential of population PK/PD modeling to inform personalized warfarin dosing in populations typically underrepresented in clinical studies, potentially leading to improved treatment outcomes and patient safety. By integrating genetic factors and clinical data, this approach could pave the way for more effective and tailored anticoagulation therapy in diverse patient groups.

Abbreviations: PK, pharmacokinetics; PD, pharmacodynamics; PK/PD, pharmacokinetic/pharmacodynamic; INR, international normalized ratio; CYP2C9, cytochrome P4502C9 gene; VKORC1, vitamin K epoxide reductase complex subunit 1 gene; VACHS, Veteran Affairs Caribbean Healthcare System; CI, confidence intervals; OFV, objective function value; IIV, inter-individual variability; RUV, residual unexplained variability; GOF, goodness of fit; NPDE, normalized prediction distribution errors; pc-VPC, prediction-corrected visual predictive checks; SAEM, Stochastic Approximation of the Expectation Maximization; IMP, Importance Sampling Estimation; F, bioavailability fraction; CL, clearance; V, volume of distribution; MTT, mean transit time; I_{max}, maximum inhibitory effect; IC_{50}, concentration resulting in 50% of I_{max}; DV, dependent variable; PRED, population prediction; K-PD, kinetic-pharmacodynamic model; MIPD, model-informed precision dosing; GGCX, γ-glutamyl carboxylase.

* Correspondence to: Medical Sciences Campus, Pharmaceutical Sciences Dept./ Pharmacogenomics Lab B-214, PO Box 365067, San Juan, PR 00936-5067, USA.
E-mail address: jorge.duconge@upr.edu (J. Duconge).

https://doi.org/10.1016/j.biopha.2023.115977
Received 1 September 2023; Received in revised form 17 November 2023; Accepted 29 November 2023
Available online 6 December 2023

1. Introduction

Warfarin is an oral anticoagulant that has been used for over six decades to prevent thromboembolic events, such as stroke and deep vein thrombosis [1]. It works by inhibiting the synthesis of vitamin K-dependent clotting factors in the liver, thus reducing the production of blood clots [2]. Despite its widespread use, warfarin therapy is associated with several challenges, including a narrow therapeutic window, a high risk of bleeding, and significant interpatient variability in response [3,4]. The management of warfarin therapy involves maintaining a stable therapeutic international normalized ratio (INR) range, which is typically between 2.0 and 3.0 for most indications [5]. However, achieving and maintaining this target range can be challenging due to the wide interpatient variability in warfarin exposure and response. This variability can be attributed to various factors, including age, sex, body weight, diet, comorbidities, and concomitant medications, as well as genetic variations [4].

The impact of genetic polymorphisms on warfarin response has been extensively studied, particularly for two relevant pharmacogenes: the *CYP2C9* gene encodes the cytochrome P450 isoform 2C9, a member of the cytochrome P450 superfamily of enzymes, and the *VKORC1* gene encodes the catalytic subunit 1 of the vitamin K epoxide reductase complex enzyme [3,4]. CYP2C9 is responsible for the metabolism of S-warfarin, the more active enantiomer of warfarin, and genetic polymorphisms in this gene have been associated with altered warfarin clearance (CL) and higher INR values [4,6,7]. VKORC1 is responsible for the reduction of inactive vitamin K 2,3-epoxide to active vitamin K in the endoplasmic reticulum membrane and, therefore, is involved in the synthesis of vitamin K-dependent clotting factors [6]. Genetic polymorphisms affecting this gene have been associated with reduced sensitivity to warfarin [8,9]. Given the impact of genetic polymorphisms on warfarin response, the use of a pharmacogenetic-driven algorithm has been recommended to guide warfarin dosing in clinical setting, particularly in patients starting warfarin therapy [6,10–12]. The results of genetic testing for *CYP2C9* and *VKORC1* polymorphisms can be used to inform initial warfarin dosing and subsequent dose adjustments, leading to more effective and personalized therapy [6,11–14].

In recent years, population pharmacokinetic (PK) and pharmacokinetic/pharmacodynamic (PK/PD) models that incorporate genetic information have been developed to predict optimal warfarin doses for individual patients, improving therapeutic efficacy and reducing the risk of adverse events and thromboembolic events [7,15–19]. The models use a two-step approach: first, a suitable starting dose is estimated based on patient factors that have been previously identified as predictors for dose individualization, which is referred to as a priori individualization. Second, once the treatment has started, the dosing can be further personalized based on feedback observations from the patient, which is referred to as a posteriori individualization [7,15,20].

However, the development of a reliable and accurate PK/PD model that incorporates genetic information can be challenging due to the complex interplay between genetic and non-genetic factors affecting warfarin dosing. Furthermore, the predictive performance and comparability of different PK/PD models that incorporate genetic information have not been extensively evaluated. External validation studies are necessary to assess the accuracy and reliability of these models in different populations, allowing for more personalized and effective warfarin dosing. While PK/PD modeling has shown promise in predicting the optimal warfarin dose for individual patients, most of the studies have been conducted in Caucasian populations, with few studies focusing on non-Caucasian populations. Furthermore, there is limited data on the application of PK/PD models incorporating *CYP2C9* and *VKORC1* genotypes information in Caribbean Hispanic patients.

In this study, we aimed to (i) externally validate a population PK/PD model of INR after concomitant administration of warfarin in clinical practice, and (ii) evaluate optimal dosing strategies of warfarin in Caribbean Hispanic patients based on the selected covariates.

2. Materials and methods

2.1. Ethics approval

This is a secondary analysis of a previous pharmacogenetic study of warfarin in Puerto Rican patients (IRB approval #A4070109). Proper safeguards against any potential violation of privacy and/or breach of confidentiality will be ensured. Authorization to use the data for the purpose stated in this project was previously obtained from individual patients by an informed consent process. Accordingly, the study was conducted following Helsinki's declaration for human subject protection in clinical surveys.

2.2. Study design

Data for analyses were available from elderly patients, mostly males, followed upon at the anticoagulation clinic in the Veteran Affairs Caribbean Healthcare System (VACHS) at San Juan, PR. The patients received long-term warfarin anticoagulant therapy for different thromboembolic disorders in total weekly doses ranged from 7 to 82 mg, depending on the 24- or 48-hour dosing interval. Also, they carried eight different *CYP2C9* alleles (*1/*2, *1/*3, *1/*5, *1/*8, *2/*2, *2/*3, *2/*5) and three *VKORC1* genotypes (G/A, G/G, A/A). Detailed information was recorded, including demographics and clinical response, evaluated longitudinally using the assessment tool INR.

2.3. Base population PK/PD model

Due to the absence of longitudinal PK information of warfarin in the current study, a previously published population PK model was implemented to retrieve the structural PK parameter estimates for each subgroup of *CYP2C9* genotype [20]. Given the absence of experimental PK values in the recruited patients, inter-individual variability (IIV) was not associated to the PK parameters.

The structural definition of a previously published PD model for INR was implemented, which relies on an indirect response model coupled to a series of transit compartments to account for the delay between warfarin exposure and INR levels [7,17]. The effect of warfarin concentration was incorporated using a sigmoid response function based on the typical longitudinal PK levels for each *CYP2C9* genotype. IIV associated to the PK/PD model parameters was modeled exponentially preventing negative values for the individual estimates, and residual unexplained variability (RUV) was described with a proportional model. The population PD parameters were re-estimated as part of the development of the base PD model from the experimental information (INR) available in the recruited patients. The significance of the non-diagonal elements of the Ω variance-covariance matrix and subject specific RUV were also evaluated.

2.4. Final population PK/PD model

A numerical evaluation of the parameter-covariate relationship was performed manually in a univariate testing. A decrease in 6.63 units (p value <0.01) of the objective function value (OFV) provided by NONMEM®. Covariates evaluated included: body weight, age, *CPY2C9* and *VKORC1* genotypes, race, diabetes mellitus and smoking status. For categorical covariates the relative size of the different categories had to be larger than 5% to be considered for covariate testing. Covariates were also investigated for co-linearity. If two covariates had a correlation coefficient $> |0.6|$ then one of the two covariates was excluded from testing.

Assessment of model adequacy was influenced by convergence stability, biological plausibility, and parsimony. Additional evaluation of standard goodness-of-fit (GOF) plots together with the normalized prediction distribution errors (NPDE) plots was conducted [21].

Model evaluation of the selected models was performed through

prediction-corrected visual predictive checks (pc-VPC) [22] with 1000 datasets obtained by Monte Carlo simulation using the final parameter estimates for both fixed and random effects. Each simulated dataset has the study design features (covariates, dosing times, PK sampling times) identical to those in the analysis dataset. For each simulated dataset, the 2.5th, 50th, and 97.5th percentiles of the simulated concentrations in each bin were calculated. Then, the 95% prediction intervals of the above-described percentiles were calculated and displayed graphically together with corresponding percentiles computed from raw data.

2.5. Optimal dosing regimen evaluation

A simulation-based analysis using a Monte Carlo approach (n = 10,000) was conducted assuming log-normal distribution of PD parameters and different combinations of statistically significant covariates. A multiple dose regimen of daily oral administration of 1, 3, 5, 7, and 10 mg of warfarin to achieve steady-state concentrations were assumed. Individual INR levels were computed at 23 h post-dose of the 10th administration cycle (PK steady-state conditions) of warfarin. Dosing regimen selection was established with the goal of achieving the highest probability of INR levels within the therapeutic range (2.0–3.0).

2.6. Data analysis

All data analyses were performed based on the population approach with the software NONMEM® (v7.5, Icon Development Solutions, Ellicott City, MD). The population parameters were estimated using the Stochastic Approximation of the Expectation Maximization and the Importance Sampling Estimation (SAEM) and the Importance Sampling Estimation (IMP) method.

For graphical and statistical analysis, the R® software v4.2.1 was used (R Foundation for Statistical Computing, Vienna, Austria). The pc-VPC were performed using PsN version 5.0.0 [23].

3. Results

The modelling dataset consisted of 1033 INR observations from 138 patients with Table 1 presenting subject demographics. Fig. 1 shows the individual INR (PD) profiles available. Distributions of continuous covariates at baseline are displayed in Supplementary Fig. S1.

Table 1
Summary of patients' characteristics.

Demographics	Value
N	138
Median age, years (range)	68 (31–90)
Median body weight, kg (range)	83 (51–159)
Race, n (%), self-reported	
White Hispanics	33 (24)
Black Hispanics	26 (19)
Admixed	37 (27)
Others or not reported	42 (30)
Smoking status, n (%)	
Yes	59 (43)
No	79 (57)
type 2 DM status, n (%)	
Yes	39 (28)
No	72 (57)
CYP2C9 genotypes, n (%)	
** 1/* 1* (wild type)	98 (71)
** 1/* 2*	21 (15)
** 1/* 3*	7 (5.1)
** 1/* 5*	1 (0.72)
** 1/* 8*	2 (1.44)
** 2/* 2*	2 (1.44)
** 2/* 3*	6 (4.34)
** 2/* 5*	1 (0.72)
VKORC1 haplotypes, n (%)	
G/A	62 (45)
G/G	57 (41.3)
A/A	19 (13.7)

INR, international normalized ratio; DM, diabetes mellitus.

3.1. Base population PK/PD model

A previously developed one-compartment model with first-order oral absorption and *CYP2C9* genotype effect on CL was considered for generating longitudinal PK profiles across different *CYP2C9* genotypes [20]. Since the population PK models were developed from oral administration of warfarin, the bioavailability fraction (F) is unknown, and the estimates of CL and V represent the apparent estimates.

Parameter estimates of the base population PK/PD model are summarized in Supplementary Table S1 and the corresponding GOF, NPDE and VPC are shown in Supplementary Fig. S2. The structural definition of the base PK/PD, which incorporates two transit compartment chains with three compartments each to account for the delay between exposure and INR response, can satisfy the overall INR trend with no appreciable systematic bias that suggest model inadequacies. System-related PD parameters (MTT_1, and MTT_2) were fixed to the values reported by Hamberg et al., 2010 (MTT_1: 27.2 h or 1.13 d, and MTT_2: 110.9 h or 4.62 d). A typical INR at baseline (INR_{base} =1.86) was estimated and the maximum INR was set to 20 as previously reported [7,17]. An inhibitory sigmoid E_{max} model of warfarin on the zero-order synthesis rate constants for each chain was assumed. The model assumes a complete (100%) inhibition of warfarin (I_{max}) to the vitamin K epoxide reductase, as previously reported [7,17,24], and the IC_{50} was estimated (15.4 mg/L). This parametrization helps to enhance the model stability. Due to the lack of intensive PD sampling, inter-individual variability was only incorporated on INR_{base} (25%) and IC_{50} (35%) parameters.

3.2. Final population PK/PD model

The final population PK/PD model incorporates *CYP2C9* on CL and body weight on V, as previously reported [20] and for the pharmacodynamic parameters, *VKORC1* polymorphisms as statistically significant

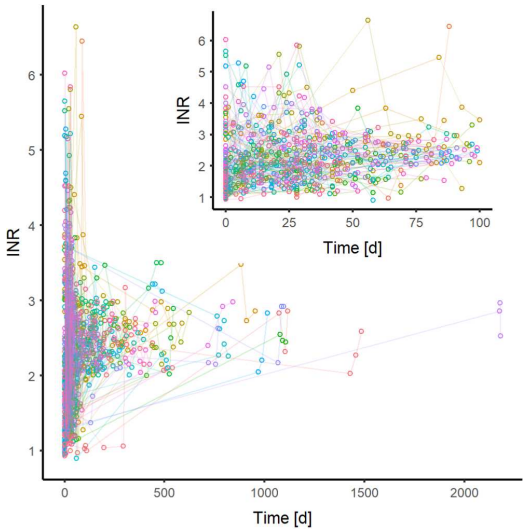

Fig. 1. Experimental raw data of INR observations vs time for all subjects included in the study (N = 138). The open circles represent the measured INRs in each patient and each color line represents an individual time profile of INR variations. INR: international normalized ratio.

covariate on INR_{base} and IC_{50} ($p < 0.01$, $\Delta OFV = -11.8$), respectively (Table 2). Other covariates, binary or (normalized) continuous variables, were investigated during the modeling process, but no statistical improvement ($p < 0.01$) after their inclusion was observed.

Supplementary Fig. S3 depicts the eta-distribution values of INR_{base} (ETA1) and IC_{50} (ETA2) across the different covariates available from the base population PK/PD model. Based on the GOF and NPDE plots (Fig. S4A), no systematic bias was observed and a slight improvement in the DV vs PRED plot is detected after the inclusion of the covariate effects. Individual observed vs predicted longitudinal INR profiles are shown in Supplementary Fig. S4B. The examination of the pc-VPC (Fig. 2) suggests a reasonable agreement between the observed data and model predictions for the median (50th percentile) and the variability (2.5th and 97.5th percentiles). The impact of *VKORC1* haplotypes on IC_{50} was modelled by accounting for the effects of individual alleles (G and A), which provides a more robust estimation in uncommon genotypes. The gamma parameter (1.47) of the sigmoid-Emax function was estimated, which is in accordance with other published values [7, 15]. Warfarin IC_{50} for G/G, G/A, and A/A were 11.76, 10.49, and 9.22 mg/L, respectively, which are higher than the reported ranges [7, 15,17,25]. The INR_{base} for the G/A, G/G, and A/A *VKORC1* haplotypes were 1.78, 1.84, and 2.18, respectively. After the covariate analysis, the IIV on INR_{base} and IC_{50} was reduced to 23% and 34%, respectively. Supplementary Fig. S5 depicts the eta-distribution values of INR_{base} (ETA1) and IC_{50} (ETA2) across the different covariates available from the final population PK/PD model.

3.3. Optimal dosing regimen evaluation

Based on the PD model developed, including the significant covariates on PK (*CYP2C9* genotypes on CL) and PD (*VKORC1* haplotypes on baseline and IC_{50}), we aimed to optimize the oral dosing strategy of warfarin in Caribbean Hispanic patients to achieve the optimal benefit/risk ratio. Fig. 3 represents the simulated INR levels across the dosing regimens tested. Table 3 summarizes the optimal dosing regimen selected for each combination of *CYP2C9* genotypes and *VKORC1* haplotypes.

4. Discussion

Currently, treatment with warfarin in the Caribbean Hispanic population generates certain therapeutic gaps since there are no clinical guidelines that evaluate the impact of different *CYP2C9* and *VKORC1* genotypes on routine INR measures (efficacy surrogate endpoint) in this population. Consequently, patients show sub-optimal clinical response rates, according to individual INR values. To address this, we have adapted a population PK/PD model of warfarin from individual data and dose records over 2 years in Caribbean Hispanic patients from a local anticoagulation clinic to optimize the dosing regimens in this population. In this paper, a simulation-based analysis to calculate the probability of guaranteeing therapeutic INR levels (2−3) for different daily regimens of warfarin was performed. The simulations accommodated different patient's genotypes resulting from combinatorial *CYP2C9* and *VKORC1* polymorphisms.

A relevant aspect of this work is that it provides external validation of previously published PK and PD models. The combination of both has made it possible to establish a PK/PD model capable of collecting behavior in the Hispanic Caribbean population, which is different from that used in previous studies. Longitudinal PK model predictions between the structural PK definition of Hamberg *et al.* [7,17] and Reyes-González *et al.* [20] can be found in Fig. 4, where no relevant differences were observed across both PK model structures. This highlights the importance of adapting published structural models to predict the behavior of anticoagulant therapy and corroborates their predictive capacity at the structural level.

Due to the paucity of longitudinal profiles with a high number of INR samples, the maturation times (MTT_1 and MTT_2) of each of the transit-compartment chains were fixed to published values. Although some authors propose a K-PD structure [7], whereby the INR response is not governed by warfarin concentrations, in this article we have generated the PK profiles from the pharmacogenetic information available in each patient to predict the change in response over time as a consequence of warfarin concentrations. Despite the limitation of not having observed concentrations of warfarin and the fact that all patients with the same genetic profile present the same longitudinal profile of warfarin, we believe that this strategy makes it possible to partly mitigate the excessive IIV of warfarin observed in clinical practice.

One of the most surprising results of this study is the IC_{50} values obtained for each of the *VKORC1* haplotypes studied in the Caribbean Hispanic population, which were clearly higher (9.22–11.76 mg/L) than those earlier reported in other populations (1.56–3.11 mg/L) [7,17]. This is consistent with the therapeutic gaps observed in this underrepresented population and suggests increased resistance of Caribbean Hispanic patients to warfarin, who may require more intensive dosing regimens to achieve similar target INR responses. This phenomenon may be the consequence of a longer longitudinal evaluation than in previous studies (>2000 d), as well as a slightly higher distribution of G/G and G/A polymorphisms that may be partially affecting the point estimate. The underlying cause for these increased IC_{50} values remains unclear. However, we also speculate it might in part be linked to the presence of the *NQO1** 2 allele (g .559 C>T, p. P187S) that has been previously associated with warfarin resistance in Hispanics [26,27]. The *NQO1* gene encodes a NAP(H)-dependent quinone oxide reductase enzyme, responsible for catalyzing the reduction of quinones, including vitamin K, into hydroquinone. This mechanism could potentially serve as an alternate vitamin K recycling pathway to VKORC1 in carriers of the haplotype A, who show a lower *VKORC1* gene expression. Nevertheless, this hypothesis needs further validation.

On the other hand, when taking into account the INR values at baseline (INR_{base}) across different *VKORC1* haplotypes, we observed higher measures in A/A carriers (2.18) compared to those in patients with haplotypes containing the G allele (1.78 and 1.84, respectively). This could be explained by a more prolonged prothrombin time and lower levels of functional (active) prothrombin-dependent coagulation factors in carriers of the *VKORC1*-A allele due to their reduced expression of the hepatic VKORC1 enzyme, which plays a pivotal role in the vitamin K cycle in the liver [28]. Vitamin K dihydroquinone is oxidized to vitamin K epoxide during this process and γ-glutamyl carboxylase (GGCX) carboxylates the various hypofunctional coagulation factors

Table 2
Final parameter estimates of the final population pharmacokinetic-pharmacodynamic model of warfarin in Caribbean Hispanic patients.

		Population PK Model Estimates		Bootstrap Results	
Fixed-Effect		Value	Shrinkage (%)	Median	95%CI
MTT_1 (d)		1.13 FIX		1.13 FIX	
MTT_2 (d)		4.62 FIX		4.62 FIX	
Baseline					
	G/A	1.78		1.76	1.48–1.91
	G/G	1.84		1.85	1.53–2.05
	A/A	2.18		2.14	1.97–2.23
IC_{50}					
	G	5.88		5.91	5.61–6.37
	A	4.61		4.63	4.41–4.98
γ		1.47		1.48	1.27–1.61
Inter-individual variability					
Baseline (%)		23	13	24	19–30
IC_{50} (%)		34	44	34	28–39
Residual unexplained variability					
Proportional (%)		27	6	26	22–31

MTT: mean transit time; IC_{50}: concentration resulting in 50% of I_{max}.

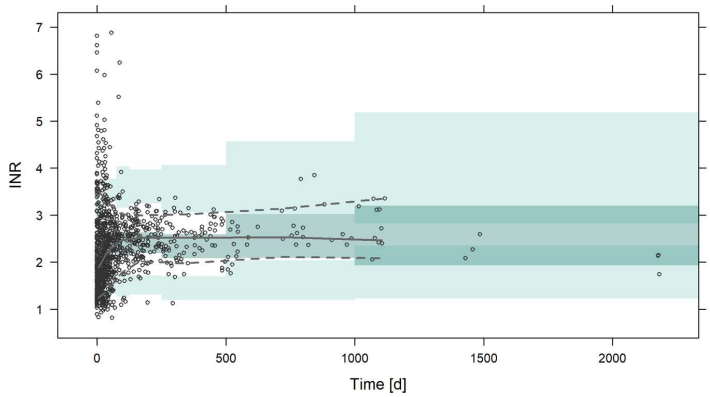

Fig. 2. Prediction-corrected visual predictive check of the final population pharmacodynamic model of INR after warfarin administration. Grey lines represent the median of 2.5th, 50th and 97.5th percentiles of the experimental INR observations. Green shaded areas encompass the 95% confidence intervals of prediction interval at 2.5th, 50th and 97.5th percentiles for the simulated INR data (n = 1000). Empty grey dots represent the experimental INR observations. INR: international normalized ratio.

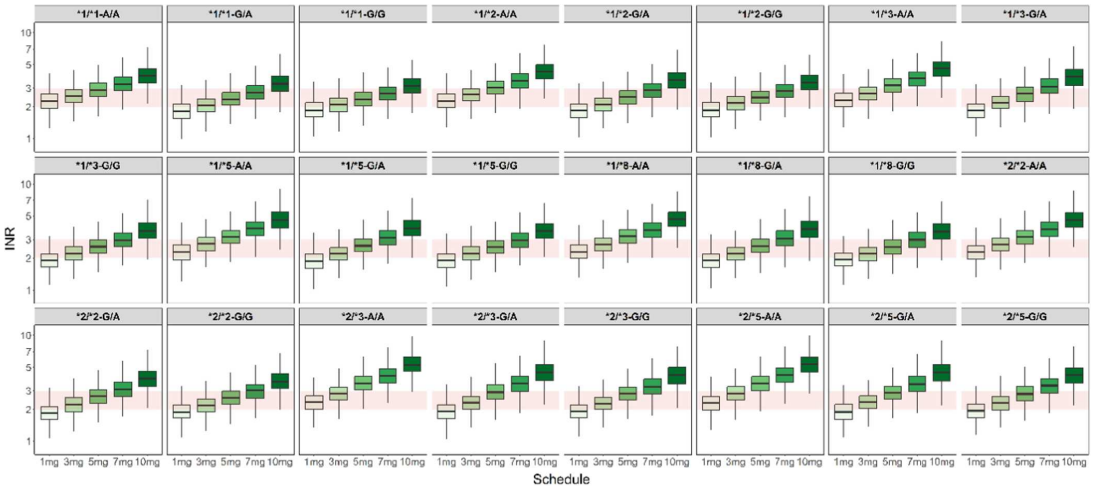

Fig. 3. Stochastic simulations (n = 10,000) of INR levels using the final population PK/PD model assuming different daily dosing regimens for each sub-population of CYP2C9 and VKORC1 polymorphisms. The red band represents the therapeutic INR interval (2–3). INR: international normalized ratio.

involved in the clotting cascade including prothrombin (FII). VKORC1 is responsible for the reduction of vitamin K epoxide back to vitamin K1 and vitamin K dihydroquinone, which is the rate-limiting step in vitamin K recycling. Therefore, even in the absence of any competitive inhibition by warfarin (baseline), reduced VKORC1 levels in carriers of the group A haplotype will deplete the formation of vitamin K1 dihydroquinone. Since vitamin K1 dihydroquinone is the essential cofactor to GGCX, further post-translational activation of hypofunctional coagulation factors is critically compromised in this situation. As a result, the prothrombin time will be prolonged, and the INR level will rise accordingly. This would open the door to hypothesize that *VKORC1* polymorphisms not only affect the potency of warfarin but also influence basal INR levels, partially explaining the excessive inter-individual variability in INR_{base}.

A model-informed optimal dosing regimen selection has been conducted based on the probability of achieving therapeutic INR levels in a virtual population using the fixed and random parameters from the final population PK/PD model. The different sub-populations considered are the result of the combination of *CYP2C9* and *VKORC1* polymorphisms. Overall, the predicted probability in all scenarios reaches therapeutic INR levels in at least 60% of the patients. Previous authors stated that due to the moderate inter-individual variability and residual error and independently of the structural definition of the PK/PD model, probabilities less than 70% are not expected for warfarin dose selection [7, 29]. In this regard, 3–5 mg of daily warfarin would achieve therapeutic INR levels in most of the scenarios considered. The sub-group of patients with * 2/* 2-, * 2/* 3- and * 2/* 5-A/A would require only 1 mg daily of warfarin to achieve therapeutic INR levels at steady-state conditions.

The absence of tailored clinical guidelines considering the impact of distinct *CYP2C9* and *VKORC1* genotypes on routine INR measures in Caribbean Hispanics has led to therapeutic gaps, contributing to suboptimal clinical response rates within this population. Through simulation-based analyses encompassing various patient genotypes resulting from *CYP2C9* and *VKORC1* polymorphisms, this study delved

Table 3
Model-informed dosing regimen selection of daily warfarin in patients with combinatorial *CYP2C9* and *VKORC1* polymorphisms.

Type of patient	Schedule	Probability
* 1/* 1-A/A	3 mg/d	67
* 1/* 1-G/A	5 mg/d	66.7
* 1/* 1-G/G	5 mg/d	66.2
* 1/* 2-A/A	3 mg/d	64.7
* 1/* 2-G/A	5 mg/d	67.3
* 1/* 2-G/G	5 mg/d	69.2
* 1/* 3-A/A	3 mg/d	64.6
* 1/* 3-G/A	3 mg/d	60.7
* 1/* 3-G/G	5 mg/d	65.9
* 1/* 5-A/A	3 mg/d	60.6
* 1/* 5-G/A	5 mg/d	63.6
* 1/* 5-G/G	5 mg/d	65.2
* 1/* 8-A/A	3 mg/d	63.5
* 1/* 8-G/A	5 mg/d	62.4
* 1/* 8-G/G	5 mg/d	63.6
* 2/* 2-A/A	1 mg/d	60.8
* 2/* 2-G/A	5 mg/d	62.5
* 2/* 2-G/G	5 mg/d	63.5
* 2/* 3-A/A	1 mg/d	64.3
* 2/* 3-G/A	3 mg/d	63
* 2/* 3-G/G	3 mg/d	64.9
* 2/* 5-A/A	1 mg/d	63.2
* 2/* 5-G/A	3 mg/d	67.3
* 2/* 5-G/G	3 mg/d	62.4

into optimizing dosing regimens to ensure therapeutic INR levels. Our findings support the significance and clinical relevance of using a population PK/PD approach in elucidating the role of genetic polymorphisms (e.g., *CYP2C9* and *VKORC1* haplotypes) for the optimal design of warfarin dosing schemes in Caribbean Hispanic patients. The simulations provided a comprehensive understanding of how a broader range of *CYP2C9* variants and, specifically, the *VKORC1*-1636 A allele influence the PK and PD of warfarin, as well as baseline INR measures, within this diverse population and shed light on potential underlying mechanisms linked to increased IC_{50} values.

The participants in our study are mainly elderly men, which is a limitation of the study as sex differences in warfarin PK have been suggested in previous studies [30,31]. However, the genotypes included as covariates in the PK/PD analyses were based on the *CPY2C9* and *VKORC1* polymorphisms, which are not sex-linked variants and are therefore unlikely to represent significant sex bias.

5. Conclusions

By performing an external validation of the PK/PD model, we can confidently extrapolate findings from the model to real-world patient scenarios, enabling tailored and precise warfarin dosing recommendations for Caribbean Hispanic individuals. Therefore, this model-informed precision dosing (MIPD) approach is expected to minimize the risk of adverse events linked to inaccurate warfarin dosing due to genetic differences at individual level and enhances therapeutic outcomes. This strategy will ultimately foster safer and more effective clinical management of personalized anticoagulation therapy in this specific patient subgroup, which is often underrepresented in clinical studies. In conclusion, by adapting this MIPD strategy to the Caribbean Hispanic population's unique characteristics, this research underscores the predictive capacity of the PK/PD modeling approach in guiding anticoagulant therapy.

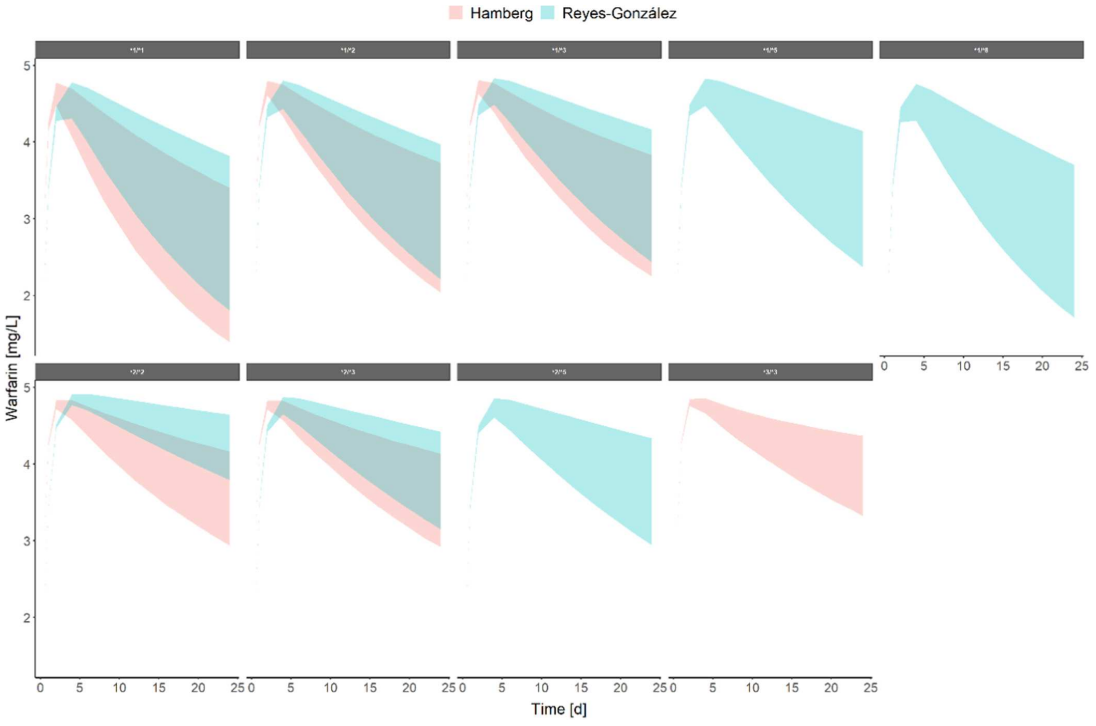

Fig. 4. Comparison of the longitudinal PK model predictions between the structural PK definition of Hamberg et al. (2007, 2010) and Reyes-González et al. (2020).

Funding

This research was financially sponsored in part by NASA grant # 80 NSSC19M0148 from the EPSCoR program, and by grant # 1R16 GM149372 from the National Institute of General Medical Sciences (NIGMS) of the National Institutes of Health (NIH). The content of this manuscript does not represent the views of the National Institutes of Health, NASA or the United States Government. No funded writing assistance was utilized in the production of this manuscript.

CRediT authorship contribution statement

Rodríguez-Fernández Karine: Formal analysis, Methodology, Visualization, Writing – original draft, Writing – review & editing. **Reynaldo-Fernández Gledys:** Data curation, Formal analysis, Methodology, Visualization, Writing – original draft, Writing – review & editing. **Reyes-González Stephanie:** Data curation, Investigation. **de las Barreras Alonso Camila de las Mercedes:** Data curation, Formal analysis, Investigation. **Rodríguez-Vera Leyanis:** Data curation, Methodology. **Vlaar Cornelis:** Conceptualization, Funding acquisition, Resources. **Monbaliu Jean-Christophe M.:** Conceptualization, Funding acquisition, Resources. **Stelzer Torsten:** Conceptualization, Funding acquisition, Resources. **Duconge Jorge:** Conceptualization, Project administration, Resources, Supervision, Validation, Writing – review & editing. **Mangas-Sanjuan Victor:** Formal analysis, Supervision, Validation, Visualization, Writing – original draft, Writing – review & editing.

Declaration of Competing Interest

The authors declare that they have no known competing financial interests or personal relationships that could have appeared to influence the work reported in this paper.

Acknowledgements

We want to thank the patients for voluntarily participating in the original study where data used in this analysis were gathered. A special acknowledgement to the personnel at the Veteran Affairs Caribbean Healthcare System (VACHS) at San Juan, PR for their support.

Appendix A. Supporting information

Supplementary data associated with this article can be found in the online version at doi:10.1016/j.biopha.2023.115977.

References

[1] J. Ansell, J. Hirsh, E. Hylek, A. Jacobson, M. Crowther, G. Palareti, Pharmacology and management of the vitamin K antagonists: American College of Chest Physicians Evidence-Based Clinical Practice Guidelines (8th Edition), Chest 133 (6 Suppl) (2008) 160s–198s, https://doi.org/10.1378/chest.08-0670.

[2] R. Wallin, S.M. Hutson, Warfarin and the vitamin K-dependent gamma-carboxylation system, Trends Mol. Med. 10 (7) (2004) 299–302, https://doi.org/10.1016/j.molmed.2004.05.003.

[3] R. Liu, X. Li, W. Zhang, H.H. Zhou, Comparison of nine statistical model based warfarin pharmacogenetic dosing algorithms using the racially diverse international warfarin pharmacogenetic consortium cohort database, PloS One 10 (8) (2015), e0135784, https://doi.org/10.1371/journal.pone.0135784.

[4] I.G. Asiimwe, M. Pirmohamed, Ethnic diversity and warfarin pharmacogenomics, Front. Pharmacol. 13 (2022), 866058, https://doi.org/10.3389/fphar.2022.866058.

[5] K. Huynh, Milestone 6: Birth of the INR, Nat. Rev. Cardiol. (2017), https://doi.org/10.1038/nrcardio.2017.176.

[6] J.A. Johnson, K.E. Caudle, L. Gong, M. Whirl-Carrillo, C.M. Stein, S.A. Scott, M. T. Lee, B.F. Gage, S.E. Kimmel, M.A. Perera, J.L. Anderson, M. Pirmohamed, T. E. Klein, N.A. Limdi, L.H. Cavallari, M. Wadelius, Clinical Pharmacogenetics Implementation Consortium (CPIC) Guideline for Pharmacogenetics-Guided Warfarin Dosing: 2017 Update, Clin. Pharmacol. Ther. 102 (3) (2017) 397–404, https://doi.org/10.1002/cpt.668.

[7] A.K. Hamberg, M. Wadelius, J.D. Lindh, M.L. Dahl, R. Padrini, P. Deloukas, A. Rane, E.N. Jonsson, A pharmacometric model describing the relationship between warfarin dose and INR response with respect to variations in CYP2C9, VKORC1, and age, Clin. Pharmacol. Ther. 87 (6) (2010) 727–734, https://doi.org/10.1038/clpt.2010.37.

[8] International Warfarin Pharmacogenetics Consortium, N.A. Limdi, M. Wadelius, L. Cavallari, N. Eriksson, D.C. Crawford, M.-T.M. Lee, C.-H. Chen, A. Motsinger-Reif, H. Sagreiya, N. Liu, A.H.B. Wu, B.F. Gage, A. Jorgensen, M. Pirmohamed, J.-G. Shin, G. Suarez-Kurtz, S.E. Kimmel, J.A. Johnson, T.E. Klein, M.J. Wagner, Warfarin pharmacogenetics: a single VKORC1 polymorphism is predictive of dose across 3 racial groups, Blood 115 (18) (2010) 3827–3834, https://doi.org/10.1182/blood-2009-12-255992.

[9] H.Y. Yuan, J.J. Chen, M.T. Lee, J.C. Wung, Y.F. Chen, M.J. Charng, M.J. Lu, C. R. Hung, C.Y. Wei, C.H. Chen, J.Y. Wu, Y.T. Chen, A novel functional VKORC1 promoter polymorphism is associated with inter-individual and inter-ethnic differences in warfarin sensitivity, Hum. Mol. Genet. 14 (13) (2005) 1745–1751, https://doi.org/10.1093/hmg/ddi180.

[10] International Warfarin Pharmacogenetics Consortium, T.E. Klein, R.B. Altman, N. Eriksson, B.F. Gage, S.E. Kimmel, M.T. Lee, N.A. Limdi, D. Page, D.M. Roden, M. J. Wagner, M.D. Caldwell, J.A. Johnson, Estimation of the warfarin dose with clinical and pharmacogenetic data, N. Engl. J. Med. 360 (8) (2009) 753–764, https://doi.org/10.1056/NEJMoa0809329.

[11] M. Pirmohamed, G. Burnside, N. Eriksson, A.L. Jorgensen, C.H. Toh, T. Nicholson, P. Kesteven, C. Christersson, B. Wahlström, C. Stafberg, J.E. Zhang, J.B. Leathart, H. Kohnke, A.H. Maitland-van der Zee, P.R. Williamson, A.K. Daly, P. Avery, F. Kamali, M. Wadelius, A Randomized Trial of Genotype-Guided Dosing of Warfarin, N. Engl. J. Med. 369 (24) (2013) 2294–2303, https://doi.org/10.1056/NEJMoa1311386.

[12] P.J. Avery, A. Jorgensen, A.K. Hamberg, M. Wadelius, M. Pirmohamed, F. Kamali, A proposal for an individualized pharmacogenetics-based warfarin initiation dose regimen for patients commencing anticoagulation therapy, Clin. Pharmacol. Ther. 90 (5) (2011) 701–706, https://doi.org/10.1038/clpt.2011.186.

[13] N.S. Ferder, C.S. Eby, E. Deych, J.K. Harris, P.M. Ridker, P.E. Milligan, S. Z. Goldhaber, C.R. King, T. Giri, H.L. McLeod, R.J. Glynn, B.F. Gage, Ability of VKORC1 and CYP2C9 to predict therapeutic warfarin dose during the initial weeks of therapy, J. Thromb. Haemost.: JTH 8 (1) (2010) 95–100, https://doi.org/10.1111/j.1538-7836.2009.03677.x.

[14] U.S. Foods and Drug Administration (FDA), Coumadin (warfarin sodium) tablets label – FDA. Full prescribing information. ⟨https://www.accessdata.fda.gov/drugsatfda_docs/label/2011/009218s107lbl.pdf⟩, 2011 (Accessed 5 August 2023).

[15] A.K. Hamberg, M. Wadelius, L.E. Friberg, T.T. Biss, F. Kamali, E.N. Jonsson, Characterizing variability in warfarin dose requirements in children using modelling and simulation, Br. J. Clin. Pharmacol. 78 (1) (2014) 158–169, https://doi.org/10.1111/bcp.12308.

[16] A.K. Hamberg, L.E. Friberg, K. Hanséus, B.M. Ekman-Joelsson, J. Sunnegårdh, A. Jonzon, B. Lundell, E.N. Jonsson, M. Wadelius, Warfarin dose prediction in children using pharmacometric bridging–comparison with published pharmacogenetic dosing algorithms, Eur. J. Clin. Pharmacol. 69 (6) (2013) 1275–1283, https://doi.org/10.1007/s00228-012-1466-4.

[17] A.K. Hamberg, M.L. Dahl, M. Barban, M.G. Scordo, M. Wadelius, V. Pengo, R. Padrini, E.N. Jonsson, A PK-PD model for predicting the impact of age, CYP2C9, and VKORC1 genotype on individualization of warfarin therapy, Clin. Pharmacol. Ther. 81 (4) (2007) 529–538, https://doi.org/10.1038/sj.clpt.6100084.

[18] U. Falkenhagen, J. Knöchel, C. Kloft, W. Huisinga, Deriving mechanism-based pharmacodynamic models by reducing quantitative systems pharmacology models: an application to warfarin, CPT: Pharmacomet. Syst. Pharmacol. 12 (4) (2023) 432–443, https://doi.org/10.1002/psp4.12903.

[19] J. Deng, V. Vozmediano, M. Rodriguez, L.H. Cavallari, S. Schmidt, Genotype-guided dosing of warfarin through modeling and simulation, Eur. J. Pharm. Sci. Off. J. Eur. Fed. Pharm. Sci. 109s (2017) S9–s14, https://doi.org/10.1016/j.ejps.2017.05.017.

[20] S. Reyes-González, C. de Las Barreras, G. Reynaldo, L. Rodríguez-Vera, C. Vlaar, V. L. Mejías, J.M. Monbaliu, T. Stelzer, V. Mangas, J. Duconge, Genotype-driven pharmacokinetic simulations of warfarin levels in Puerto Ricans, Drug Metab. Pers. Ther. (2020), https://doi.org/10.1515/dmdi-2020-0135.

[21] E. Comets, K. Brendel, F. Mentré, Computing normalised prediction distribution errors to evaluate nonlinear mixed-effect models: the npde add-on package for R, Comput. Methods Prog. Biomed. 90 (2) (2008) 154–166, https://doi.org/10.1016/j.cmpb.2007.12.002.

[22] M. Bergstrand, A.C. Hooker, J.E. Wallin, M.O. Karlsson, Prediction-corrected visual predictive checks for diagnosing nonlinear mixed-effects models, AAPS J. 13 (2) (2011) 143–151, https://doi.org/10.1208/s12248-011-9255-z.

[23] L. Lindbom, P. Pihlgren, E.N. Jonsson, PsN-Toolkit–a collection of computer intensive statistical methods for non-linear mixed effect modeling using NONMEM, Comput. Methods Prog. Biomed. 79 (3) (2005) 241–257, https://doi.org/10.1016/j.cmpb.2005.04.005.

[24] E.M. Hylek, S. Regan, A.S. Go, R.A. Hughes, D.E. Singer, S.J. Skates, Clinical predictors of prolonged delay in return of the international normalized ratio to within the therapeutic range after excessive anticoagulation with warfarin, Ann. Intern. Med. 135 (6) (2001) 393–400, https://doi.org/10.7326/0003-4819-135-6-200109180-00008.

[25] S.M. Saffian, S.B. Duffull, R.L. Roberts, R.C. Tait, L. Black, K.A. Lund, A. H. Thomson, D.F. Wright, Influence of Genotype on Warfarin Maintenance Dose Predictions Produced Using a Bayesian Dose Individualization Tool, Ther. Drug Monit. 38 (6) (2016) 677–683, https://doi.org/10.1097/ftd.0000000000000347.

[26] D.F. Hernandez-Suarez, K. Claudio-Campos, J.E. Mirabal-Arroyo, B.A. Torres-Hernández, A. López-Candales, K. Melin, J. Duconge, Potential of a pharmacogenetic-guided algorithm to predict optimal warfarin dosing in a high-risk Hispanic patient: role of a novel NQO1*2 Polymorphism, J. Invest. Med. High. Impact Case Rep. 4 (4) (2016), 2324709616682049, https://doi.org/10.1177/2324709616682049.

[27] N. El Rouby, L. Rodrigues Marcatto, K. Claudio, L. Camargo Tavares, H. Steiner, M. R. Botton, S.A. Lubitz, E.N. Fallon, K. Yee, J. Kaye, S.A. Scott, J. Karnes, P. Caleb Junior de Lima Santos, J. Duconge, L.H. Cavallari, Multi-site Investigation of Genetic Determinants of Warfarin Dose Variability in Latinos, Clin. Transl. Sci. 14 (1) (2021) 268–276, https://doi.org/10.1111/cts.12854.

[28] PharmGKB website, Warfarin Pathway Pharmacodynamics. ⟨https://www.pharmgkb.org/pathway/PA145011114⟩, (Accessed 5 August 2023).

[29] PAGE. Abstracts of the Annual Meeting of the Population Approach Group in Europe. ISSN 1871–6032 Reference: PAGE 31 (2023) Abstr 10711 ⟨[]⟨www.page-meeting.org/?abstract=10711⟩].

[30] J. Hirsh, J. Dalen, D.R. Anderson, et al., Oral anticoagulants: mechanism of action, clinical effectiveness, and optimal therapeutic range, Chest 119 (1_suppl) (2001) 8S–21S.

[31] A.E. Rettie, L.C. Wienkers, F.J. Gonzalez, W.F. Trager, K.R. Korzekwa, Impaired (S)-warfarin metabolism catalysed by the R144C allelic variant of CYP2C9, Pharmacogenetics 4 (1) (1994) 39–42.

SUPLEMENTARY MATERIAL

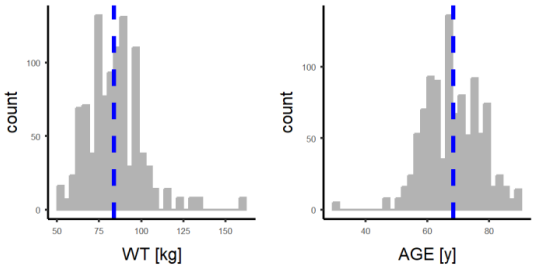

Figure S1. Distribution of body weight and age covariates included in the dataset. WT: body weight.

Table S1. Final parameter estimates of the base population pharmacokinetic-pharmacodynamic model of warfarin in Caribbean Hispanic patients

	Population PK Model Estimates		**Bootstrap Results**	
Fixed-Effect	**Value**	**Shrinkage (%)**	**Median**	**95%CI**
MTT_1 (d)	1.13 FIX		1.13 FIX	
MTT_2 (d)	4.62 FIX		4.62 FIX	
Baseline	1.86		1.88	1.45-2.17
IC_{50}	15.4		15.3	11.9-19.2
γ	1.29		1.30	1.14-1.52
Inter-individual variability				
Baseline (%)	25	16	24	20-33
IC_{50} (%)	35	43	36	27-40
Residual unexplained variability				
Proportional (%)	27	7	26	21-31

MTT: mean transit time; IC_{50}: concentration resulting in 50% of I_{max}.

A

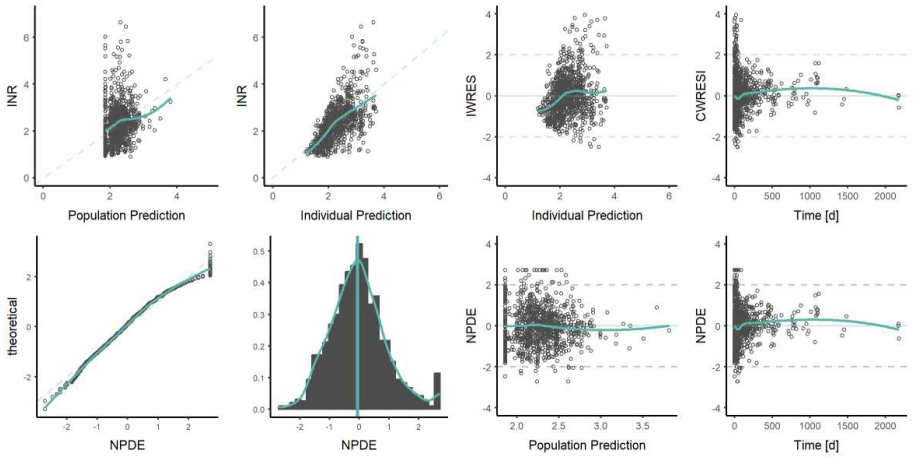

B

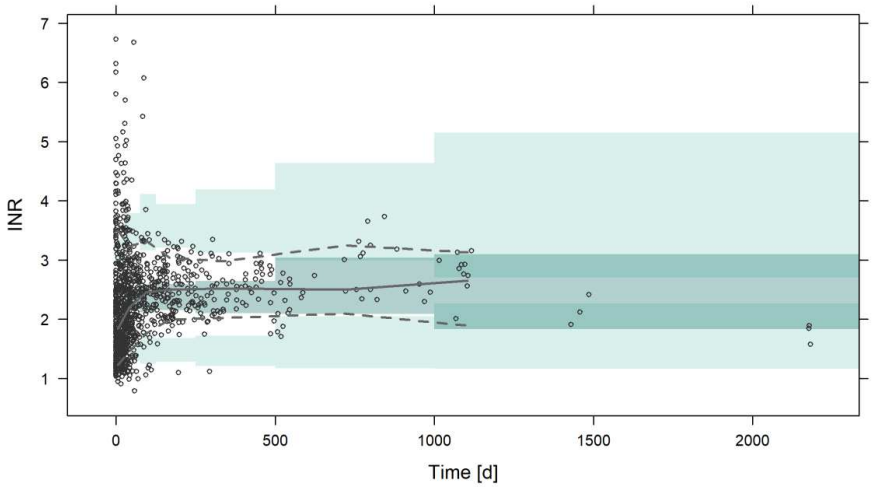

Figure S2. A. Goodness-of-fit and NPDE plots and of the base population pharmacokinetic-pharmacodynamic model of INR after warfarin administration. The green solid line represents the non-linear regression, and the grey dotted line represents the line of identity. IWRES: individual weighted residuals, CWRESI: conditional weighted residuals, NPDE: Normalised prediction distribution errors. INR: international normalized ratio. **B.** Prediction-Corrected Visual Predictive check of the base population pharmacodynamic model of INR after warfarin administration. Grey lines represent the 2.5th, 50th and 97.5th experimental percentiles. Green shaded areas represent the 95% prediction interval of the 2.5th, 50th and 97.5th percentiles. Empty grey dots represent the experimental INR observations. INR: international normalized ratio.

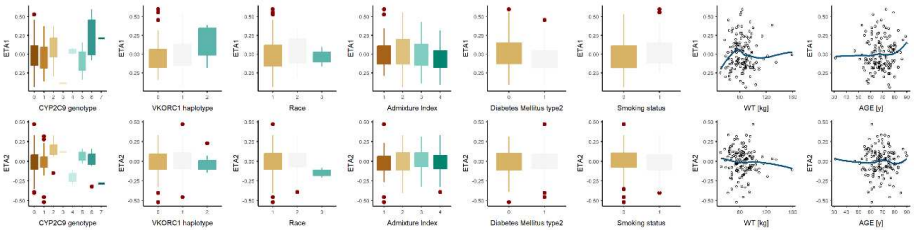

Figure S3. Eta-distribution plots of the continuous and categorical covariates available using the base population PK/PD model. WT: body weight; *CYP2C9*: cytochrome P4502C9 gene; *VKORC1*: vitamin K epoxide reductase complex subunit 1 gene.

A

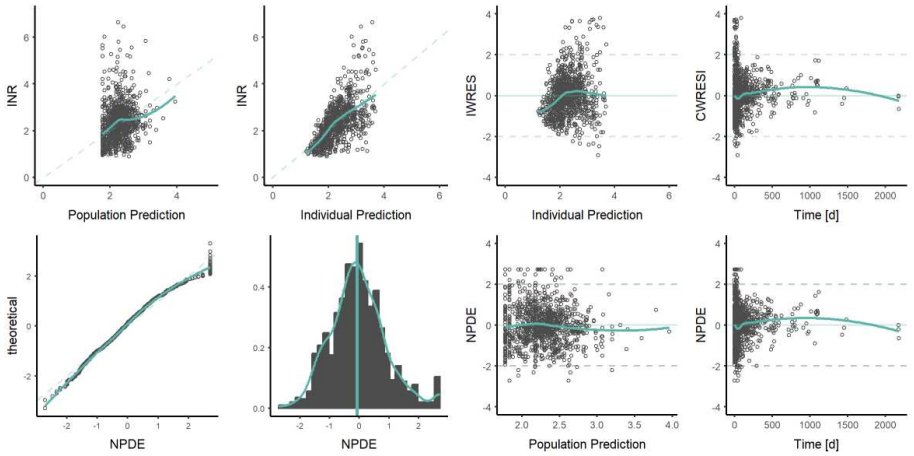

B

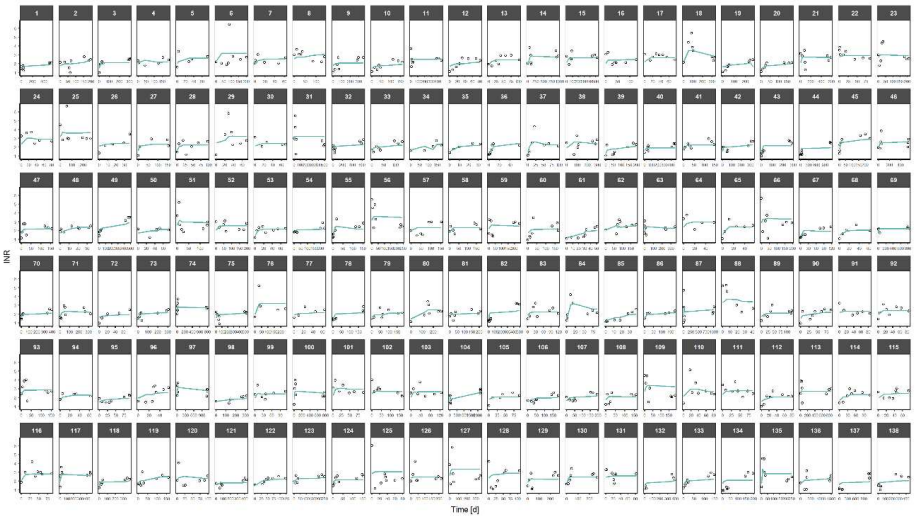

Figure S4. A. Goodness-of-fit and NPDE plots and of the final population pharmacokinetic-pharmacodynamic model of INR after warfarin administration. The green solid line represents the non-linear regression, and the grey dotted line represents the line of identity. IWRES: individual weighted residuals, CWRESI: conditional weighted residuals, NPDE: Normalised prediction distribution errors. INR: international normalized ratio. **B.** Individual predicted and observed INR after warfarin administration in Hispanic Caribbean patients obtained with the final PK/PD model. The blue solid line represents the non-linear regression and empty grey dots represent the experimental INR observations. INR: international normalized ratio.

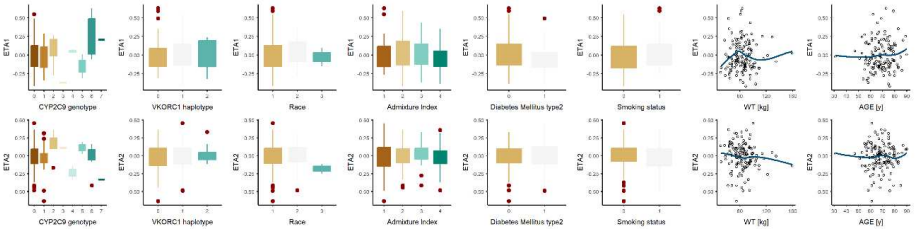

Figure S5. Eta-distribution plots of the continuous and categorical covariates available using the final population PK/PD model.

Annex 4: Model-Informed Precision Dosing for Personalized Ustekinumab Treatment in Plaque Psoriasis

pharmaceutics

MDPI

Article

Model-Informed Precision Dosing for Personalized Ustekinumab Treatment in Plaque Psoriasis

Karine Rodríguez-Fernández [1,2,†], Javier Zarzoso-Foj [1,2,†], Marina Saez-Bello [3], Almudena Mateu-Puchades [4], Antonio Martorell-Calatayud [5], Matilde Merino-Sanjuan [1,2], Elena Gras-Colomer [6], Monica Climente-Martí [3] and Victor Mangas-Sanjuan [1,2,*]

[1] Department of Pharmacy and Pharmaceutical Technology and Parasitology, University of Valencia, 46100 Valencia, Spain; karofer@alumni.uv.es (K.R.-F.); javier.zarzoso@uv.es (J.Z.-F.); matilde.merino@uv.es (M.M.-S.)
[2] Interuniversity Research Institute for Molecular Recognition and Technological Development, Polytechnic University of Valencia-University of Valencia, 46100 Valencia, Spain
[3] Pharmacy Service, Doctor Peset University Hospital, Foundation for the Promotion of Health and Biomedical Research in the Valencian Region (FISABIO), 46017 Valencia, Spain; saez_marbel@gva.es (M.S.-B.); climente_mon@gva.es (M.C.-M.)
[4] Dermatology Service, Doctor Peset University Hospital, Foundation for the Promotion of Health and Biomedical Research in the Valencian Region (FISABIO), 46017 Valencia, Spain; mateu_alm@gva.es
[5] Dermatology Service, Hospital Manises of Valencia, 46940 Valencia, Spain; martorell_antcal@gva.es
[6] Pharmacy Service, Hospital Manises of Valencia, 46940 Valencia, Spain; gras_ele@gva.es
* Correspondence: victor.mangas@uv.es; Tel.: +34-963-543-351
† These authors contributed equally to this work.

Abstract: Background/Objectives: Implementing model-informed precision dosing (MIPD) strategies guided by population pharmacokinetic/pharmacodynamic (PK/PD) models could enhance the management of inflammatory diseases such as psoriasis. However, the extent of individual experimental data gathered during MIPD significantly influences the uncertainty in estimating individual PK/PD parameters, affecting clinical dose selection decisions. Methods: This study proposes a methodology to individualize ustekinumab (UTK) dosing strategies for 23 Spanish patients with moderate to severe chronic plaque psoriasis., considering the uncertainty of individual parameters within a population PK/PD model. Results: An indirect response model from previous research was used to describe the PK/PD relationship between UTK serum concentrations and the Psoriasis Area and Severity Index (PASI) score. A maximum inhibition drug effect (I_{max}) model was selected, and a first-order remission constant rate of psoriatic skin lesion (k_{out} = 0.016 d^{-1}) was estimated. Conclusions: The MIPD approach predicted that 35% and 26% of the patients would need an optimized and intensified dosage regimen, respectively, compared to the regimen typically used in clinical practice. This analysis demonstrated its utility as a tool for selecting personalized UTK dosing regimens in clinical practice in order to optimize the probability of achieving targeted clinical outcomes in patients with psoriasis.

Keywords: psoriasis; ustekinumab; pharmacokinetic/pharmacodynamic

Citation: Rodríguez-Fernández, K.; Zarzoso-Foj, J.; Saez-Bello, M.; Mateu-Puchades, A.; Martorell-Calatayud, A.; Merino-Sanjuan, M.; Gras-Colomer, E.; Climente-Martí, M.; Mangas-Sanjuan, V. Model-Informed Precision Dosing for Personalized Ustekinumab Treatment in Plaque Psoriasis. *Pharmaceutics* **2024**, *16*, 1295. https://doi.org/10.3390/pharmaceutics16101295

Academic Editors: Katarina Vučićević and Branislava Miljković

Received: 3 September 2024
Revised: 29 September 2024
Accepted: 2 October 2024
Published: 4 October 2024

1. Introduction

The management of psoriasis, a chronic immune-mediated condition, has been revolutionized with the introduction of therapeutic monoclonal antibody (mAb), with ustekinumab (UTK) constituting one of the available treatment choices [1,2]. UTK targets with high specificity and affinity the shared p40 subunit of interleukin (IL)-12 and IL-23 [3,4]. Both cytokines play an important role in the immune cascade that leads to psoriasis, particularly in modulating the differentiation of naïve T-cells into Th1 and Th17 cells [5–7].

Under the brand name Stelara® (Janssen Biotech, Inc., Horsham, PA, USA) UTK is available in solution for injection and can be administered subcutaneously. The latter formulation offers flexibility in administration, autoinjectors being the most recent [8].

The clinical development programs for UTK have been the most extensive for a biologic agent. Phase III clinical trials [9–12] for UTK in psoriasis have specified a significant decrease in Psoriasis Area and Severity Index (PASI) scores, supporting considerable improvements in the severity of the disease. Additionally, UTK has been directly compared to the tumor necrosis factor inhibitor etanercept [13], representing the first-ever head-to-head comparison of biological agents in psoriasis treatment. UTK is dosed according to body weight, as indicated in the summary of product characteristics (SmPC) [8]. For individuals weighing $\leq$ 100 kg and those weighing > 100 kg, a 45 and 90 mg dose is given, respectively, at weeks 0 and 4 (induction period), followed by subsequent doses every 12 weeks (the maintenance period). UTK typically reaches a steady state within approximately 28 weeks of regular dosing.

A population pharmacokinetic (PK) modeling approach was developed for UTK in clinical trial adult patients with moderate to severe plaque psoriasis [14] and psoriatic arthritis [15] and in real-world data patients [16], using a one-compartment model with first-order absorption and first-order-elimination, demonstrating a comparable PK between adult patients from clinical trials and real-world data. The same model was developed in clinical trial pediatric patients with moderate to severe plaque psoriasis [17]. In addition, an integrated population PK analysis was performed to describe the PK behavior of UTK in healthy subjects and individuals with psoriasis, psoriatic arthritis, Crohn's disease, and ulcerative colitis [18]. The chosen structural PK model for UTK was a two-compartment open model incorporating first-order absorption and elimination kinetics. Notably, parameters such as clearance (CL) and the volume of distribution were found to increase nonlinearly with body weight. This model effectively incorporates the PK characteristics of UTK across all approved inflammatory conditions and in healthy individuals, providing a consistent framework for understanding UTK's PK profile in diverse patient populations. The relationship between serum concentration–time data with longitudinal measures of the PASI in patients with moderate to severe plaque psoriasis was described via an indirect response model in a clinical trial and real-world patient data [16,17,19,20]. The contribution of the UTK effect to the inhibition of the formation rate of psoriatic skin lesions was described by a maximum inhibition drug effect (I_{max}) model [21].

Dermatologists often follow labeled dosing recommendations for initial treatment with UTK, which may not be optimal or safe for every patient [22]. Due to variable psoriasis disease progression in individual patients and the variability in response, they perform changes in the dosing regimen of UTK during the maintenance period of treatment. These changes in routine clinical practice are called optimizations and intensifications of SmPC dosage regimens. Dose regimen optimization involves maintaining the dose but extending the dosing interval or decreasing the dose while maintaining the dosing interval. On the contrary, dose regimen intensification implies maintaining the dose but decreasing the dosing interval or increasing the dose while maintaining the dosing interval. With this approach, the risk of adverse events increases due to drug concentrations that are either supratherapeutic or subtherapeutic because of the lack of a model-informed decision-making process [23]. Additionally, the methods for individualization commonly used in standard clinical practice, such as those based on clinical response and therapeutic drug monitoring (TDM), demand strict adherence to the sampling schedule. Intervention typically occurs only after the drug has reached a steady state, and adjustments are made by comparing the patient's exposure to a target range. If the exposure falls outside this range, the dose is adjusted under the assumption of dose–exposure proportionality at steady state or based on clinical experience [24–27].

Consequently, dermatologists require a flexible approach for psoriasis treatment that considers non-labeled dosing regimens and transitions between different therapeutic modalities of psoriasis to select the optimal treatment for each patient and to solve the cases of suboptimal response, the loss of efficacy over time, or the emergence of adverse effects. These challenges highlight the critical importance of transitioning to model-informed precision dosing (MIPD) strategies guided by population pharmacokinetic/pharmacodynamic

(PK/PD) models. With MIPD, any timed sample can be utilized, allowing interventions at any point, from before the first dose to when a steady state is reached. The intervention method involves calculating a dose that achieves a predefined PK/PD target [27–32]. Implementing PK/PD models in dosing decisions for psoriasis management improves precision dosing and addresses the interindividual variability (IIV) observed in psoriasis treatment responses, enhancing therapeutic outcomes and patient safety [14,17,19,33]. Therefore, the objective of this study was to propose a methodology capable of individualizing dosing strategies of UTK in patients with moderate to severe chronic plaque psoriasis based on the uncertainty of the individual parameters of a population PK/PD model.

2. Materials and Methods

2.1. Study Design

A post-authorization, prospective, and observational clinical practice follow-up study was conducted on Spanish patients with moderate to severe chronic plaque psoriasis from Manises Hospital of Valencia. The authors affirm that all procedures undertaken in this study adhere to the ethical standards established by the pertinent national and institutional committees overseeing human experimentation. Furthermore, they ensure compliance with the Helsinki Declaration of 1975, with revisions made in 2008. The study received approval from the Ethics Committee of La Fe University and Polytechnic Hospital (protocol code VMS-UTK-2020-01 EPA-SP). All participants provided written informed consent. The enrollment period spanned from February 2021 to December 2022, encompassing individuals who had received at least one dose of UTK (Stelara®) and who were under treatment at the time of inclusion. The patients included in the study were receiving dosage regimens individualized (optimized/intensified or not) and authorized by the dermatologist based on their clinical response. Exclusion criteria included individuals below 18 years of age, pregnant individuals, and those with cognitive impairment. Treatment-related variables such as dosage regimen, time, and line of treatment were collected for each patient. Moreover, demographic data were extracted from the hospital's electronic clinical records, including age, sex, weight, and height.

2.2. Blood Sampling and Analytical Quantification of Samples

Patients were administered UTK via subcutaneous injection in the abdomen or upper thigh. The patients received the following dosage regimen as a current treatment: 45 or 90 mg of UTK every 12, 14, and 16 weeks (q12w, q14w, and q16w), 45 mg of UTK every 18 weeks (q18w), and 90 mg of UTK every 8, 10, and 15 weeks (q8w, q10w, q15w). Blood samples for PK analysis were collected using plain red vacutainer tubes immediately before UTK administration and approximately 2, 6, 10, 12, 14, 16, and 18 weeks afterward. After centrifugation, serum samples were transferred to separate tubes and frozen at temperatures between −20 and −80 °C until processing. Serum concentrations of UTK were measured in the laboratory of Manises Hospital using an enzyme-linked immunosorbent assay (ELISA; Promonitor-UTK assay, Progenika Biopharma, Grifols®, Derio, Spain). The Promonitor-UTK quantifies concentrations of UTK in the range of 0.63–20 μg/mL.

2.3. Psoriasis Area and Severity Index Score Measurement

In the dermatology service from Manises Hospital, patients initiating UTK therapy undergo PASI assessments every 3 months during the first year of treatment. Following the initial year, PASI evaluations occur every 6 months. Baseline PASI values, recorded at the onset of UTK therapy, were extracted from patient clinical records. All available PASI scores documented in patient clinal records during the approximately 1.5-year follow-up period were collected.

2.4. Modeling Data Analysis

Figure 1 summarizes the modeling strategy performed. The data analysis was initiated by simulation using the population PK parameters of the 7 reference PK models published

for UTK [14–18,34]. This aided in identifying the model that most accurately represented our data. Subsequently, we applied the chosen model along with the individual UTK serum concentrations gathered during TDM to estimate individual PK parameters.

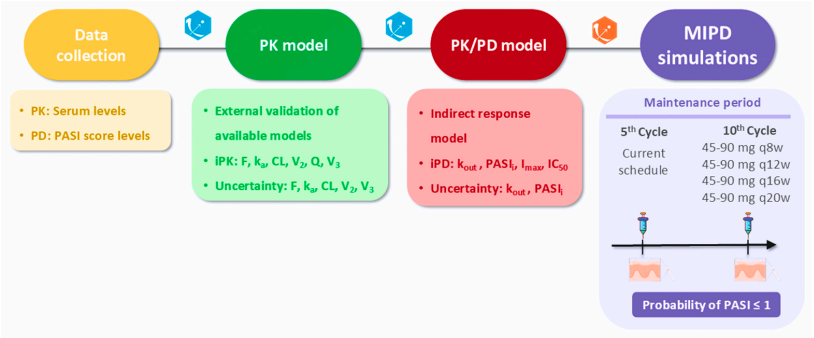

Figure 1. Modeling workflow. PK: pharmacokinetic; PD: pharmacodynamic; PASI: Psoriasis Area and Severity Index; iPK: individual pharmacokinetic parameter; iPD: individual pharmacodynamic parameter; F: bioavailability; k_a: absorption rate constant; CL: clearance; Q: intercompartmental transfer clearance; V_2: central volume of distribution; V_3: peripheral volume of distribution; k_{out}: first-order remission constant rate of psoriatic skin lesion; I_{max}: maximum inhibition drug effect model; $PASI_i$: estimated baseline levels of PASI response; IC_{50}: concentration of the drug needed to inhibit 50% of the response; MIPD: model-informed precision dosing; q8w: once every 8 weeks, q12w: once every 12 weeks; q16w: once every 16 weeks; q20w: once every 20 weeks.

A previously published indirect response model with PASI synthesis inhibition [16] was considered to describe the PK/PD relationship between UTK serum concentrations and the PASI (Figure 2). The ordinary differential equations of the PK/PD model can be found in the Supplementary Materials. This model structure was also previously applied to other mAbs designed for the treatment of psoriasis [19,35–38]. Linear, I_{max}, and sigmoid drug effects functions were evaluated [21].

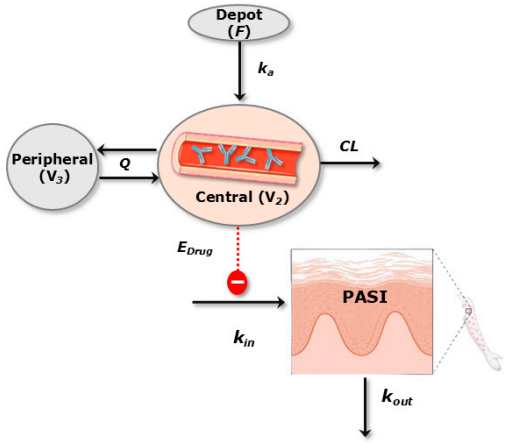

Figure 2. Schematic representation of the final PK/PD model. E_{Drug}: effect of the drug; k_{in}: zero-order progression constant rate of psoriatic skin lesion.

Baseline levels of PASI response ($PASI_i$) were estimated using the B2 method [39], where $PASI_i$ represents the individual predicted baseline level of the PASI, $PASI_{i,o}$ is the

individual observed baseline and $\eta_{i,RV}$ is the estimated individual random component accounting for the difference between $PASI_i$ and $PASI_{i,o}$. This variable has a mean equal to zero and, during parameter estimation, is restricted to having the same variance as the residual unexplained variability (RUV) (Equation (1)). Consequently, we assumed that the variability observed in the rest of the data also applies to the baseline data.

$$PASI_i = PASI_{i,0} \cdot e^{\eta_{i,RV}} \quad (1)$$

The selection of the PK/PD model was based on the comparison of the minimum value of the objective function, a visual exploration of goodness-of-fit plots and the precision of model parameters stated in the standard errors. An evaluation of the selected PK/PD models was performed through simulation-based diagnostics prediction-corrected visual predictive checks (pcVPCs) [40,41]. All data analyses were performed based on the population approach with the software Monolix 2024R1 (Lixoft SAS, a Simulations Plus company, Lancaster, CA, USA) [42]. For graphical and statistical analysis, R software (http://cran.r-project.org, version 4.4.1, accessed on 30 September 2024) was employed [43,44].

2.5. Individual Dosing Regimen Strategy

To explore the performance of the final PK/PD model and its impact on clinical practice, the optimal MIPD regimen in each patient was determined, for which the PK and PD individual parameters and their uncertainties were considered. The individual conditional distributions of PK/PD parameters were estimated in Monolix, which represented the PK and PD individual parameter estimates and their corresponding uncertainty [45]. Uncertainty refers to the degree of accuracy with which PK and PD individual parameters can be determined based on the observed data and covariate value for that individual, considering that the individual belongs to the population for which the typical parameter value (fixed effects) and the variability (standard deviation of the random effects) were previously estimated [45,46].

The determination of individual conditional distributions ($p(\psi_i|y_i)$, with ψ_i being the individual parameters for individual i and y_i the data observations for individual i), was performed with a Markov Chain Monte Carlo (MCMC) procedure called the Metropolis–Hastings algorithm that samples parameter values from these distributions, using the following expression:

$$p(\psi_i|y_i) = \frac{p(y_i|\psi_i) \cdot p(\psi_i)}{p(y_i)} \quad (2)$$

where $p(y_i|\psi_i)$ is the conditional density function of the data when knowing the individual parameter values, $p(\psi_i)$ is the density function for the individual parameters and $p(y_i)$ is a constant that represents the likelihood.

With individual conditional distributions, one hundred clones per patient were generated and were imputed to Simulx 2024R1 (Lixoft SAS, a Simulations Plus company) [47] to predict through stochastic simulations, and the PASI levels expected at the 5th and 10th cycle (maintenance period) of treatment with UTK were as follows:

- 5th cycle: individual simulations of dosing regimens were generated considering 5 cycles of UTK (steady-state conditions) administration with the administered dosage regimen of each patient.
- 10th cycle: following the 5th cycle, we simulated the combination of alternative dose levels (45 and 90 mg) with different posology (q8w, q12w, q16w, and q20w) for each patient during 5 more cycles of treatment with UTK.

For each patient, the probabilities of achieving the response target (a PASI score ≤ 1) with each simulated dose regimen were calculated in cycle 5 and 10 using the following formula:

$$Probability = \frac{n_{PASI}}{T_{PASI}} \times 100 \quad (3)$$

where n_{PASI} represent the amount of simulated PASI score values that reach the response target (a PASI score ≤ 1), and T_{PASI} represent the total amount of simulated PASI score values (100 clones). In the 10th cycle, the regimen with which the patient achieved a probability $\geq 90\%$ (i.e., $\geq$90 virtual patients) was selected as the final dosage regimen. In case the patient achieved the response target with more than one dosage regimen, the optimized dosing regimen was selected as the final regimen, which represented a maintenance of the dose over a wider dosing interval or a decrease in the dose within the same dosing interval. The dosage regimen selected in the 10th cycle was compared with the current dosage regimen from the clinical practice of each patient to determine if the patients continued with their current regimen or required a change (optimization or intensification) in the dosage regimen.

3. Results

3.1. Study Population

The modeling dataset consisted of 23 patients including 75 observations in serum samples (PK), a baseline PASI ($PASI_{i,0}$) for each patient, and 117 individual PASI (PD). Table 1 summarizes the characteristics of the study, including demographic data, comorbidities, TDM data, and treatment characteristics that describe the current dosage regimen from the clinical practice of the subjects enrolled.

Table 1. Summary of patients' characteristics and PK/PD experimental data collected during TDM.

	Mean ± SD	**Range**	**n (%)**
Demographic data			
Age (years)	62 ± 8.19	45–76	
Body weight (kg)	92 ± 18.4	70–135	
Height (m)	1.67 ± 0.06	1.54–1.83	
BMI (kg/m^2)	32.3 ± 6.8	24–50.19	
Gender (male)			14 (64)
Treatment period (years)	5.43 ± 3.3	0.304–11.4	
Biological "naive"			20 (87)
Comorbidities			
AHT			2 (9)
Dyslipidemia			2 (9)
Diabetes			1 (4)
Obesity			4 (16)
Psoriatic arthropathy			2 (9)
Non-alcoholic fatty liver			2 (9)
Anxious–depressive disorder			2 (9)
Others			4 (16)
TDM data			
Total of patients			23
UTK concentration (mg/L)	4.1 ± 3.06	0.27–12.7	
Total of UTK concentrations			75
PASI (no units)	1.096 ± 2.13	0–12	
Total of PASIs			117
$PASI_{i,0}$	14.4 ± 6.23	5–31.9	

Current treatment characteristics							
SmPC		Optimized		Intensified		Summary	
45 mg q12w	1	45 mg q14w	1	90 mg q10w	1	SmPC	9 (40%)
90 mg q12w	8	45 mg q16w	3	90 mg q8w	2	Optimized	11 (48%)
		45 mg q18w	1			Intensified	3 (12%)
		90 mg q14w	1				
		90 mg q15w	2				
		90 mg q16w	3				

SD: standard deviation; BMI: body mass index; AHT: arterial hypertension; TDM: therapeutic drug monitoring; UTK: ustekinumab; PASI: Psoriasis Area and Severity Index; $PASI_{i,o}$: individual observed baseline; SmPC: summary of product characteristics; q8w: once every 8 weeks; q10w: once every 10 weeks; q12w: once every 12 weeks; q14w: once every 14 weeks; q15w: once every 15 weeks; q16w: once every 16 weeks; q18w: once every 18 weeks.

3.2. Population PK Model

A two-compartment model with first-order absorption and linear disposition processes, previously published by Shao et al. [18], was considered as the population PK model (Figure 2). Then, the statistical significance of covariates included in the reference model was tested with the available information and patient population collected. Only the effect of body weight was maintained on CL, intercompartmental transfer clearance (Q), the central volume of distribution (V_2), and the peripheral volume of distribution (V_3). Therefore, body weight was the only covariate that influenced the determination of individual PK parameter values. The results from the model evaluation exercise indicate that the model could capture the individual PK profiles with adequate accuracy since most of the observations were aligned to the identity line (Figure 3). The pcVPC of the PK model is shown in Supplementary Figure S1.

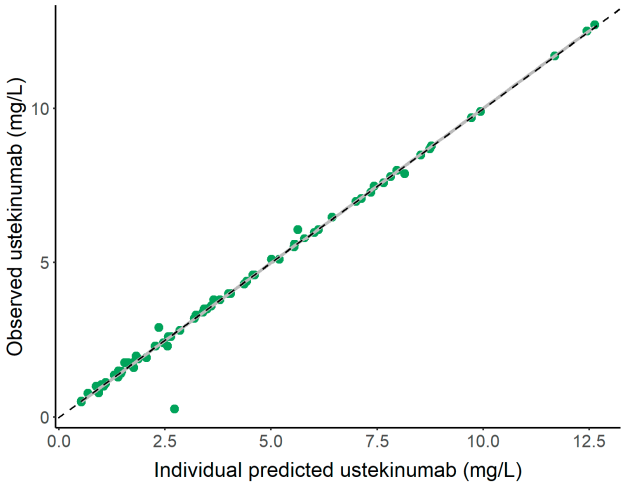

Figure 3. Individual predicted vs. the observed concentrations of UTK in patients with chronic plaque psoriasis.

3.3. Population PK/PD Model

The relationship between UTK concentration and PASI observations was described by an indirect response [48] in which UTK inhibited the zero-order progression constant rate of psoriatic skin lesion (k_{in}) through an I_{max} model. The first-order remission constant rate of psoriatic skin lesion (k_{out}) and the baseline PASI levels using the B2 method were estimated. The concentration of the drug needed to inhibit 50% of the response (IC_{50}) was fixed to a published value [16]. Longitudinal individual PK and PD profiles are shown in Figure 4. Overall, the PK/PD model can characterize the longitudinal behavior of the PASI at the individual level, suggesting that the current framework considers properly the combined drug effect and PASI turnover. The pcVPC of the PK/PD model is shown in Supplementary Figure S2. Parameter estimates of the final population PK/PD model are summarized in Table 2. The mean and standard deviation of individual PK/PD parameters are summarized in Supplementary Tables S1 and S2, respectively.

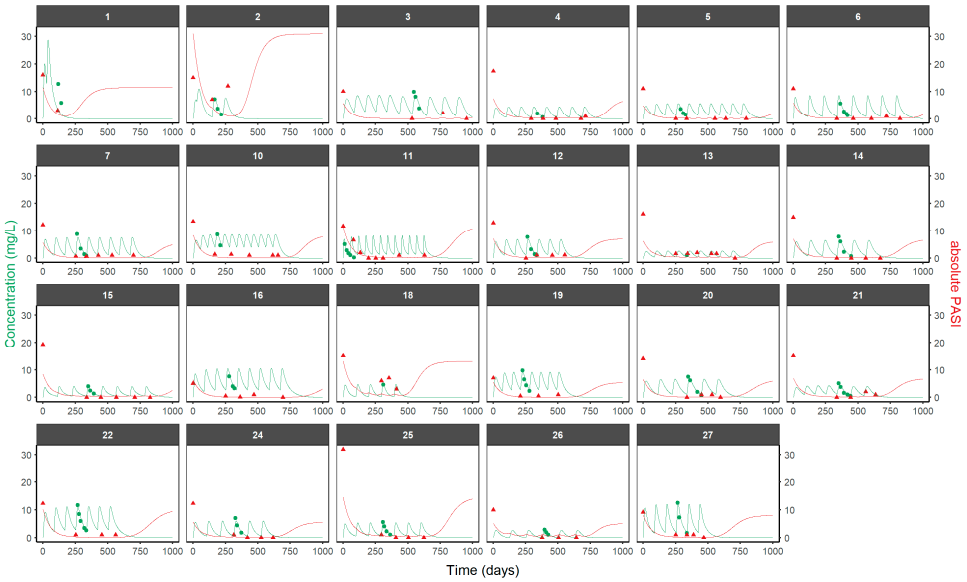

Figure 4. Individual predicted and observed UTK serum concentrations (green) and PASI (red) after UTK administration in patients with chronic plaque psoriasis. The line represents the individual prediction, and the green and red dots represent the UTK and PASI observations, respectively.

Table 2. Population PK/PD estimates after administration of UTK in patients with psoriasis.

Parameter (Units)	Value	RSE (%)
Fixed effect		
k_{out} (d^{-1})	0.016	22
I_{max}	0.97	0.7
IC_{50} (mg/L)	0.07 FIX	
Inter-individual variability		
k_{out} (%)	55.87	38.9
Residual unexplained variability		
Error (%)	0.86	9.95

k_{out}: first-order remission constant rate of psoriatic skin lesion; I_{max}: maximum inhibition drug effect; IC_{50}: concentration of the drug needed to inhibit 50% of the response.

3.4. Individual Dosing Regimen Evaluation

Probabilities across the cycles of treatment evaluated per patient are represented in Supplementary Figure S3. The MIPD strategy predicted that 8/23 (35%) and 6/23 (26%) of patients would require an optimized and intensified dosage regimen, respectively, compared with the current regimen received in clinical practice for the maintenance period. A change to the approved regimen of 45 mg q12w is proposed in 3/23 (13%), representing 38% (3/8) of the total optimized patients. Also, in the optimized patients, non-labeled dosing regimens of 45 mg q16w and 45 mg q8w are suggested in 2/8 (24%) and 3/8 (38%) of patients, respectively. Regarding the patients with intensified dosage regimens, a change to 90 mg q8w (3/6) and 45 mg q8w (3/6), respectively, is recommended. No change in the dosing regimen was predicted in 5/23 (22%) patients. This MIPD strategy additionally allowed us to identify that 4/23 (17%) patients would not achieve the efficacy endpoint selected (a 90% probability of a PASI ≤ 1), contributing to the early identification of patients with therapeutic failure (Figure 5).

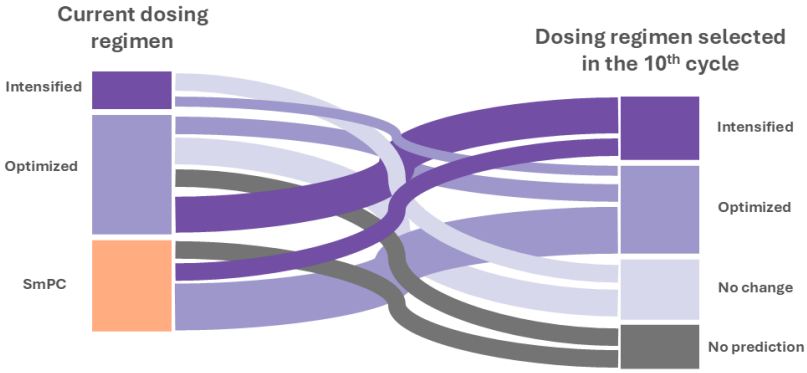

Figure 5. Sankey diagram to indicate the main flows of changes in the individual dose regimen from the current dosage regimen of clinical practice to the predicted dosage regimen in the maintenance period of treatment with UTK (cycle 10). SmPC: summary of product characteristics.

PK and PD simulations with the current dosage regimen from the clinical practice of each subject and the individual optimal dosing regimen established in the 10th cycle are depicted in Supplementary Figure S4. Figure 6 represents the relationship between the absolute PASI and a trough concentration at a steady state ($C_{trough\text{-}ss}$) for each patient, with all dosage regimens tested. Overall, the results suggest a non-linear relationship, indicating that the range of concentration 1.6–1.8 mg/L allows to achieve 90% of patients with a PASI ≤ 1.

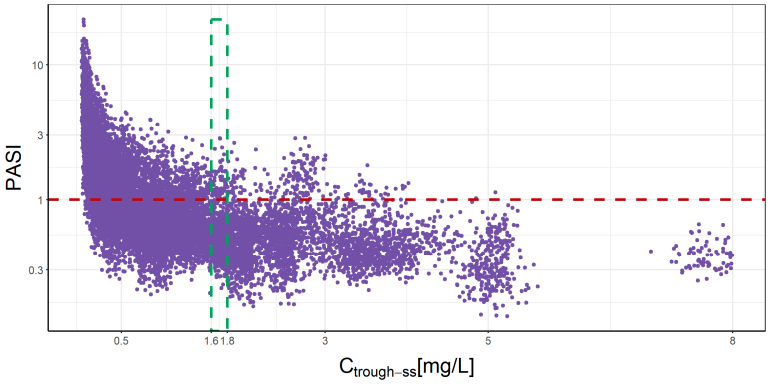

Figure 6. Simulated absolute PASI and trough concentration for each patient after 10 cycles of UTK administration using labeled and non-labeled dosing schemes. $C_{trough\text{-}ss}$: trough concentration at steady state.

4. Discussion

In this study, we developed a procedure capable of individualizing dosing strategies of UTK in clinical practice Spanish patients with moderate to severe chronic plaque psoriasis based on the uncertainty of the individual parameter estimates of a population PK/PD model. Additionally, the inclusion of the uncertainty during the simulation step for a personalized dosing regimen selection facilitates the evaluation of the degree of certainty in model-informed predictions in the clinical setting, providing a probabilistic framework for the MIPD of UTK.

Of the total number of patients who need a dosage regimen modification, 35% would be oriented towards an optimized dosage regimen. In 22% of patients, this optimization is

proposed to be performed using a non-labeled dosage regimen. This represents a reduction of one dose per year, meaning that patients, instead of receiving five doses of UTK in the first year of treatment with SmPC dosing regimens and four from the second year onwards, would receive four doses and three doses, respectively. According to the database of health information on medicines and parapharmacy products [49] the price of Stelara® 45 mg solution for injection in a pre-filled syringe is EUR 2915.4. Assuming the reduction in dosage, this will entail an annual cost per patient of EUR 11,661.6, which will represent a saving of 25%. In addition to fewer expenses related to the purchase of medication, with the lower number of administrations, there is less risk of an occurrence of injection site reactions due to SmPC. The previous fact includes patients who are to receive 45 mg q16w and also those who are to receive 45 mg q8w because the latter take much more intensive dosage regimens during clinical practice, for example, 90 mg q10w.

From our pool of patients, an intensification of the dosage regimen in comparison with the one received in clinical practice is proposed in 26% of the patients. In these patients, individual CL values higher than the typical value are observed; hence, this type of patient will require higher levels of UTK to achieve a successful therapeutic response. It should be taken into consideration that after performing our strategy for MIPD in UTK, dosage regimen optimization is recommended for most of the patients. As a result, an improvement in patient well-being and health system management can be achieved because, in the end, the patients would always be in an optimal therapeutic response range.

The MIPD strategy did not allow us to reach the efficacy endpoint (a 90% probability of a PASI $\leq$ 1) in 17% of patients. This strategy represents an advantage in identifying non-responding patients at the early stages of treatment, improving the effectiveness in the management of psoriasis for those patients, and avoiding the cost of treating these patients during successive cycles. A more in-depth analysis of these patients reveals CL or k_{out} values higher and lower, respectively, than the population average (Supplementary Figure S3), which could serve as a threshold to characterize patients with a low probability of optimal response to UTK.

For the estimation of individual PK/PD parameters, all the PASI and UTK concentration values available at the time of recruitment were used. To implement the proposed MIPD strategy, an adaptive procedure might be implemented. This procedure would involve re-estimating the individual parameters as additional data points become available to ensure the model remains accurate and reflective of the patient's evolving condition. On the other hand, this analysis confirms the need to collect PASI samples from patients during the first weeks of treatment (the induction phase), which enhances the characterization of PK and PD processes and increases the number of observations per patient, leading to a precise and accurate estimation of their individual PD parameters. The non-linear relationship between the PASI score and trough concentration levels of UTK (Figure 6) demonstrates both the impact of the PK and PD parameters to guarantee satisfactory treatment efficacy. Therefore, although it is possible to establish global exposure values for a PASI value, the individualization of treatment through this MIPD strategy allows for the achievement of a greater number of patients with effective therapeutic regimens, reducing therapeutic failure only for non-responding patients. In our study, a $C_{trough\text{-}ss}$ range of 1.6–1.8 mg/L was able to help 90% of patients achieve a PASI $\leq$ 1. Even though the $C_{trough\text{-}ss}$ range obtained in a previous population PK/PD study [17] was 0.0914–0.978 mg/L, it should be noted that this range is representative only for patients weighing 60 to 100 kg with a dosing regimen of 45 mg q12w. Correspondingly, it was generated from the simulated data of patients who were exclusively starting treatment with UTK in pivotal phase III clinical trials, with the efficacy objective of PASI 75 in week 12. However, the range of our study represents a more demanding PD endpoint (PASI $\leq$ 1 or PASI 99), and it is representative of patients with no body weight limit (92 $\pm$ 18.4 [70–135] kg) receiving eight dosage regimens used in clinical practice (45 or 90 mg q8, 12, 16 and 20w) under steady-state UTK therapy conditions. Furthermore, this range provides target $C_{trough\text{-}ss}$ values that are associated with an optimal

response in line with current clinical guideline recommendations (PASI $\leq$ 1) intended to maximize both clinical outcomes and the quality of life of patients with psoriasis [50,51].

Our work is based on previously published PK /PD models, thus recycling data and using previously developed knowledge, but in addition to our model, we have taken a step forward in the characterization of the relationship between UTK concentrations and response through the PASI observed in real-world clinical data. But also, this study is an example of individual-level precision dosing, which involves a more comprehensive and effective use of precision dosing strategies by recognizing, characterizing, and quantifying the various sources of variability in drug response through PK/PD modeling [23,33]. Such studies are particularly valuable for drugs like UTK that are used to treat heterogeneous conditions like psoriasis, where response variability is significant. While improving our understanding of PK/PD relationships within specific patient subgroups during clinical trials can enhance the identification of precise dosing targets, real-world patients remain significantly more diverse than those in controlled trial settings. Therefore, robust post-marketing surveillance is essential to explore unique precision dosing targets [52]. Advances in data collection and analysis methods from real-world patients offer opportunities to identify new precision dosing algorithms and refine existing ones established in clinical trials. These methods enable the continuous updating and extension of dosing strategies to better meet the individualized needs of patients [33,53]. Thus, our strategy based on MIPD in real-world clinical data could be the first attempt to ensure the most precise individual dosing of patients with plaque psoriasis treated with UTK.

Similar to any real-world study cohort, notable challenges involve the lack of patients (a small patient sample size), a few points available per patient, and therefore the presence of missing data. Due to the study design conditions, many PK/PD observations were taken very spaced out in time, without a continuous characterization (sparse data). For this reason, some unquantified changes in the physiology or the progression of the psoriasis disease could directly impact the obtained results. In the future, similar models could be implemented into a conditional distribution dashboard system [54,55]. This would allow for real-time predictions of treatment response, aiding in informed decisions regarding dosing adjustments and treatment transitions for UTK. In this way, as suggested by Mould and Upton in their recently published review [56], options for alternative dosing strategies based on MIPD and/or TDM could be included in the SmPC of UTK.

5. Conclusions

In conclusion, this study proposes a methodology to individualize UTK dosing strategies considering the uncertainty of individual parameters within a population PK/PD model to optimize the probability of achieving targeted clinical outcomes in patients with moderate to severe chronic plaque psoriasis. This represents an initial step towards performing MIPD for biologics that act on the interleukin pathways of psoriasis, which has been explored very little. Future studies should implement our proposal in a greater cohort of real-world patients.

Supplementary Materials: The following supporting information can be downloaded at: https://www.mdpi.com/article/10.3390/pharmaceutics16101295/s1, Ordinary differential equations for the PK/PD model of UTK and PASI; Figure S1: Prediction-corrected visual predictive check obtained from one thousand simulated studies using the selected population PK model; Figure S2: Prediction-corrected visual predictive check obtained from one thousand simulated studies using the selected population PK/PD model; Table S1: Mean of the individual PK/PD parameters drawn from the conditional distribution task in Monolix; Table S2: Standard deviation of the individual PK/PD parameters drawn from the conditional distribution task in Monolix; Figure S3: Bar plot of 100 simulated absolute PASI for each patient after UTK administration at cycles 5 and 10, using the individual parameters from the final population PK/PD model and their uncertainties; Figure S4: PK and PD simulations with the current dosage regimen from clinical practice and the individual optimal dosing regimen established after simulations in 10th cycle for each patient.

Author Contributions: Conceptualization, M.M.-S., E.G.-C., M.C.-M. and V.M.-S.; methodology, K.R.-F., J.Z.-F., M.M.-S., E.G.-C., M.C.-M. and V.M.-S.; software, K.R.-F., J.Z.-F. and V.M.-S.; validation, K.R.-F., J.Z.-F., M.S.-B., M.M.-S., A.M.-P., A.M.-C., E.G.-C., M.C.-M. and V.M.-S.; formal analysis, K.R.-F., J.Z.-F. and V.M.-S.; investigation, K.R.-F., J.Z.-F. and V.M.-S.; resources, A.M.-P., A.M.-C., E.G.-C. and M.C.-M.; data curation, K.R.-F.; writing—original draft preparation, K.R.-F., J.Z.-F. and V.M.-S.; writing—review and editing, K.R.-F., J.Z.-F., M.S.-B., M.M.-S., A.M.-P., A.M.-C., E.G.-C., M.C.-M. and V.M.-S.; visualization, K.R.-F. and J.Z.-F. ; supervision, E.G.-C., M.C.-M. and V.M.-S.; project administration, E.G.-C., M.C.-M. and V.M.-S.; funding acquisition, A.M.-P., E.G.-C. and M.C.-M. All authors have read and agreed to the published version of the manuscript.

Funding: This research received no external funding.

Institutional Review Board Statement: The study was conducted following the Declaration of Helsinki and approved by the Ethics Committee of La Fe University and Polytechnic Hospital (protocol code: VMS-UTK-2020-01 and date of approval: 27 January 2021).

Informed Consent Statement: Informed consent was obtained from all subjects involved in the study.

Data Availability Statement: The data presented in this study are available on request from the corresponding author due to ethical and legal restrictions.

Conflicts of Interest: The authors declare no conflicts of interest.

Abbreviations

AHT	Arterial hypertension
BMI	Body mass index
$C_{trough\text{-}ss}$	Trough concentration at steady state
CL	Clearance
E_{Drug}	Effect of the drug
F	Bioavailability
IC_{50}	Concentration of the drug needed to inhibit 50% of the response
I_{max}	Maximum inhibition drug effect
IIV	Interindividual variability
IL	Interleukin
k_a	Absorption rate constant
k_{in}	Zero-order progression constant rate of psoriatic skin lesion
k_{out}	First-order remission constant rate of psoriatic skin lesion
mAb	monoclonal antibody
MCMC	Markov Chain Monte Carlo
MIPD	Model-informed precision dosing
n_{PASI}	Amount of simulated PASI score values that reach the response target (PASI score ≤ 1)
$\eta_{i,RV}$	Estimated individual random component accounting for the difference between $PASI_i$ and $PASI_{i,o}$
PASI	Psoriasis Area and Severity Index
$PASI_i$	Estimated baseline levels of PASI response
$PASI_{i,o}$	Individual observed baseline levels of PASI response
pcVPC	Prediction-corrected visual predictive check
PD	Pharmacodynamic
PK	Pharmacokinetic
PK/PD	Pharmacokinetic/pharmacodynamic
Q	Intercompartmental transfer clearance
q8w	Once every 8 weeks
q10w	Once every 10 weeks
q12w	Once every 12 weeks
q14w	Once every 14 weeks
q15w	Once every 15 weeks
q16w	Once every 16 weeks

q18w	Once every 18 weeks
q20w	Once every 20 weeks
RUV	Residual unexplained variability
SD	Standard deviation
SmPC	Summary of product characteristics
TDM	Therapeutic drug monitoring
T_{PASI}	Total amount of simulated PASI score values (100 clones)
UTK	Ustekinumab
V_2	Central volume of distribution
V_3	Peripheral volume of distribution

References

1. Schadler, E.D.; Ortel, B.; Mehlis, S.L. Biologics for the primary care physician: Review and treatment of psoriasis. *Disease-a-Month* **2018**, *65*, 51–90. [CrossRef] [PubMed]
2. Rendon, A.; Schäkel, K. Psoriasis Pathogenesis and Treatment. *Int. J. Mol. Sci.* **2019**, *20*, 1475. [CrossRef] [PubMed]
3. Koutruba, N.; Emer, J.; Lebwohl, M. Review of ustekinumab, an interleukin-12 and interleukin-23 inhibitor used for the treatment of plaque psoriasis. *Ther. Clin. Risk Manag.* **2010**, *6*, 123–141. [CrossRef] [PubMed]
4. Weber, J.; Keam, S.J. Ustekinumab. *BioDrugs Clin. Immunother. Biopharm. Gene Ther.* **2009**, *23*, 53–61. [CrossRef] [PubMed]
5. Mahil, S.K.; Capon, F.; Barker, J.N. Update on psoriasis immunopathogenesis and targeted immunotherapy. *Semin. Immunopathol.* **2016**, *38*, 11–27. [CrossRef]
6. Murphy, K.M.; Reiner, S.L. The lineage decisions of helper T cells. *Nat. Rev. Immunol.* **2002**, *2*, 933–944. [CrossRef]
7. Tesmer, L.A.; Lundy, S.K.; Sarkar, S.; Fox, D.A. Th17 cells in human disease. *Immunol. Rev.* **2008**, *223*, 87–113. [CrossRef]
8. FDA. Approved Drug Products: STELARA (Ustekinumab) Injection, for Subcutaneous or Intravenous Use. March 2024. Available online: https://www.accessdata.fda.gov/drugsatfda_docs/label/2024/761044s013lbl.pdf (accessed on 6 August 2024).
9. Leonardi, C.L.; Kimball, A.B.; Papp, K.A.; Yeilding, N.; Guzzo, C.; Wang, Y.; Li, S.; Dooley, L.T.; Gordon, K.B. Efficacy and safety of ustekinumab, a human interleukin-12/23 monoclonal antibody, in patients with psoriasis: 76-week results from a randomised, double-blind, placebo-controlled trial (PHOENIX 1). *Lancet* **2008**, *371*, 1665–1674. [CrossRef]
10. Papp, K.A.; Langley, R.G.; Lebwohl, M.; Krueger, G.G.; Szapary, P.; Yeilding, N.; Guzzo, C.; Hsu, M.C.; Wang, Y.; Li, S.; et al. Efficacy and safety of ustekinumab, a human interleukin-12/23 monoclonal antibody, in patients with psoriasis: 52-week results from a randomised, double-blind, placebo-controlled trial (PHOENIX 2). *Lancet* **2008**, *371*, 1675–1684. [CrossRef]
11. Thein, D.; Rosenø, N.A.L.; Maul, J.T.; Wu, J.J.; Skov, L.; Bryld, L.E.; Rasmussen, M.K.; Ajgeiy, K.K.; Thomsen, S.F.; Thyssen, J.P.; et al. Drug Survival of Adalimumab, Secukinumab, and Ustekinumab in Psoriasis as Determined by Either Dose Escalation or Drug Discontinuation during the First 3 Years of Treatment–a Nationwide Cohort Study. *J. Investig. Dermatol.* **2023**, *143*, 2211–2218. [CrossRef]
12. Yiu, Z.Z.N.; Mason, K.J.; Hampton, P.J.; Reynolds, N.J.; Smith, C.H.; Lunt, M.; Griffiths, C.E.M.; Warren, R.B. Drug survival of adalimumab, ustekinumab and secukinumab in patients with psoriasis: A prospective cohort study from the British Association of Dermatologists Biologics and Immunomodulators Register (BADBIR). *Br. J. Dermatol.* **2020**, *183*, 294–302. [CrossRef] [PubMed]
13. Young, M.S.; Horn, E.J.; Cather, J.C. The ACCEPT study: Ustekinumab versus etanercept in moderate-to-severe psoriasis patients. *Expert Rev. Clin. Immunol.* **2011**, *7*, 9–13. [CrossRef] [PubMed]
14. Zhu, Y.; Hu, C.; Lu, M.; Liao, S.; Marini, J.C.; Yohrling, J.; Yeilding, N.; Davis, H.M.; Zhou, H. Population pharmacokinetic modeling of ustekinumab, a human monoclonal antibody targeting IL-12/23p40, in patients with moderate to severe plaque psoriasis. *J. Clin. Pharmacol.* **2009**, *49*, 162–175. [CrossRef] [PubMed]
15. Zhu, Y.W.; Mendelsohn, A.; Pendley, C.; Davis, H.M.; Zhou, H. Population pharmacokinetics of ustekinumab in patients with active psoriatic arthritis. *Int. J. Clin. Pharmacol. Ther.* **2010**, *48*, 830–846. [CrossRef]
16. Pan, S.; Tsakok, T.; Dand, N.; Lonsdale, D.O.; Loeff, F.C.; Bloem, K.; de Vries, A.; Baudry, D.; Duckworth, M.; Mahil, S.; et al. Using Real-World Data to Guide Ustekinumab Dosing Strategies for Psoriasis: A Prospective Pharmacokinetic-Pharmacodynamic Study. *Clin. Transl. Sci.* **2020**, *13*, 400–409. [CrossRef]
17. Zhou, W.; Hu, C.; Zhu, Y.; Randazzo, B.; Song, M.; Sharma, A.; Xu, Z.; Zhou, H. Extrapolating Pharmacodynamic Effects from Adults to Pediatrics: A Case Study of Ustekinumab in Pediatric Patients With Moderate to Severe Plaque Psoriasis. *Clin. Pharmacol. Ther.* **2020**, *109*, 131–139. [CrossRef]
18. Shao, J.; Xu, Z.; Xu, Y. Integrated Population Pharmacokinetic Analysis of Ustekinumab Across Multiple Immune-Mediated Inflammatory Disease Populations and Healthy Subjects. *Eur. J. Drug Metab. Pharmacokinet.* **2022**, *47*, 537–548. [CrossRef]
19. Zhou, H.; Hu, C.; Zhu, Y.; Lu, M.; Liao, S.; Yeilding, N.; Davis, H.M. Population-based exposure-efficacy modeling of ustekinumab in patients with moderate to severe plaque psoriasis. *J. Clin. Pharmacol.* **2010**, *50*, 257–267. [CrossRef]
20. Rodríguez-Fernández, K.; Mangas-Sanjuán, V.; Merino-Sanjuán, M.; Martorell-Calatayud, A.; Mateu-Puchades, A.; Climente-Martí, M.; Gras-Colomer, E. Impact of Pharmacokinetic and Pharmacodynamic Properties of Monoclonal Antibodies in the Management of Psoriasis. *Pharmaceutics* **2022**, *14*, 654. [CrossRef]
21. Felmlee, M.A.; Morris, M.E.; Mager, D.E. Mechanism-based pharmacodynamic modeling. *Methods Mol. Biol.* **2012**, *929*, 583–600. [CrossRef]

22. Notario, J.; Bordas, X. Practical management of ustekinumab in moderate-severe psoriasis. *Actas Dermo-Sifiliográficas* **2012**, *103*, 52–58. [CrossRef]
23. Tyson, R.J.; Park, C.C.; Powell, J.R.; Patterson, J.H.; Weiner, D.; Watkins, P.B.; Gonzalez, D. Precision Dosing Priority Criteria: Drug, Disease, and Patient Population Variables. *Front. Pharmacol.* **2020**, *11*, 420. [CrossRef] [PubMed]
24. Syversen, S.W.; Goll, G.L.; Jørgensen, K.K.; Sandanger, Ø.; Sexton, J.; Olsen, I.C.; Gehin, J.E.; Warren, D.J.; Brun, M.K.; Klaasen, R.A.; et al. Effect of Therapeutic Drug Monitoring vs Standard Therapy During Infliximab Induction on Disease Remission in Patients With Chronic Immune-Mediated Inflammatory Diseases: A Randomized Clinical Trial. *JAMA* **2021**, *325*, 1744–1754. [CrossRef] [PubMed]
25. Albader, F.; Golovics, P.A.; Gonczi, L.; Bessissow, T.; Afif, W.; Lakatos, P.L. Therapeutic drug monitoring in inflammatory bowel disease: The dawn of reactive monitoring. *World J. Gastroenterol.* **2021**, *27*, 6231–6247. [CrossRef] [PubMed]
26. D'Haens, G.R.; Sandborn, W.J.; Loftus, E.V., Jr.; Hanauer, S.B.; Schreiber, S.; Peyrin-Biroulet, L.; Panaccione, R.; Panés, J.; Baert, F.; Colombel, J.F.; et al. Higher vs Standard Adalimumab Induction Dosing Regimens and Two Maintenance Strategies: Randomized SERENE CD Trial Results. *Gastroenterology* **2022**, *162*, 1876–1890. [CrossRef]
27. Minichmayr, I.K.; Dreesen, E.; Centanni, M.; Wang, Z.; Hoffert, Y.; Friberg, L.E.; Wicha, S.G. Model-informed precision dosing: State of the art and future perspectives. *Adv. Drug Deliv. Rev.* **2024**, *2024*, 115421. [CrossRef]
28. Olivier, B.G.; Swat, M.J.; Moné, M.J. Modeling and Simulation Tools: From Systems Biology to Systems Medicine. *Methods Mol. Biol.* **2016**, *1386*, 441–463. [CrossRef]
29. Darwich, A.S.; Polasek, T.M.; Aronson, J.K.; Ogungbenro, K.; Wright, D.F.B.; Achour, B.; Reny, J.L.; Daali, Y.; Eiermann, B.; Cook, J.; et al. Model-Informed Precision Dosing: Background, Requirements, Validation, Implementation, and Forward Trajectory of Individualizing Drug Therapy. *Annu. Rev. Pharmacol. Toxicol.* **2021**, *61*, 225–245. [CrossRef]
30. Minichmayr, I.K.; Mizuno, T.; Goswami, S.; Peck, R.W.; Polasek, T.M.; Pharmacology, t.A.S.o.C.; Community, T.P.D. Recent Advances Addressing the Challenges of Precision Dosing. *Clin. Pharmacol. Ther.* **2024**, *116*, 527–530. [CrossRef]
31. Bandín-Vilar, E.; Toja-Camba, F.J.; Vidal-Millares, M.; Durán-Maseda, M.J.; Pou-Álvarez, M.; Castro-Balado, A.; Maroñas, O.; Gil-Rodríguez, A.; Carracedo, Á.; Zarra-Ferro, I.; et al. Towards precision medicine of long-acting aripiprazole through population pharmacokinetic modelling. *Psychiatry Res.* **2024**, *333*, 115721. [CrossRef]
32. Rodríguez-Fernández, K.; Reynaldo-Fernández, G.; Reyes-González, S.; de Las Barreras, C.; Rodríguez-Vera, L.; Vlaar, C.; Monbaliu, J.M.; Stelzer, T.; Duconge, J.; Mangas-Sanjuan, V. New insights into the role of VKORC1 polymorphisms for optimal warfarin dose selection in Caribbean Hispanic patients through an external validation of a population PK/PD model. *Biomed. Pharmacother. Biomed. Pharmacother.* **2024**, *170*, 115977. [CrossRef] [PubMed]
33. Polasek, T.M.; Peck, R.W. Beyond Population-Level Targets for Drug Concentrations: Precision Dosing Needs Individual-Level Targets that Include Superior Biomarkers of Drug Responses. *Clin. Pharmacol. Ther.* **2024**, *116*, 602–612. [CrossRef] [PubMed]
34. Hu, C.; Szapary, P.O.; Mendelsohn, A.M.; Zhou, H. Latent variable indirect response joint modeling of a continuous and a categorical clinical endpoint. *J. Pharmacokinet. Pharmacodyn.* **2014**, *41*, 335–349. [CrossRef] [PubMed]
35. Salinger, D.H.; Endres, C.J.; Martin, D.A.; Gibbs, M.A. A semi-mechanistic model to characterize the pharmacokinetics and pharmacodynamics of brodalumab in healthy volunteers and subjects with psoriasis in a first-in-human single ascending dose study. *Clin. Pharmacol. Drug Dev.* **2014**, *3*, 276–283. [CrossRef]
36. Chigutsa, E.; Velez de Mendizabal, N.; Chua, L.; Heathman, M.; Friedrich, S.; Jackson, K.; Reich, K. Exposure-Response Modeling to Characterize the Relationship Between Ixekizumab Serum Drug Concentrations and Efficacy Responses at Week 12 in Patients with Moderate to Severe Plaque Psoriasis. *J. Clin. Pharmacol.* **2018**, *58*, 1489–1500. [CrossRef]
37. Hu, C.; Yao, Z.; Chen, Y.; Randazzo, B.; Zhang, L.; Xu, Z.; Sharma, A.; Zhou, H. A comprehensive evaluation of exposure-response relationships in clinical trials: Application to support guselkumab dose selection for patients with psoriasis. *J. Pharmacokinet. Pharmacodyn.* **2018**, *45*, 523–535. [CrossRef]
38. van Huizen, A.; Bank, P.; van der Kraaij, G.; Musters, A.; Busard, C.; Menting, S.; Rispens, T.; de Vries, A.; van Doorn, M.; Prens, E.; et al. Quantifying the Effect of Methotrexate on Adalimumab Response in Psoriasis by Pharmacokinetic-Pharmacodynamic Modeling. *J. Investig. Dermatol.* **2024**, *144*, 794–801. [CrossRef]
39. Dansirikul, C.; Silber, H.E.; Karlsson, M.O. Approaches to handling pharmacodynamic baseline responses. *J. Pharmacokinet. Pharmacodyn.* **2008**, *35*, 269–283. [CrossRef]
40. Bergstrand, M.; Hooker, A.C.; Wallin, J.E.; Karlsson, M.O. Prediction-corrected visual predictive checks for diagnosing nonlinear mixed-effects models. *AAPS J.* **2011**, *13*, 143–151. [CrossRef]
41. Upton, R.N.; Mould, D.R. Basic concepts in population modeling, simulation, and model-based drug development: Part 3-introduction to pharmacodynamic modeling methods. *CPT Pharmacomet. Syst. Pharmacol.* **2014**, *3*, e88. [CrossRef]
42. Lixoft. Monolix Suite 2024R1. 2024. Available online: https://lixoft.com/products/monolix/ (accessed on 25 July 2024).
43. Ito, K.; Murphy, D. Application of ggplot2 to Pharmacometric Graphics. *CPT Pharmacomet. Syst. Pharmacol.* **2013**, *2*, e79. [CrossRef] [PubMed]
44. R Core Team. *R: A Language and Environment for Statistical Computing*; R Foundation for Statistical Computing: Vienna, Austria, 2024. Available online: http://www.R-project.org/ (accessed on 30 July 2024).
45. Monolix 2024R1 User Guide. Available online: https://monolix.lixoft.com/single-page/ (accessed on 25 January 2024).
46. Kümmel, A.; Bonate, P.L.; Dingemanse, J.; Krause, A. Confidence and Prediction Intervals for Pharmacometric Models. *CPT Pharmacomet. Syst. Pharmacol.* **2018**, *7*, 360–373. [CrossRef] [PubMed]

47. Lixoft. Simulx 2024R1. 2024. Available online: https://simulx.lixoft.com/ (accessed on 25 July 2024).
48. Dayneka, N.L.; Garg, V.; Jusko, W.J. Comparison of four basic models of indirect pharmacodynamic responses. *J. Pharmacokinet. Biopharm.* **1993**, *21*, 457–478. [CrossRef] [PubMed]
49. BOT PLUS. Available online: https://botplusweb.farmaceuticos.com/ (accessed on 29 August 2024).
50. Torres, T.; Puig, L. Treatment goals for psoriasis: Should PASI 90 become the standard of care? *Actas Dermo-Sifiliográficas* **2015**, *106*, 155–157. [CrossRef] [PubMed]
51. Nast, A.; Smith, C.; Spuls, P.I.; Avila Valle, G.; Bata-Csörgö, Z.; Boonen, H.; De Jong, E.; Garcia-Doval, I.; Gisondi, P.; Kaur-Knudsen, D.; et al. EuroGuiDerm Guideline on the systemic treatment of Psoriasis vulgaris–Part 1: Treatment and monitoring recommendations. *J. Eur. Acad. Dermatol. Venereol.* **2020**, *34*, 2461–2498. [CrossRef]
52. Kamal, M.A.; Ganguly, S.; Kadambi, A.; Smith, P.F. Extended Model-Informed Drug Development: Beyond Clinical Trials and Regulatory Approval. *Clin. Pharmacol. Ther.* **2024**, *116*, 518–521. [CrossRef]
53. Darwich, A.S.; Ogungbenro, K.; Vinks, A.A.; Powell, J.R.; Reny, J.L.; Marsousi, N.; Daali, Y.; Fairman, D.; Cook, J.; Lesko, L.J.; et al. Why has model-informed precision dosing not yet become common clinical reality? lessons from the past and a roadmap for the future. *Clin. Pharmacol. Ther.* **2017**, *101*, 646–656. [CrossRef]
54. Dolan, J.G.; Veazie, P.J.; Russ, A.J. Development and initial evaluation of a treatment decision dashboard. *BMC Med. Inform. Decis. Mak.* **2013**, *13*, 51. [CrossRef]
55. Mould, D.R.; Upton, R.N.; Wojciechowski, J. Dashboard systems: Implementing pharmacometrics from bench to bedside. *AAPS J.* **2014**, *16*, 925–937. [CrossRef]
56. Mould, D.R.; Upton, R.N. "Getting the Dose Right"-Revisiting the Topic with Focus on Biologic Agents. *Clin. Pharmacol. Ther.* **2024**, *116*, 613–618. [CrossRef]

Supplementary materials

Model-Informed Precision Dosing for Personalized Ustekinumab Treatment in Plaque Psoriasis

Karine Rodriguez-Fernandez [1,2,†], Javier Zarzoso-Foj [1,2,†], Marina Saez-Bello [3], Almudena Mateu-Puchades [4], Antonio Martorell-Calatayud [5], Matilde Merino-Sanjuan [1,2], Elena Gras-Colomer [6], Monica Climente-Marti [3] and Victor Mangas-Sanjuan [1,2,*]

[1] Department of Pharmacy and Pharmaceutical Technology and Parasitology, University of Valencia. Valencia, Spain; karofer@alumni.uv.es (K.R.-F.); javier.zarzoso@uv.es (J.Z.-F.); matilde.merino@uv.es (M.M.-S.)
[2] Interuniversity Research Institute for Molecular Recognition and Technological Development, Polytechnic University of Valencia-University of Valencia. Valencia, Spain
[3] Pharmacy Service, Doctor Peset University Hospital, Valencia. Foundation for the Promotion of Health and Biomedical Research in the Valencian Region (FISABIO), Valencia, Spain; saez_marbel@gva.es (M.S.-B.); climente_mon@gva.es (M.C.-M.)
[4] Dermatology Service, Doctor Peset University Hospital, Valencia. Foundation for the Promotion of Health and Biomedical Research in the Valencian Region (FISABIO), Valencia, Spain; mateu_alm@gva.es
[5] Dermatology Service, Hospital Manises of Valencia, Spain; martorell_antcal@gva.es
[6] Pharmacy Service, Hospital Manises of Valencia, Spain; gras_ele@gva.es
* Correspondence: victor.mangas@uv.es; Tel.: +34963543351
† These authors contributed equally to this work.

Ordinary differential equations for the PK/PD model of UTK and PASI

$$\frac{dA}{dt} = -k_a \cdot A \qquad \text{Equation S1}$$

$$\frac{dC_C}{dt} = k_a \cdot A - CL \cdot C_C + Q \cdot (C_p - C_c) \qquad \text{Equation S2}$$

$$\frac{dC_P}{dt} = -Q \cdot (C_p - C_c) \qquad \text{Equation S3}$$

$$\frac{dPASI}{dt} = k_{in} \cdot \left(1 - \frac{I_{max} \cdot C_C}{(IC_{50} + C_C)}\right) - k_{out} \cdot PASI \qquad \text{Equation S4}$$

Where k_a: absorption rate constant; A: amount of UTK in the depot compartment.; CL: clearance; C_c: concentration of UTK in the central compartment; Q: intercompartmental transfer clearance; C_p: concentration of UTK in the peripheral compartment; k_{in}: zero-order progression constant rate of psoriatic skin lesion; k_{out}: first-order remission constant rate of psoriatic skin lesion; I_{max}: maximum inhibition drug effect model; IC_{50}: concentration of UTK needed to inhibit 50% of the response; PASI: Psoriasis Area and Severity Index.

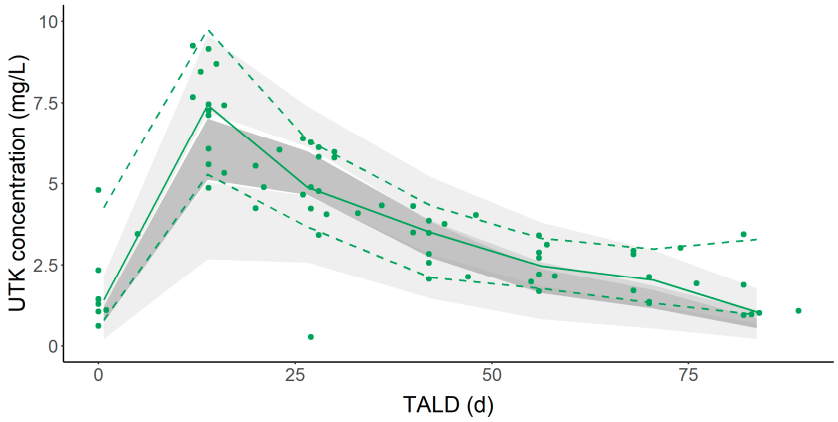

Figure S1. Prediction-corrected visual predictive check obtained from one thousand simulated studies using the selected population PK model. Points represent the observed serum UTK concentrations; lines, 2.5th, 50th, and 97.5th percentiles of the simulated data. Shaded areas represent the 95% prediction intervals of the 5th, 50th, and 95th percentiles of the simulated studies. TALD: time after last dose.

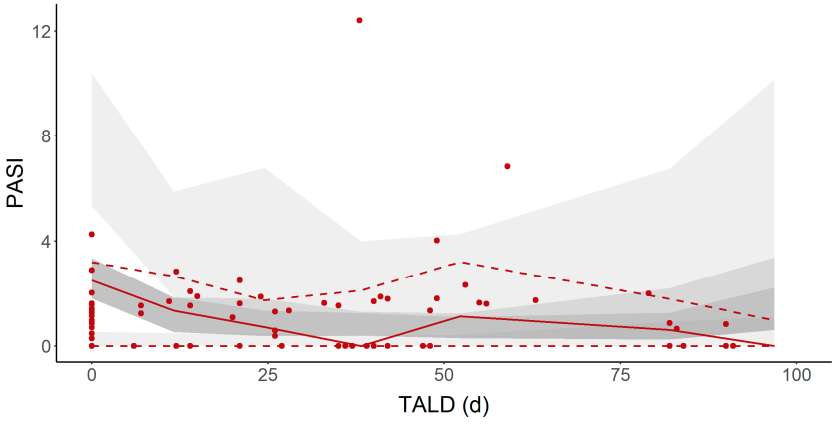

Figure S2. Prediction-corrected visual predictive check obtained from one thousand simulated studies using the selected population PK/PD model. Points represent the observed serum UTK concentrations; lines, 2.5th, 50th, and 97.5th percentiles of the simulated data. Shaded areas represent the 95% prediction intervals of the 5th, 50th, and 95th percentiles of the simulated studies. TALD: time after last dose.

Table S1. Mean of the individual PK/PD parameters draws from the conditional distribution task in Monolix.

ID	k_a (d^{-1})	F (%)	CL (L/d)	V_2 (L)	Q (L/d)	V_3(L)	k_{out}(d^{-1})	I_{max}	$PASI_i$
1	0.40	93	0.20	3.52	0.20	2.10	0.019	0.968	13.722
2	0.15	65	0.18	2.97	0.16	1.68	0.006	0.968	19.995
3	0.15	80	0.16	2.85	0.16	1.59	0.017	0.968	11.616
4	0.13	81	0.19	3.21	0.18	1.87	0.016	0.968	9.075
5	0.09	80	0.17	2.97	0.16	1.72	0.019	0.968	5.564
6	0.11	55	0.16	2.90	0.16	1.76	0.016	0.968	7.346
7	0.20	86	0.24	3.83	0.22	2.53	0.018	0.968	9.860
10	0.14	75	0.20	3.17	0.18	1.78	0.019	0.968	14.508
11	0.33	51	0.25	3.89	0.23	2.52	0.017	0.968	10.643
12	0.18	61	0.18	3.08	0.17	1.98	0.018	0.968	11.624
13	0.15	79	0.24	3.72	0.21	2.31	0.017	0.968	16.094
14	0.17	74	0.19	3.36	0.19	2.56	0.015	0.968	8.238
15	0.19	70	0.19	3.46	0.20	2.33	0.016	0.968	9.736
16	0.09	83	0.18	3.15	0.18	1.85	0.018	0.968	7.360
18	0.14	65	0.30	4.30	0.25	2.85	0.007	0.968	18.845
19	0.17	74	0.17	3.20	0.18	2.15	0.021	0.968	8.616
20	0.22	97	0.12	3.38	0.19	1.89	0.017	0.968	10.079
21	0.15	51	0.21	3.68	0.21	2.78	0.017	0.968	11.062
22	0.19	75	0.13	3.00	0.17	2.21	0.017	0.968	12.280
24	0.21	68	0.23	3.84	0.22	2.73	0.015	0.968	7.104
25	0.21	82	0.17	3.13	0.17	1.96	0.017	0.968	16.983
26	0.17	57	0.21	3.22	0.18	1.87	0.014	0.968	5.963
27	0.25	70	0.14	2.67	0.14	1.73	0.014	0.968	9.557

k_a: absorption rate constant; F: bioavailability CL: clearance; Q: intercompartmental transfer clearance; V_2: central volume of distribution; V_3: peripheral volume of distribution; k_{out}: first-order remission constant rate of psoriatic skin lesion; I_{max}: maximum inhibition drug effect model; $PASI_i$: estimated baseline levels of PASI response.

Table S2. Standard deviation of the individual PK/PD parameters draws from the conditional distribution task in Monolix.

ID	k_a	F	CL	V_2	Q	V_3	k_{out}	I_{max}	$PASI_i$
1	0.02	0.03	0.01	0.04	0	0.27	0.01	0	0.31
2	0.04	0.05	0.01	0.03	0	0.21	0.00	0	0.44
3	0.01	0.06	0.01	0.03	0	0.21	0.01	0	0.29
4	0.03	0.08	0.02	0.04	0	0.21	0.01	0	0.14
5	0.04	0.06	0.02	0.04	0	0.24	0.01	0	0.19
6	0.03	0.05	0.02	0.03	0	0.24	0.01	0	0.20
7	0.02	0.05	0.01	0.04	0	0.28	0.01	0	0.18
10	0.02	0.06	0.02	0.04	0	0.24	0.01	0	0.23
11	0.05	0.04	0.01	0.05	0	0.26	0.00	0	0.27
12	0.02	0.05	0.01	0.04	0	0.23	0.01	0	0.22
13	0.05	0.10	0.02	0.04	0	0.32	0.01	0	0.20
14	0.01	0.04	0.01	0.04	0	0.29	0.01	0	0.20
15	0.03	0.05	0.02	0.04	0	0.30	0.01	0	0.17
16	0.01	0.07	0.02	0.04	0	0.24	0.01	0	0.37
18	0.04	0.11	0.03	0.05	0	0.38	0.01	0	0.60
19	0.02	0.05	0.01	0.04	0	0.27	0.01	0	0.29
20	0.02	0.02	0.00	0.04	0	0.19	0.01	0	0.18
21	0.02	0.04	0.02	0.04	0	0.35	0.01	0	0.21
22	0.03	0.04	0.01	0.03	0	0.26	0.01	0	0.26
24	0.02	0.05	0.02	0.04	0	0.32	0.01	0	0.20
25	0.03	0.05	0.01	0.04	0	0.25	0.01	0	0.19
26	0.03	0.05	0.02	0.04	0	0.25	0.01	0	0.22
27	0.03	0.04	0.01	0.03	0	0.22	0.01	0	0.27

k_a: absorption rate constant; F: bioavailability CL: clearance; Q: intercompartmental transfer clearance; V_2: central volume of distribution; V_3: peripheral volume of distribution; k_{out}: first-order remission constant rate of psoriatic skin lesion; I_{max}: maximum inhibition drug effect model; $PASI_i$: estimated baseline levels of PASI response.

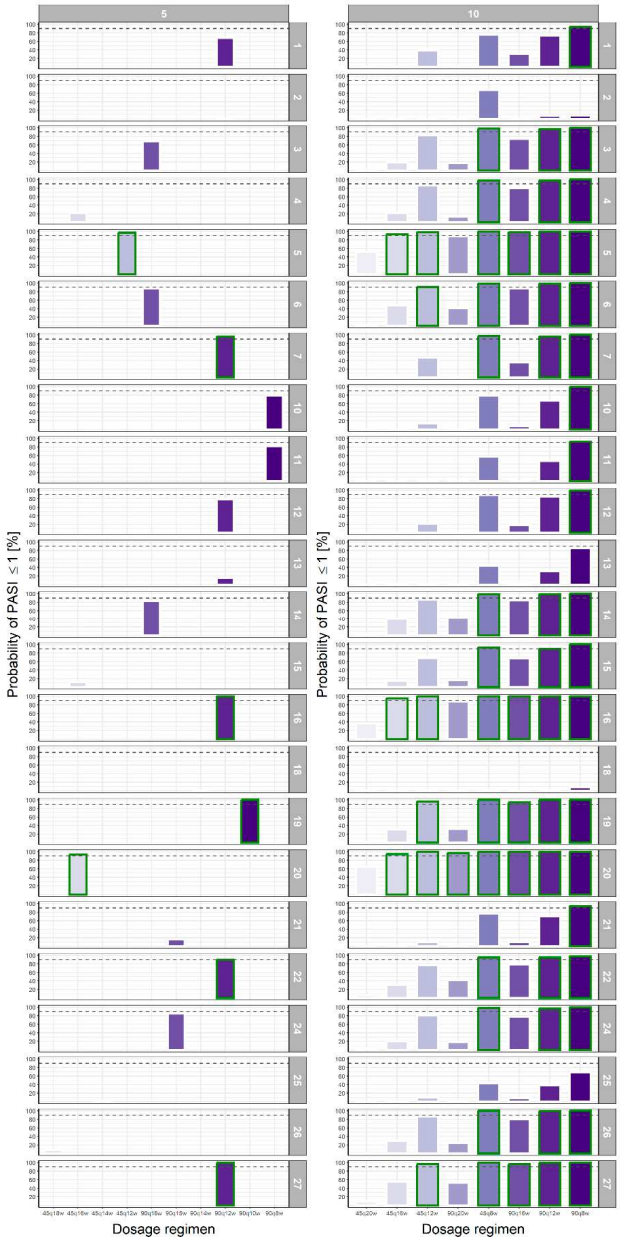

Figure S3. Bar plot of 100 simulated absolute PASI for each patient after UTK administration at cycles 5 and 10, using the individual parameters from the final population PK/PD model and their uncertainties. In green it is represented the probability ≥ 90% of PASI level ≤1. The dose regimens in which a probability ≥ 90% is reached are indicated in green.

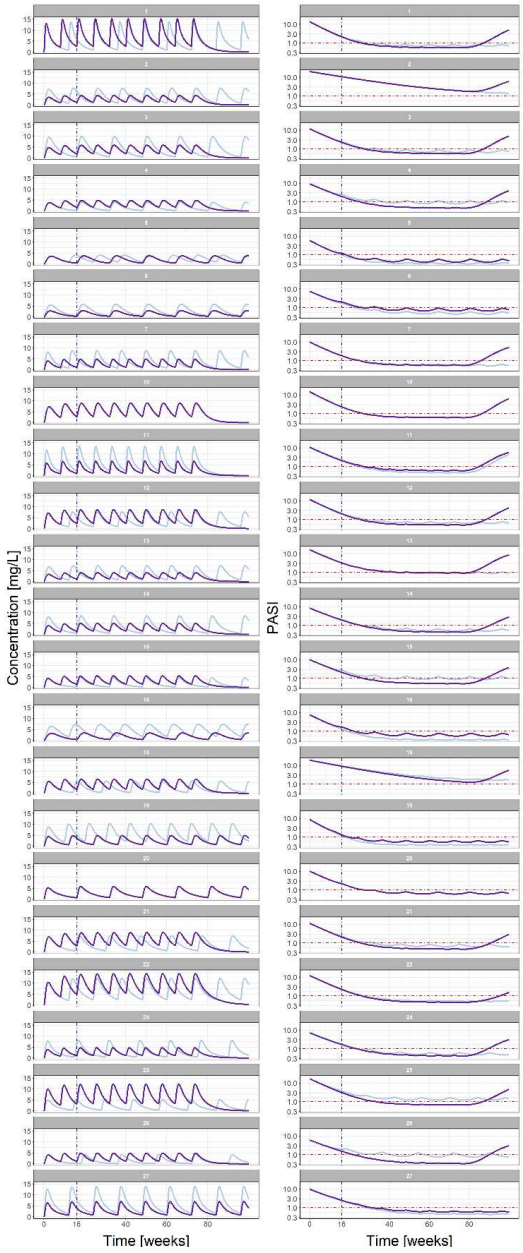

Figure S4. PK and PD simulations with the current dosage regimen from clinical practice (blue) and the individual optimal dosing regimen established after simulations in 10th cycle (purple) for each patient. The vertical dashed line represents the starting point of the maintenance period at week 16. The horizontal dashed line represents the PASI value of 1.

Annex 5: Personalized Secukinumab Treatment in Patients with Plaque Psoriasis Using Model-Informed Precision Dosing

pharmaceutics

MDPI

Article

Personalized Secukinumab Treatment in Patients with Plaque Psoriasis Using Model-Informed Precision Dosing

Karine Rodriguez-Fernandez [1,2,†], Javier Zarzoso-Foj [1,2,†], Marina Saez-Bello [3], Almudena Mateu-Puchades [4], Antonio Martorell-Calatayud [5], Matilde Merino-Sanjuan [1,2], Elena Gras-Colomer [6], Monica Climente-Marti [3,*] and Victor Mangas-Sanjuan [1,2,*]

[1] Department of Pharmacy and Pharmaceutical Technology and Parasitology, University of Valencia, 46100 Valencia, Spain; karofer@alumni.uv.es (K.R.-F.); javier.zarzoso@uv.es (J.Z.-F.); matilde.merino@uv.es (M.M.-S.)
[2] Interuniversity Research Institute for Molecular Recognition and Technological Development, Polytechnic University of Valencia–University of Valencia, 46100 Valencia, Spain
[3] Pharmacy Service, Doctor Peset University Hospital, Foundation for the Promotion of Health and Biomedical Research in the Valencian Region (FISABIO), 46017 Valencia, Spain; saez_marbel@gva.es
[4] Dermatology Service, Doctor Peset University Hospital, Foundation for the Promotion of Health and Biomedical Research in the Valencian Region (FISABIO), 46017 Valencia, Spain; mateu_alm@gva.es
[5] Dermatology Service, Hospital Manises of Valencia, 46940 Manises, Spain; martorell_antcal@gva.es
[6] Pharmacy Service, Hospital Manises of Valencia, 46940 Manises, Spain; gras_ele@gva.es
* Correspondence: climente_mon@gva.es (M.C.-M.); victor.mangas@uv.es (V.M.-S.)
† These authors contributed equally to this work.

Abstract: Background/Objectives: Patient care and control of inflammatory disorders, such as psoriasis, can be improved by model-informed precision dosing (MIPD) techniques based on population pharmacokinetic/pharmacodynamic (PK/PD) models. Clinical dose selection decisions based on MIPD strategies need to take account of the uncertainty associated with the individual PK/PD model parameters, which is determined by the quantity of individual observational data collected in clinical practice. **Methods:** The aim of this study was to propose an approach for personalized dosage regimens of secukinumab (SCK) in 22 Spanish patients with plaque psoriasis, whose severity level was considered moderate to severe, taking into account the uncertainty associated with individual parameters in a population-based PK/PD model. **Results:** The link between SCK serum concentrations and Psoriasis Area and Severity Index (PASI) scores was explained using an indirect response model. A maximum inhibition (I_{max}) drug effect model was applied to limit the progression of psoriatic skin lesions within the turnover PD mechanism, which explains the changes in PASI scores during treatment. A first-order remission rate constant for psoriatic lesions (k_{out} = 0.11 day^{-1}) was estimated. **Conclusions:** According to the MIPD strategy, 50% of patients would require an optimized regimen and 14% would require an intensified dosage regimen in comparison to current clinical treatment. This research has shown its usefulness as a tool for choosing individualized SCK dosage regimens in patients with long-lasting plaque psoriasis to improve the probability of achieving satisfactory response levels.

Keywords: psoriasis; secukinumab; pharmacokinetic/pharmacodynamic

Citation: Rodriguez-Fernandez, K.; Zarzoso-Foj, J.; Saez-Bello, M.; Mateu-Puchades, A.; Martorell-Calatayud, A.; Merino-Sanjuan, M.; Gras-Colomer, E.; Climente-Marti, M.; Mangas-Sanjuan, V. Personalized Secukinumab Treatment in Patients with Plaque Psoriasis Using Model-Informed Precision Dosing. *Pharmaceutics* **2024**, *16*, 1576. https://doi.org/10.3390/pharmaceutics16121576

Academic Editor: Neal M. Davies

Received: 31 October 2024
Revised: 3 December 2024
Accepted: 9 December 2024
Published: 10 December 2024

1. Introduction

Secukinumab (SCK) is a fully human immunoglobulin G1k (IgG1k) monoclonal antibody (mAb) designated for the treatment of psoriasis [1,2], a chronic autoimmune skin disorder characterized by pro-inflammatory cytokines and keratinocyte hyperproliferation [3–5]. Psoriasis disease is partially explained by an elevation of proinflammatory interleukin (IL)-17A, which binds to the IL-17 receptor present in keratinocytes, triggering the signaling pathway associated with inflammatory processes [6,7]. The pharmacological

mechanism of action of SCK consists in selective binding to IL-17A, which diminishes its interaction with the IL-17 receptor, and therefore, reduces the inflammatory cascade [8].

Currently, SCK (Cosentyx®) is approved as an injection for subcutaneous (SC) use for treating plaque psoriasis, also called psoriasis vulgaris, from moderate to severe modality in adults. As indicated in the summary of product characteristics (SmPC) [9], SCK should be administered in a dose of 300 mg in weeks 0, 1, 2, 3, and 4 (induction period), and then every 4 weeks (maintenance period). For patients with a body weight of 90 kg or more, a maintenance dose of 300 mg every 2 weeks may provide additional benefit [10]. Clinical trials evaluating the efficacy of SCK in psoriasis have reported notable reductions in Psoriasis Area and Severity Index (PASI) scores, reflecting a substantial improvement in disease severity [11–17].

The population pharmacokinetics (PK) properties of SCK have been characterized using pooled results from six clinical trials: one phase I, three phase II, and two phase III studies in patients with psoriasis [11–13,18–20]. A two-compartment PK model with first-order absorption for SC administration and with zero-order infusion for intravenous administration successfully characterized its longitudinal PK behavior in patients with moderate to severe psoriasis [21,22]. SCK shows a terminal half-life of 27 days and slow clearance (CL) (0.19 L/day). Low central (V_2 = 3.61 L) and peripheral (V_3 = 2.87 L) volumes of distribution were estimated. An allometric relationship between body weight and CL and V_2 characterized the influence of body weight on PK disposition parameters of SCK. A disease progression model incorporating a symptomatic drug effect was recently developed for SCK [23]. In this model, the proportion of patients achieving PASI 75 and PASI 90 reported in clinical trials was used as the efficacy index.

The initial treatment with SCK is indicated by dermatologists following the labeled dosing recommendations. This procedure may not be the most favorable or harmless for all patients [24]. When the patient is in the maintenance phase of treatment with SCK because of the variable psoriasis disease progression and the fluctuation in individual response, modifications in SmPC dosage regimens become necessary. These modifications in the routine clinical practice of a dermatology service are called intensifications and optimizations. The goal of dosage regimen optimization is to either decrease the dose while keeping the dosing interval the same or retain the dose whereas the dosing interval is expanded. In contrast, dosage regimen intensification results in keeping the dose but cutting the dosing interval or increasing the dose but keeping the dosing interval. Due to the lack of a model-informed decision-making process, this strategy raises the likelihood of adverse outcomes caused by the emergence of e subtherapeutic or supratherapeutic drug concentrations [25]. Furthermore, rigorous adherence to the sample schedule is required by the individualization techniques that are frequently employed in conventional clinical practice, like those related to therapeutic drug monitoring (TDM) and clinical response. During these techniques, the drug's exposure in patients is compared to an objective range to make modifications, and intervention usually happens only after the medication has achieved a steady state. In cases when the exposure deviates from this range, the dosage is modified based on either clinical experience or the hypothesis of proportionality in dose exposure at a steady state [26–29].

For dosage selection in a patient, the ideal treatment and addressing events of insufficient response, gradual depletion of efficacy, or the advent of side effects, dermatologists must adopt an adaptable approach for treating chronic psoriasis vulgaris that contemplates dosage regimens not included in the SmPC (non-labeled) and transitions between various therapeutic alternatives of the disease. These obstacles underline how crucial it is to switch in the direction of model-informed precision dosing (MIPD) techniques based on population pharmacokinetic/pharmacodynamic (PK/PD) models. Because MIPD allows for the use of any timed sample, interventions can be carried out before the initial dosage or until a steady state is attained. The procedure of intervention determines a dosage that meets a predetermined target for PK/PD [29–34]. Therapeutic results and patient safety are improved when PK/PD models are used in dosage selection for the control of chronic plaque

psoriasis, since they address the interindividual variability (IIV) in therapy responses and increase precision dosing [35–37]. Therefore, this study aims to suggest a strategy for individualizing dosage regimens of SCK in patients with moderate to severe long-lasting psoriasis vulgaris reflecting the uncertainty associated with individual parameters obtained from a population PK/PD model.

2. Materials and Methods

2.1. Research Design

A prospective, observational, post-authorization clinical practice follow-up study was carried out at Dr. Peset University Hospital of Valencia on Spanish patients with chronic psoriasis vulgaris from moderate to severe modality. The study's authors certify that the methods used in the investigation comply with the moral guidelines set out by relevant institutional and national bodies that regulate the use of human subjects in research. Additionally, they guarantee adherence to the 1975 Helsinki Declaration, which underwent amendments in 2008. The Dr. Peset University Hospital Ethics Committee approved the study (protocol code VMS-SCK-2020-01 EPA-SP). Prior to beginning any study procedures, the patients' written informed consent was obtained. The time frame for the study was July 2020–December 2022. Patients who were receiving therapy at the time of registration and had received at least one dose of SCK (Cosentyx®) were eligible to participate. Personalized (optimized/intensified) dose regimens were prescribed to the study participants by the dermatologist, considering their clinical responses. Pregnant women, those under the age of 18, and people with cognitive impairments were all excluded. For every patient, therapy-related information including time, dose, and treatment line were gathered. Demographic information, such as weight, sex, height, and age, were also obtained from the hospital's electronic medical records.

2.2. Blood Collection and Sample Analytical Quantification

The patients received 150 or 300 mg of SCK by SC injection (abdomen or upper thigh) every 4, 5 and 6 weeks (q4w, q5w and q6w). Blood samples for PK analysis were collected using plain red vacutainer tubes immediately before SCK administration and approximately 2, 7, 14, 22, 30, and 40 days afterwards. The collected blood samples were centrifuged for 10 to 15 min at 3500–4000 rpm, and subsequently, the remaining was transferred to another tube and frozen until processing. Concentrations of SCK in serum were measured by A. Menarini Diagnostics (08918 Badalona, Barcelona, Spain) using an ISO 15189 [38] validated enzyme-linked immunosorbent assay (ELISA) in a freedom Evolyzer Tecan. The concentration range of the calibration curve was 0.2 μg/mL to 225 μg/mL.

2.3. Assessment of Psoriasis Area and Severity Index Score

Patients which began SCK therapy at Dr. Peset University Hospital's dermatological service received PASI evaluations between weeks 5 and 6 and weeks 16 and 24 after the induction period. Following this, PASI measurements were performed every 6 months. All the PASI scores that were available and registered in patients' clinical records through the almost 1.5-year follow-up period were used for this investigation. Medical records of the patients were additionally examined to extract the baseline PASI values registered at the beginning of the SCK therapy.

2.4. Modeling Data Analysis

A summary of the modeling approach used is shown in Figure 1. The population PK parameters of the published reference model for SCK [21] were employed for simulation to determine if the available model was able to accurately represent our data. A two-compartment model with an absorption compartment through linear processes (Figure 2) represents the structural PK model. Then, a population PK/PD model was developed to characterize the time course of PASI response [39,40]. Several structural PK/PD models were proposed to characterize the time delay between PK and PD ob-

servations. Linear, maximum inhibition (I_{max}), and functions for sigmoid drug effects were assessed [41]. The first section of the Supplementary Materials provides the ordinary differential equations of the PK/PD model.

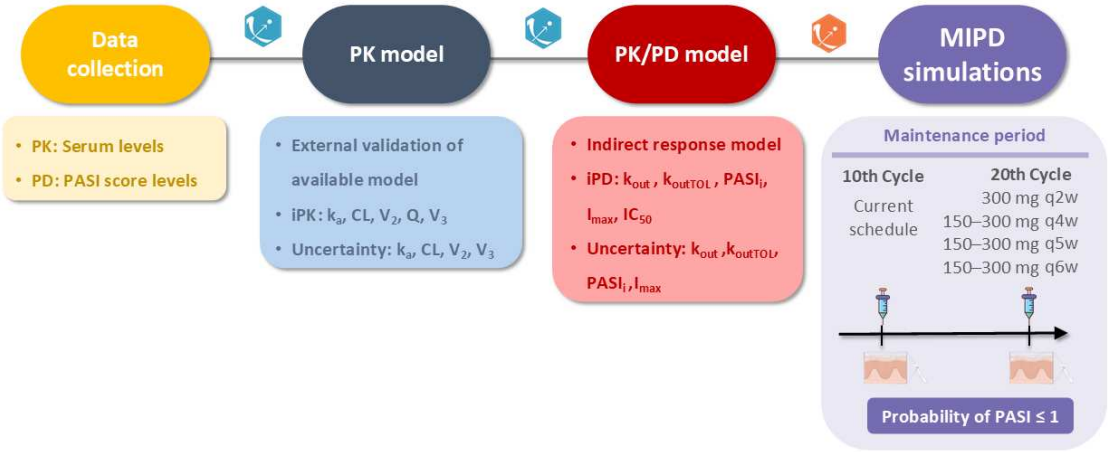

Figure 1. Workflow of the modeling process. PASI: Psoriasis Area and Severity Index; PD: pharmacodynamic; PK: pharmacokinetic; iPK: individual pharmacokinetic parameters; k_a: absorption rate constant; CL: clearance; Q: intercompartmental transfer clearance; V_2: central volume of distribution; V_3: peripheral volume of distribution; iPD: individual pharmacodynamic parameters; k_{out}: first-order reduction constant rate of psoriatic skin lesion; $k_{outTOLt}$: first-order remission constant rate of tolerance; $PASI_i$: estimated baseline levels of PASI response; I_{max}: maximum inhibition drug effect model; IC_{50}: concentration of the drug needed to inhibit 50% of the response; MIPD: model-informed precision dosing; q2w: once every 2 weeks, q4w: once every 4 weeks, q5w: once every 5 weeks, q6w: once every 6 weeks.

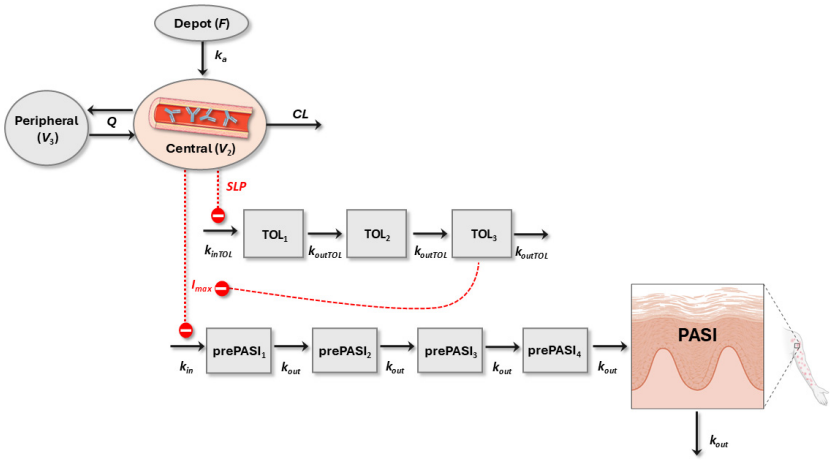

Figure 2. Final PK/PD model representation. *F*: bioavailability; k_{in}: zero-order evolution constant rate of psoriatic skin lesion; k_{inTOL}: zero-order progression constant rate of tolerance; SLP: linear drug effect model.

The B2 method [42] was applied to estimate baseline levels of PASI response, where $PASI_i$ characterizes the individual predicted baseline level of PASI, the individual observed

baseline are represented by $PASI_{i,0}$, and the distinguishing features between $PASI_i$ and $PASI_{i,0}$ are incorporated in the estimated individual random component $\eta_{i,RV}$. The mean of this random component is equal to zero, and its variance is constrained to have the same value as the residual unexplained variability (RUV) (Equation (1)). Hence, we expected that the baseline data would likewise exhibit the variability seen in the remaining data.

$$PASI_i = PASI_{i,0} \cdot e^{\eta_{i,RV}} \quad (1)$$

A comparison of the minimum value of the objective function, a visual examination of goodness-of-fit plots, and the accuracy of model parameters as indicated by the relative standard errors (RSE) were the basis for selecting the PK/PD model. By applying simulation-based diagnostics called prediction-corrected visual predictive checks (pcVPC), the evaluation of the elected PK/PD models was completed [40,43]. The data analyses were conducted via the population approach established in the software Monolix 2024R1 (Lixoft SAS, a Simulations Plus company, Lancaster, CA, USA) [44]. The R software (version 4.4.1; http://cran.r-project.org, accessed on 15 November 2024) [45,46] was used for statistical and graphical analysis.

2.5. Individual Dosage Regimen Approach

The most appropriate MIPD regimen for each patient was found by simulation analysis incorporating the PK and PD individual parameters and their uncertainties, in order to investigate the performance of the final PK/PD model and its influence on clinical practice. The PK and PD individual parameter estimates and their corresponding uncertainty were obtained by computing the individual conditional distributions of PK/PD parameters in Monolix 2024R1 [47]. The degree to which PK and PD individual parameters can be accurately obtained based on the observed data and covariate value for that individual, reflecting that the individual is a member of the population for which the typical parameter value (fixed effects) and the variability (standard deviation of the random effects) were previously estimated, is known as uncertainty [47,48].

A Markov chain Monte Carlo (MCMC) process known as Metropolis–Hastings algorithms was used to determine individual conditional distributions ($p(\psi_i|y_i)$, where ψ_i indicates the individual parameters for individual i , and y_i symbolizes the data observations for individual i. The following expression was used to sample parameter values from these distributions:

$$p(\psi_i|y_i) = \frac{p(y_i|\psi_i) \cdot p(\psi_i)}{p(y_i)} \quad (2)$$

where the constant that denotes the likelihood is $p(y_i)$, the density function for the individual parameters is referred as $p(\psi_i)$, and $p(y_i|\psi_i)$ reflects the conditional density function of the data when the individual parameter values are known.

In order to predict, via stochastic simulations, the PASI levels and trough concentrations at steady state ($C_{trough\text{-}ss}$) expected at the 10th and 20th cycle (maintenance period) of treatment with SCK, one hundred clones per patient were created applying individual conditional distributions and later imputed to Simulx 2024R1 (Lixoft SAS, a Simulations Plus company) [49]. Simulations were performed as follows:

- 10th cycle: using each patient's prescribed dosage regimen, simulations of individual dosage regimens were generated considering 10 cycles of SCK (steady-state conditions) administration
- 20th cycle: once 10 cycles were applied, 10 more cycles of SCK treatment for each patient were implemented additionally, to simulate the combination of alternative dose levels (150 and 300 mg) with different posology (q2w, q4w, q5w, and q6w) (Figure 1).

The probabilities of reaching the response aim (PASI score ≤ 1) in the 10th and 20th cycle for each patient, with each simulated dosage regimen, were calculated applying the following expression:

$$Probability = \frac{n_{PASI}}{T_{PASI}} \times 100 \quad (3)$$

The total quantity of simulated PASI score values (100 clones) corresponds to T_{PASI} , whereas n_{PASI} is the number of simulated PASI score values that accomplish the response target (PASI score ≤ 1). The regimen with a probability $\geq 90\%$ (i.e., $\geq$90 virtual patients) in the 20th cycle was chosen as the final dosage regimen. For methodological reasons, intensified dosing regimens were tested at the 20th cycle; a successful response was achieved even at the 10th cycle. When the response target was reached by the patient with several dosage regimens, it was selected as the final regimen, the one that was the most optimized among all. The most optimized dosage regimen stands for a lower dose while maintaining the dosing interval or equally a larger dosing interval but keeping the dose. After selecting a dosage regimen in the 20th cycle, it was compared with the clinical practice dosing regimen in each patient to determine if it was optimized or intensified, if the patients maintained their current regimen, or if it had not been possible to make a prediction for the patient.

3. Results

3.1. Research Subjects

A total of 22 patients were included in the study. The modeling dataset consisted of 85 concentrations of SCK in samples of serum (PK), 106 individual values of PASI score (PD) and for each patient a baseline PASI ($PASI_{i,0}$). Comorbidities, demographic and TDM data are presented in Table 1. Moreover, the current dosage regimens of the subjects who participated in the study are described as treatment characteristics in Table 1.

Table 1. Overview of the PK/PD experimental data and patient characteristics gathered within TDM.

	Mean ± SD	**Range**	**n (%)**
Demographic data			
Body weight (kg)	74.5 ± 15	46–97	
Height (m)	1.7 ± 0.09	1.54–1.85	
BMI (kg/m^2)	25.5 ± 4.9	16–41	
Age (years)	50.07 ± 13.4	28–76	
Gender (male)			14 (64)
Treatment period (years)	2 ± 1.7	0.005–5.1	
Biological “naive”			19 (86)
Comorbidities			
AHT			5 (23)
Dyslipidemia			7 (32)
Diabetes			3 (14)
Obesity			2 (9.1)
Psoriatic arthropathy			5 (23)
Non-alcoholic fatty liver			1 (4.5)
Anxious–depressive disorder			2 (9.1)
Others			11 (50)
TDM data			
Total of patients			22
SCK concentration (mg/L)	48.2 ± 18.5	7.4–89	85
PASI (no units)	1 ± 1.7	0–12.3	106
$PASI_{i,0}$	11.6 ± 5.8	2–27.5	22

Table 1. *Cont.*

		Mean ± SD		Range	n (%)
Clinical practice treatment characteristics					
SmPC		Optimized		Summary	
300 mg q4w	18	150 mg q4w	2	SmPC	18 (82%)
		300 mg q5w	1	Optimized	4 (18%)
		300 mg q6w	1	Intensified	none

SD: standard deviation; BMI: body mass index; AHT: arterial hypertension; TDM: therapeutic drug monitoring; SCK: secukinumab; PASI: Psoriasis Area and Severity Index; SmPC: summary of product characteristics; q4w: once every 4 weeks; q5w: once every 5 weeks; q6w: once every 6 weeks.

3.2. Population PK Model

The population PK model was a two-compartment model with first-order absorption and linear disposition processes that had been formerly issued by Bruin et al. [21]. The available data and patient population were then used to examine the statistical significance of the covariates enclosed in the original paper. Only body weight on CL (0.8) and V_2 (1) were maintained through an allometric relationship. Given that most of the observations were in line with the identity line, individual characterization of the individual PK profiles was confirmed (Supplementary Figure S1).

3.3. Population PK/PD Model

An indirect response [50] was selected to describe the relationship between SCK concentration and PASI observations in which SCK inhibits the zero-order evolution constant rate of psoriatic skin lesion (k_{in}). The inhibition of k_{in} through an I_{max} model provided a statistically significant reduction in the objective function value (p-value < 0.01). Other mAbs intended to treat moderate to severe chronic psoriasis vulgaris have previously used this model structure [51–56]. To capture the delay between SCK administration and observable effects, an additional chain of four turnover prePASI compartments was added, each representing a step in the disease progression (Figure 2).

The $PASI_i$ was estimated using the B2 method. Also, the value of first-order reduction constant rate of psoriatic skin lesion (k_{out}) was computed. Due to difficulties during the minimization and convergence processes, the concentration of the drug needed to inhibit 50% of the response (IC_{50}) could not be estimated and was fixed to a published value (9.35 mg/L) [23]. A tolerance mechanism was incorporated to account for the increase in PASI score over time during the administration of SCK in four patients (ID: 5, 10, 13, and 16). Tolerance and desensitization phenomena have been previously modeled in preclinical data for proinflammatory cytokines that determine the triggering of plaque psoriasis [57]. A turn-over mechanism including three mediator-like compartments was proposed, where the rate of progression of tolerance (k_{inTOL}) is triggered by drug effects incorporated as a linear function (SLP) of the predicted levels of SCK in serum.

Individual PK and PD profiles across time are reproduced in Figure 3. According to the PK/PD model, the current framework appropriately takes into account the combined action of SCK and PASI turnover, since it can describe the longitudinal behavior of PASI at the individual level. Individual predicted vs. the observed PASI in patients with chronic plaque psoriasis and the pcVPC of the PK/PD model are shown in Supplementary Figures S2 and S3, respectively. Table 2 provides a summary of parameter estimates for the final population PK/PD model. Supplementary Tables S1 and S2 include an overview of the mean and standard deviation of the PK/PD parameters in each patient, respectively.

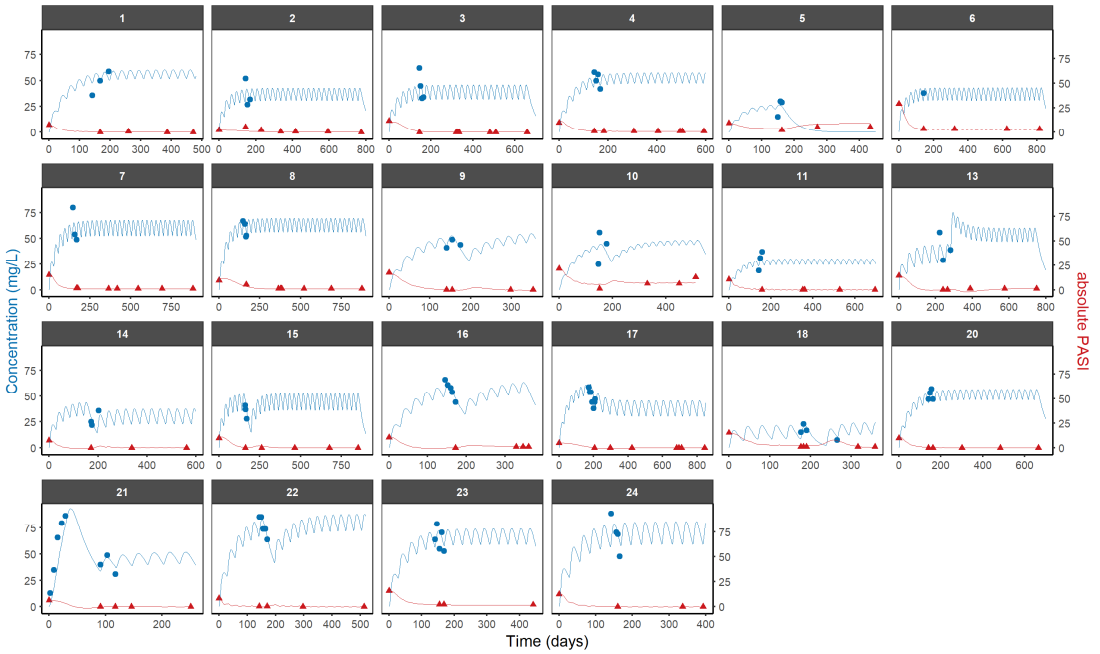

Figure 3. Predicted and observed PASI score (red) and SCK concentrations (blue) after the administration of SCK in patients with long-lasting psoriasis vulgaris. Individual predictions are represented by lines, and the SCK and PASI observations are represented by blue and red dots, respectively.

Table 2. Population PK/PD estimates in patients with chronic plaque psoriasis after administration of SCK.

Parameter (Units)	Value	RSE (%)
Fixed-effect		
k_{out} (day^{-1})	0.11	26.1
k_{outTOL} (day^{-1})	0.003	106
I_{max}	1.19	1.88
IC_{50} (mg/L)	9.35 FIX	
Inter-individual variability		
k_{out} (%)	91.3	20
k_{outTOL} (%)	37.15	431
I_{max} (%)	7.63	18
Residual unexplained variability		
Error (%)	0.76	9.2

RSE: relative standard error; k_{out}: first-order reduction constant rate of psoriatic skin lesion; I_{max}: maximum inhibition drug effect; $k_{outTOLt}$: first-order remission constant rate of tolerance; IC_{50}: concentration of the drug needed to inhibit 50% of the response.

3.4. Individual Dosage Regimen Evaluation

Supplementary Figure S4 illustrates the probabilities across treatment cycles for each patient. The MIPD strategy indicated that 50% (11/22) of patients would require an optimized dose regimen, while 14% (3/22) would need an intensified regimen compared to the clinical practice regimen used during the maintenance period of treatment with SCK. The optimized patients are suggested to follow non-standard dosage regimens: 150 mg q4w

for 9% (1/11), 150 mg q5w for 9% (1/11), 150 mg q6w for 18% (2/11), 300 mg q5w for 45% (5/11), and 300 mg q6w for 18% (2/11) of patients. In patients requiring intensified regimens, switching to 300 mg q2w is advised for all. For 18% (4/22) of patients, no changes to their current regimen were predicted. Furthermore, this MIPD strategy helped identify 18% (4/22) of patients who would not reach the efficacy target (90% probability of PASI $\leq$ 1), enabling early recognition of those at risk of therapeutic failure. Figure 4 specifies the changes from the dose regimen in clinical practice to the predicted regimen during the maintenance phase of therapy with SCK (cycle 20).

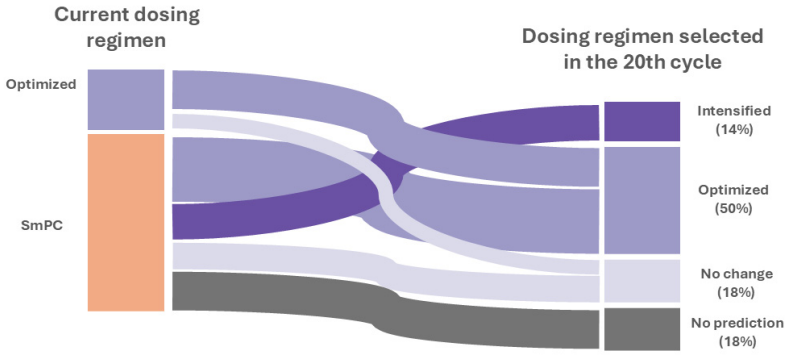

Figure 4. Sankey diagram of the shifts in individual dosage regimens. SmPC: summary of product characteristics.

Supplementary Figure S5 depicts the PK and PD simulations for each patient, comparing the current clinical practice regimen with the optimized dosing regimen determined by the 20th cycle. Figure 5 highlights the connection between absolute PASI scores and steady-state $C_{trough\text{-}ss}$ under all tested regimens. The general findings show a non-linear association, establishing that a $C_{trough\text{-}ss}$ varying from 64.2 to 69.3 mg/L allows a PASI score $\leq$ 1 in 90% of patients.

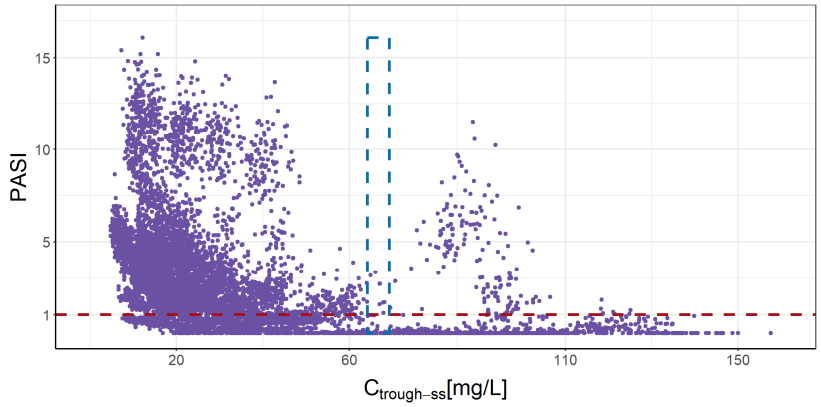

Figure 5. Simulated trough level and absolute PASI score for all subjects after receiving 150 mg q4w, q5w, and q6w; and 300 mg q2w, q4w, q5w and q6w of SCK SC administration in the 20th cycle. The purple dots represent the simulated PASI score and their corresponding $C_{trough\text{-}ss}$. The blue dashed box represents the $C_{trough\text{-}ss}$ (64.2–69.3 mg/L) that allows a PASI score $\leq$ 1 in 90% of patients. The red dashed line represents the PASI value of 1. $C_{trough\text{-}ss}$: trough concentration at steady state.

4. Discussion

In this study, an exposure–response model was developed for PASI, the most employed endpoint for efficacy in clinical practice patients with persistent psoriasis vulgaris. An indirect-response model was evaluated to characterize the effects of SCK, incorporating an additional series of turnover compartments for prePASI and a tolerance mechanism. This approach was based on the expectation of a time lag between the peak concentrations of SCK and the maximum drug effect on psoriatic lesions, represented by PASI scores. Since SCK inhibits the IL-17A, the exposure–efficacy model represented SCK as having an inhibitory pharmacological effect on the development of psoriatic lesions following drug administration. However, we are aware of the drawbacks in the developed PK/PD model reflected in the low precision in parameter estimation of the tolerance mechanism (RSE of k_{outTOL} and RSE of k_{outTOL} IIV), which is only activated in four patients (5, 10, 13, and 16).

The cornerstone of this study was the development of a procedure for tailoring dosing approaches of SCK in Spanish patients with moderate to severe long-lasting psoriasis vulgaris, based on the uncertainty surrounding individual parameter estimates from a population PK/PD model. Moreover, by integrating uncertainty into the simulation stage designed for personalized dosing regimen choice, it becomes possible to assess the confidence level of model-informed forecasts in clinical practice, offering an approach with probabilistic character for MIPD of SCK. Among the patients needing a modification to their dosage regimen, an optimized dosage regimen is suggested in 50% of them. In almost all optimized patients (91%), the optimization should be to a non-labeled dosage regimen, with 300 mg q5w being recommended in 45% of patients. This adjustment would lead to a decrease of 3 doses for each year, meaning that as an alternative to receiving 14 doses in the following years after the first year of treatment with SKC according to the SmPC dosing guidelines, patients would receive 11 doses. Corresponding to the health information database for medicines and pharmacy products [58], the cost of Cosentyx® 300 mg injection in a pre-filled syringe is EUR 1246.98. With the optimization of SCK therapy, the annual cost per patient would amount to EUR 13717, resulting in savings of 21%. Additionally, fewer medication purchases and a smaller quantity of administrations would decrease the threat of injection site reactions.

In contrast to the clinical practice's dose regimen schedule, intensification was recommended in 14% of the subjects. Because in these patients the I_{max} values were lower (1.06–1.13) than the typical value (1.19), a higher level of SCK dose would be required to achieve a successful therapeutic response. Note that most of the included patients required a dose regimen optimization following the implementation of our MIPD method in SCK. Consequently, since patients are more likely to be within the appropriate treatment response range, it is possible to enhance patient welfare and health system administration. In 18% of subjects, the efficacy endpoint (90% probability of PASI ≤ 1) was not obtained. Therefore, the MIPD strategy proposed in this investigation implies a benefit for identifying patients who are not responding to treatment in the beginning. In this way, the management of plaque psoriasis can be enhanced in these individuals, and unnecessary costs associated with treating them in subsequent cycles could be avoided. Furthermore, their k_{out} values are lower (0.07) than the typically observed (0.11), which might be used as a cutoff point for distinguishing patients who are unlikely to respond optimally to SCK.

The full data of SCK concentrations and PASI scores that were acquirable in each patient included in this study were applied to estimate the individual PK/PD parameters. An adaptable process might be employed to apply the suggested MIPD approach into practice. To make sure the model continues to be accurate and still represent the patient's progressing state, this approach would involve a refining process of the individual parameters as novel data points appear. In this study, the importance of collecting samples of absolute PASI from patients throughout the initial weeks of treatment to accurately determine their individual PD parameters is highlighted. The significance of both PK and PD parameters in ensuring effective treatment outcomes is demonstrated by the non-linear relationship between the simulated absolute PASI and $C_{trough\text{-}ss}$ of SCK

(Figure 5). While it is feasible to set general exposure values corresponding to an absolute PASI, the use of this MIPD approach to personalize treatment can lead to a higher proportion of patients reaching efficient dosage regimens, thereby minimizing treatment failure among non-responders.

A more exigent $C_{trough\text{-}ss}$ range (64.2–69.3 mg/L) was proposed in this study to accomplish in 90% of patients an absolute PASI ≤ 1. A previously reported $C_{trough\text{-}ss}$ range (12.9–62.9 mg/L) was established in a prior population PK modeling investigation [21], which included individuals on a 300 mg q4w dosage regimen, and it was produced using simulated data from clinical trials in patients who were only beginning therapy with SCK, in which the efficacy objective was to achieve in week 12 the PASI 75. Conversely, the $C_{trough\text{-}ss}$ range found in this research stand for a more rigorous PD endpoint (PASI ≤ 1 or PASI 99) from patients in routine clinical practice. Also, the proposed $C_{trough\text{-}ss}$ range aligns with optimal response criteria consistent with current clinical guidelines (PASI ≤ 1), intended to enhance the quality of life and clinical results for those with persistent psoriasis vulgaris [59,60].

This research is based on PK/PD models previously reported. Nevertheless, our work is an example of how to effectively use established knowledge. However, we have gone one step further in the description of the relationship among SCK concentrations and patient responses measured by absolute PASI under real-world circumstances. In addition, this investigation exemplifies individualized precision dosing, representing a more thorough and effective application of precision dosing approaches by identifying, characterizing, and quantifying the different causes of variability in drug response via PK/PD modeling [25,35]. While gaining a deeper comprehension of PK/PD interrelation in particular patient populations during clinical studies can aid in identifying precise dosing objectives, patients from clinical practice are often much more distinct than those in supervised study environments. As a result, efficient post-marketing monitoring is crucial for investigating distinctive precision-dosing aims [61]. Improvements in methods for gathering and analyzing data from real-world patients present chances to discover novel precision-dosing procedures and improve those confirmed in clinical trials. These techniques facilitate the ongoing renewing and enhancement of dosing strategies to more effectively address patient requirements [35,62]. That is why our approach, which is based on MIPD under real-world circumstances, may be a first effort to guarantee the most accurate individual dosage for patients with psoriasis vulgaris receiving SCK.

Some limitations have been played against our investigation. Firstly, as a consequence of the study design conditions, there was a small patient sample size. Secondly, many PK/PD observations were either missing or were captured very distant in time (sparse data), resulting in a small number of points per patient. Because of that, the progression of psoriasis vulgaris or unmeasured physiological transformations may have straightforwardly affected the outcomes obtained. Looking ahead, similar models could be incorporated into a provisional distribution dashboard system for enhanced analysis [63,64]. Regarding the proposed optimization with the unlabeled dosage regimen of 300 mg q5w, and despite its advantages in terms of efficiency and safety, sometimes such optimizations may not be carried out because it would mean extending the frequency of administration by one more week. Changing the dosage could cause some confusion in, for example, elderly patients, patients who are seriously ill at the start of SCK therapy, and patients who have been heavily pretreated with multi-resistant forms. Furthermore, we incorporated tolerance mechanisms because we first developed a PKPD model with all the experimental evidence and then conducted an MIPD approach for evaluating the optimal dosing regimen. Therefore, the tolerance mechanisms could not be anticipated in a traditional TDM approach for prospective prediction without measured PK and PD levels.

The results of this study confirm the recommendations already formulated by other authors, who propose incorporating alternatives for different dosing schemes based on MIPD and/or TDM into the SmPC [65]. This proposal could enhance treatment management in chronic diseases, such as plaque psoriasis, and could facilitate real-time predictions

of treatment responses, helping healthcare providers make informed decisions regarding dosing modifications and therapy transitions for SCK.

5. Conclusions

In conclusion, this study represents a significant initial step for biologists to implement MIPD that targets the IL routes in long-lasting psoriasis vulgaris, an area that has been largely understudied. We propose a methodology to personalize dosing strategies for SCK, which considers the uncertainty of individual parameters within a population PK/PD model to enhance the likelihood of succeeding targeted clinical effects in patients with psoriasis vulgaris from moderate to severe modality. Future research should focus on applying our approach to a larger group of real-world patients and validating the proposed dosing strategies.

Supplementary Materials: The following supporting information can be downloaded at: https://www.mdpi.com/article/10.3390/pharmaceutics16121576/s1, Ordinary differential equations for the PK/PD model of SCK and absolute PASI; Figure S1: Individually predicted vs. the observed concentrations of SCK in patients with chronic psoriasis vulgaris; Figure S2: Individually predicted vs. the observed PASI in patients with chronic psoriasis vulgaris; Figure S3: Prediction-corrected visual predictive check obtained from one thousand simulated studies using the selected population PK/PD model; Table S1: Means of the individual PK/PD parameters drawn from the conditional distribution task in Monolix; Table S2: Standard deviation of the individual PK/PD parameters drawn from the conditional distribution task in Monolix; Figure S4: Bar plot of 100 simulated absolute PASI for each patient after SCK administration at cycles 10 and 20, using the individual parameters from the final population PK/PD model and their uncertainties; Figure S5: PK and PD simulations with the current dosage regimen from clinical practice and the individual optimal dosing regimen established after simulations in 20th cycle for each patient.

Author Contributions: Conceptualization, M.M.-S., E.G.-C., M.C.-M. and V.M.-S.; methodology, K.R.-F., J.Z.-F., M.M.-S., E.G.-C., M.C.-M. and V.M.-S.; software, K.R.-F., J.Z.-F. and V.M.-S.; validation, K.R.-F., J.Z.-F., M.S.-B., M.M.-S., A.M.-P., A.M.-C., E.G.-C., M.C.-M. and V.M.-S.; formal analysis, K.R.-F., J.Z.-F. and V.M.-S.; investigation, K.R.-F., J.Z.-F. and V.M.-S.; resources, A.M.-P., A.M.-C., E.G.-C. and M.C.-M.; data curation, K.R.-F.; writing—original draft preparation, K.R.-F., J.Z.-F. and V.M.-S.; writing—review and editing, K.R.-F., J.Z.-F., M.S.-B., M.M.-S., A.M.-P., A.M.-C., E.G.-C., M.C.-M. and V.M.-S.; visualization, K.R.-F. and J.Z.-F.; supervision, E.G.-C., M.C.-M. and V.M.-S.; project administration, E.G.-C., M.C.-M. and V.M.-S.; funding acquisition, A.M.-P., E.G.-C. and M.C.-M. All authors have read and agreed to the published version of the manuscript.

Funding: This research received no external funding.

Institutional Review Board Statement: This study was conducted following the Declaration of Helsinki and approved by the Ethics Committee of Dr. Peset University Hospital (protocol code: VMS-SCK-2020-01 and date of approval: 30 March 2020).

Informed Consent Statement: Informed consent was obtained from all subjects involved in the study.

Data Availability Statement: The data presented in this study are available on request from the corresponding author due to ethical and legal restrictions.

Conflicts of Interest: The authors declare no conflicts of interest.

Abbreviations

AHT	Arterial hypertension
BMI	Body mass index
$C_{trough\text{-}ss}$	Trough concentration at steady state
CL	Clearance
ELISA	Enzyme-linked immunosorbent assay
F	Bioavailability
IC_{50}	Concentration of the drug needed to inhibit 50% of the response
I_{max}	Maximum inhibition

IIV	Interindividual variability
IL	Interleukin
k_a	Absorption rate constant
k_{in}	Zero-order evolution constant rate of psoriatic skin lesion
k_{inTOL}	Zero-order progression constant rate of tolerance
k_{out}	First-order reduction constant rate of psoriatic skin lesion
k_{outTOL}	First-order remission constant rate of tolerance
mAb	Monoclonal antibody
MCMC	Markov chain Monte Carlo
MIPD	Model-informed precision dosing
PASI	Psoriasis Area and Severity Index
$PASI_i$	Estimated baseline levels of PASI response
$PASI_{i,0}$	Individual observed baseline levels of PASI response
pcVPC	Prediction-corrected visual predictive checks
PD	Pharmacodynamic
PK	Pharmacokinetic
PK/PD	Pharmacokinetic/pharmacodynamic
Q	Intercompartmental transfer clearance
q2w	Once every 2 weeks
q4w	Once every 4 weeks
q5w	Once every 5 weeks
q6w	Once every 6 weeks
RSE	Relative standard error
RUV	Residual unexplained variability
SC	Subcutaneous
SD	Standard deviation
SmPC	Summary of product characteristics
SLP	Linear drug effect model
TDM	Therapeutic drug monitoring
SCK	Secukinumab
V_2	Central volume of distribution
V_3	Peripheral volume of distribution

References

1. Frieder, J.; Kivelevitch, D.; Menter, A. Secukinumab: A review of the anti-IL-17A biologic for the treatment of psoriasis. *Ther. Adv. Chronic Dis.* **2018**, *9*, 5–21. [CrossRef] [PubMed]
2. Garnock-Jones, K.P. Secukinumab: A review in moderate to severe plaque psoriasis. *Am. J. Clin. Dermatol.* **2015**, *16*, 323–330. [CrossRef] [PubMed]
3. Nestle, F.O.; Kaplan, D.H.; Barker, J. Psoriasis. *N. Engl. J. Med.* **2009**, *361*, 496–509. [CrossRef]
4. Schadler, E.D.; Ortel, B.; Mehlis, S.L. Biologics for the primary care physician: Review and treatment of psoriasis. *Disease-a-Month* **2018**, *65*, 51–90. [CrossRef] [PubMed]
5. Rendon, A.; Schäkel, K. Psoriasis Pathogenesis and Treatment. *Int. J. Mol. Sci.* **2019**, *20*, 1475. [CrossRef] [PubMed]
6. Patel, D.D.; Lee, D.M.; Kolbinger, F.; Antoni, C. Effect of IL-17A blockade with secukinumab in autoimmune diseases. *Ann. Rheum. Dis.* **2012**, *72* (Suppl. 2), ii116–ii1123. [CrossRef]
7. Mahil, S.K.; Capon, F.; Barker, J.N. Update on psoriasis immunopathogenesis and targeted immunotherapy. *Semin. Immunopathol.* **2016**, *38*, 11–27. [CrossRef]
8. Lynde, C.W.; Poulin, Y.; Vender, R.; Bourcier, M.; Khalil, S. Interleukin 17A: Toward a new understanding of psoriasis pathogenesis. *J. Am. Acad. Dermatol.* **2014**, *71*, 141–150. [CrossRef]
9. EMA: COSENTYX-EPAR-product information. Available online: https://www.ema.europa.eu/en/documents/product-information/cosentyx-epar-product-information_en.pdf (accessed on 17 September 2024).
10. Phung, M.; Ighani, A.; Georgakopoulos, J.R.; Vender, R.; Giroux, L.; Lansang, P.; Yeung, J. Off-Label High-Dose Secukinumab for the Treatment of Moderate-to-Severe Psoriasis. *J. Cutan. Med. Surg.* **2019**, *23*, 391–393. [CrossRef]
11. Rich, P.; Sigurgeirsson, B.; Thaci, D.; Ortonne, J.P.; Paul, C.; Schopf, R.E.; Morita, A.; Roseau, K.; Harfst, E.; Guettner, A.; et al. Secukinumab induction and maintenance therapy in moderate-to-severe plaque psoriasis: A randomized, double-blind, placebo-controlled, phase II regimen-finding study. *Br. J. Dermatol.* **2013**, *168*, 402–411. [CrossRef]
12. Papp, K.A.; Langley, R.G.; Sigurgeirsson, B.; Abe, M.; Baker, D.R.; Konno, P.; Haemmerle, S.; Thurston, H.J.; Papavassilis, C.; Richards, H.B. Efficacy and safety of secukinumab in the treatment of moderate-to-severe plaque psoriasis: A randomized, double-blind, placebo-controlled phase II dose-ranging study. *Br. J. Dermatol.* **2013**, *168*, 412–421. [CrossRef] [PubMed]

13. Langley, R.G.; Elewski, B.E.; Lebwohl, M.; Reich, K.; Griffiths, C.E.; Papp, K.; Puig, L.; Nakagawa, H.; Spelman, L.; Sigurgeirsson, B.; et al. Secukinumab in plaque psoriasis--results of two phase 3 trials. *N. Engl. J. Med.* **2014**, *371*, 326–338. [CrossRef]
14. Augustin, M.; Jullien, D.; Martin, A.; Peralta, C. Real-world evidence of secukinumab in psoriasis treatment—A meta-analysis of 43 studies. *J. Eur. Acad. Dermatol. Venereol. JEADV* **2020**, *34*, 1174–1185. [CrossRef] [PubMed]
15. Yiu, Z.Z.N.; Mason, K.J.; Hampton, P.J.; Reynolds, N.J.; Smith, C.H.; Lunt, M.; Griffiths, C.E.M.; Warren, R.B. Drug survival of adalimumab, ustekinumab and secukinumab in patients with psoriasis: A prospective cohort study from the British Association of Dermatologists Biologics and Immunomodulators Register (BADBIR). *Br. J. Dermatol.* **2020**, *183*, 294–302. [CrossRef]
16. Leonardi, C.; Zhu, B.; Malatestinic, W.N.; Eastman, W.J.; Guo, J.; Murage, M.J.; Choong, C.K.; Burge, R.; Blauvelt, A. Real-World Biologic Adherence, Persistence, and Monotherapy Comparisons in US Patients with Psoriasis: Results from IBM MarketScan(®) Databases. *Adv. Ther.* **2022**, *39*, 3214–3224. [CrossRef]
17. Thein, D.; Rosenø, N.A.L.; Maul, J.T.; Wu, J.J.; Skov, L.; Bryld, L.E.; Rasmussen, M.K.; Ajgeiy, K.K.; Thomsen, S.F.; Thyssen, J.P.; et al. Drug Survival of Adalimumab, Secukinumab, and Ustekinumab in Psoriasis as Determined by Either Dose Escalation or Drug Discontinuation during the First 3 Years of Treatment—A Nationwide Cohort Study. *J. Investig. Dermatol.* **2023**, *143*, 2211–2218.e2214. [CrossRef] [PubMed]
18. Hueber, W.; Patel, D.D.; Dryja, T.; Wright, A.M.; Koroleva, I.; Bruin, G.; Antoni, C.; Draelos, Z.; Gold, M.H.; Psoriasis Study Group; et al. Effects of AIN457, a Fully Human Antibody to Interleukin-17A, on Psoriasis, Rheumatoid Arthritis, and Uveitis. *Sci. Transl. Med.* **2010**, *2*, 52ra72. [CrossRef]
19. Reich, K.; Papp, K.A.; Matheson, R.T.; Tu, J.H.; Bissonnette, R.; Bourcier, M.; Gratton, D.; Kunynetz, R.A.; Poulin, Y.; Rosoph, L.A.; et al. Evidence that a neutrophil-keratinocyte crosstalk is an early target of IL-17A inhibition in psoriasis. *Exp. Dermatol.* **2015**, *24*, 529–535. [CrossRef]
20. Paul, C.; Lacour, J.P.; Tedremets, L.; Kreutzer, K.; Jazayeri, S.; Adams, S.; Guindon, C.; You, R.; Papavassilis, C. Efficacy, safety and usability of secukinumab administration by autoinjector/pen in psoriasis: A randomized, controlled trial (JUNCTURE). *J. Eur. Acad. Dermatol. Venereol. JEADV* **2015**, *29*, 1082–1090. [CrossRef]
21. Bruin, G.; Loesche, C.; Nyirady, J.; Sander, O. Population pharmacokinetic modeling of secukinumab in patients with moderate to severe psoriasis. *J. Clin. Pharmacol.* **2017**, *57*, 876–885. [CrossRef]
22. Rodríguez-Fernández, K.; Mangas-Sanjuán, V.; Merino-Sanjuán, M.; Martorell-Calatayud, A.; Mateu-Puchades, A.; Climente-Martí, M.; Gras-Colomer, E. Impact of Pharmacokinetic and Pharmacodynamic Properties of Monoclonal Antibodies in the Management of Psoriasis. *Pharmaceutics* **2022**, *14*, 654. [CrossRef] [PubMed]
23. Liu, Y.; Xu, L.; Wang, X.; Wu, L.; Cai, R.; Li, L.; Zheng, Q. Optimization of secukinumab dose regimens in patients with moderate-to-severe plaque psoriasis via exposure-response modeling. *Expert Rev. Clin. Pharmacol.* **2023**, *16*, 999–1008. [CrossRef]
24. Notario, J.; Bordas, X. Practical management of ustekinumab in moderate-severe psoriasis. *Actas Dermo-Sifiliogr.* **2012**, *103*, 52–58. [CrossRef]
25. Tyson, R.J.; Park, C.C.; Powell, J.R.; Patterson, J.H.; Weiner, D.; Watkins, P.B.; Gonzalez, D. Precision Dosing Priority Criteria: Drug, Disease, and Patient Population Variables. *Front. Pharmacol.* **2020**, *11*, 420. [CrossRef] [PubMed]
26. Syversen, S.W.; Goll, G.L.; Jørgensen, K.K.; Sandanger, Ø.; Sexton, J.; Olsen, I.C.; Gehin, J.E.; Warren, D.J.; Brun, M.K.; Klaasen, R.A.; et al. Effect of Therapeutic Drug Monitoring vs Standard Therapy During Infliximab Induction on Disease Remission in Patients with Chronic Immune-Mediated Inflammatory Diseases: A Randomized Clinical Trial. *JAMA* **2021**, *325*, 1744–1754. [CrossRef] [PubMed]
27. Albader, F.; Golovics, P.A.; Gonczi, L.; Bessissow, T.; Afif, W.; Lakatos, P.L. Therapeutic drug monitoring in inflammatory bowel disease: The dawn of reactive monitoring. *World J. Gastroenterol.* **2021**, *27*, 6231–6247. [CrossRef]
28. D'Haens, G.R.; Sandborn, W.J.; Loftus, E.V., Jr.; Hanauer, S.B.; Schreiber, S.; Peyrin-Biroulet, L.; Panaccione, R.; Panés, J.; Baert, F.; Colombel, J.F.; et al. Higher vs Standard Adalimumab Induction Dosing Regimens and Two Maintenance Strategies: Randomized SERENE CD Trial Results. *Gastroenterology* **2022**, *162*, 1876–1890. [CrossRef]
29. Minichmayr, I.K.; Dreesen, E.; Centanni, M.; Wang, Z.; Hoffert, Y.; Friberg, L.E.; Wicha, S.G. Model-informed precision dosing: State of the art and future perspectives. *Adv. Drug Deliv. Rev.* **2024**, *215*, 115421. [CrossRef]
30. Olivier, B.G.; Swat, M.J.; Moné, M.J. Modeling and Simulation Tools: From Systems Biology to Systems Medicine. In *Systems Medicine*; Schmitz, U., Wolkenhauer, O., Eds.; Methods in Molecular Biology; Humana Press: New York, NY, USA, 2016; Volume 1386, pp. 441–463. [CrossRef]
31. Darwich, A.S.; Polasek, T.M.; Aronson, J.K.; Ogungbenro, K.; Wright, D.F.B.; Achour, B.; Reny, J.L.; Daali, Y.; Eiermann, B.; Cook, J.; et al. Model-Informed Precision Dosing: Background, Requirements, Validation, Implementation, and Forward Trajectory of Individualizing Drug Therapy. *Annu. Rev. Pharmacol. Toxicol.* **2021**, *61*, 225–245. [CrossRef]
32. Minichmayr, I.K.; Mizuno, T.; Goswami, S.; Peck, R.W.; Polasek, T.M.; American Society of Clinical Pharmacology; Therapeutics Precision Dosing Community. Recent Advances Addressing the Challenges of Precision Dosing. *Clin. Pharmacol. Ther.* **2024**, *116*, 527–530. [CrossRef]
33. Bandín-Vilar, E.; Toja-Camba, F.J.; Vidal-Millares, M.; Durán-Maseda, M.J.; Pou-Álvarez, M.; Castro-Balado, A.; Maroñas, O.; Gil-Rodríguez, A.; Carracedo, Á.; Zarra-Ferro, I.; et al. Towards precision medicine of long-acting aripiprazole through population pharmacokinetic modelling. *Psychiatry Res.* **2024**, *333*, 115721. [CrossRef] [PubMed]

34. Rodríguez-Fernández, K.; Reynaldo-Fernández, G.; Reyes-González, S.; de Las Barreras, C.; Rodríguez-Vera, L.; Vlaar, C.; Monbaliu, J.M.; Stelzer, T.; Duconge, J.; Mangas-Sanjuan, V. New insights into the role of VKORC1 polymorphisms for optimal warfarin dose selection in Caribbean Hispanic patients through an external validation of a population PK/PD model. *Biomed. Pharmacother.=Biomed. Pharmacother.* **2024**, *170*, 115977. [CrossRef] [PubMed]
35. Polasek, T.M.; Peck, R.W. Beyond Population-Level Targets for Drug Concentrations: Precision Dosing Needs Individual-Level Targets that Include Superior Biomarkers of Drug Responses. *Clin. Pharmacol. Ther.* **2024**, *116*, 602–612. [CrossRef]
36. Zhu, Y.; Hu, C.; Lu, M.; Liao, S.; Marini, J.C.; Yohrling, J.; Yeilding, N.; Davis, H.M.; Zhou, H. Population pharmacokinetic modeling of ustekinumab, a human monoclonal antibody targeting IL-12/23p40, in patients with moderate to severe plaque psoriasis. *J. Clin. Pharmacol.* **2009**, *49*, 162–175. [CrossRef] [PubMed]
37. Zhou, W.; Hu, C.; Zhu, Y.; Randazzo, B.; Song, M.; Sharma, A.; Xu, Z.; Zhou, H. Extrapolating Pharmacodynamic Effects From Adults to Pediatrics: A Case Study of Ustekinumab in Pediatric Patients With Moderate to Severe Plaque Psoriasis. *Clin. Pharmacol. Ther.* **2020**, *109*, 131–139. [CrossRef]
38. *ISO 15189*; Medical Laboratories—Requirements for Quality and Competence. International Organization for Standardization: Geneva, Switzerland, 2022.
39. Mould, D.R.; Upton, R.N. Basic concepts in population modeling, simulation, and model-based drug development. *CPT Pharmacomet. Syst. Pharmacol.* **2012**, *1*, e6. [CrossRef]
40. Upton, R.N.; Mould, D.R. Basic concepts in population modeling, simulation, and model-based drug development: Part 3-introduction to pharmacodynamic modeling methods. *CPT Pharmacomet. Syst. Pharmacol.* **2014**, *3*, e88. [CrossRef]
41. Felmlee, M.A.; Morris, M.E.; Mager, D.E. Mechanism-based pharmacodynamic modeling. In *Computational Toxicology*; Reisfeld, B., Mayeno, A., Eds.; Methods in Molecular Biology; Humana Press: Totowa, NJ, USA, 2012; Volume 929, pp. 583–600. [CrossRef]
42. Dansirikul, C.; Silber, H.E.; Karlsson, M.O. Approaches to handling pharmacodynamic baseline responses. *J. Pharmacokinet. Pharmacodyn.* **2008**, *35*, 269–283. [CrossRef]
43. Bergstrand, M.; Hooker, A.C.; Wallin, J.E.; Karlsson, M.O. Prediction-corrected visual predictive checks for diagnosing nonlinear mixed-effects models. *AAPS J.* **2011**, *13*, 143–151. [CrossRef]
44. Lixoft. Monolix Suite 2024R1 (2024). Available online: https://lixoft.com/products/monolix/ (accessed on 25 July 2024).
45. Ito, K.; Murphy, D. Application of ggplot2 to Pharmacometric Graphics. *CPT Pharmacomet. Syst. Pharmacol.* **2013**, *2*, e79. [CrossRef]
46. R Core Team. *R: A Language and Environment for Statistical Computing*; R Foundation for Statistical Computing: Vienna, Austria, 1999–2024; Available online: http://www.R-project.org/ (accessed on 30 July 2024).
47. Monolix 2024R1 User Guide. Available online: https://monolix.lixoft.com/single-page/ (accessed on 25 January 2024).
48. Kümmel, A.; Bonate, P.L.; Dingemanse, J.; Krause, A. Confidence and Prediction Intervals for Pharmacometric Models. *CPT Pharmacomet. Syst. Pharmacol.* **2018**, *7*, 360–373. [CrossRef] [PubMed]
49. Lixoft. Simulx 2024R1 (2024). Available online: https://simulx.lixoft.com/ (accessed on 25 July 2024).
50. Dayneka, N.L.; Garg, V.; Jusko, W.J. Comparison of four basic models of indirect pharmacodynamic responses. *J. Pharmacokinet. Biopharm.* **1993**, *21*, 457–478. [CrossRef]
51. Zhou, H.; Hu, C.; Zhu, Y.; Lu, M.; Liao, S.; Yeilding, N.; Davis, H.M. Population-based exposure-efficacy modeling of ustekinumab in patients with moderate to severe plaque psoriasis. *J. Clin. Pharmacol.* **2010**, *50*, 257–267. [CrossRef] [PubMed]
52. Salinger, D.H.; Endres, C.J.; Martin, D.A.; Gibbs, M.A. A semi-mechanistic model to characterize the pharmacokinetics and pharmacodynamics of brodalumab in healthy volunteers and subjects with psoriasis in a first-in-human single ascending dose study. *Clin. Pharmacol. Drug Dev.* **2014**, *3*, 276–283. [CrossRef]
53. Tham, L.-S.; Tang, C.-C.; Choi, S.-L.; Satterwhite, J.H.; Cameron, G.S.; Banerjee, S. Population exposure-response model to support dosing evaluation of ixekizumab in patients with chronic plaque psoriasis. *J. Clin. Pharmacol.* **2014**, *54*, 1117–1124. [CrossRef] [PubMed]
54. Pan, S.; Tsakok, T.; Dand, N.; Lonsdale, D.O.; Loeff, F.C.; Bloem, K.; de Vries, A.; Baudry, D.; Duckworth, M.; Mahil, S.; et al. Using Real-World Data to Guide Ustekinumab Dosing Strategies for Psoriasis: A Prospective Pharmacokinetic-Pharmacodynamic Study. *Clin. Transl. Sci.* **2020**, *13*, 400–409. [CrossRef]
55. Kerbusch, T.; Li, H.; Wada, R.; Jauslin, P.M.; Wenning, L. Exposure-response characterisation of tildrakizumab in chronic plaque psoriasis: Pooled analysis of 3 randomised controlled trials. *Br. J. Clin. Pharmacol.* **2020**, *86*, 1795–1806. [CrossRef]
56. Rodríguez-Fernández, K.; Zarzoso-Foj, J.; Saez-Bello, M.; Mateu-Puchades, A.; Martorell-Calatayud, A.; Merino-Sanjuan, M.; Gras-Colomer, E.; Climente-Martí, M.; Mangas-Sanjuan, V. Model-Informed Precision Dosing for Personalized Ustekinumab Treatment in Plaque Psoriasis. *Pharmaceutics* **2024**, *16*, 1295. [CrossRef]
57. DeBonis, J.; Veiseh, O.; Igoshin, O.A. Uncovering the interleukin-12 pharmacokinetic desensitization mechanism and its consequences with mathematical modeling. *CPT Pharmacomet. Syst. Pharmacol.* **2024**. [CrossRef]
58. BOT PLUS. Available online: https://botplusweb.farmaceuticos.com/ (accessed on 29 August 2024).
59. Torres, T.; Puig, L. Treatment goals for psoriasis: Should PASI 90 become the standard of care? *Actas Dermo-Sifiliogr.* **2015**, *106*, 155–157. [CrossRef]
60. Nast, A.; Smith, C.; Spuls, P.I.; Avila Valle, G.; Bata-Csörgö, Z.; Boonen, H.; De Jong, E.; Garcia-Doval, I.; Gisondi, P.; Kaur-Knudsen, D.; et al. EuroGuiDerm Guideline on the systemic treatment of Psoriasis vulgaris—Part 1: Treatment and monitoring recommendations. *J. Eur. Acad. Dermatol. Venereol. JEADV* **2020**, *34*, 2461–2498. [CrossRef] [PubMed]

61. Kamal, M.A.; Ganguly, S.; Kadambi, A.; Smith, P.F. Extended Model-Informed Drug Development: Beyond Clinical Trials and Regulatory Approval. *Clin. Pharmacol. Ther.* **2024**, *116*, 518–521. [CrossRef] [PubMed]
62. Darwich, A.S.; Ogungbenro, K.; Vinks, A.A.; Powell, J.R.; Reny, J.L.; Marsousi, N.; Daali, Y.; Fairman, D.; Cook, J.; Lesko, L.J.; et al. Why has model-informed precision dosing not yet become common clinical reality? lessons from the past and a roadmap for the future. *Clin. Pharmacol. Ther.* **2017**, *101*, 646–656. [CrossRef]
63. Dolan, J.G.; Veazie, P.J.; Russ, A.J. Development and initial evaluation of a treatment decision dashboard. *BMC Med. Inform. Decis. Mak.* **2013**, *13*, 51. [CrossRef] [PubMed]
64. Mould, D.R.; Upton, R.N.; Wojciechowski, J. Dashboard systems: Implementing pharmacometrics from bench to bedside. *AAPS J.* **2014**, *16*, 925–937. [CrossRef]
65. Mould, D.R.; Upton, R.N. "Getting the Dose Right"—Revisiting the Topic with Focus on Biologic Agents. *Clin. Pharmacol. Ther.* **2024**, *116*, 613–618. [CrossRef]

Supplementary materials

Personalized Secukinumab Treatment in Patients with Plaque Psoriasis Using Model-Informed Precision Dosing

Karine Rodriguez-Fernandez [1,2,†], Javier Zarzoso-Foj [1,2,†], Marina Saez-Bello [3], Almudena Mateu-Puchades [4], Antonio Martorell-Calatayud [5], Matilde Merino-Sanjuan [1,2], Elena Gras-Colomer [6], Monica Climente-Marti [3,*] and Victor Mangas-Sanjuan [1,2,*]

[1] Department of Pharmacy and Pharmaceutical Technology and Parasitology, University of Valencia, 46100 Valencia, Spain
[2] Interuniversity Research Institute for Molecular Recognition and Technological Development, Polytechnic University of Valencia–University of Valencia, 46100 Valencia, Spain
[3] Pharmacy Service, Doctor Peset University Hospital, Foundation for the Promotion of Health and Biomedical Research in the Valencian Region (FISABIO), 46017 Valencia, Spain
[4] Dermatology Service, Doctor Peset University Hospital, Foundation for the Promotion of Health and Biomedical Research in the Valencian Region (FISABIO), 46017 Valencia, Spain
[5] Dermatology Service, Hospital Manises of Valencia, 46940 Manises, Spain
[6] Pharmacy Service, Hospital Manises of Valencia, 46940 Manises, Spain
* Correspondence: climente_mon@gva.es (M.C.-M.); victor.mangas@uv.es (V.M.-S.); Tel.: +34-963543351
† These authors contributed equally to this work.

Ordinary differential equations for the PK/PD model of SCK and absolute PASI for patients without tolerance mechanism.

$$\frac{dA}{dt} = -k_a \cdot A$$

$$\frac{dC_C}{dt} = k_a \cdot A - CL \cdot C_C + Q \cdot (C_p - C_c)$$

$$\frac{dC_P}{dt} = -Q \cdot (C_p - C_c)$$

$$\frac{dprePASI_1}{dt} = k_{in} \cdot \left(1 - \frac{I_{max} \cdot C_C}{(IC_{50} + C_C)}\right) - k_{out} \cdot prePASI_1$$

$$\frac{dprePASI_2}{dt} = k_{out} \cdot prePASI_1 - k_{out} \cdot prePASI_2$$

$$\frac{dprePASI_3}{dt} = k_{out} \cdot prePASI_2 - k_{out} \cdot prePASI_3$$

$$\frac{dprePASI_4}{dt} = k_{out} \cdot prePASI_3 - k_{out} \cdot prePASI_4$$

$$\frac{dPASI}{dt} = k_{out} \cdot prePASI_4 - k_{out} \cdot PASI$$

where k_a: absorption rate constant; A: amount of SCK in the depot compartment.; CL: clearance; C_c: concentration of SCK in the central compartment; Q: intercompartmental transfer clearance; C_P: concentration of SCK in the peripheral compartment; $prePASI_{1-4}$: pre Psoriasis Area and Severity Index compartment; k_{in}: zero-order progression constant rate of psoriatic skin lesion; I_{max}: maximum inhibition drug effect model; IC_{50}: concentration of SCK needed to inhibit 50% of the response; k_{out}: first-order remission constant rate of psoriatic skin lesion; PASI: Psoriasis Area and Severity Index compartment.

Ordinary differential equations for the PK/PD model of SCK and PASI for patients with tolerance mechanisms

$$\frac{dA}{dt} = -k_a \cdot A$$

$$\frac{dC_C}{dt} = k_a \cdot A - CL \cdot C_C + Q \cdot (C_p - C_c)$$

$$\frac{dC_P}{dt} = -Q \cdot (C_p - C_c)$$

$$\frac{dTOL_1}{dt} = k_{in_{TOL}} \cdot (1 - SLP \cdot C_C) - k_{out_{TOL}} \cdot TOL_1$$

$$\frac{dTOL_2}{dt} = k_{out_{TOL}} \cdot TOL_1 - k_{out_{TOL}} \cdot TOL_2$$

$$\frac{dTOL_3}{dt} = k_{out_{TOL}} \cdot TOL_2 - k_{out_{TOL}} \cdot TOL_3$$

$$\frac{dprePASI_1}{dt} = k_{in} \cdot \left(1 - \frac{(I_{max} \div TOL_3) \cdot C_C}{(IC_{50} + C_C)}\right) - k_{out} \cdot prePASI_1$$

$$\frac{dprePASI_2}{dt} = k_{out} \cdot prePASI_1 - k_{out} \cdot prePASI_2$$

$$\frac{dprePASI_3}{dt} = k_{out} \cdot prePASI_2 - k_{out} \cdot prePASI_3$$

$$\frac{dprePASI_4}{dt} = k_{out} \cdot prePASI_3 - k_{out} \cdot prePASI_4$$

$$\frac{dPASI}{dt} = k_{out} \cdot prePASI_4 - k_{out} \cdot PASI$$

where k_a: absorption rate constant; A: amount of SCK in the depot compartment.; CL: clearance; C_C: concentration of SCK in the central compartment; Q: intercompartmental transfer clearance; C_P: concentration of SCK in the peripheral compartment; TOL_{1-3}: tolerance compartment; k_{inTOL}: zero-order progression constant rate of tolerance; $k_{outTOLt}$: first-order remission constant rate of tolerance; $prePASI_{1-4}$: pre Psoriasis Area and Severity Index compartment; k_{in}: zero-order progression constant rate of psoriatic skin lesion; I_{max}: maximum inhibition drug effect model; IC_{50}: concentration of SCK needed to inhibit 50% of the response; k_{out}: first-order remission constant rate of psoriatic skin lesion; PASI: Psoriasis Area and Severity Index compartment.

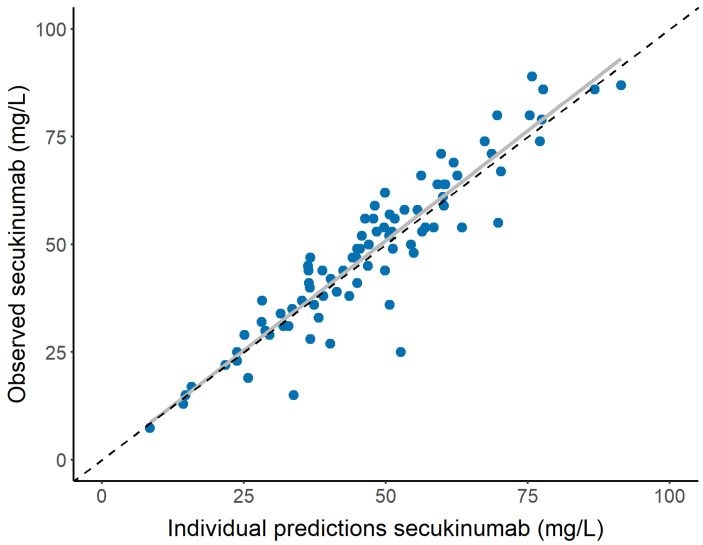

Figure S1. Individual predicted vs the observed concentrations of SCK in patients with chronic psoriasis vulgaris.

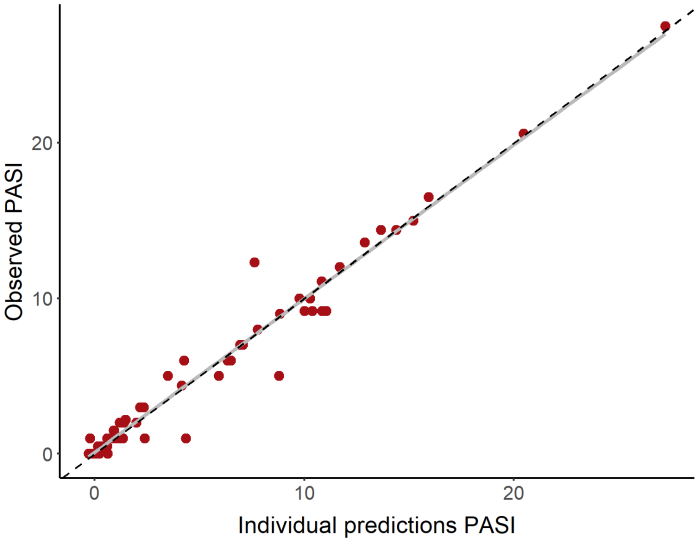

Figure S2. Individual predicted vs the observed PASI in patients with chronic psoriasis vulgaris.

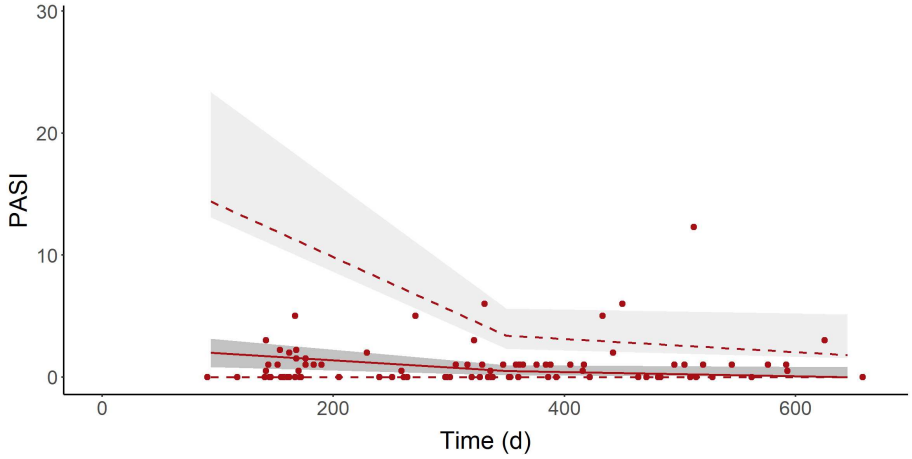

Figure S3. Prediction-corrected visual predictive check obtained from one thousand simulated studies using the selected population PK/PD model. Points represent the observed serum SCK concentrations; lines, 2.5th, 50th, and 95th percentiles of the simulated data. Shaded areas represent the 95% prediction intervals of the 5th, 50th, and 95th percentiles of the simulated studies.

Table S1. Mean of the individual PK/PD parameters drawn from the conditional distribution task in Monolix. For all patients F = 72.9 % and IC_{50} = 9.35 mg/L.

Subjects	PK					PD			
	k_a (day^{-1})	CL (L/d)	V_2 (L)	Q (L/d)	V_3 (L)	k_{out} (day^{-1})	k_{outTOL} (day^{-1})	I_{max}	$PASI_i$
1	0.20	0.15	3.72	0.40	2.93	0.47	0.0027	1.17	7.05
2	0.18	0.20	4.34	0.45	3.46	0.02	0.0033	1.10	1.98
3	0.20	0.11	1.99	0.26	1.71	0.09	0.0033	1.27	10.66
4	0.18	0.17	4.16	0.44	3.35	0.13	0.0033	1.13	10.78
5	0.18	0.26	4.60	0.47	3.62	0.07	0.0033	1.17	8.81
6	0.18	0.18	3.37	0.37	2.68	0.12	0.0033	1.13	27.40
7	0.19	0.15	3.31	0.37	2.68	0.08	0.0033	1.12	14.37
8	0.18	0.14	2.80	0.32	2.24	0.04	0.0033	1.09	10.99
9	0.18	0.17	4.34	0.45	3.37	0.25	0.0033	1.21	15.88
10	0.17	0.17	4.38	0.45	3.39	0.14	0.0044	1.20	20.38
11	0.19	0.17	3.22	0.38	2.80	0.12	0.0035	1.42	9.73
13	0.19	0.17	3.67	0.39	2.94	0.07	0.0028	1.34	12.76
14	0.20	0.19	3.52	0.39	2.82	0.09	0.0031	1.29	6.92
15	0.19	0.17	2.69	0.32	2.15	0.11	0.0032	1.20	10.35
16	0.17	0.15	4.19	0.44	3.42	0.12	0.0035	1.22	10.22
17	0.16	0.15	3.00	0.31	2.19	0.06	0.0030	1.27	4.12
18	0.18	0.26	4.00	0.42	3.17	0.15	0.0033	1.27	13.81
20	0.17	0.20	3.92	0.43	3.26	0.29	0.0033	1.24	9.95
21	0.34	0.16	3.38	0.42	3.17	0.18	0.0033	1.21	6.27
22	0.17	0.11	2.79	0.32	2.20	0.07	0.0034	1.13	7.73
23	0.18	0.13	2.63	0.30	2.09	0.09	0.0033	1.06	15.13
24	0.16	0.12	2.67	0.31	2.11	0.20	0.0033	1.15	11.59

k_a: absorption rate constant; F: bioavailability CL: clearance; Q: intercompartmental transfer clearance; V_2: central volume of distribution; V_3: peripheral volume of distribution; k_{out}: first-order remission constant rate of psoriatic skin lesion; $k_{outTOLt}$: first-order remission constant rate of tolerance; I_{max}: maximum inhibition drug effect model; $PASI_i$: estimated baseline levels of PASI response.

Table S2. Standard deviation of the individual PK/PD parameters drawn from the conditional distribution task in Monolix.

Subjects	PK					PD			
	k_a (day^{-1})	CL (L/d)	V_2 (L)	Q (L/d)	V_3 (L)	k_{out} (day^{-1})	k_{outTOL} (day^{-1})	I_{max}	$PASI_i$
1	0.023	0.006	0.284	0	0.073	0.216	0.0012	0.011	0.097
2	0.024	0.013	0.370	0	0.100	0.006	0.0012	0.098	0.106
3	0.018	0.014	0.287	0	0.088	0.034	0.0012	0.034	0.167
4	0.023	0.010	0.374	0	0.102	0.152	0.0013	0.023	0.103
5	0.021	0.020	0.405	0	0.105	0.131	0.0014	0.062	0.089
6	0.021	0.015	0.301	0	0.078	0.178	0.0012	0.028	0.100
7	0.025	0.009	0.283	0	0.077	0.131	0.0013	0.019	0.101
8	0.026	0.008	0.255	0	0.070	0.011	0.0013	0.022	0.100
9	0.022	0.004	0.664	0	0.119	0.063	0.0011	0.005	0.068
10	0.019	0.010	0.433	0	0.112	0.163	0.0012	0.059	0.098
11	0.028	0.010	0.207	0	0.091	0.016	0.0012	0.026	0.074
13	0.018	0.007	0.269	0	0.084	0.054	0.0012	0.035	0.119
14	0.022	0.008	0.279	0	0.056	0.075	0.0013	0.021	0.081
15	0.018	0.012	0.200	0	0.064	0.012	0.0014	0.014	0.065
16	0.031	0.006	0.372	0	0.175	0.090	0.0006	0.027	0.100
17	0.023	0.007	0.207	0	0.077	0.035	0.0013	0.015	0.107
18	0.021	0.021	0.368	0	0.089	0.087	0.0013	0.048	0.095
20	0.012	0.022	0.206	0	0.096	0.019	0.0013	0.027	0.092
21	0.022	0.010	0.179	0	0.097	0.053	0.0013	0.017	0.145
22	0.022	0.005	0.254	0	0.074	0.054	0.0012	0.024	0.110
23	0.021	0.007	0.245	0	0.065	0.103	0.0013	0.030	0.101
24	0.006	0.005	0.109	0	0.047	0.169	0.0012	0.006	0.123

k_a: absorption rate constant; F: bioavailability CL: clearance; Q: intercompartmental transfer clearance; V_2: central volume of distribution; V_3: peripheral volume of distribution; k_{out}: first-order remission constant rate of psoriatic skin lesion; $k_{outTOLt}$: first-order remission constant rate of tolerance; I_{max}: maximum inhibition drug effect model; $PASI_i$: estimated baseline levels of PASI response.

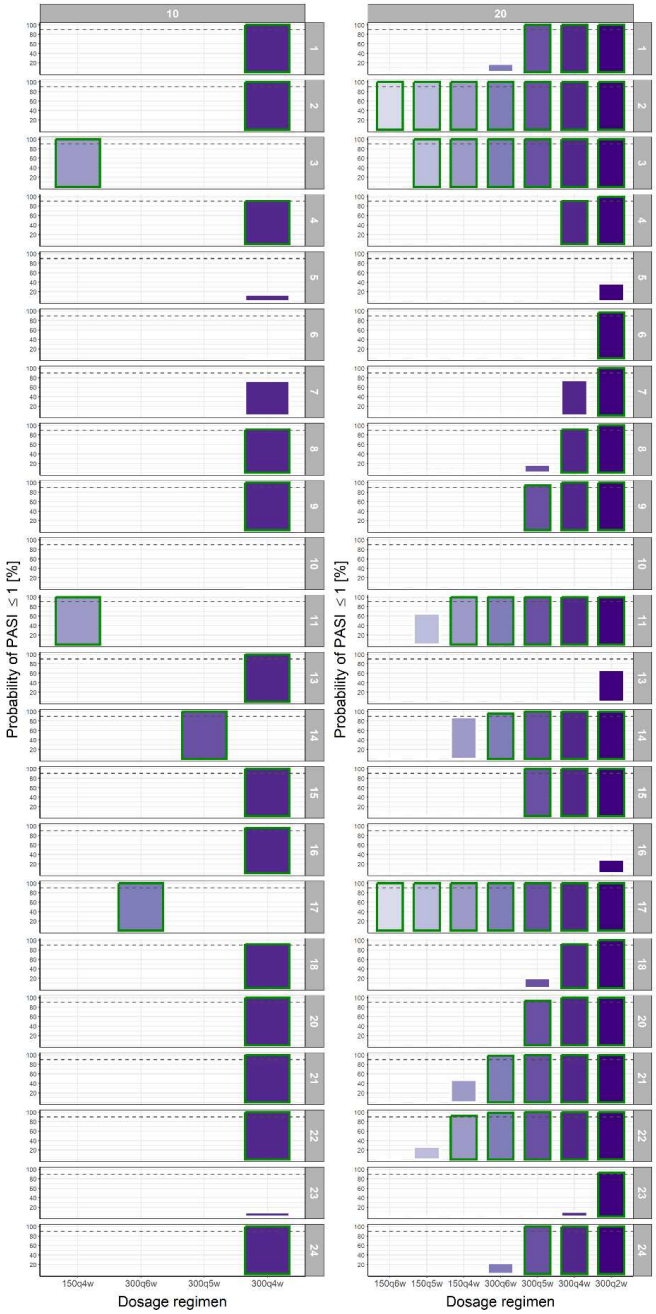

Figure S4. Bar plot of 100 simulated absolute PASI for each patient after SCK administration at cycles 10 and 20, using the individual parameters from the final population PK/PD model and their uncertainties. In green it is represented the probability ≥ 90% of PASI level ≤1. The dose regimens in which a probability ≥ 90% is reached are indicated in green.

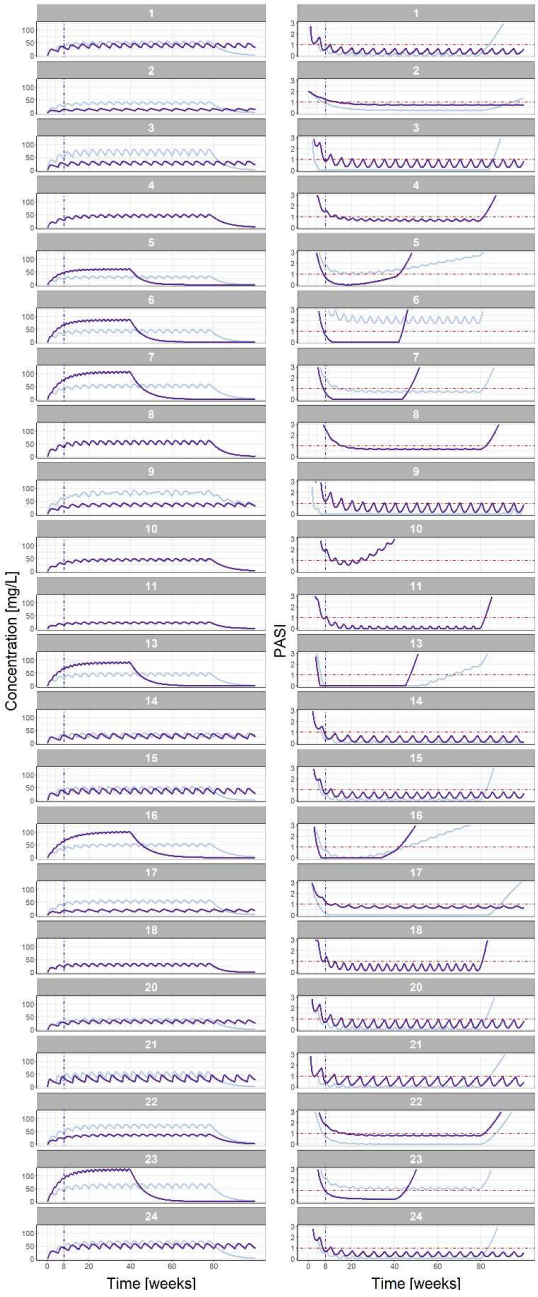

Figure S5. PK and PD simulations with the current dosage regimen from clinical practice (blue) and the individual optimal dosing regimen established after simulations in the 20th cycle (purple) for each patient to compare the plasmatic concentration tendency (left panel) and the PASI score behavior (right panel) according to the dosage regimen that the patient receives. The vertical dashed line represents the starting point of the maintenance period at week 8. The horizontal dashed line represents the PASI value of 1.

VNIVERSITAT DE VALÈNCIA